The Danish Meteorological Institute

Danish Ministry of Energy and Climate

DMI Scientific Report SR-16-22

The Polar Cap (PC) Index

Derivation Procedures and Quality Control

Peter Stauning

Research Department,Danish Meteorological Institute (DMI)
Lyngbyvej 100, 2100 Copenhagen Ø, Denmark

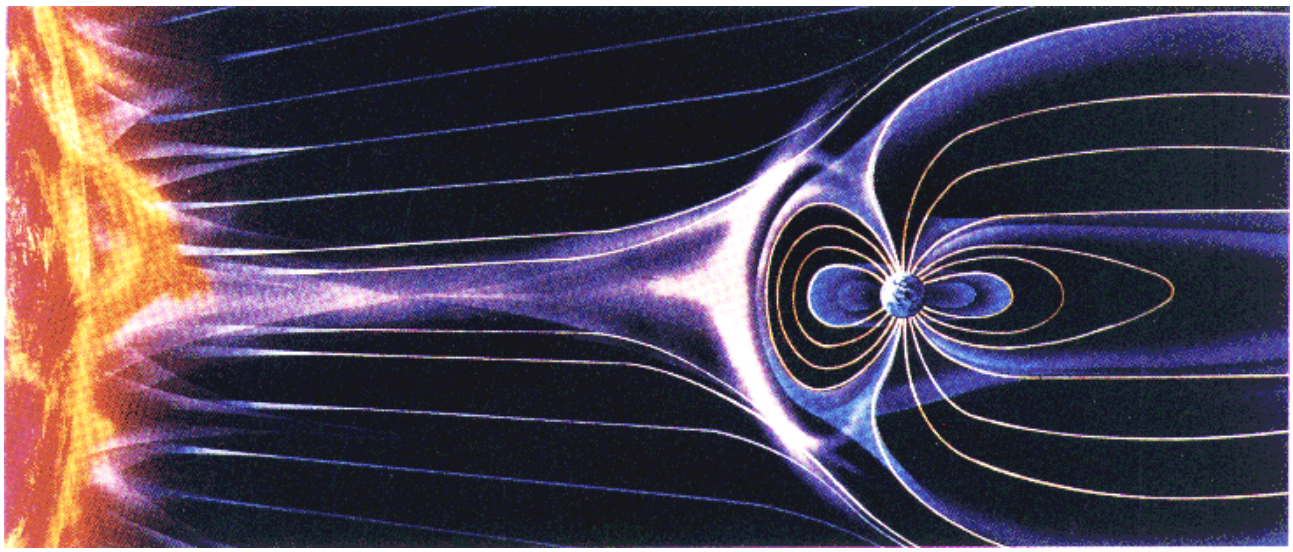

DMI Scientific Report SR-16-22. Copenhagen 2016

Colophon

Serial title:
DMI Scientific Report SR-16-22

Title:
The Polar Cap (PC) Index

Subtitle:
Derivation Procedures and Quality Control

Author:
Peter Stauning (emeritus scientist), Danish Meteorological Institute, Copenhagen.

Responsible institution:
Danish Meteorological Institute (DMI)

Language:
English

Keywords:
Polar Cap Index, PCN, PCS index, Polar magnetic disturbances, Geomagnetism, Solar Wind

Url:
http://www.dmi.dk/

Digital ISBN:
978-87-7478-667-2

ISSN:
2445-9127

Version:
Version 1 November 2016

Website:
www.dmi.dk

Contents:

Appendix A:

Appendix B :

Appendix C :

List of acronyms

AARI	Arctic and Antarctic Research Institute (located in St. Petersburg, Russia)
ACE	Advanced Composition Explorer (satellite)
BL	Base Line (level for internal geomagnetic field)
BSN	Bow Shock Nose (appr. 12 Re in front of the Earth)
DMI	Danish Meteorological Institute (located in Copenhagen, Denmark)
DP	Disturbance Polaire (polar magnetic disturbance types)
DP1	DP related to substorms
DP2	DP related to forward convection patterns (antisunward over polar cap)
DP3	DP related to reverse convection (sunward over polar cap)
DP4	(=DPY) DP related to IMF B_Y component. (convection system near Cusp)
DTU	Danish Technical University (located in Lyngby, Denmark)
DTU Space	DTU Space Research Institute
GSFC	Goddard Space Flight Center (NASA facility)
HSRW	Half Solar Rotation Weighted (for QDC calculations)
IAGA	International Association of Geomagnetism and Aeronomy
IMF	Interplanetary Magnetic Field
KL	Kan and Lee (ref. publication 1979)
LT	Local Time
MEF	Merging Electric Field (parameter in the solar wind)
OD	Optimum Direction (max. correlation between MEF and polar magnetic variations)
ODA	Optimum Direction Angle (angle between OD and E-W meridian)
OMNIweb	Interface to multiple sources of satellite-related data. Resides at GSFC, NASA
OMNIfiles	Used here for satellite data referred to Bow Shock Nose by time shifts
PC	Polar Cap
PCN	Polar Cap North (index)
PCS	Polar Cap South (index)
Q	Quiet (magnetically)
QDC	Quiet Day Curve (daily magnetic variation during quiet conditions)
QL	Quiet Level (magnetically)
QQ	Quietest (magnetically)
RE	Radius of the Earth
SRW	Solar Rotation Weighted (for QDC calculations)
SW	Solar Wind
UT	Universal Time (=Greenwich Mean Time, GMT)

The Polar Cap (PC) Index.

Derivation Procedures and Quality Control .

Abstract

The Polar Cap (PC) indices are derived from analyses of polar magnetic variations. PCN (North) values are based on magnetic data from Qaanaaq (Thule) in Greenland, while PCS (South) values are based on data from Vostok at Antarctica. The observatory in Qaanaaq is operated by the Danish Meteorological Institute (DMI), while the magnetometer instrument there is run by DTU Space. The magnetometer at Vostok is operated by the Russian Arctic and Antarctic Research Institute (AARI).

The PC indices primarily provide measures of the intensities of the transpolar ionospheric currents related to the polar cap antisunward ionospheric plasma convection driven by dawn-dusk electric fields generated by the solar wind. The index values are calibrated on a statistical basis to approximate values in units of mV/m of the interplanetary “merging” (or "geo-effective") electric field (*Kan and Lee, 1979)* conveyed by the solar wind. The index thus provides a measure of the energy input from the solar wind to the magnetosphere to cause global magnetic activity related to solar wind conditions. The PC indices can be used to analyze magnetically disturbed conditions and may provide forecasts of substorm activity and ring current development during geomagnetic storms.

The present report provides a comprehensive description of recent PC index derivation procedures developed at DMI. The report uses data from the epoch 1997-2009. The solar wind properties are described by OMNI data files (http://omniweb.gsfc.nasa.gov), while the polar magnetic data are provided from Thule and Vostok geomagnetic observatories. Thus, the data basis for determining the index coefficients and the PC index values presented here is the same as that used for the index version recently endorsed by IAGA but found to be immature (*Stauning*, 2015). The issues of particular concern in the IAGA-endorsed index procedure are discussed thoroughly in a separate section. Differences between the present derivation procedure and the IAGA-endorsed procedure as well as earlier PC index versions are discussed.

The comprehensive description provided here of the index procedure and of the more intricate features of the derivation process such as the effects of reverse convection cases, solar wind sector structure, averaging and smoothing of parameters, and choice of data epoch and reference quiet level, may hopefully inspire future suppliers of PCN and PCS index values to provide adequate descriptions of their methods along with the indices.

1. Introduction

The Polar Cap (PC) index was suggested by *Troshichev and Andrezen* (1985), further developed by *Troshichev et al.* (1988), *Vennerstrøm* (1991), and defined roughly (cf. sections 17.7 and 18) into its present form by *Troshichev et al.* (2006) to become an important parameter for analyses of solar-terrestrial relations and associated geomagnetic disturbances.

The concept of a polar cap index is based on the separation of the geomagnetic field into distinct parts. The main part, around 97%, comes from internal sources, that is, the Earth's core and crust. The field from electric currents in the core, the main field, has relatively slow (secular) variations in magnitude as well as in direction (cf. section 5.1). The crustal remnant magnetization is constant on geological time scales. The remaining field contributions generated by external current systems and their induced counterparts in the ground are generally found by subtracting a set of base line values, formed by the core and crust contributions, from the measured field components.

The external contributions from current systems in the ionosphere and the magnetosphere, in turn, can be subdivided into two fractions. One is associated with the effects of the slowly varying solar UV and EUV fluxes and the rather steady flow of solar wind plasma past the Earth's magnetosphere during calm solar conditions. These contributions form the rather regular daily geomagnetic variations often described by a Quiet Day Curve (QDC) for each component. The other fraction is associated with effects relating to active solar conditions with enhanced solar wind and the presence of a magnetic field in the solar wind. This interplanetary magnetic field (IMF) in the solar wind may strongly enhance the interaction of the solar wind with the Earths magnetosphere. The interaction manifests itself, among other, though strong magnetic variations in the Polar Regions.

PC index values are primarily derived from the intensity of geomagnetic variations associated with the transpolar part of the ionospheric forward two-cell convection patterns in the polar cap. The magnetic variations are scaled with respect to the driving interplanetary "merging" (or "geo-effective") electric field to make the resulting index independent of local daily and seasonal variations. The PCN (North) index is based on geomagnetic variation data from Qaanaaq (Thule) in Greenland while the PCS (South) index is based on data from Vostok in Antarctica.

Since the original concept of a Polar Cap index was introduced by *Troshichev and Andrezen* (1985) several different calculation procedures have been developed to derive PC-North (PCN) and PC-South (PCS) indices from polar cap magnetic variations. In the past there have been 7 different version of the PCN index and 5 versions of the PCS index (see *Stauning*, 2013b and Appendix C). The International Association of Geomagnetism and Aeronomy (IAGA) has recently endorsed new Polar Cap (PCN and PCS) index versions to supersede the previous different versions (cf. sections 17 and 18).

The various versions of the PC indices have been used to study interplanetary geoeffective electric fields (e.g., *Troshichev et al.*, 2006), solar wind pressure pulses (*Lukianova*, 2003; *Huang*, 2005), cross polar cap voltage and polar cap diameter (*Troshichev et al.*, 1996, 2000; *Ridley and Kihn*, 2004), ionospheric Joule heating (*Chun et al.*, 1999, 2002), and general polar cap dynamics (*Stauning et al.*, 2008; *Fiori et al.*, 2009; *Gao et al.*, 2012). The PC indices were also used to predict auroral electrojet intensities (*Vennerstrom et al.*, 1991; *Vassiliadis et al.*, 1996; *Takalo and Timonen*, 1999), global auroral power (*Liou et al.*, 2003), and ring current intensities (*Stauning et al.*, 2008, *Troshichev et al.*, 2011b, 2012). For specific space weather purposes the PC indices can be used to predict substorm development (*Janzhura et al.*, 2007; *Troshichev and Janzhura*, 2009; *Troshichev et al*., 2011c, 2014), and power line disturbances in the subauroral regions (*Stauning*, 2013c).

The new PC index version endorsed by IAGA in 2013 was supplied jointly by Arctic and Antarctic Research Institute (AARI), Russia, and DTU Space and published since 2014 at http://pcindex.org. However, a comprehensive description of the derivation procedure is not yet available. Some documentation is found at the DTU Space (2014) ftp site: ftp://ftp.space.dtu.dk/WDC/indices/pcn, where reference is made to the following sources for more extended descriptions of the PC index procedures: *Troshichev et al.* (2006), *Janzhura and Troshichev* (2008), *Janzhura and Troshichev* (2011), *Troshichev*

and Janzhura (2012). The new IAGA-endorsed PC index has some adverse features which should be known and taken into account by possible users of the index (*Stauning*, 2015). The aim here is primarily to provide a full description of the most up-to-date DMI PCN and PCS index procedures. In addition, characteristic features of the IAGA-endorsed versions and other PC index versions still in use or used in the past are outlined.

2. Polar convection modes and PC index basics

2.1 Convection modes

Polar magnetic variations beyond the quiet daily variations (QDC) are predominantly caused by the horizontal and field-aligned currents related to the convection systems sketched in Fig. 1. The horizontal currents are related to oppositely directed ionospheric drift motions. The DP2 (forward) and DP3 (reverse) convection modes could be considered the basic modes for the transpolar convection and currents while DP1 (substorm) and DP4 (DPY) convection modes may generate perturbations of the two basic transpolar convection systems.

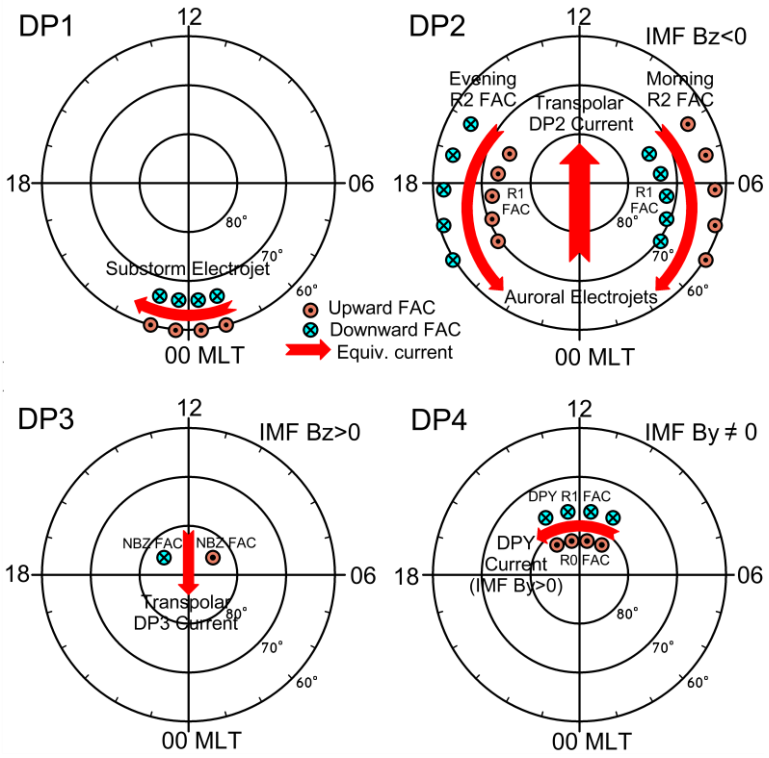

Fig. 1. Sketches of ionospheric and field-aligned currents related to DP1 (substorm), DP2 (forward), DP3 (reverse), and DP4 (DPY) polar convection systems (*Stauning*, 2015).

2.2 PC index definition

The basic definition of the Polar Cap (PC) index could be found in *Troshichev et al.* (2006). In summary, (cf. *Stauning*, 2013b), the PC index is derived from an assumed linear relation between the "merging" (or "geo-effective") electric field, E_M, in the solar wind encountering the Earth and ΔF_{PROJ}, the polar cap horizontal magnetic variation (at ground) projected to the so-called "optimum direction".

With constants α [nT/(mV/m)] and β [nT], the linear relation is expressed as:

$$\Delta F_{PROJ} = \alpha E_M + \beta \quad (1)$$

The optimum direction (cf. section 8) is close to perpendicular to the average DP2 transpolar equivalent current direction (see Fig. 1) and makes an angle φ to the dawn-dusk direction. The projection enhances the coupling of the PC index to the dominant DP2 forward convection mode.

The merging electric field (*Kan and Lee*, 1979) is defined through:

$$E_M = V_{SW} B_T \sin^2(\theta/2) \quad (2)$$

where V_{SW} is the solar wind velocity, B_T is the transverse component of the interplanetary magnetic field ($B_T=\sqrt{(B_Y^2+B_Z^2)}$, while θ is the polar angle between the Z-axis of the Geocentric Solar-Magnetospheric (GSM) coordinate system and the transverse IMF component.

Equation (1) is now inverted to give a definition of the PC index by equivalence with the merging electric field measured in mV/m:

$$PC = (\Delta F_{PROJ} - \beta)/\alpha \quad (\sim E_M) \quad (3)$$

The scaling parameters comprise the optimum direction angle, φ, derived to give maximum correlation between the solar wind intensities (Eq. 2) and the projected magnetic variations (Eq. 1), while the coefficients, α (slope) and β (intercept), are found from Eq. 1 through regression analyses based on an ensemble of concurrent (contemporary with a time delay, cf. section 8.2) values of the merging electric field, E_M, and the polar cap horizontal magnetic variation vector, $\boldsymbol{\Delta F}$, counted from the quiet level, $\boldsymbol{F}_{QL}$.

3. Summary of PC index derivation procedures.

The Polar Cap (PC) index represents the geomagnetic disturbance in the central polar cap caused by the encounter of the magnetized solar wind with the Earth's magnetosphere and scaled to equal, on the average, the solar wind merging electric field in order to remove dependencies on local time of day and season, and on specific observatory location. Before giving a detailed description of the steps in the derivation procedure, a short summary is provided in this section.

3.1. Data series.

3.1.1. Solar wind data. Recordings of solar wind parameters for the interplanetary magnetic field (IMF B_Y and IMF B_Z) and the solar wind velocity (V_{SW}) are needed. Data from the IMP8, WIND, and ACE spacecrafts have been used in past PC index derivation. These solar wind parameters selected from available satellites and referred to Earth's bow shock nose are conveniently made available in the OMNI data series via http://omniweb.gsfc.nasa.gov, e.g. in the 5-min resolution values used for the statistical processing to derive PC index scaling parameters. There, one can also find a full description of the derivation and of the uncertancies involved in the shift of solar wind parameters from the satellite positions to the nose of the magnetosphere. The solar wind data are here converted into values of the merging electric field by using the Kan and Lee (1979) formula presented in Eq. 2.

3.1.2. Geomagnetic data. Geomagnetic recordings from a polar cap observatory are needed. Data from Qaanaaq (Thule) in Greenland in 1-min resolution are used for standard PCN index while 1-min data from Vostok in Antarctica are used for standard PCS index values. Past data from Thule are available via Intermagnet (www.intermagnet.org) or from DTU Space (http://space.dtu.dk). Past data from Vostok are available on request from Arctic and Antarctic Research Institute (AARI) or via the web site http://pcindex.org.

3.1.3. Baseline. The secularly varying baseline values (X_{BL}, Y_{BL}) could either be subtracted in an initial step or built into the QDC. The end results would be the same but isolating the QDC contribution may facilitate quality control. When to be used, the yearly values are linearly interpolated to give daily values of (X_{BL},Y_{BL}).

3.1.4. QDC derivation. Recent PC index procedures are based on magnetic variation data corrected for the quiet daily variation, which largely depends on the flow of ionospheric plasma across the polar cap in response to the residual cross-polar cap voltage and to the heating and ionization by solar radiation at the dayside and subsequent expansion of the ionosphere toward the nightside. The quiet daily variation is characterized by the so-called "Quiet Day Curve" (QDC), the elements of which, in principle, are found as the magnetic variations at corresponding times of day and season during "*extremely quiet intervals*" (e.g., *Troshichev et al.*, 2006).

For derivation of QDC values, the "Solar Rotation Weighting" (SRW) method (see *Stauning*, 2011) is used here in contrast to the method used for the IAGA-endorsed index procedure. It relies on building hourly QDC values through each day by averaging contributions from corresponding hours from the selected day and neighboring days weighted to give preference to the quietest recordings made during days closest to the day in question and with the same face of the Sun turned toward the Earth. Thus:

$$X_{QDC} = \sum (X_i \cdot wf_i)/\sum wf_i \quad (4a)$$

$$Y_{QDC} = \sum (Y_i \cdot wf_i)/\sum wf_i \quad (4b)$$

where wf_i is the combined weight factor for the i'th sample (see section 6).

When to be used, the hourly QDC values for the day in question are interpolated to give 15-min, 5-min or 1-min values of (X_{QDC},Y_{QDC}).

3.1.5. Corrected geomagnetic data series. For the derivation of PC index coefficients here, the baseline- and QDC-corrected geomagnetic data are converted into series of sorted average values of the horizontal components, e.g., (ΔX,ΔY) in local geographic (rotating) coordinates, where:

$$\Delta X = X_{RAW} - X_{BL} - X_{QDC} \quad (5a)$$

$$\Delta Y = Y_{RAW} - Y_{BL} - Y_{QDC} \quad (5b)$$

In a spike suppression effort, the handling of the 1-min raw data exempts the max and min samples from the averaging to give 15-min or 5-min values. For the baseline (X_{BL},Y_{BL}) the daily values are sufficiently accurate since the variations through a day are less than 1 nT (cf. section 15).

3.2. Delay from Earth's bow shock to Polar Cap. Optimum direction angle.

The first step in the processing to calculate index parameter values is the derivation of the delay between solar wind parameters at the bow shock nose and the related Polar Cap geomagnetic effects. In the same step the so-called "Optimum direction angle" (φ=ODA) is found. The optimum direction angle is the varying angle counted CW between the dawn-dusk meridian and the meridian onto which the projected horizontal magnetic disturbance vectors have the highest correlation with the merging electric fields. The optimum direction angle is also the angle between the direction to the Sun and the direction of the sunward equivalent ionospheric current (the current causing the geomagnetic disturbance).

The delay and the optimum direction angle are found by stepping both the delay value and the angle through ranges of values searching for the highest value of the correlation between the time-shifted merging electric field at the bow shock nose and the projected magnetic disturbance (ΔF_{PROJ}), i.e.:

$$\Delta F_{PROJ} = \Delta X \cdot \sin(V_{PROJ}) \pm \Delta Y \cdot \cos(V_{PROJ}) \quad (6)$$

+ for Vostok; - for Thule, while V_{PROJ} is defined as a function of *UThr* (UT time in hours) through:

$$V_{PROJ} = Longitude + UThr \cdot 15^o + optimum\ direction\ angle \quad (7)$$

The optimum direction angle (φ=*ODA*) varies with location, season and local time (cf. section 8.2).

3.3. Slope and intercept coefficients. PC index values.

The PC index concept relies on equivalence between the scaled geomagnetic disturbance and the merging electric field in the impinging solar wind. Assuming that the projected magnetic variations, statistically, are proportional to the merging electric field, time shifted by *td* to the polar cap, gives the relation:

$$\Delta F_{PROJ}(t) = \alpha \cdot E_M(t - td) + \beta \qquad (8)$$

where α is the "Slope" while β is the "Intercept" parameter named from a visualized graphical display of ΔF_{PROJ} against the delayed E_M. These coefficients are found by least squares regression analyses on a large amount of corresponding values of the (time-shifted) merging electric field and the projected magnetic variations. They depend, like the optimum direction angle, on local time of day and season, and on observatory location. With the optimum angle and the slope and intercept coefficients derived on a statistical basis, the PC index is now derived from actual values of the projected disturbance through:

$$\mathrm{PC}(t) = (\Delta F_{PROJ}(t) - \beta)/\alpha \quad (\sim E_M(t\text{-}td)) \qquad (9)$$

where the coefficients, α and β, are given the values derived for the relevant time of day and day of the year, but invariable over years. In the standard version the PC index is provided in 1-min resolution.

3.4. Particular features in the selection and handling of data samples.

The DP2 mode (cf. Fig. 1) is the primary convection mode for the PC index. The disturbing effects from substorms (DP1 convection mode), described by the auroral electrojet indices, are minimized by using data from an observatory, such as Thule, located close to the magnetic pole.

The alternative DP3 reverse convection mode is established during intervals of strong northward IMF B_Z (NBZ) conditions, when also the magnitude of IMF B_Y is less the IMF B_Z. In such cases the IMF polar angle, θ, is small, and the non-negative merging electric field takes small positive values (cf. Eq. 2), while the projected magnetic variations may take large negative values such that any proportionality (Eq. 8) is excluded. These cases belong to a different class. To make the PC index representative of the merging electric field, NBZ cases should be excluded from the data base in the calculations of index coefficients (not from deriving actual PC index values).

The DP4 (DPY) convection mode is related to current systems predominantly operating in and around the Cusp region at the Earth's dayside at geomagnetic latitudes around ± 75°. These currents are caused by the Y-component, IMF B_Y, of the interplanetary magnetic field. The contribution from an IMF B_Y component to the merging electric field is independent on the its sign (cf. Eq. 2) while the effects on the convection and thus on the resulting magnetic disturbance is highly asymmetric and may enhance or reduce PC index values compared to the values expected from the intensity of the merging electric field. The adverse effects are mitigated by using a QDC procedure that takes the IMF B_Y effects into account.

The solar wind magnetic field could be represented by large loops of field lines extending from the Sun. The field orientation, i.e., outward or inward, depends on the direction of the field along the loop and on the observer's position relative to the field's meridian plane. Due to the solar rotation the loops are dragged into a spiral configuration (Parker spiral) by the outward streaming solar wind plasma. Hence, the component along the field line is systematically shared between the IMF *X*- and *Y*-components. Outward field orientation gives positive IMF B_X and negative B_Y values, and vice versa for inward fields.

The field line loops extending from the Sun are generally organized with the same orientation along extended stretches of the circumference of the Sun. Thus the signs of the IMF B_X and B_Y components at the Earth may alternate two or more times during a 27 days solar rotation period. The sector structure is not stationary and may shift between two, three, and multi-sector modes. The largest IMF B_Y effects are usually associated with the two-sector structure (see Fig. 3).

The processing of solar wind and polar cap data to derive PCN and PCS index values is described in considerable details the following sections 4 to 14. The choice of methods and the selection of parameters are discussed more extensively in sections 15 and 16.

4. Solar Wind satellite observations.

During the time interval from 1975 to present, where high-quality digital magnetic data are available from Thule and in some years also from Vostok, there are three main sources of solar wind plasma and interplanetary magnetic field data. These sources are IMP 8, WIND and ACE satellite data. Further solar wind data are, at times, acquired by the Geotail satellite. At Goddard Space Flight Center (GSFC) at NASA, the available data are combined into OMNI files using the best possible selection of spacecraft measurements. The OMNI data series extend back to 1981 and is available at http://omniweb.gsfc.nasa.gov along with format descriptions and thorough descriptions of the selection and processing of the satellite data. By appropriate time-shifting of the measurements, data in the OMNI files are referred to the magnetospheric bow shock nose (BSN) located at a distance of approximately 12 earth radii in front of the Earth toward the Sun.

4.1. IMP 8 satellite

The IMP 8 satellite was launched 1973-10-26 into an orbit with apogee and perigee around 40 and 25 earth radii, respectively, and inclination varying between 0 deg and 55 deg.. Solar wind data are available up to year 2000. The spacecraft was located in the solar wind for 7 to 8 days of every 12.5 days orbit. Telemetry coverage has been varying between around 60 and 90%.

With around 25 years (i.e. more than two solar activity cycles) of steady operation and stable orbit conditions at positions relatively close to the Earth, but still in the undisturbed solar wind during most of the time, this satellite, compared to Wind and ACE, provides by far the best basis for statistical studies of relations between solar wind parameters and polar geomagnetic disturbances since for such studies one can select cases where the satellite is close to the magnetosphere but still in the undisturbed solar wind.

4.2. Wind satellite

The Wind satellite was launched 1994-11-01 to spend the first 9 months of operation (1995) in a double-lunar swing-by orbit near the ecliptic plane, with apogee from 80 to 250 Re and perigee ranging from 5 to 10 Re. During the next couple of years Wind was inserted in a halo orbit around the L1 point in front of the Earth at distances varying from 235 to 265 Re. During more recent years Wind has been moved around to various positions ranging from orbits near the frontal magnetopause and in the near-Earth tail to highly eccentric orbits taking the satellite far away from the Sun-Earth line.

The drastic changes in satellite orbit make the data less useful for studies involving long-term correlation with ground-based observations. However, the strongly varying satellite position provides unique opportunities to investigate the effects of variations in the distance between the satellite and the Earth along the Sun-Earth line (varying delay) as well as variations in solar wind uniformity with the transverse distance from the Sun-Earth line.

4.3. ACE satellite

The ACE satellite was launched 1997-08-25 into a halo orbit around the L1 Earth-Sun liberation point. The satellite instruments and telemetry has provided almost 100% recovery of magnetic data and solar wind plasma and velocity data since the beginning of 1998. The satellite is still active. An example of ACE data through year 2000 is presented in Fig. 2. The figure displays the measured IMF B_X, B_Y, and B_Z components, and the solar wind velocity, V_{SW}. Values of the derived merging electric field, E_M, are shown in the bottom field. The slowly varying curves (in red lines) superimposed on the fast variations (in blue lines) indicate Gaussian-smoothed values. All parameters are time-shifted from the ACE position to the bow shock nose (BSN) position at around X_{GSE}=12 R_E (cf. description at http://omniweb.gsfc.nasa.gov).

For space weather forecasts, in addition to the convenient continuity of solar wind observations, the main advantage of using ACE data is the large distance of around 240 Re (~1.500.000 km) from the Earth to the satellite. This large distance causes a delay of typically around 1 hour for the solar wind with its

embedded magnetic field to travel from the satellite position to the encounter with the Earth's magnetosphere. For real-time space weather forecasts this delay is quite useful.

However, in addition to possible telemetry or spacecraft failures one has to make reservations concerning the reliability of the measurements of solar wind plasma parameters, in particular, the solar wind velocities. During events of strong high-energy solar proton outbursts, which often precede and accompany solar wind enhancements leading to geomagnetic storms, the plasma detectors might be disabled by the hard radiation leading to false solar wind velocity data.

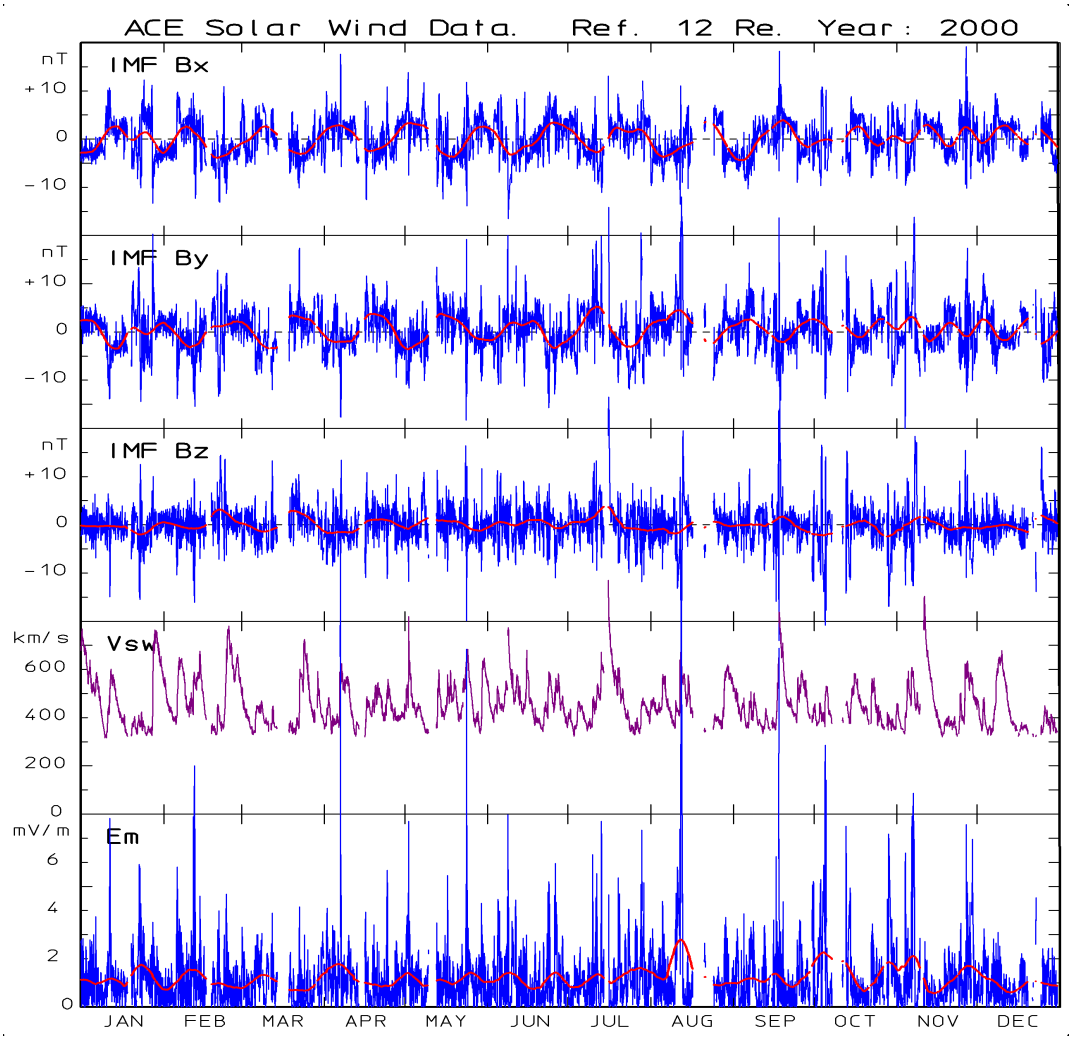

Fig. 2. ACE solar wind data. From top: interplanetary magnetic field (IMF) components B_X, B_Y, B_Z, solar wind velocity (V_{SW}), and merging electric field (E_M). All data shifted to bow shock nose.

In Fig. 2 one may note the data gaps in mid-March, in mid July (the Bastille event), in mid-August, in beginning of October and in some days in November and December. During the July and November events, the cause of missing data was the occurrence of strong high-energy solar proton fluxes, which disabled the plasma detectors. Such events are particularly troublesome for space weather forecasts since they may disguise the onset of major enhancements of solar wind intensities associated with strong coronal mass ejections (CME), which in turn may cause violent geomagnetic storms like it happened during the Bastille event on 14 July, 2000. In the OMNIweb data the WIND satellite has a similar problem. The IMP 8 data series terminated on 9 June 2000 and are no longer available for space weather forecasts.

In addition to the disruptions of the ACE data, note in Fig. 2. the systematic modulation of IMF B_X and B_Y intensities in opposite phases with a period of mostly around 27 days, i.e., the solar rotation period. This is an indication of the solar wind sector structure, where the general solar magnetic field has consistently organized structures through considerable parts of the rotating Sun's circumference. Here, in 2000, the structure indicates a two-sector mode through most months except October-December where the sector structure shifts to a four-sector mode.

The recurrence features for IMF B_Y, i.e., the sector structure, are further illustrated in Fig. 3. that displays the smoothed B_Y values from 1998 through 2008 against time of year. The larger amplitudes are generally associated with the two-sector structures reflecting the solar 27 days rotation period.

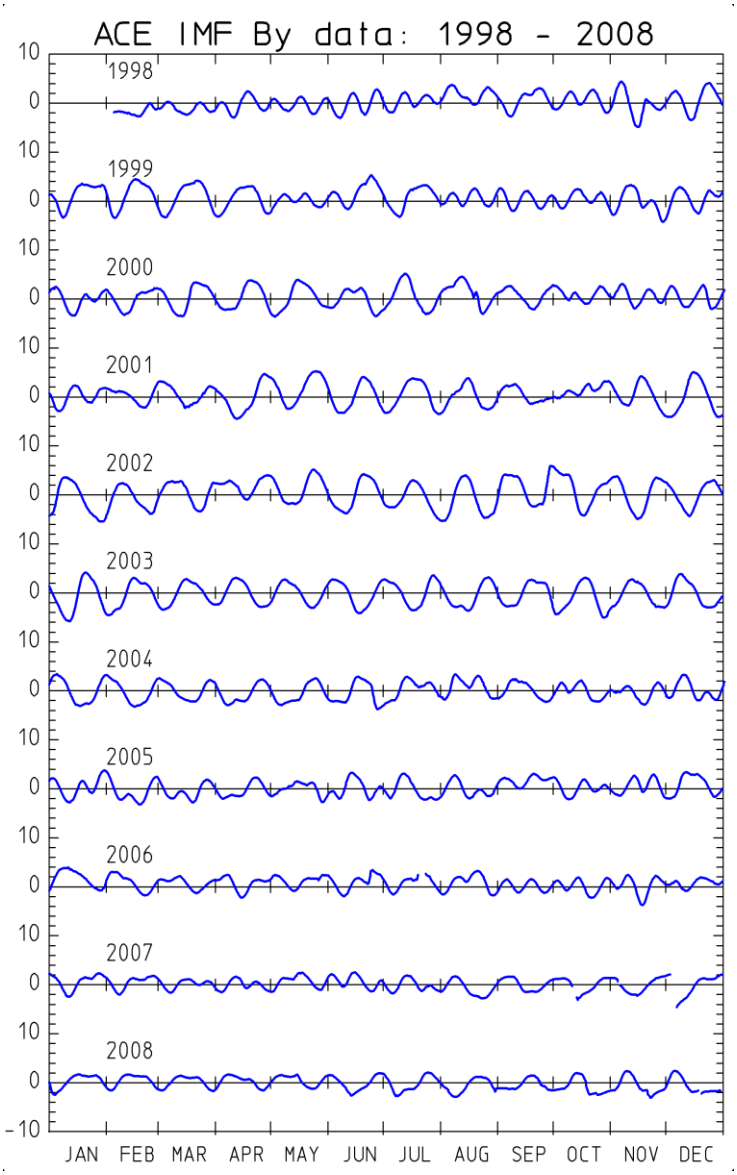

Fig. 3. Recurrence features (sector structure) for IMF B_Y. The IMF B_X data have the same features (in antiphase).

Further reservations concerning the use of ACE satellite data for space weather forecasts relate to the problem of shifting solar wind properties from the ACE position to the position of the bow shock nose and transporting the effects from there to related geomagnetic disturbances within the Earth's magnetosphere and the polar ionospheres. The possible effects of the shifting of parameters from the ACE position to the BSN position are illustrated by comparing time-shifted ACE data to corresponding data from the IMP 8 satellite.

Fig. 4. compares ACE solar wind measurements time-shifted from the ACE position at X_{GSE} around 240 R_E to the bow shock nose (BSN) position at X_{GSE}~12 R_E in front of the Earth, with corresponding BSN-shifted IMP 8 measurements conducted at X_{GSE} positions between 0 and 40 R_E, i.e., much closer to BSN. The parameters noted in the plots indicate average difference (S0), robust (magnitude) difference (S1) and RMS difference (S2).

There is a considerable scatter particularly in the IMF components and this scatter is reflected in the derived values of the merging electric field. However, the average values matches quite well between the BSN-shifted ACE data and the BSN-shifted IMP 8 data collected much closer to the Earth (and closer to the BSN position). For the present main purpose, i.e., to derive PC index coefficients by statistical methods from a large data base, this average matching gives confidence in the use of the OMNI data files built from ACE, Wind, and Geotail data in addition to IMP 8 measurements, and with all data time-shifted to the BSN position. The

time-shifting from the BSN position to the Polar Cap is dealt with in section 8. On the other hand, the scatter, e.g., in corresponding values of E_M displayed in Fig. 4d, should be borne in mind in direct comparisons of L1 satellite measurements with near-Earth observations such as the geomagnetic variations used to derive actual PC index values.

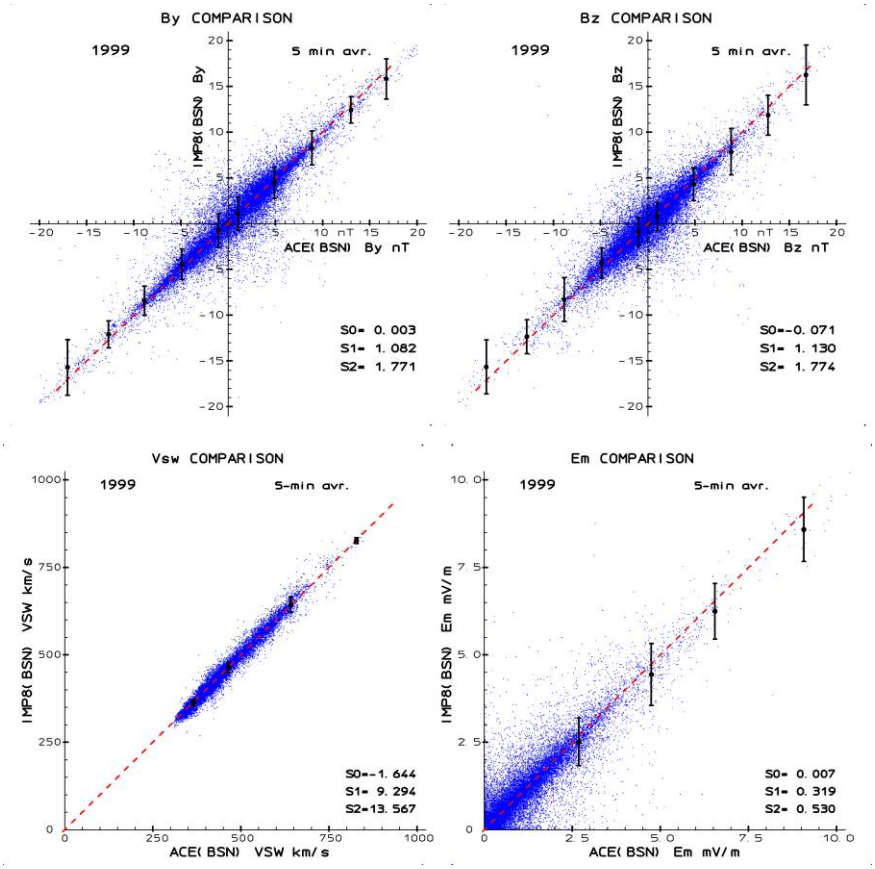

Figure 4. Comparison of ACE solar wind measurements, time-shifted from the ACE position at X_{GSE} around 240 R_E to the Bow Shock Nose (BSN) position at X_{GSE}~12 R_E in front of the Earth, with corresponding BSN-shifted IMP 8 measurements conducted at X_{GSE} positions between 0 and 40 R_E. The dashed lines indicate equality.

5. Thule and Vostok geomagnetic data.

The PCN index for the northern polar cap is based on data from the Danish geomagnetic observatory in Thule (Qaanaaq) in Greenland while the PCS index for the southern polar cap is based on data from the Russian geomagnetic observatory at Vostok in Antarctica. Important parameters at 100 km altitude are listed in Table 1 for the geodetic as well as the corrected geomagnetic coordinate system (Vitmo GSFC).

Table 1. PC geomagnetic observatories in the northern and southern polar caps. Epoch 2000

Station name	IAGA code	Geodetic Latitude	Geodetic Longitude	Corr. geomag. Latitude	Corr. geomag. Longitude	Solar Noon	MLT Noon
Qaanaaq	THL	77.48°	290.83°	85.29°	31.30°	16.61 UT	15.05 UT
Vostok	VOS	-78.46°	106.84°	-83.57°	54.80°	04.88 UT	13.02 UT

As mentioned in section 3.1., the geomagnetic variations to be used for the PC index need correction for the base level and for the quiet daily variation, QDC (cf. Eqs. 5a and 5b). The base level could be included in the QDC.

For the present derivation of PC index coefficients, the 1-min BL- and QDC-corrected geomagnetic data are converted into series of sorted 5-min and 15-min average values of the horizontal components, (ΔX,ΔY), in the geographic coordinate system. The choice of coordinate system was shown in *Stauning et al.* (2006) to have little effects on the derivation of PC index coefficients and values.

5.1. Base level for Thule.

For Thule geomagnetic data the base level is quite steady and free of level jumps. Hence it is convenient to address the base level issue and subtract the base level from the raw data before further processing is made. The base levels for the individual components are listed in the comments to the (obsolete) polar cap index, PCN2, provided by DTU Space at ftp://ftp.space.dtu/WDC/pcn and listed here in Table A1 in appendix A.

Over the years, the secular variations in the base levels are quite significant. The declination changes from 282.25° in 1973 to 308.40° in 2012, i.e., by 0.67° each year on the average. The X component changes by 44 nT and the Y component by 17 nT each year. However, from day to day the secular changes are much less than 1 nT. Hence, daily baseline values are quite adequate in determining the quiet levels for the present purpose (cf. section 15.1).

The yearly average *X* and *Y* component values through the international quiet days are very close to the quiet winter night level (QWNL) considering that these values refer to the start of the year while the year-means refer to the middle of the year. The year-mean quiet values could also be used for the baseline for our purposes. The yearly joint variations in QWNL and the year-mean *X* and *Y* baseline values are shown in Fig. 5. It is also evident that baseline values through the year can be derived by simple interpolation.

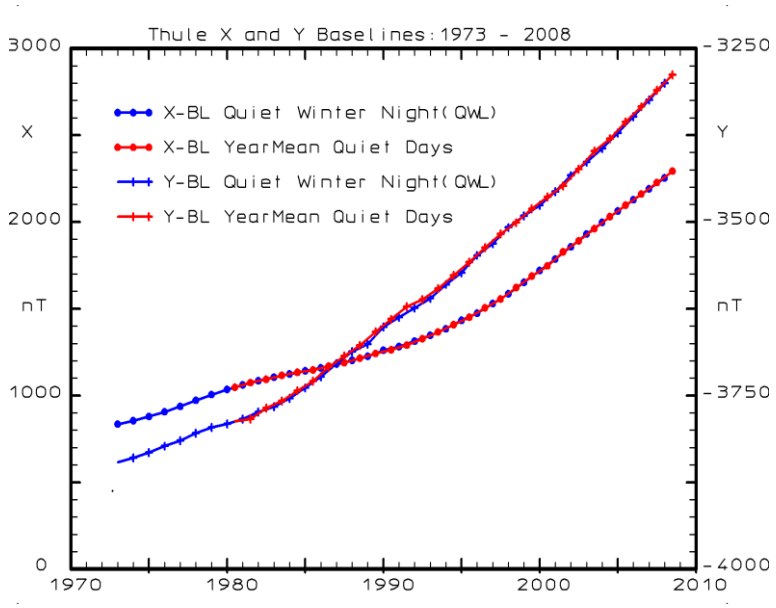

Fig. 5. Thule QWNL and Yearmean X and Y Baselines 1973-2008.

5.2 Baseline for Vostok.

For Vostok the baseline changes are less systematic. Hence, for the QL determination there is not so much gained in deriving these values separately. However, for illustration of the stability of the magnetometer the baseline values could still be useful. The baseline values shown in Table B1a in appendix B have been derived as the yearly averages of the component values during quiet conditions defined by the international classification of the 5 quietest days each month. It is recognized that the international quietest days are determined from midlatitude variabilities and that the conditions at polar latitudes could be different.

Actually, for Vostok the monthly baseline values are used here in the determination of QDC values. Like the yearly average component values these monthly averages are based on measurements during the international quiet days. These values are well suited to disclose possible baseline jumps related to the difficult observational conditions at Vostok and possible instrument replacements. A segment of such values are shown in Table 2 for the years 1994 and 1996. These years have been selected for the table

since there are lengthy disruptions and level jumps in the data caused either by the harsh climatic conditions in Antarctica or instrument replacements. The full set of monthly baseline values for 1997-2009 are listed in Table B1b in appendix B.

In Table 2 of monthly averages through quiet days one may note the jumps in level from just before to just after the breaks in the data series. Such cases require particular attention when forming QDCs.

Table 2. Vostok magnetometer. Monthly averages of component values during quiet days.

Year	Mn	X nT	Y nT	Z nT	Year	Mn	X nT	Y nT	Z nT
1994	1	-6659	-11591	-58486	1996	1	-7042	-11443	-58371
1994	2	-6658	-11577	-58507	1996	2	-7045	-11448	-58430
1994	3	0	0	0	1996	3	0	0	0
1994	4	0	0	0	1996	4	0	0	0
1994	5	0	0	0	1996	5	0	0	0
1994	6	0	0	0	1996	6	0	0	0
1994	7	0	0	0	1996	7	0	0	0
1994	8	0	0	0	1996	8	0	0	0
1994	9	0	0	0	1996	9	0	0	0
1994	10	0	0	0	1996	10	0	0	0
1994	11	0	0	0	1996	11	-6743	-11593	-58325
1994	12	-6988	-11408	-58378	1996	12	-6749	-11600	-58326

6. Quiet Daily Variations (the QDC)

The regular quiet day variation for any given day should be derived from segments of data recorded during quiet but otherwise similar conditions as those in effect on the day in question. Methods that may work at middle latitudes might not perform well at polar latitudes. Hence, special procedures are needed. Here, the "Solar Rotation Weighted" (SRW) procedure is used. The method is outlined in this section and further discussed in sec. 15.5. A detailed description is provided in *Stauning* (2011b).

6.1. Principles of the Solar Rotation Weighted (SRW) QDC method.

The QDC procedure applied here for the horizontal components of auroral or polar magnetometer recordings taking into account the recurrence properties of, among others, the varying sector structure, is based on weighting of contributions based on the following principles (*Stauning*, 2011b):

(i) *The data segments to build a QDC must be quiet with small variances in both components of the horizontal magnetic vectors (not just one component at a time).*

(ii) *The optimum interval for selecting data segments to define a QDC for any given day is within a few days around (and inclusive) the day in question where the season and, most likely, the sector structure, the average solar wind velocity, and the solar UV and X-ray fluxes are the same.*

(iii) *The second best intervals for the selection of quiet segments to the QDC are the days one solar rotation before and after the day in question. On these days the sector structure, the average solar wind velocities, and the solar UV and X-ray fluxes with good probability are close to the conditions on the day in question. Using the days one solar rotation before together with the days one solar rotation after the day in question compensates for the seasonal changes that are most pronounced around equinoxes.*

(iv) *Days, where the opposite face of the sun is directed toward the earth, should be avoided. On these days, most likely, the sector structure (the direction of IMF Bx) is opposite and the solar wind velocities*

as well as the UV and X-ray fluxes could be different from the conditions prevailing on the day in question.

(v) *The data processing functions and all QDC smoothing functions should be simple and reproducible such that independent calculations could be made to derive identical QDCs from the original data.*

These principles are implemented by constructing relevant weight functions, WF_{XX} , for each of the parameters (*XX*) of particular importance for the QDC, that is, the variance in the recorded data, the date difference, and the relative solar rotation phase. The product of these partial weight functions is then applied to hourly average values, (X_{OBS} , Y_{OBS}), of the recorded data through an interval extending from the days one and a half solar rotation period before the QDC day in question, through the QDC day, and including days one and a half solar rotation after the QDC day. Using the combined weight function, *WF*, the hourly (initial) QDC values are then determined by the superposition:

$$X_{QDC} = \Sigma\,(X_{OBS} \cdot WF) \,/\, \Sigma\, WF \quad \text{and} \quad Y_{QDC} = \Sigma(\, Y_{OBS} \cdot WF) \,/\, \Sigma\, WF \qquad (10)$$

The actual value of the weight factor sum, Σ *WF*, provides a measure of the QDC quality. Thus, high values indicate good quality (i.e. a QDC value based on quiet samples near the day in question). There is a potential for warning of poor QDC quality at low values of the weight function (i.e. QDC values based on somewhat disturbed samples away from the best or second best data intervals).

The QDC procedure and the application of the above criteria are explained more detailed in the next sections and in section 15.5. The parameters are defined and explained in *Stauning* (2011b). We use here 1-min samples of the horizontal field vector defined in a local geographic coordinate system with the X-component in the local North direction, the Y-component in East and the Z-component downward in the northern hemisphere, upward in the southern. The various functions and parameters used here are presented in sections 6.2 to 6.8. The scaling parameters and data intervals are defined in Table 3. The steps in the SRW QDC procedure are the following:

(i) Processing of basic data by subtraction of baselines, calculation of hourly means, and calculation of hourly values of variances for all hours of the QDC data base interval extending from -40 to + 40 days of the day in question.

(ii) Calculation of variance weight function values and look-up of tabular values (cf. Fig. 6) for the combined solar rotation and date distance weight function values for each hour of the data base interval.

(iii) Multiplication of all hourly mean component values by the related total weight function values.

(iv) Summation of all weighted hourly mean component values and (separately) all weight function values for each UT hour of the day. Division of the sum of weighted component values by the sum of weights to derive hourly initial values of the QDC.

(v) Smoothing of the initial values to derive final hourly QDC values for the day in question.

(vi) Interpolation of hourly QDC values to any desired sample rate (e.g., 1-min).

6.2. Basic data for QDC.

At the initial data processing step, the magnetic components are reduced by subtracting baseline (BL) values from the recorded (OBS) values. With recorded field components (X_{OBS},Y_{OBS},Z_{OBS}) and the slowly (secularly) varying baseline values (X_{BL}, Y_{BL}, Z_{BL}) the reduced magnetic component data (*x, y, z)* are then:

$$x = X_{OBS} - X_{BL} \quad y = Y_{OBS} - Y_{BL} \quad z = Z_{OBS} - Z_{BL} \quad \text{(e.g., 1-min samples)} \qquad (11)$$

In addition to removing the secular changes from the magnetic variations to be analyzed, this procedure also ensures that drift in instrument zero level as well as changes at possible replacements of measuring instruments have no effects on the QDC values. For a stable magnetometer the reductions are not strictly necessary but provide the benefit that the calculated QDCs now more directly represent the ionospheric conditions and may be judged and compared more easily. The sum of baseline and QDC values are termed “Quiet Level” (QL) values.

6.3. Data variability weight function.

With the baseline-reduced values the actual magnetic field components are examined to define intervals of particularly small variability. Two variance parameters are calculated. One is the maximum value of the time derivative of the 1-min samples of the horizontal field vector ***F*** through the QDC sample interval, *LSQ* (here 1 hr), i.e. the maximum change, δFt, in vector magnitude from one minute to the next:

$$\delta Ft(NHR) = max \{ \sqrt{((x(t) - x(t-1))^2 + (y(t) - y(t-1))^2)} \} \quad (12)$$

This parameter being a function of the hour, *NHR*, of the day provides an indication of the "smoothness" of the values recorded through the hour. The other parameter is the average variance in the horizontal field vector ***F*** through the sample interval, i.e.:

$$\delta Fv(NHR) = avr \{ \sqrt{(\delta x(t)^2 + \delta y(t)^2)} \} \quad (13)$$

where $\delta x(t) = x(t) - x_M(NHR)$ and $\delta y(t) = y(t) - y_M(NHR)$ are the deviations from the mean values, $x_M(NHR)$, $y_M(NHR)$. This parameter provides an indication of the slope of the values recorded through the hour.

For each QDC sample interval (1 hr) the average component values and the variances are calculated and a weight function related to the "normalized" variances is defined as shown below:

$$WF_{VV} = exp- \{(\delta Ft/RTL)^{WP} + (\delta Fv/RVL)^{WP}\} \quad (14)$$

where the normalized variances are raised to the power *WP*. The variance normalization constants, *RTL* and *RVL* and the power exponent value, *WP*, (cf. Table 3) determine in the averaging process the weight given to magnetic field values with small variances (i.e., smooth recordings with small slopes) relative to those of larger variances.

6.4. Date difference weight function.

Ideally, the contributions to the superposition of quiet data segments should come from dates, *DD*, within a few days around the QDC date, *D0*, in question. Due to the frequent occurrences of lengthy intervals of magnetic disturbances it may not always be possible to construct a QDC based solely on data from nearby dates. Instead, a Gaussian weight function with a half width scale parameter *RDD* is defined in order to give higher weight to nearby days and corresponding lesser weight to days separated more from the QDC day.

$$WF_{DD} = exp\{- (DD-D0)^2/RDD^2 \} \quad (15)$$

6.5. Solar rotation weight function.

There is general agreement that the QDC values shall reflect the 11-year solar activity cycle. However, the question remains whether the QDC shall vary with the varying UV- and X-ray fluxes emitted from the different sides of the rotating Sun facing the Earth, with persistent variations in the solar wind velocity, and with the varying solar wind sector structure experienced during the varying phases of the solar 27 days average rotational period (*LSR*). It is, of course, not possible to provide complete account for such changes but the stronger and longer-lasting variations could be included in the calculations of a varying QDC.

The simplest way to accomplish an integration of such variations in the QDCs is to include a weighting with solar rotation phase in the superposition of quiet intervals. The weighting factor used here is:

$$WF_{SR} = \cos^2(\pi \cdot XDD/LSR) \quad (16)$$

where $XDD = abs\{DD-D0\}$ is the deviation in days from the actual day. This factor has a maximum (=1) when at *LSR*=27 days interval, the same side of the Sun is facing the Earth and a minimum (=0) when the opposite side is facing Earth. In the procedure described here, the collection of quiet intervals to form the QDC is extended over a range from *LDD* (here 40 days) before to *LDD* days after the day in question.

The display in Fig. 6. presents graphically the combined solar rotation and date difference weight function, WF_{DR}:

$$WF_{DR} = WF_{SR} \cdot WF_{DD} = \cos^2(\pi \cdot XDD/LSR) \cdot \exp(-XDD^2/RDD^2) \quad (17)$$

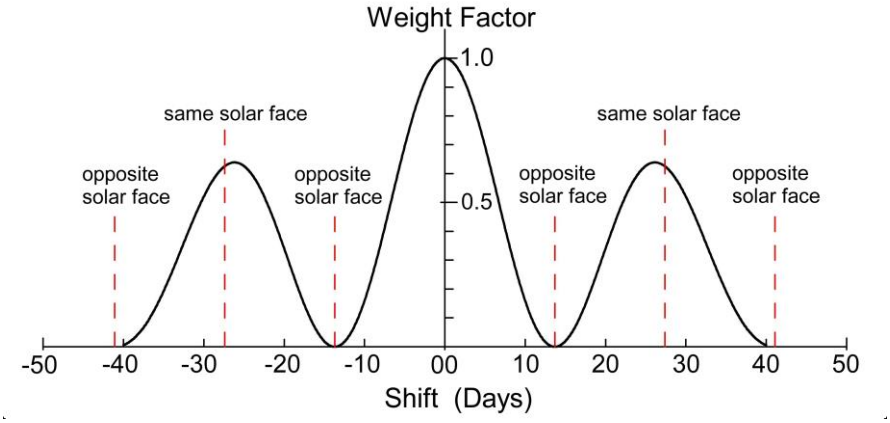

Fig. 6. Combined date-difference and solar rotation weight factor (*Stauning*, 2011b).

The longer dashed lines in Fig. 6 mark the dates where the Sun has the same face turned towards the Earth as on the day in question. The shorter dashed lines mark dates with the opposite side of the Sun facing the Earth. The total weight of the main lobe around *XDD*=0 and the total weight of each of the side lobes one solar rotation earlier or later can be adjusted by the selection of the parameter *RDD*. It should be noted that the solar rotation weight factor as well as the date separation weight factor can be calculated and tabulated in advance.

6.6. Calculation of initial QDC hourly values.

The QDC values are then composed from the hourly segments available within a span of *LDD* days to either side of the day in question. Each segment is weighted with the combined weight factor, $WF_{VDR} = WF_{VV} \cdot WF_{DD} \cdot WF_{SR} = WF_{VV} \cdot WF_{DR}$. Thus the quiet intervals closest to the day in question count most while quiet intervals one solar rotation apart are also included but count less. Quiet intervals on days, where the opposite side of the Sun faces the Earth, are neglected. Thus, for UT hour *NHR*, the resulting (non-smoothed, NS) initial QDC hourly values, $X_{QDC}(NHR)_{NS}$, and $Y_{QDC}(NHR)_{NS}$, are then:

$$X_{QDC}(NHR)_{NS} = \Sigma\,(X_M\,(NHR) \cdot WF_{VDR})\,/\,\Sigma\,WF_{VDR} \quad (18a)$$

$$Y_{QDC}(NHR)_{NS} = \Sigma\,(Y_M\,(NHR) \cdot WF_{VDR})\,/\,\Sigma\,WF_{VDR} \quad (18b)$$

where the summation is extended over all valid hourly average values of the magnetic variation data for this UT hour within the interval from – to + *LDD* days of the day in question. The sum of weight function values, $\Sigma\,WF_{VDR}$, is a QDC quality parameter.

6.7. Smoothing of QDC hourly values.

In order to approach the ideal quiet day variation (see section 15.5) and, furthermore, enhance the systematic variations and suppress excursions related to singular events, the QDC values are finally smoothed with respect to the UT hour of the day. The smoothing is done by averaging over a series of consecutive hours around the selected UT hour, *NHR0*, using a Gaussian weight function:

$$WF_{HR} = exp\{ - (XHR - NHR0)^2/RHR^2 \} \quad (19)$$

Hence, the final QDC values are:

$$X_{QDC}(NHR0) = \Sigma\,(X_{QDC}\,(NHR)_{NS} \cdot WF_{HR})\,/\,\Sigma\,WF_{HR} \quad (20a)$$

$$Y_{QDC}(NHR0) = \Sigma\,(Y_{QDC}\,(NHR)_{NS} \cdot WF_{HR}\,/\,\Sigma\,WF_{HR} \quad (20b)$$

where *NHR* is the variable UT hour while *RHR* is the half width of the Gaussian weight function for the time-of-day. The summations involved in the averaging are extended from – to + *LHR* hours, where the interval parameter, *LHR*, is set to twice the width of the weight function scale parameter (*RHR*).

6.8. Conversion of QDC hourly values to 5- or 1-min values.

The above procedure has been used to calculate for each day a QDC comprising hourly values that refer to the middle of the hour. Thus, for example, $X_{QDC}(00)$ refers to the midpoint of the interval from 00 to 01 UT. Here, to give smooth variations, the hourly values are converted to 1-min QDC values by using quadratic interpolation. The interpolation requires that a parabola of interpolated values between two mid-hourly reference points agree with these hourly values, and that its continuations have least squares deviation from the preceding and the following hourly values. For the interpolation to work at the beginning and the end of the day, the hourly QDC values are extended in both ends by using values from the preceding and the following day.

The formula used for the interpolation is:

$$X_{QDC}(NHR+DHR) = X_{QDC}(NHR) + AQ \cdot DHR^2 + BQ \cdot DHR \qquad (21)$$

where *NHR* is the hour, *DHR* is the deviation (in decimal hours) from the middle of the hour, while the constants *AQ* and *BQ* valid for the interval between *NHR-1* and *NHR*, i.e., *DHR* = -1 to 0 hours , are:

$$AQ=0.25\cdot(X_{QDC}(NHR-2) - X_{QDC}(NHR-1) - X_{QDC}(NHR) + X_{QDC}(NHR+1)) \qquad (22a)$$

$$BQ=0.25\cdot(X_{QDC}(NHR-2) - 5\cdot X_{QDC}(NHR-1) + 3\cdot X_{QDC}(NHR) + X_{QDC}(NHR+1)) \qquad (22b)$$

The parabolic interpolation has been chosen instead of more sophisticated interpolation schemes, like the Cubic Spline, for its robustness to odd data and data gaps. The parabolic interpolation scheme provides a continuous QDC during almost all conditions albeit not quite as smooth as that delivered by Cubic Spline interpolation when conditions are best.

6.9. Summary.

The parameters used in the QDC procedure are listed in Table 3.

Table 3. QDC weight function parameters and integration intervals (*Stauning*, 2011b).

Parameter	Symbol	Value
Interval of QDC summation	*LDD*	40 days
Data sample interval	*LDI*	1 minute
Interval of variability calculations	*LSD*	1 hr (=*LSQ*)
Variability exponent parameter	*WP*	2
Variability time derivative const.	*RTL*	6 nT
Variability variation norm. const.	*RVL*	12 nT
Date difference norm. const.	*RDD*	40 days
Solar rotation recurrence period	*LSR*	27 days
QDC sample interval	*LSQ*	1 hr
QDC smoothing interval	*LHR*	8 hours
QDC smoothing norm. const.	*RHR*	4 hours

With these parameters, the combined weight factor for the initial QDC is:

$$WF_{TOT} = exp- \{(\delta Ft/6)^2 + (\delta Fv/12)^2 + (\Delta D/40)^2\} \cdot \cos^2(\pi \cdot \Delta D/27) \qquad (23)$$

where δFt is the hourly max time derivative and δFv the hourly variance in nT for the horizontal disturbance vector, $\boldsymbol{F}$. ΔD is the numerical value of the date difference in days. The weight factor is calculated for each hour through an interval of ±40 days around the day in question. For each hour of the day, all hourly average component values for that hour are multiplied by the weight factor (same for both horizontal components) and added. The sum of these products is divided by the sum of weight factors to give the unsmoothed hourly QDC value for each component for the day in question (cf. Eqs. 4a and 4b).

Finally, the hourly QDC values are Gaussian smoothed over time of day by using the weight function:

$$WF_{SMOOTH} = exp\text{-}\{(\Delta Hr/4)^2\} \qquad (24)$$

where ΔHr is the time difference in hours from the hour in question. All QDC samples within ±8 hours are multiplied by the weight factor, added, and divided by the sum of weight factors to provide the final hourly QDC values. QDC values in finer resolutions are produced by parabolic interpolation.

7. Examples of the use of the SRW procedure to derive QDC for Thule

In order to demonstrate the QDC procedure, magnetic data from Thule are used in the examples. The recorded data from Thule are 1-min samples of absolute field vector value either in WDC (World Data Center) format or in BIN (Intermagnet) format, which is now the standard format. The data are available via Intermagnet (http://www.intermagnet.org).

7.1 QDC integration and weight function parameters.

The integration and weight function parameters used in the examples are all displayed in Table 3. These parameters in combination with standard functions (cosine and exp.) found on every computer define completely the processing of data samples to derive QDC values. The parameters are invariant to the coordinate system (X,Y or H,D) used for the horizontal components. Hence, it is quite straight-forward to make programs in any programming language to recalculate or verify the QDC values from the original data.

7.2. Baseline reduction.

For convenience, the baseline geomagnetic field intensities are subtracted. For Thule the baseline geomagnetic field components are estimated every year referring to 1 January (northern winter). This quiet winter night (QWNL) data set forms the table spanning the years 1973 to 2012 shown in Table A1 in appendix A. For Thule the secular variations are steady enough (see Fig. 5) to make linear interpolation in-between years and extrapolation beyond latest yearly QWNL values quite adequate. Now, for every day of the year the actual baseline values, X_{BL}, Y_{BL}, Z_{BL} to be used in Eq. 5 are derived by linear interpolation between the values defined at 1 January in the present year and those from 1 January in the next year.

7.3. Data variability.

As an example, the hourly variability parameters (δFt, δFv), derived by using Eqs. 12 and 13, are listed in Table 4 along with the hourly means (x_{HR},y_{HR},z_{HR}) of the reduced field components for Thule for the first day of the year 2002. Since the total variation over a quiet day is typically sinusoidal-like with amplitudes in both components on the order of 30 - 100 nT then the "quiet" derivative, δFt (in 1 min), would be less than 1 nT , and the "quiet" hourly variance, δFv, would typically be less than 5 nT. Actual values beyond these are indicative of magnetic disturbances. The QDC results for this day and for July 1, 2002, are presented in Table 5.

Table 4. Example hourly averages of Thule magnetic field components (x_{HR}, y_{HR}, z_{HR}) with baselines subtracted, and variances (δFt, δFv) for 1 January 2002.

Year	Mth	Day	Hr	x_{HR}	y_{HR}	z_{HR}	δFt	δFv
2002	1	1	0	-23	-25	1	4.2	11.1
2002	1	1	1	-15	-24	4	5.1	10.2
2002	1	1	2	-15	-50	2	4.5	8.4
2002	1	1	3	-4	-55	7	6.0	10.0
2002	1	1	4	14	-36	16	4.2	8.9
2002	1	1	5	41	-13	19	6.1	10.1
2002	1	1	6	39	-18	18	7.1	10.5
2002	1	1	7	51	-10	21	8.2	16.2
2002	1	1	8	25	-2	32	5.4	10.9
2002	1	1	9	21	11	25	4.5	4.3
2002	1	1	10	29	33	26	8.0	13.9
2002	1	1	11	13	55	24	5.8	9.4
2002	1	1	12	5	63	25	7.1	13.8
2002	1	1	13	-7	46	14	7.6	8.5
2002	1	1	14	-10	9	14	8.5	9.0
2002	1	1	15	-8	-7	13	6.1	8.2
2002	1	1	16	-36	18	-3	8.6	15.3
2002	1	1	17	-53	30	-14	5.1	9.6
2002	1	1	18	-72	21	-2	3.6	15.3
2002	1	1	19	-53	20	14	5.1	11.0
2002	1	1	20	-33	14	13	5.1	6.0
2002	1	1	21	-29	4	11	3.2	10.1
2002	1	1	22	-26	-8	9	3.6	11.7
2002	1	1	23	-37	-22	13	3.6	10.4

7.4. Example QDC calculation for Thule.

When the data variability values have been calculated (like shown in Table 4) then the hourly variability weight function values can be calculated. The date deviation and solar rotation weight functions are derived from the tabulated values (cf. Fig. 6) depending only on the deviation (in days) between the QDC day in question and the day of the hourly sample to be used in the construction of an initial QDC. The QDC values are smoothed and stored as sets of hourly values, for instance, through each day of the year. Segments of final hourly QDC data and weight function sums ($\Sigma\ WF_{VDR}$) referring to the 1st of January and 1st July 2002, respectively, are displayed in Table 5. The baseline values of the *X* and *Y* components are shown by the values listed at hour 24 for each day such that the absolute QL values can also be derived from the table by adding for each hour the daily baseline value to the relative hourly QDC values listed for each of the two components.

In Table 5 note the daily variations in the hourly X_{QDC} and Y_{QDC} components displayed within each section and the seasonal variations seen in the differences in amplitudes between the two sections that represent winter and summer conditions, respectively. The weight function sums in the last columns also display daily and seasonal variations having minima at the middle of the day (around 16 hrs UT) and in the summer season, where the variability in the data is largest.

Table 5. Thule QDC hourly values (X_{QDC}, Y_{QDC}) in nT and sum of weight function values (SWF) at 00 to 23 Hr (UT). Daily baseline values (X_{BL},Y_{BL}) at Hr=24. Dates: 1 January and 1 July 2002, 00-24 UT.

Year	Mth	Day	Hr	X_{QDC}	Y_{QDC}	*SWF*	Year	Mth	Day	Hr	X_{QDC}	Y_{QDC}	*SWF*
2002	1	1	0	-11	-14	15.64	2002	7	1	0	-14	-28	3.71
2002	1	1	1	-8	-15	15.24	2002	7	1	1	-4	-32	4.16
2002	1	1	2	-4	-13	16.52	2002	7	1	2	6	-33	4.49
2002	1	1	3	-1	-11	17.70	2002	7	1	3	16	-31	6.31
2002	1	1	4	2	-9	19.28	2002	7	1	4	26	-28	7.07
2002	1	1	5	4	-5	17.82	2002	7	1	5	34	-21	5.65
2002	1	1	6	6	-1	18.41	2002	7	1	6	41	-13	6.05
2002	1	1	7	6	2	17.32	2002	7	1	7	47	-3	5.91
2002	1	1	8	5	6	16.91	2002	7	1	8	51	8	5.23
2002	1	1	9	3	9	14.75	2002	7	1	9	53	18	3.09
2002	1	1	10	0	12	11.58	2002	7	1	10	51	27	2.70
2002	1	1	11	-3	14	9.94	2002	7	1	11	47	35	0.70
2002	1	1	12	-7	15	8.22	2002	7	1	12	37	40	0.70
2002	1	1	13	-12	15	8.83	2002	7	1	13	24	44	0.16
2002	1	1	14	-16	14	7.72	2002	7	1	14	8	44	0.73
2002	1	1	15	-19	12	8.31	2002	7	1	15	-8	42	0.23
2002	1	1	16	-22	10	9.92	2002	7	1	16	-23	37	0.20
2002	1	1	17	-24	7	9.58	2002	7	1	17	-35	30	0.96
2002	1	1	18	-25	3	10.70	2002	7	1	18	-42	21	1.03
2002	1	1	19	-25	-1	12.73	2002	7	1	19	-45	11	1.53
2002	1	1	20	-24	-5	14.12	2002	7	1	20	-44	1	0.92
2002	1	1	21	-22	-8	14.05	2002	7	1	21	-39	-8	2.31
2002	1	1	22	-19	-11	14.61	2002	7	1	22	-32	-16	2.61
2002	1	1	23	-15	-13	15.32	2002	7	1	23	-24	-23	4.43
2002	1	1	24	1857	-3433		2002	7	1	24	1893	-3424	

The QDC values for the extraordinarily low weight sum values spotted in Table 5 at around 13 and 15-16 hours UT on 1 July, 2002, represent "worst cases" and might be given extra attention in anticipation of stronger fluctuations than normal due to the sparse amount of quiet samples (cf. Fig. 7b). However, the smoothing process, probably, has evened out possible odd excursions since nothing abnormal is seen in the QDCs for this day in the displays in Figs. 7, 8, and 9.

The relations between the recorded data and the calculated QDC values are displayed in diagrams that present the original raw Thule data (corrected for the base level) in thin line and the QDC levels derived from the above outlined calculations in heavy line. Some examples are shown in Fig. 7 for January and July 2002. This year, 2002, is a solar maximum year. In these diagrams the recorded *X*-component data (with baseline subtracted) are displayed against UT hour of the day for the 5 quietest (QQ) days of the month. The QDCs for the middle of the month (in full line), for the 1st (in dashed line), and for the 30th (in dotted line) have been superposed. The top panel displays the X-component data for January 2002 while the bottom panels display the X-component data for July 2002. Note, particularly in the bottom panel, how the QDC changes gradually through the month.

a.

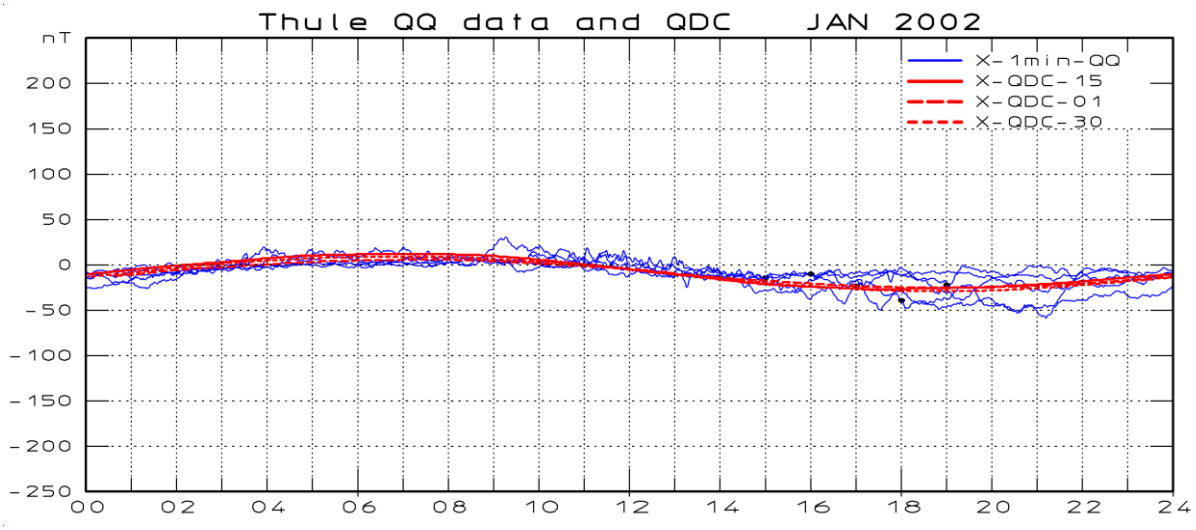

b.

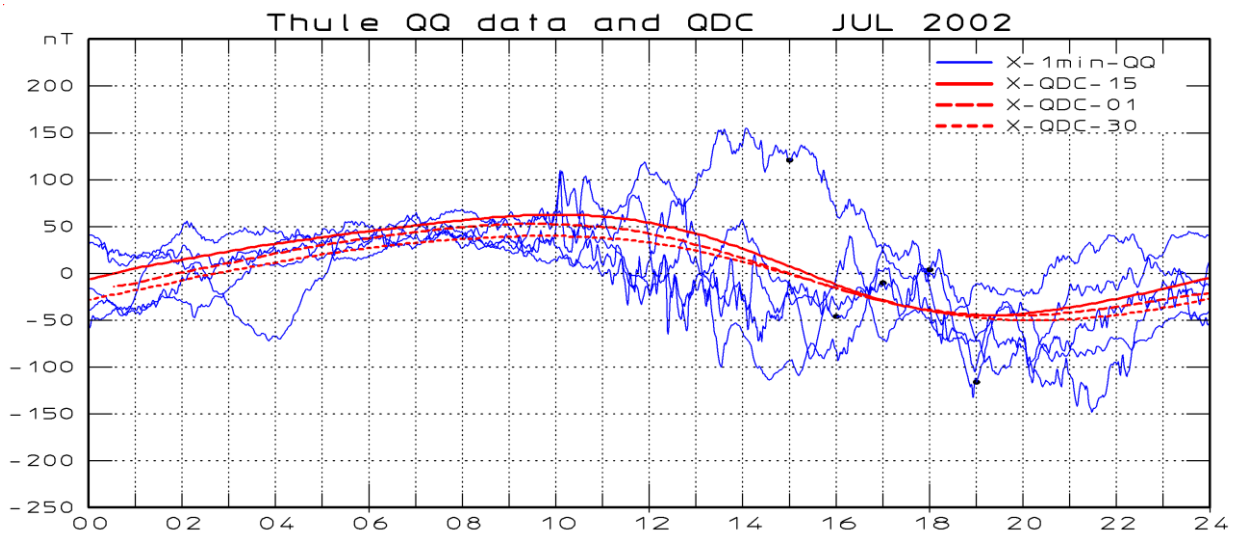

Figure 7. Recorded values (thin, blue line) from the five international quietest (QQ) days of January (top panel) and July (lower panels). Dates are noted at the curves. The QDCs derived by the Solar Rotation Weighted (SRW) minimum variance method for the 15th day of the months are displayed in heavy red line.The QDCs for the 1st and 30th are shown in dashed and dotted lines.

Further diagrams are shown in Figs. 8 and 9 for solar quiet (1996) and active (2002) years, respectively. Note in these examples, particularly for July 2002 in Fig. 8, that the QDC values not only display daily sinusoidal-like variations but also indicate changing levels (in mid-July slightly higher X_{QDC} and lower Y_{QDC} level) and changing ratio between the X_{QDC} and Y_{QDC} amplitudes as a consequence mainly of solar wind sector variations in IMF B_Y .

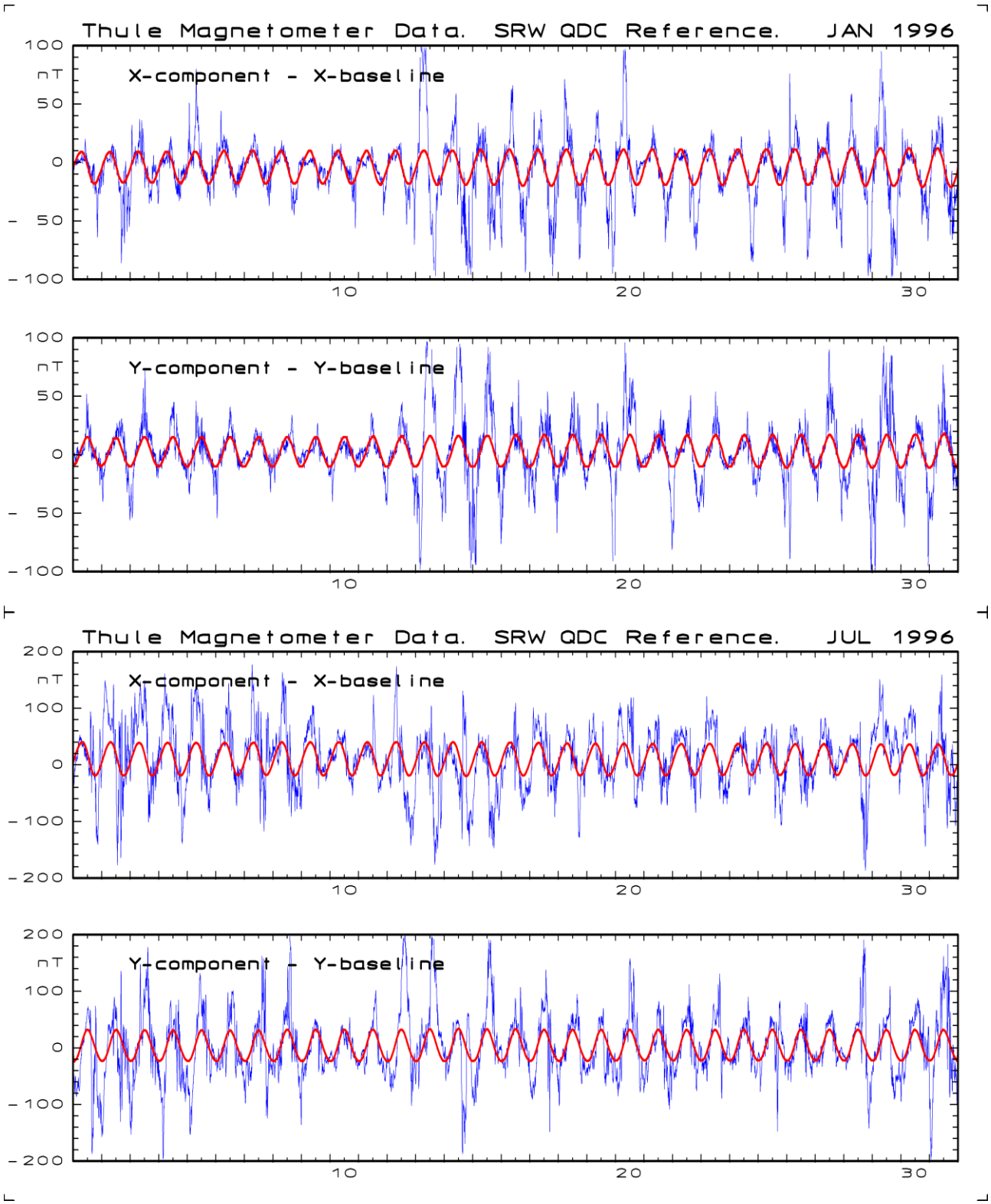

Figure 8. Thule raw magnetometer data corrected for the secularly varying base level (thin blue line), and the QDC values (heavy red line) calculated by using the solar rotation weighted (SRW) minimum variance method. Data for January (minimum QDC variation) and July (maximum QDC variation) are presented. Note the different amplitude scales for January and July. This year, 1996, is a solar minimum year.

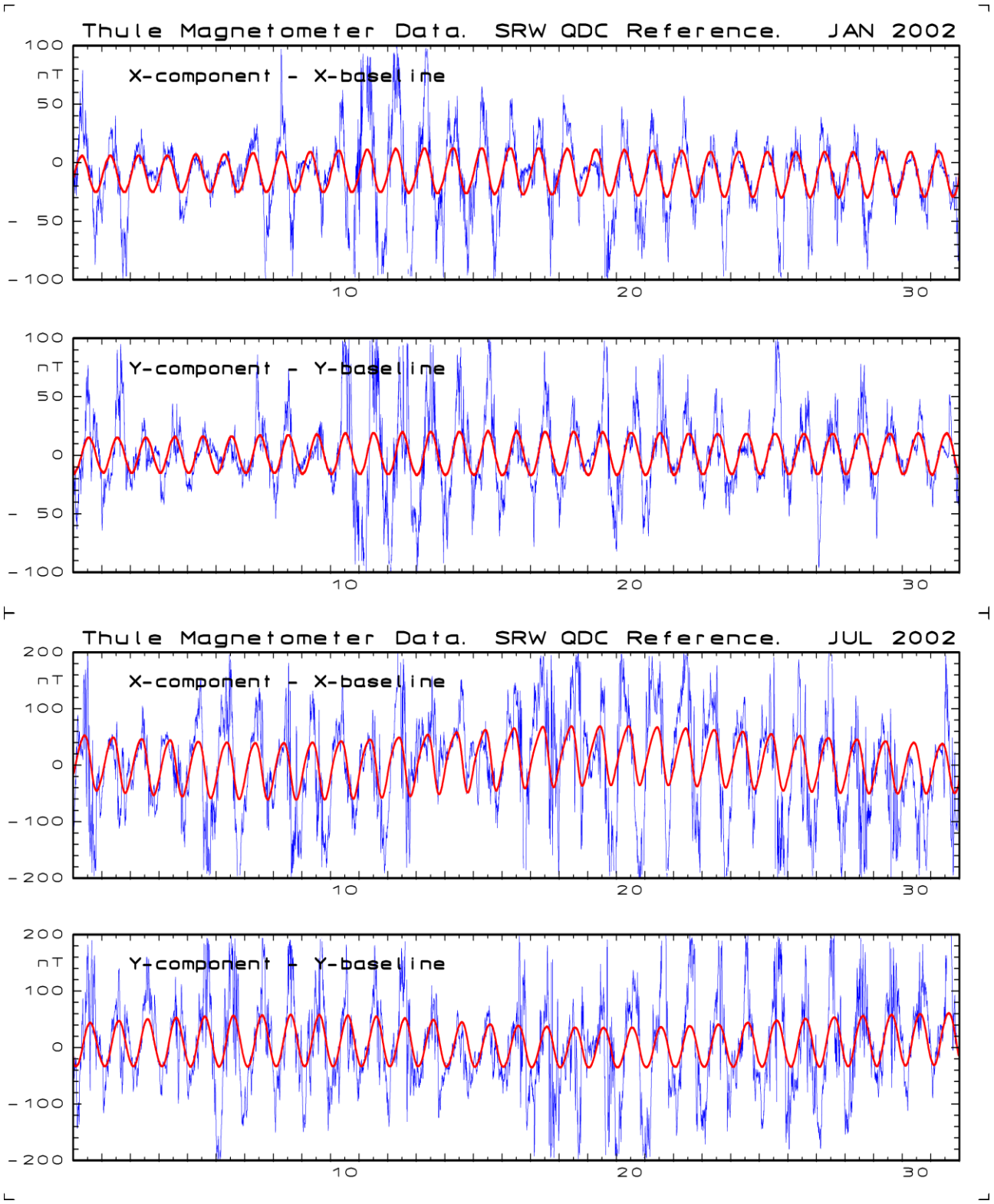

Figure 9. Thule raw magnetometer data corrected for the secularly varying base level (thin blue line), and the QDC values (heavy red line) calculated by using the solar rotation weighted (SRW) minimum variance method. Data for January (minimum QDC variation) and July (maximum QDC variation) are presented. Note the different amplitude scales for January and July. This year, 2002, is a solar maximum year.

7.5. Overview of QDCs through one year. On-line real-time QDC calculations.

The above outlined automated solar rotation weighted (SRW) minimum variance method has been used to calculate QDC data sets through all intervals with available Thule and Vostok digital data. The diagram displayed in the top panel of Fig. 10 is intended to provide an overview of the resulting QDCs for the *X*-component for Thule through one year (2002). The vertical axis has a scale for the QDC values. The horizontal axis is divided into 12 monthly fields. For each monthly field there is a scale for the UT hour (00-24) of the day and all the *X*-component QDCs for that month have been plotted on top of each other within the narrow field. The QDCs for the first, the middle, and the end day of the month are plotted in different colours. The QDCs for the other days are plotted in thin blue line. For neighbouring fields the QDC for the first day should be close to the QDC for the last day of the foregoing month.

The diagram provides an overview of the seasonal variations in the QDC amplitudes as well as an illustration of the irregular variations associated, for instance, with the changing sector structure. Furthermore, it is fairly simple to spot strange QDC data sets that could incur if invalid data had slipped into the data base or if the variance parameters were set too tight such that the QDC was built on few singular data segments.

A further application of the outlined SRW QDC technique could be to produce immediate QDCs to be used, for instance, for on-line calculations and presentations of actual PC index values. For such applications only half the data base (data through -40 to 0 days) is available for QDC calculations. However, the procedure could be operated with the same program and parameters as usual since days without data (those following the QDC day in question) are automatically omitted in the summations of weighted contributions. The middle panel in Fig. 10 displays an overview of the results of such QDC calculations over half the range (HSRW). Due to the reduced data basis, the derived QDCs now have larger spreads.

The bottom panel in Fig. 10 displays, still for the *X*-component, the differences between the normal (SRW) QDC values and the "on-line real-time" (HSRW) QDC values calculated from the reduced data base of days prior to the day in question. The differences are largest around equinoxes due to the lack of compensation of seasonal effects. Part of the differences seen in August relate to solar sector effects. As noted in the diagram, the average difference is 0.35 nT and the RMS difference is 4.45 nT. The peak differences are less than 10 nT in winter and 20 nT in equinox and summer seasons. The year in question (2002) is a solar maximum year. Hence, the differences shown here are maximum values through the solar cycle.

Fig. 11 displays for the *Y*-component the corresponding yearly summary plots through 2002 of the normal (SRW) QDC values in the upper field and the HRSW QDC values in the middle field, while the differences between the two sets of QDC values are plotted in the bottom field.

The differences (nearly the same in QDC *X*- and *Y*-components) would give RMS errors in the PC indices on the order of 0.2 units (mV/m) compared to values calculated by using QDC data derived from the full data basis and less than 0.5 mV/m in worst case peak differences.

To convey a proper perspective of these differences, PC index values below 2 signal quiet conditions, values between 2 and 5 predict moderately disturbed conditions, while values above 5 units indicate strong magnetic disturbances (e.g., *Troshichev et al*., 2006; *Stauning, 2007*; *Stauning et al*., 2008), (cf. also section 15.1). With the small RMS and peak errors (0.2 and 0.5 mV/m), the HRSW procedure is indeed well suited to deliver immediate QDC values for on-line, real-time space weather forecast applications. As time goes on the QDCs could be re-calculated with gradually enhanced precision up to the day, 40 days later, where final QDC values may be calculated (on the provision that the basic magnetic data are final values then).

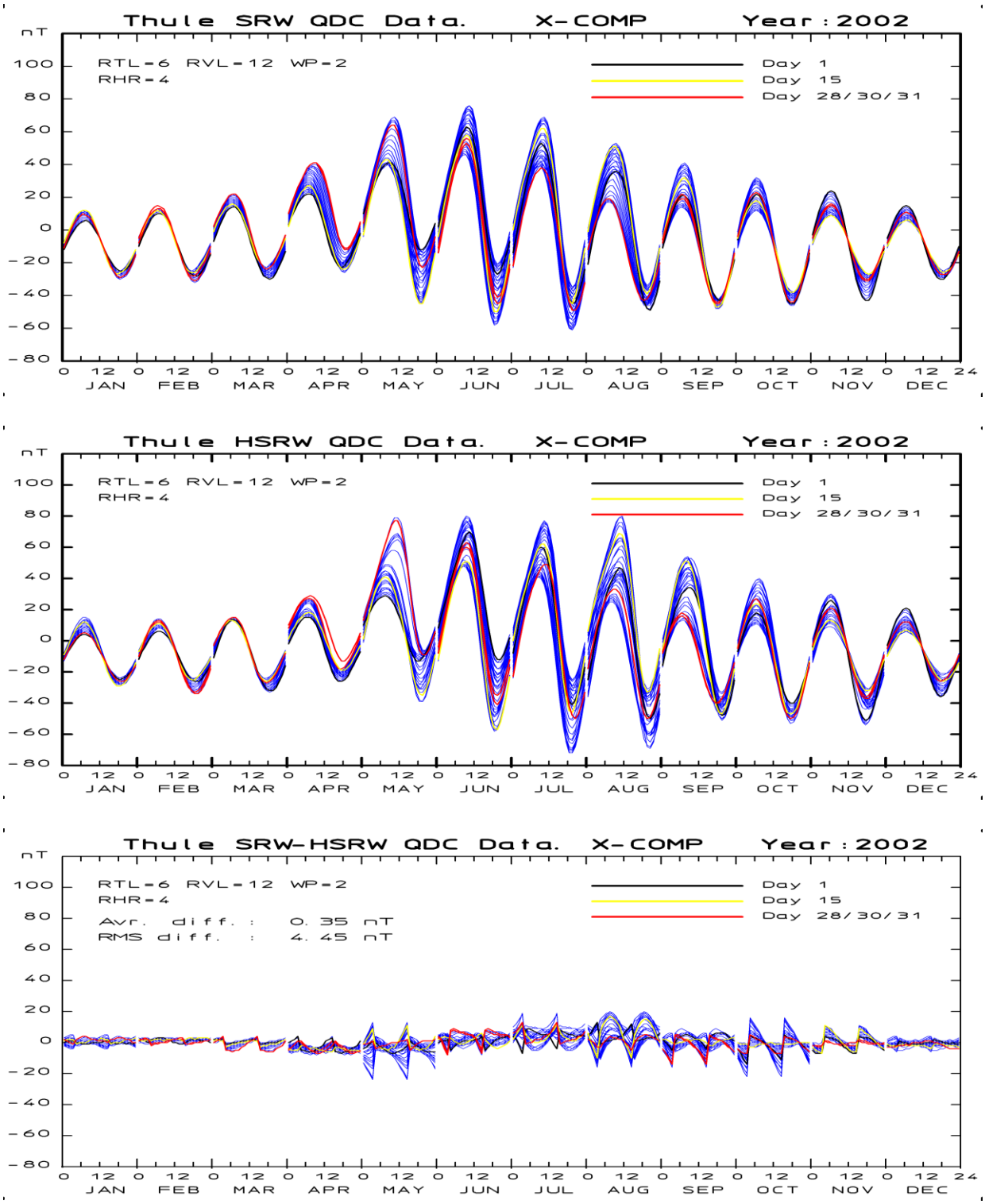

Figure 10. QDCs for *X*-component. Top: Full Solar rotation (through - to + 40 days) weighted (SRW) minimum variance hourly QDC values through 2002. There is a scale for the UT hour (00-24) in each monthly section. QDCs for start, middle, and end days of the months are plotted in different colours. The QDCs for the other days are plotted in thin blue line. Middle: Half Solar rotation (through -40 to 0 days) weighted (HSRW) QDCs. Bottom: Differences between SRW and HSRW QDCs. Average (0.35 nT) and RMS (4.45 nT) differences are noted on the figure.

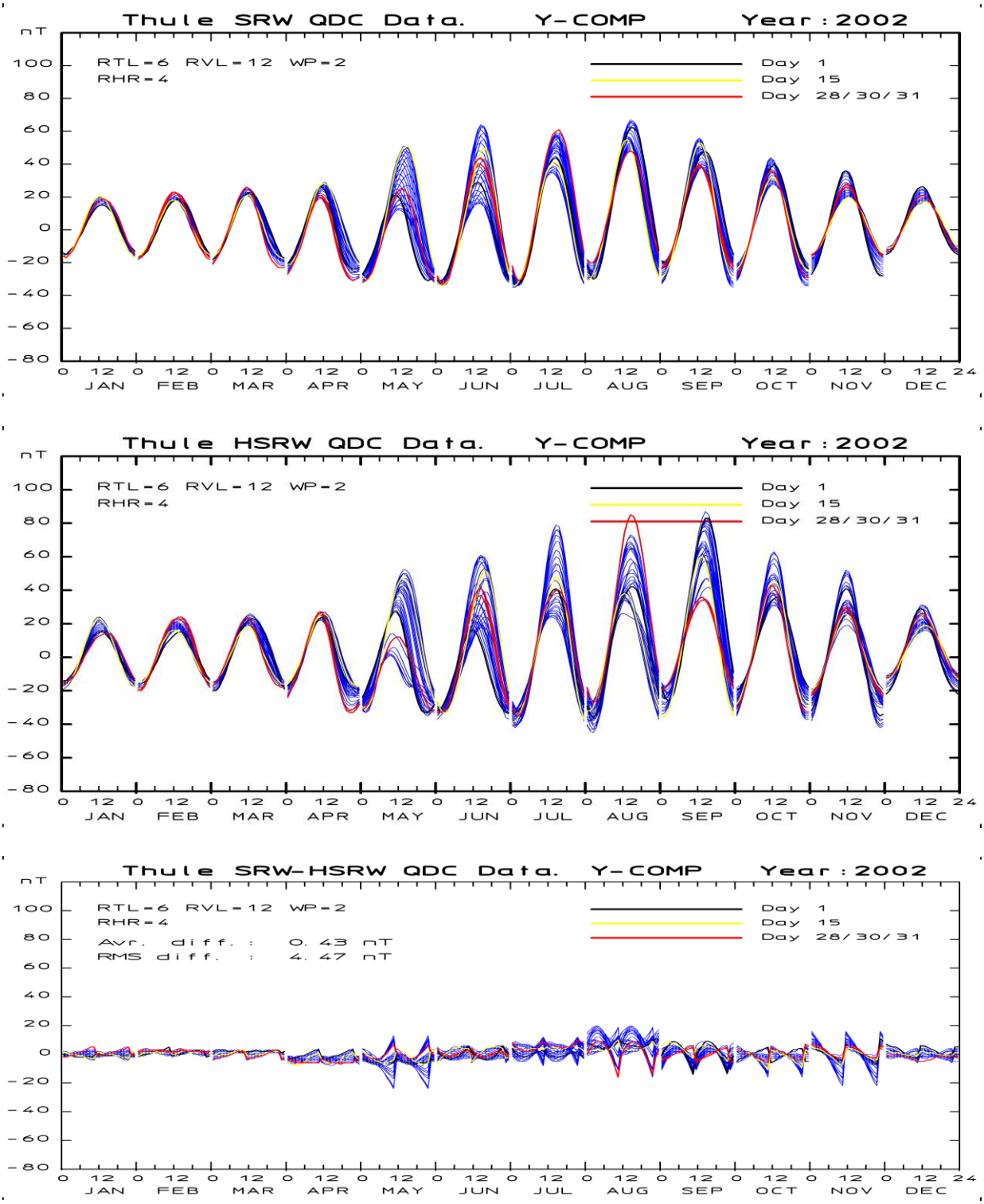

Figure 11. QDCs for *Y*-component. Top: Full Solar rotation (through - to + 40 days) weighted (SRW) minimum variance hourly QDC values through 2002. There is a scale for the UT hour (00-24) in each monthly section. QDCs for start, middle, and end days of the months are plotted in different colours. The QDCs for the other days are plotted in thin blue line. Middle: Half Solar rotation (through -40 to 0 days) weighted (HSRW) QDCs. Bottom: Differences between SRW and HSRW QDCs. Average (0.43 nT) and RMS (4.47 nT) differences are noted on the figure.

8. Optimum direction angle calculations for Thule

Searching for a proxy based on polar magnetic disturbances to represent the solar wind "Merging Electric Field" (E_M = MEF = V_{SW} B_T $sin^2(\theta/2)$), the correlation between the horizontal disturbance vector $\Delta\boldsymbol{F}$ (corrected for the quiet daily variations) and the MEF could be maximized by projecting $\Delta\boldsymbol{F}$ to a specific direction, "the optimum direction". This direction is not fixed in space but varies slowly with local time and season.

8.1. Definition of the optimum direction angle.

To estimate the optimum direction the horizontal magnetic vector is resolved in an X-component (northward in a rotating geographical coordinate system) and a Y-component (eastward). The vertical Z-component is downward in the northern polar cap. For the horizontal components, as stated in the summary (Eq. 5), we first subtract from the raw data the baseline values and then subtract QDC values:

$$\Delta X = (X_{RAW} - X_{BL}) - X_{QDC} \quad (25a)$$

$$\Delta Y = (Y_{RAW} - Y_{BL}) - Y_{QDC} \quad (25b)$$

here, X_{BL} is the baseline value for the X-component defined yearly (every 1 January) and now adjusted to the actual day-of-year. X_{QDC} is the reference QDC level provided as a table of hourly values for each day of the year and now adjusted to the proper day and time-of-day. The Y-component is handled correspondingly.

For Thule, the projection of the disturbance vector $\Delta\boldsymbol{F}$ to the optimum direction is given through:

$$\Delta F_{PROJ} = \Delta X \cdot cos\,(U_{PROJ}) + \Delta Y \cdot sin(U_{PROJ}) \quad (26)$$

where U_{PROJ} (counted anticlockwise) is the angle between the X-component axis and the optimum direction. This angle varies with local time, $LThr$ (LT in hours), according to:

$$U_{PROJ} = U_0 + LThr \cdot 15^o \quad (27)$$

In order to explain the projection angles the diagram in Fig. 12 displays the northern polar region in geographical latitude (latitude circles every 5^O from 75^O to the pole) and local time (LT). For Thule the geographic coordinates are θ= 77.47N, λ = 290.77^OE. The varying position of Thule through a day has been marked in the diagram by a latitude circle with tics every LT hour.

The red arrow indicates the average equivalent DP2 current direction. The optimum direction is the direction of the magnetic variations, $\Delta\boldsymbol{F}$, generated by the equivalent DP2 currents that, in turn, relate to the merging electric field, E_M.

The position of Thule at local midnight, 00 LT, (04:37 UT), and at 06, 12 and 18 LT are indicated by the plots of axes of the local (X,Y) coordinate system and the magnetic variation vector $\Delta\boldsymbol{F}$ shifted to the observatory position.

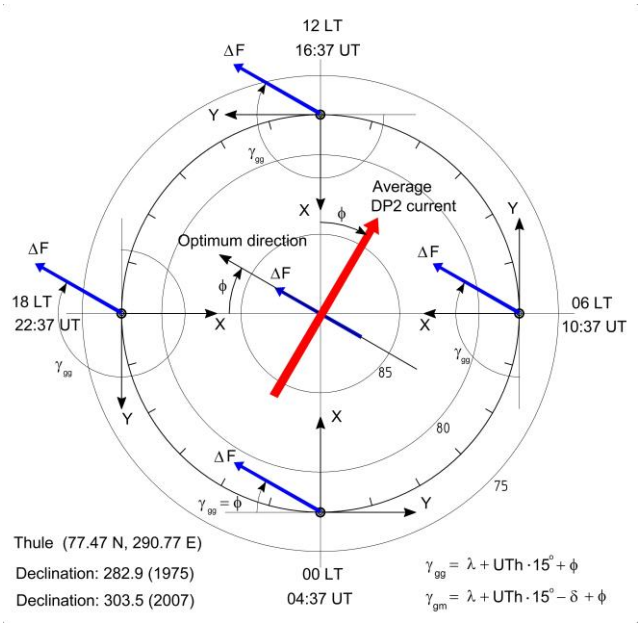

Figure 12. Transpolar current direction (CD), optimum direction (OD), and magnetic component directions X and Y for Thule.

Using instead the complement angle $V_{PROJ} = U_{PROJ} - 270°$, and UT time instead of LT, then for Thule the projections of components ΔX and ΔY are now given by:

$$\Delta F_{PROJ} = \Delta X \cdot sin\,(V_{PROJ}) - \Delta Y \cdot cos(V_{PROJ}) \quad (28)$$

where V_{PROJ} now counted clockwise is defined as a function of *UThr* (UT time in hours) through:

$$V_{PROJ} = Longitude + UThr \cdot 15^{o} + optimum\ direction\ angle\ (ODA) \quad (29)$$

As seen in Fig. 12, the projection angles, V_{PROJ}, indicated by the circle segments, are now the angle between the negative Y-axis and the optimum direction (OD). The optimum direction angle (φ=ODA) is also the angle between the midnight-noon direction and the transpolar equivalent current direction (CD).

Values of the optimum direction angle are calculated from analyses to find the maximum correlation between the projected QL-corrected geomagnetic variations measured in the polar cap and solar wind merging electric field values derived from interplanetary spacecraft data. In addition to depending on local time and season, the optimum direction values depend on observatory location.

8.2. Procedure for calculation of optimum direction.

In order to correlate the satellite data with polar ground-based magnetic data it is important to adjust the relative timing of samples. For the OMNI data files, the timing has been shifted to the reference position at the bow shock nose (BSN) at appr. 12 R_E in front of the Earth, roughly by imposing a time shift equal to the difference in the X coordinates of this position and the actual satellite position in a Geocentric Solar-Ecliptic (GSE) coordinate system divided by the solar wind velocity *Vx*. For IMP 8 satellite data the time shift is usually a few minutes, while for ACE data the time shift is on the order of 1 hour (cf. http://omniweb.gsfc.nasa.gov). Here, the satellite data are further referred to the Polar Regions by imposing a shift corresponding to an anticipated delay between the estimated time for solar wind parameters at BSN and the time of the resulting effects on the polar ionospheric convection as observed through the geomagnetic recordings.

This study uses OMNI (BSN) data, provided in 5-min samples, and geomagnetic data provided in 1-min samples. The 5-min geomagnetic samples are formed from the 1-min data by omitting the maximum and minimum values (removal of singular spikes) and averaging the remaining 1-min values. These 5-min samples are the basis for correlation of the merging electric field, E_M, determined from the OMNI data and the time-shifted projected horizontal magnetic disturbance vectors. The correlation coefficients are calculated over all data from the selected sequence of years (here 1997-2009).

In order to calculate representative values of the delay, the time shift is varied through a range of values in steps of 5 min such that values of ΔF_{PROJ} at time t are correlated with values of E_M at earlier time, t-delay. The optimum direction angle is varied in steps of 5° in through all possible directions, the disturbance vector $\Delta \boldsymbol{F}$ is projected to the optimum direction according to Eq. 28, and the correlation between the projected magnetic disturbances and the solar wind merging electric field is calculated. For each month and each UT hour of the day the correlation coefficients are calculated according to textbook's product-momentum formula:

$$\boldsymbol{R} = \frac{N \Sigma XY - (\Sigma X)(\Sigma Y)}{\sqrt{[N \Sigma X^2 - (\Sigma X)^2][N \Sigma Y^2 - (\Sigma Y)^2]}} \quad (30)$$

where $X = \Delta F_{PROJ}$, and $Y = E_M$, while the summation is extended over all available 5-min samples through the data interval except NBZ cases, where IMF $B_Z > |B_Y| + 3$ nT (see section 15.6).

Among the calculated values of the correlation coefficients derived through all steps in optimum direction angle, the maximum value is found. Based on this maximum value along with the preceding 2 and the following 2 values of the correlation coefficient, the top point of a least squares parabolic function is then used to determine the precise value of the optimum direction angle for the given month and UT hour in question and for the selected delay. The value of the maximum correlation coefficient is also determined from this least squares parabolic function.

The monthly average hourly value of the correlation coefficients is then derived for all 24 hours of the 12 months. This quantity is a function of the delay initially imposed on the series of geomagnetic data to match the propagation of effects from the merging electric field at the bow shock nose (BSN) to cause magnetic disturbances recorded within the polar cap.

Table 6 displays values of the correlation coefficients for Thule for each 5-min step in the delay. The coefficients are here organized in groups according to season: winter, equinox, and summer, and in subgroups according to local time of day: night (01-07 UT), morning (07-13 UT), midday (13-19), and evening (19-01 UT). Using again least squares parabolic fit over 5 delay values, the optimum correlations (OC) and the corresponding delays (OD) are found for each group. These values are shown in the bottom two rows of Table 6.

Table 6. Coefficients for the correlation at varying delays between the merging electric field at bow shock nose (BSN) and polar geomagnetic variations at Thule projected to the optimum direction.

Delay	NOV - FEB				MAR-APR + SEP-OCT				MAY - AUG				AllYear
Min.	01-07	07-13	13-19	19-01	01-07	07-13	13-19	19-01	01-07	07-13	13-19	19-01	Avr.
0	0.619	0.651	0.647	0.622	0.684	0.679	0.652	0.663	0.673	0.653	0.554	0.692	0.649
5	0.638	0.680	0.678	0.647	0.704	0.705	0.676	0.685	0.697	0.672	0.584	0.718	0.674
10	0.659	0.709	0.707	0.675	0.725	0.733	0.702	0.711	0.722	0.692	0.618	0.745	0.700
15	0.674	**0.720**	**0.721**	0.689	0.739	**0.749**	0.718	0.726	0.738	**0.704**	0.641	0.761	0.715
20	**0.677**	0.716	0.717	**0.689**	**0.742**	0.747	**0.719**	**0.729**	**0.742**	0.703	**0.646**	**0.765**	**0.716**
25	0.674	0.706	0.703	0.683	0.739	0.735	0.709	0.725	0.739	0.696	0.635	0.759	0.709
30	0.670	0.696	0.688	0.676	0.733	0.721	0.697	0.718	0.733	0.685	0.614	0.748	0.698
35	0.663	0.688	0.675	0.669	0.727	0.708	0.683	0.709	0.726	0.673	0.589	0.737	0.687
40	0.658	0.682	0.665	0.663	0.724	0.697	0.670	0.700	0.717	0.662	0.565	0.725	0.677
Opt.corr.	0.678	0.721	0.721	0.691	0.743	0.750	0.720	0.730	0.743	0.705	0.646	0.765	0.717
Opt.delay	20.25	17.22	17.02	18.67	20.16	17.64	18.34	19.76	20.35	18.08	19.21	19.58	18.76

From the mean of subgroup averages the final values are:

Average optimum correlation: 0.717 *Average optimum delay*: 18.76 min. (31)

From Table 6 several further features may be extracted. For all groups, the best correlations marked by heavy numbers are obtained at delays close to 20 min. The delays are generally a little larger during night hours (01-07 UT) and smaller at morning and daytime hours (07-19 UT) but the variations are rather small ranging from minimum value at 17.0 minutes (winter day) to maximum at 20.4 minutes (summer night). With the small spread over different local time and season conditions for Thule, the same average delay value is assumed for Vostok. This choice is justified by Tables 7 and 8 in section 16.7.

With the delay fixed, the optimum direction angles can now be derived. For the continued processing, a time shift rounded off to 20 min is imposed on OMNI bow shock nose (BSN) samples relative to Thule and Vostok geomagnetic data series and 15-min samples are used from now on to reduce scatter and improve the correlation. In order to provide valid statistics, the data are again combined to form values for each hour of the day through each month of the year.

When based on data from a single month the hourly values of the optimum direction angle (*ODA*) will show strong fluctuations which may not be reproduced if the corresponding calculations are made for another epoch. In order to make the values more generally representative some averaging and smoothing is necessary. In the first step the averages of *ODA* hourly values was formed over each of three 4-year subintervals of the 12 years epoch, 1997-2009 (excluding 2003, since there are no data from Vostok that year). Subsequently, the average of the three set of ODA values are formed. These values are then exposed to 2-D Gaussian weighted smoothing over month and UT hour by averaging using the weight function (cf. section 15.2):

$$WF = exp\{ - (HR - HR0)^2/XHR^2 - (MD-MD0)^2/XMD^2 \} \quad (32)$$

where *HR* is the variable UT hour, *HR0* is the selected UT hour and *XHR* is the half-width of the Gaussian weight function for the time-of-day. Correspondingly, *MD* is the variable month, *MD0* is the selected month and *XMD* is the half-width of the Gaussian weight function for months. The summations involved in the averaging are extended to twice the width of the Gaussian. Assuming cyclic variations, provisions are made for summation beyond the 24 hours of a day and 12 months of a year. The values used here are *XHR*=4 hours and *XMD*=2 month. For finer resolutions, e.g., 15-min, 5-min or 1-min samples, the hourly values of the optimum angle are interpolated.

In order not to reduce the amplitudes of the parameters being smoothed or interpolated, the series are exposed to a "peak amplitude enhancement" by applying the modification (cf. section 15.2):

$$X_M(N) = X(N) - A\cdot\{X(N-1) + X(N+1) - 2\cdot X(N)\} \qquad (33)$$

With A=0.25 this modification enhances the peak values by typically a few percent, which balances the reduction imposed by the Gaussian smoothing or interpolation.

The resulting optimum angle values (with QDC correction of data) for the three subintervals and for the total epoch from 1997 to 2009 are presented in Fig. 13. Note the consistent variations during summer months and the larger spread between values derived for the subintervals during winter months.

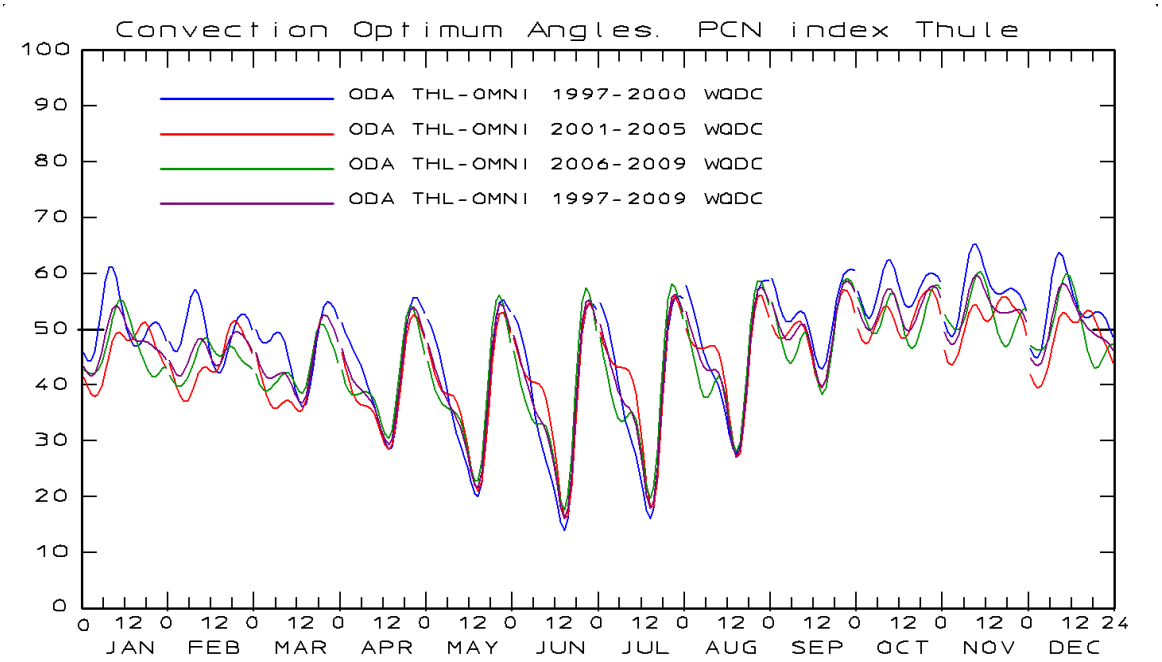

Fig. 13. Derivation of optimum direction angle for Thule using data from epoch 1997-2000 (blue line), 2001-2005 (red), 2006-2009 (green), and the average through 1997-2009 (magenta line).

An issue, which has been discussed in e.g., *Troshichev et al.* (2011), is the influence from including QDC correction in the processing of the magnetic data. In the presently used program to derive the optimum direction angles, the QDC correction is invoked in a single command line and can easily be switched on or off. Here, the QDC correction is found to have negligible effects on the optimum direction angle.

For Thule, the optimum direction angles derived with and without QDC correction as well as with and without smoothing are displayed in Fig. 14a for January and in Fig 14b for July. The stepped 1-hr values are averages through the month. The more smooth lines display 5-min values for day 15 of the month. Note, that the smoothing is 2-dimensional, that is, over hours (seen in the diagram) and over months (not directly seen).

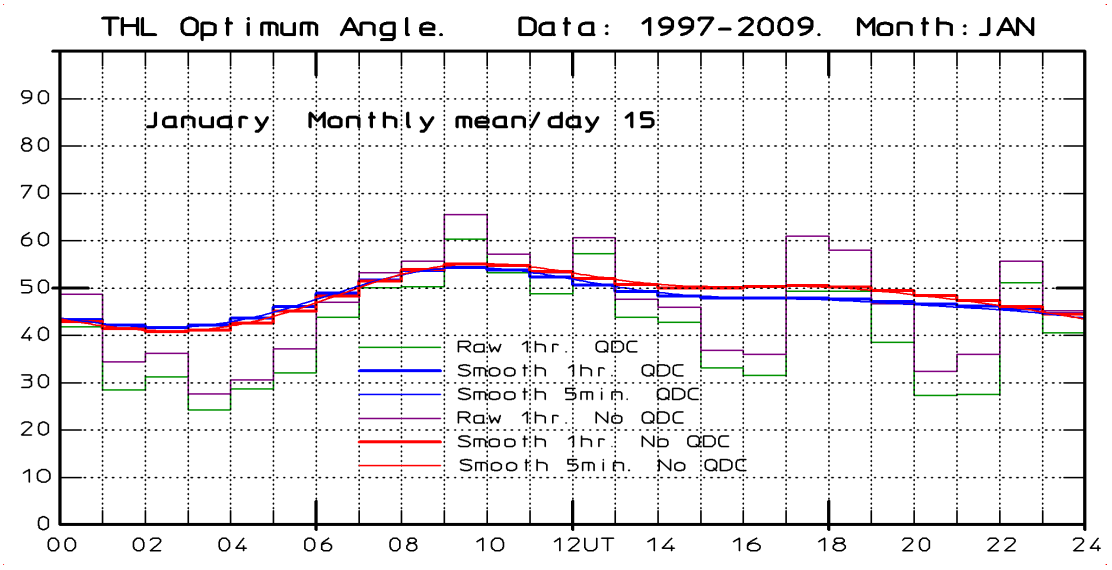

Fig. 14a. Optimum direction angle for Thule. Mean hourly values for January with/without smoothing, and with/without QDC correction. Five-min values for day 15 with/without QDC correction.

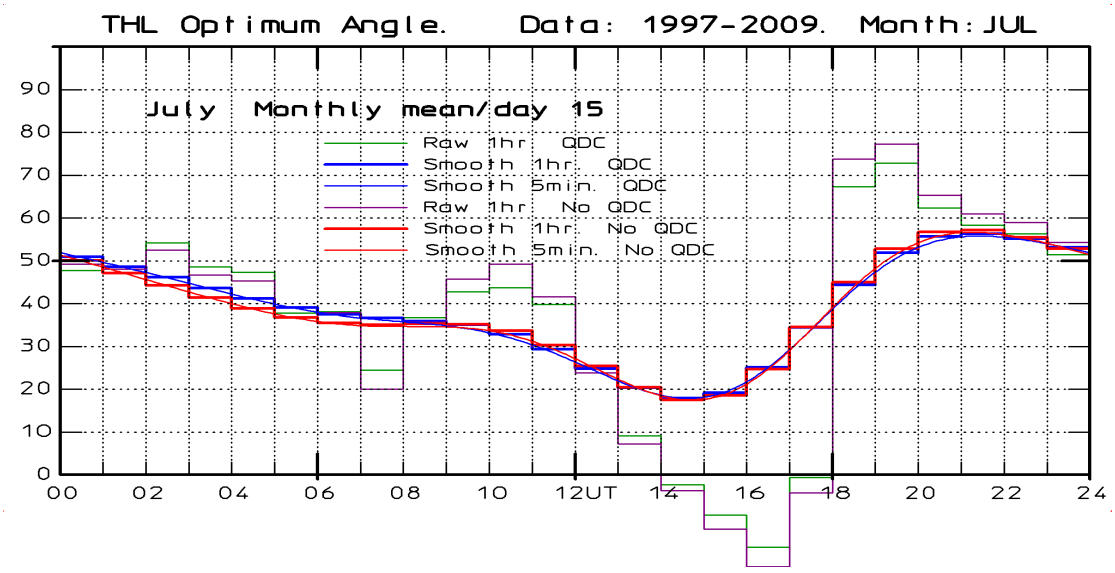

Fig. 14b. Optimum direction angle for Thule. Mean hourly values for July with/without smoothing, and with/without QDC correction. Five-min values for day 15 with/without QDC correction.

In addition to showing the close values of the optimum direction angles derived with and without QDC correction, Figs. 14a,b also demonstrate the reasonable course of the interpolated 5-min values relative to the hourly steps.

Values of the OMNI-Thule optimized correlation coefficients derived without and with QDC are listed in Tables A2a,b in appendix A. The smoothed values of the optimum direction angle (φ) for Thule are shown in Tables A3a,b in appendix A for calculations without/with QDC adjustments of the geomagnetic data.

9. Calculations of Slope and Intercept for Thule.

Recalling, that we are searching for a proxy based on polar magnetic disturbances to represent the solar wind "Merging Electric Field" ($E_M = MEF = V_{SW} B_T sin^2(\theta/2)$), the correlation between the MEF and the horizontal disturbance vector ($\Delta \boldsymbol{F}$) is maximized by projecting $\Delta \boldsymbol{F}$ to a specific direction ("optimum direction"), which varies slowly with local time and season. The general assumption is now that there is a (statistical) linear relation between the polar magnetic variations, ΔF_{PROJ}, and the solar wind electric field, E_M, and that this relation can be inverted and used to define a polar cap (PC) index by equivalence (cf. Eqs. 1-3).

Contrary to the calculation of the optimum direction, the issue of whether or not the QDC values should be subtracted from the recorded values (corrected for baseline) has importance for the calculations of slope and intercept. Also important is the question whether or not reverse convection cases should be included in the data base used for the regression. Consequently, these issues are first discussed. A more detailed discussion of the related effects is provided in sections 15 and 16.

9.1. The QDC issue

In the above sections the magnetic disturbances were found by subtracting baseline values (the “internal” field components) from the total magnetic field intensities measured in the polar cap. This level is approximated by interpolation through the year of the so-called Quiet Winter Night Level (QWNL), that is, the magnetic level recorded in the quietest winter nights where the overhead disturbance currents are minimal. Furthermore, rather regular daily variations described with the Quiet Daily Curve (QDC) and not related to the solar wind merging (geoeffective) electric field, E_M, could be subtracted before the regression analyses are performed and, correspondingly, before the PC index values are calculated from actual geomagnetic data.

In relation to the calculation of a PC index associated with the solar wind merging electric field, E_M, the QDC values refer to the current systems in effect when the solar wind electric field is insignificant. In such cases the polar magnetic variations are primarily related to current systems generated by the antisunward convection in the central polar cap ionosphere resulting from the gradient in ionization densities from the day to the night side. A further drive of the antisunward convection in the central polar cap is provided by the residual cross-polar cap voltage resulting from the steady solar wind "frictional" forcing of the polar ionospheric two-cell convection (Axford and Hines, 1965), which depends on the solar wind velocity and density.

The resulting current intensities depend on local ionospheric conductivities. Thus the QDC variations through the day depend on the solar UV flux, which varies with local season and with solar activity level, and on solar wind properties apart from the electric field. Tables of QDC values should be derived continually in order to represent the varying solar UV intensities and solar wind plasma properties. The subtraction of QDC values from the observed magnetic variations in the calculations of PC coefficient and index values provides a compensation for solar cycle effects resulting from the varying solar UV and EUV radiation and solar wind plasma intensities through the 11-year cycle.

9.2. Reverse convection.

For the large-scale polar magnetic variations there are two basic modes. One is related to the currents associated with the two-cell polar ionospheric "forward" convection mode (DP2, cf. Fig. 1), which is the most common convection mode. It applies to solar wind conditions where the interplanetary magnetic field (IMF) is either southward oriented or only weak in magnitude when northward directed. In the two-cell forward mode the convection in the central polar cap is antisunward while there is a sunward return flow at lower (auroral) latitudes. The direction of the Hall current component, which dominates the magnetic response at ground level, is opposite of the convection flow direction.

During conditions of strong, northward oriented IMF, different convection modes may appear. In the central polar cap a reverse convection system (DP3) may develop for which the transpolar flow is sunward while the return flow at lower latitudes, but still within the polar cap, is antisunward. Possible combinations of the forward two-cell and the reverse two-cell convection systems include three and four cell convection systems.

With a reverse overhead convection flow the magnetic deflections at ground are opposite of those of the forward convection mode. Accordingly, the projected disturbance vector may become less than the QDC level or even strongly negative. Since the interplanetary merging electric field (E_M) by definition (cf. Eq. 2) is always non-negative then the linear relation assumed in Eq. 1 is no longer valid. PC index values calculated during such conditions may turn out to be negative. Hence, the concept of the PC index as a proxy for the E_M value breaks down. Accordingly, reverse convection cases belong to a different class of disturbances and should be omitted from the data base in calculations of the coefficients of proportionality between the geomagnetic variations and the merging electric field.

9.3. Regression slope and intercept calculations

The task is now to calculate the slope and intercept parameters to give the highest possible correlation between the interplanetary merging electric fields and the time-shifted polar magnetic disturbances. The former parameter is here based on observations of solar wind velocity, V_{SW}, and interplanetary magnetic field, IMF B_Y and B_Z, made available in OMNI 5-min samples. The value of the merging electric field is calculated by using Eq. 2 ($E_M = V_{SW}\, B_T\, sin^2(\theta/2)$)

The horizontal magnetic vector, $\boldsymbol{F}$, like explained in section 8, is resolved in an X-component (northward in a geographical coordinate system) and a Y-component (eastward). The base line values are subtracted from the raw data and the QDC values are subtracted as defined in Eqs. 25a,b ($\Delta X = (X_{RAW} - X_{BL}) - X_{QDC}$, $\Delta Y = (Y_{RAW} - Y_{BL}) - Y_{QDC}$).

The projection of the disturbance vector $\Delta\boldsymbol{F}$ to the optimum direction is defined by Eq. 28. ($\Delta F_{PROJ} = \Delta X \cdot sin(V_{PROJ}) - \Delta Y \cdot cos(V_{PROJ})$). where the projection angle, V_{PROJ} (counted CW), is defined as a function of *UThr* (UT time in hours) through Eq. 29 ($V_{PROJ} = Longitude + UThr \cdot 15^o + optimum\ direction\ angle$)

Basis for the regression is the above-mentioned assumption of a linear relation between the merging electric field, E_M, and the projected (baseline and QDC corrected) magnetic variation, ΔF_{PROJ} as expressed in Eq. 1 from which average values of the slope, α, and the intercept parameter, β ,should be derived by statistical methods from a comprehensive and representative data base.

Like it was done for the optimum direction angle (φ) the regression coefficients are derived as series of mean hourly values through a day for each month of the year. To solve for the coefficients in the linear relation in Eq. 1 ($\Delta F_{PROJ} = \alpha\, E_M + \beta$), statistical text-books provide the least squares formulas for the regression of Y upon X:

Slope: $$\alpha = \frac{N \Sigma XY - (\Sigma X)(\Sigma Y)}{N \Sigma X^2 - (\Sigma X)^2} \qquad (34)$$

Intercept: $$\beta = \frac{(\Sigma Y)(\Sigma X^2) - (\Sigma X)(\Sigma XY)}{N \Sigma X^2 - (\Sigma X)^2} \qquad (35)$$

To conform with other PC index methods (except one, cf. sec. 17.2), in these best fit regression formulas, the projected magnetic disturbance (ΔF_{PROJ}) is parameter Y, while the merging electric field (E_M) is parameter X. For each month of the year the hourly values of α and β are formed by processing all corresponding 15-min values of E_M (t-20 min) and ΔF_{PROJ} (t) through that hour of all days through the month. In order to minimize statistical fluctuations the coefficients are first derived for each of three subintervals of 4 years each, and next averaged over the total epoch, here 1997-2009 (ex. 2003).

In order to avoid reverse convection cases in the data base used for calculations of PC index coefficients, a combination of limits on actual IMF values and projected magnetic variations is used. For the IMF it is

required that IMF B_Z < | IMF B_Y | + 3.0 nT. This condition excludes cases where strong northward IMF B_Z is the dominant component. A further condition imposed on the selection of data requires that the projected magnetic variation, ΔF_{PROJ}, is larger than -50 nT. This condition ensures that cases with strong reverse convection, which may continue for a while after the driving northward IMF has been reduced or has changed polarity, are also omitted.

The raw (non-smoothed) values of the slopes and intercept coefficients derived for Thule from using Eqs. 34 and 35 are then exposed to 2-D Gaussian smoothing over month and UT hour by averaging using the weight function defined in Eq. 32 ($WF = exp\{ - (HR - HR0)^2/XHR^2 - (MD-MD0)^2/XMD^2 \}$) and the amplitude modification shown in Eq. 33 where, again, the values used for smoothing are XHR=4 hours and XMD=2 months, while A=0.25 for the amplitude modification.

The resulting slope values for the three subintervals and for the total epoch 1997-2009 (ex. 2003, cf. section 12) are presented in Fig. 15. Depending on choice of subinterval, the slope values could vary by up to ~ 20% from the final values.

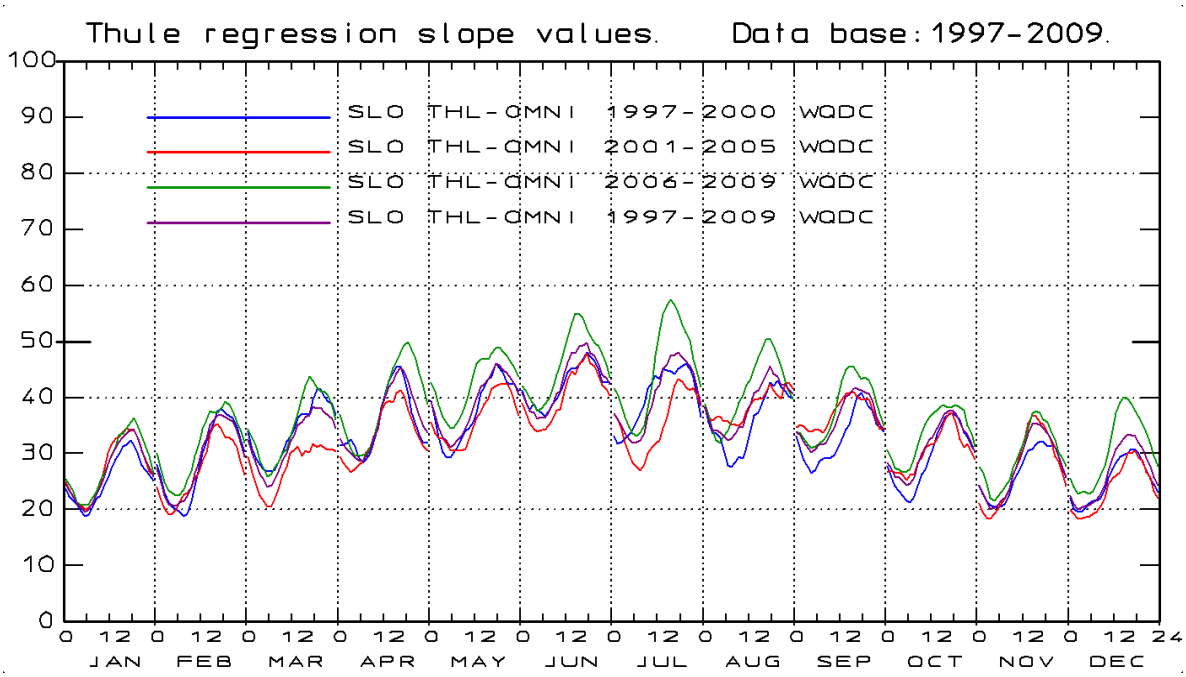

Fig. 15. Derivation of slope values for Thule using data from epoch 1997-2000 (blue line), 2001-2005 (red line), 2006-2009 (green line), and the average through 1997-2009 (magenta line).

For Thule, the raw (non-smoothed) and smoothed hourly slope values are presented in Fig. 16a for January and in Fig. 16b for July. In addition, the figures display interpolated 5-min slope values for day 15 of the months. Gaussian weight function interpolation with peak amplitude enhancement is used here. Note that the data have been 2-D smoothed such that the resulting hourly slope values in these monthly plots are not necessarily the mean of the displayed non-smoothed initial values for the presented months.

In the program to derive slope values, the QDC correction of the geomagnetic data is made in a single command line that easily can be switched on or off. Thus, all calculations can be made with the same data basis and the same program except for the subtraction of QDC values from the geomagnetic data samples. Figs. 16a and 16b for Thule includes displays of the raw and smoothed hourly slope values and of the interpolated 5-min slope values for the case where QDC correction is not used. It is evident, that the difference between cases where QDC correction of the geomagnetic data is used or not used is quite marginal for the slope values.

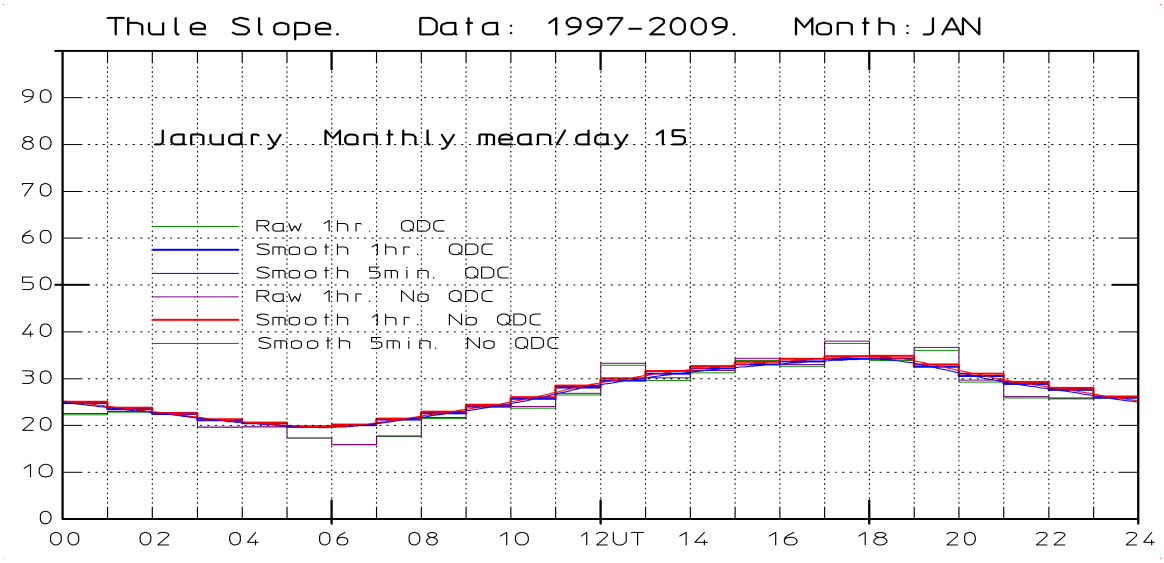

Fig. 16a. January slope values for Thule. Mean hourly values for January with/without smoothing, with and without QDC correction. Five-min values for day 15 with/without QDC correction

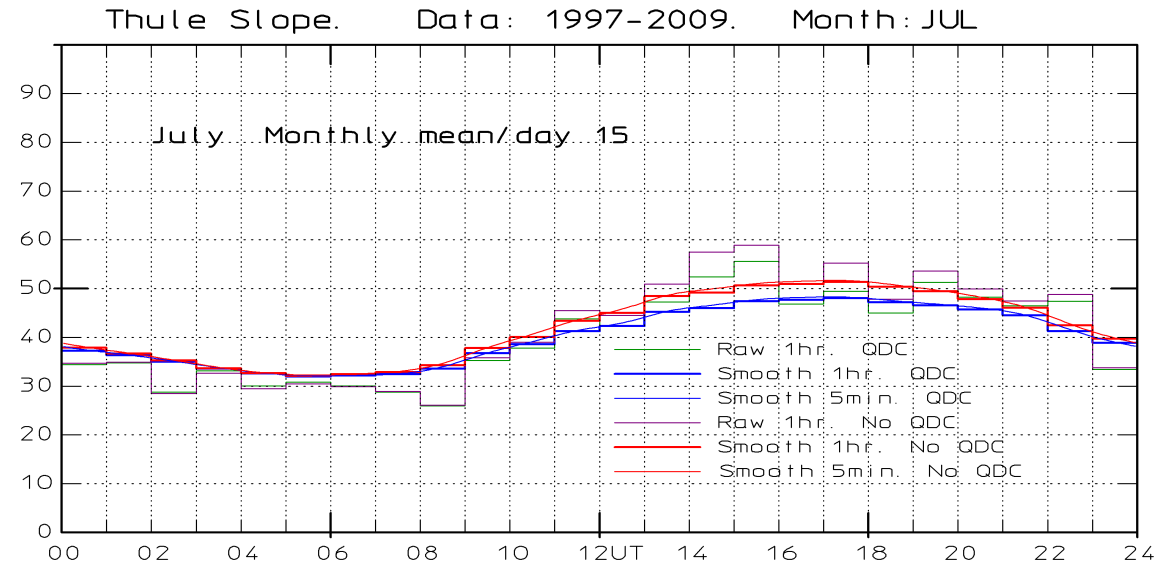

Fig. 16b. July slope values for Thule. Mean hourly values for July with/without smoothing, with and without QDC correction. Five-min values for day 15 with/without QDC correction.

Similarly, the raw (non-smoothed) hourly values of the intercept are derived for Thule by using Eq. 35 on subintervals with subsequent averaging through the entire epoch from 1997 to 2009 (ex. 2003). Smoothed values of the intercept (β) are derived using again Gaussian 2D-smoothing and amplitude enhancement (*XHR*=4 hours, *XMD*=2 months, and A=0.25).

For the QDC-corrected data, the subinterval results as well as the final result for the total epoch 1997-2009 are presented in Fig. 17. Note that the subinterval deviations from the final result are as large as the final values.

The monthly mean hourly values are interpolated to give the 5-min values. The raw/smoothed hourly intercept values and the 5-min interpolated values on day 15 are presented in Figs. 18a and 18b for Thule for January and July.

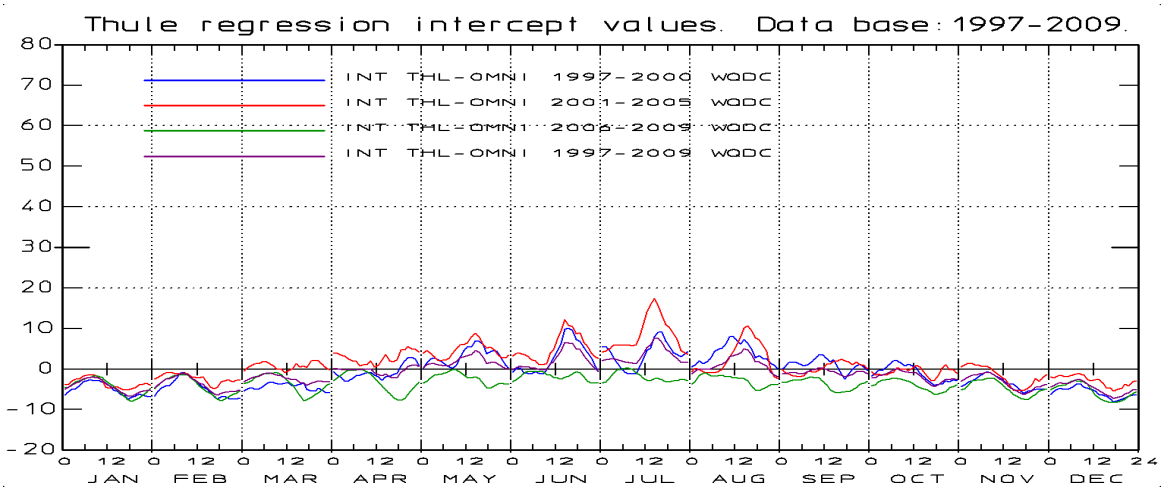

Fig. 17. Derivation of intercept values for Thule using QDC-corrected data from epoch 1997-2000 (blue line), 2001-2005 (red line), 2006-2009 (green line), and the average through 1997-2009 (magenta line).

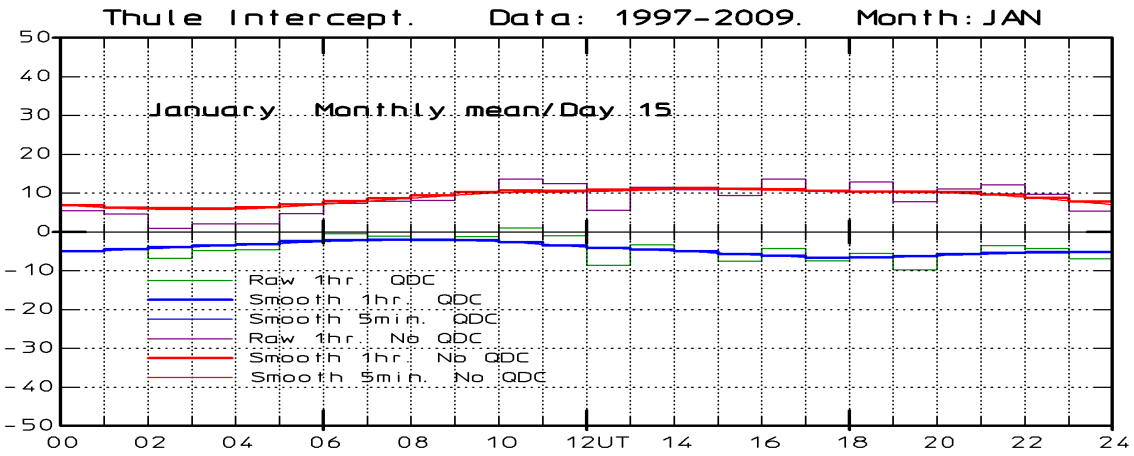

Fig. 18a. January intercept values for Thule. Mean hourly values for January with/without smoothing, with and without QDC correction. Five-min values for day 15 with/without QDC correction.

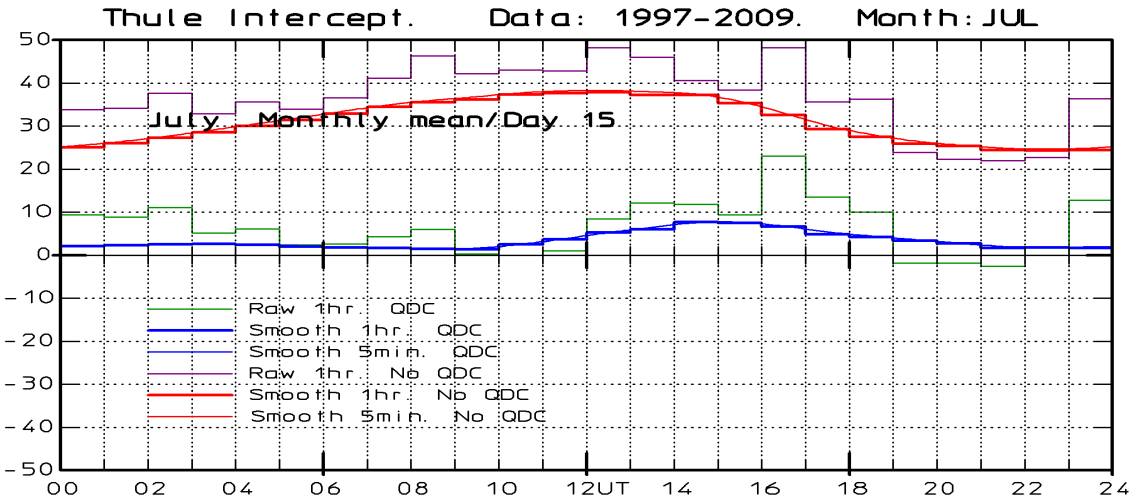

Fig. 18b. July intercept values for Thule. Mean hourly values for January with/without smoothing, with and without QDC correction. Five-min values for day 15 with/without QDC .correction.

Like for the calculations of slope values, the QDC correction of the geomagnetic data can easily be switched on and off. Both cases are presented in Figs. 18a and 18b. For the intercept values there are significant differences between the QDC and non-QDC cases.

9.4. Summary plots of angle, slope and intercept.

Fig. 19 displays combined plots of optimum direction angle, slope, and intercept coefficients for Thule. The three diagrams are divided in columnar fields (dividing lines not shown) for each month through the year marked along the horizontal axes. Each monthly field is subdivided in hours through a day. Monthly mean hourly values through a day of the index angle and coefficients are plotted within each field similar to plots provided in Figs. 13, 15, and 17 for Thule. Parameters are derived with and without QDC correction.

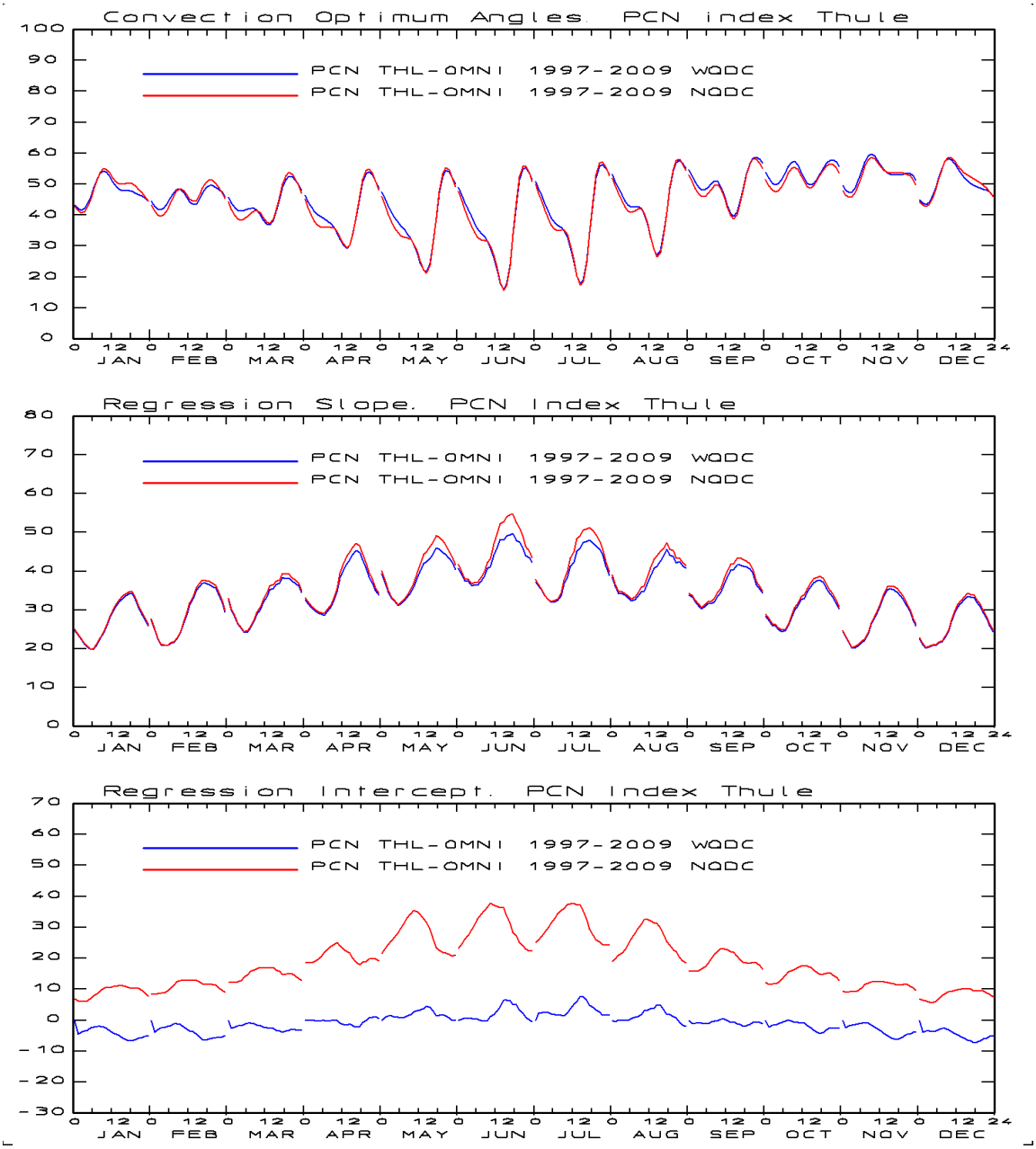

Fig. 19. Summary plot of optimum direction angle (upper field), slope (middle), and intercept (bottom field) for Thule. Parameters derived with QDC correction (blue line) and without (red line).

10. PC index calculations for Thule.

With tables of available PC index parameters, i.e., optimum direction angle, slope and intercept coefficients, interpolated to 1-min resolution, it is now straight-forward to derive PCN index values. Recorded 1-min data for the horizontal geomagnetic vector (X_{RAW},Y_{RAW}) are corrected for the baseline, and the relevant QDC values are derived using either the Solar Rotation Weighted (SRW) procedure for historical data (data from most of ±40 days must be available) or the HSRW procedure for actual (on-line) data (data from most of preceding 40 days must be available).

The QDC values (X_{QDC},Y_{QDC}) are subtracted from the baseline-corrected values in order to derive the geomagnetic variation vector value ($\Delta \boldsymbol{F}$) according to Eqs 25a,b. Now, the actual UT time and the observatory longitude are used with the tabulated optimum direction angle (φ) for that time to derive the projection angle (V_{PROJ}) according to Eq. 29. The projected scalar disturbance value (ΔF_{PROJ}) is derived according to Eq. 28. Finally, with the tabulated slope, α, and intercept, β, for the time in question, the PC index value is derived according to Eq. 3 (PC = (ΔF_{PROJ} – β)/ α)

To provide an example, PCN index values for 1-16 January 2002 are displayed (blue line) in Fig. 20. Values of the related merging electric field (shifted by 20 min) are included (black line) in the diagram for comparison. The plotting is based on 5-min samples. This year is a solar maximum year.

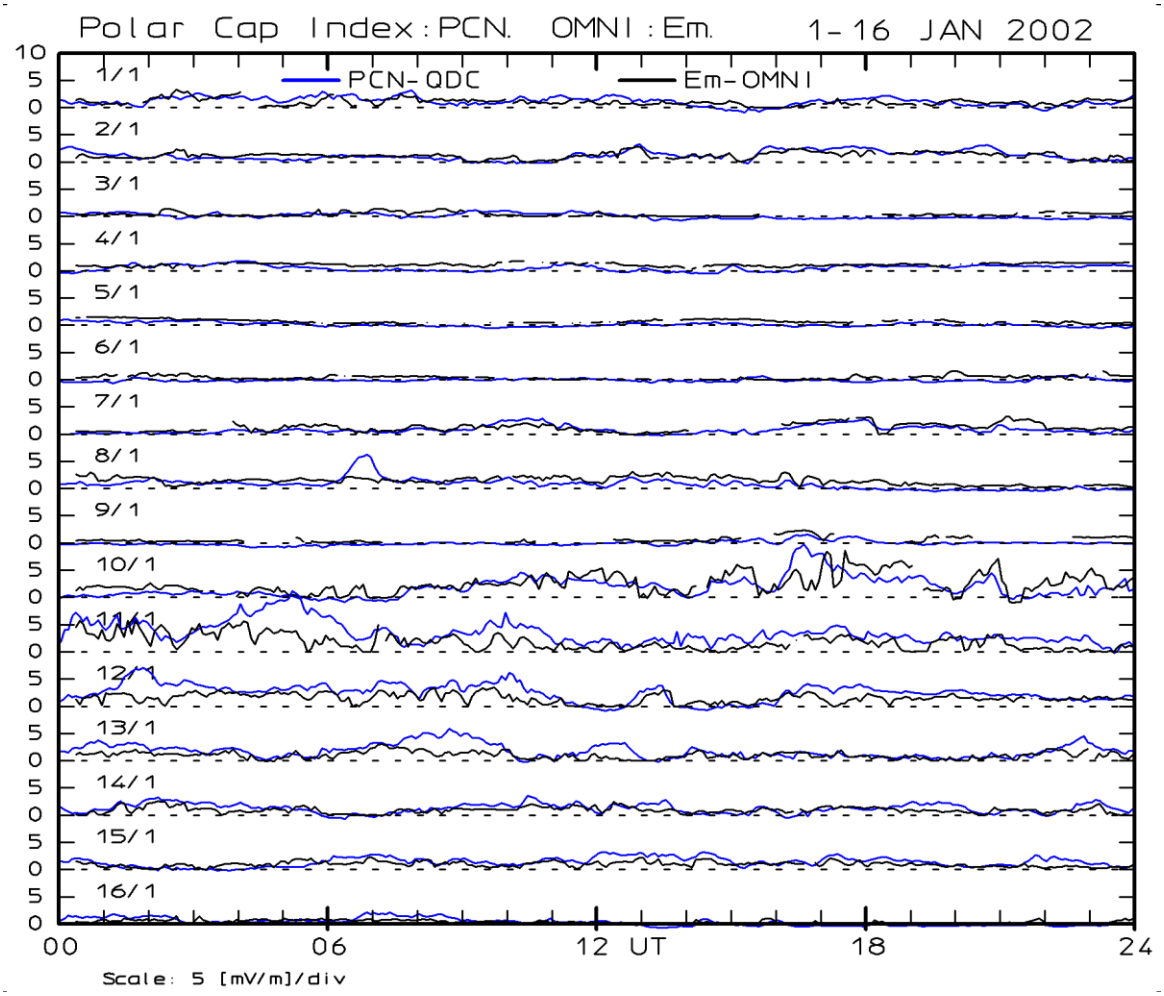

Fig. 20. Northern Polar Cap (PCN) index values (blue line) for 1-16 January 2002. Values of the merging electric field (E_M) are plotted in black line for comparison.

11. SRW procedure for calculation of QDC for Vostok.

The "Solar Rotation Weighted" (SRW) procedure used for Thule data has also been applied to Vostok magnetic data. Examples of the results are displayed in Fig. 21 in the same format as used in Figs. 8 and 9 above. In the figure the components are represented in the local geomagnetic coordinate system (H,E).

The H-component diagram of recorded values and QDCs for July 2002 compares quite accurately with Fig 2 of *JT2008* (there is an error in their naming of the month) except for the base levels. Here, the average data and QDC levels are around 0 nT while for Fig. 2 of *JT2008* the average levels are around 100 nT since baseline values were not subtracted from their data. This difference is unimportant for applications using the magnetic variations, like the calculation of PC index values, since the required absolute QL levels (sum of baseline and QDC) can easily be traced back.

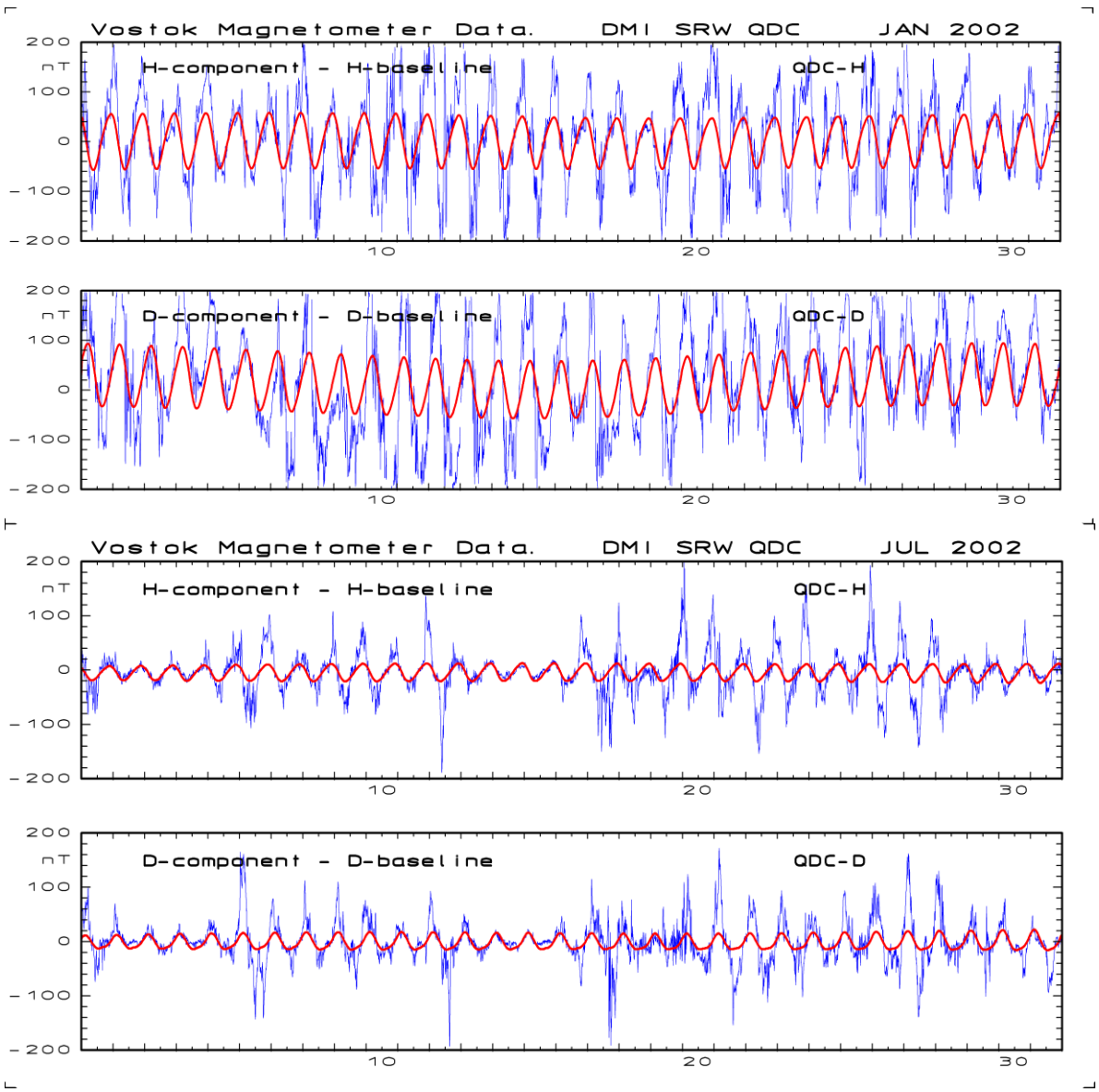

Figure 21. Vostok raw magnetometer data corrected for the secularly varying base level (thin blue line) and the QDC values (heavy red line) calculated by using the solar rotation weighted (SRW) minimum variance method. Data for January (maximum QDC variation) and July (minimum QDC variation) are presented. This year, 2002, is a solar maximum year.

The recording of geomagnetic data at Vostok is less regular than the corresponding data collection at Thule due to the much harder environment in Antarctica as well as logistic problems. Among other, the

recordings from the year 2003 are completely missing, and there are numerous shorter data gaps in the geomagnetic data series. Since the magnetometer baselines have some irregular jumps, instead of deriving baselines for one year at a time, the baselines for Vostok were derived for each month with valid data. Subsequently the monthly baselines were smoothed using the Gleisberg concept: $Xc(N)=\{X(N-2) + 2\cdot X(N-1) + 2\cdot X(N) + 2\cdot X(N+1) + X(N+2)\}/8$ with precaution for jumps and data gaps.

The entire data series was scanned (by eye) in order to detect sudden jumps. Special care was taken at the transitions between valid and invalid (or missing) data. Fortunately, like discussed in section 7.5, the SRW method is fairly robust even with lengthy data gaps or sudden disruptions of the data stream, provided that the baseline level is handled properly. The diagrams in Fig. 22 provide summaries of the QDCs for the X and Y components for Vostok through 2002 corresponding to the upper fields of Figs 10 and 11 with QDCs for Thule. Note that the sequence of months have been modified in order to ease comparisons with QDCs for Thule taking into account the hemispherical difference in season.

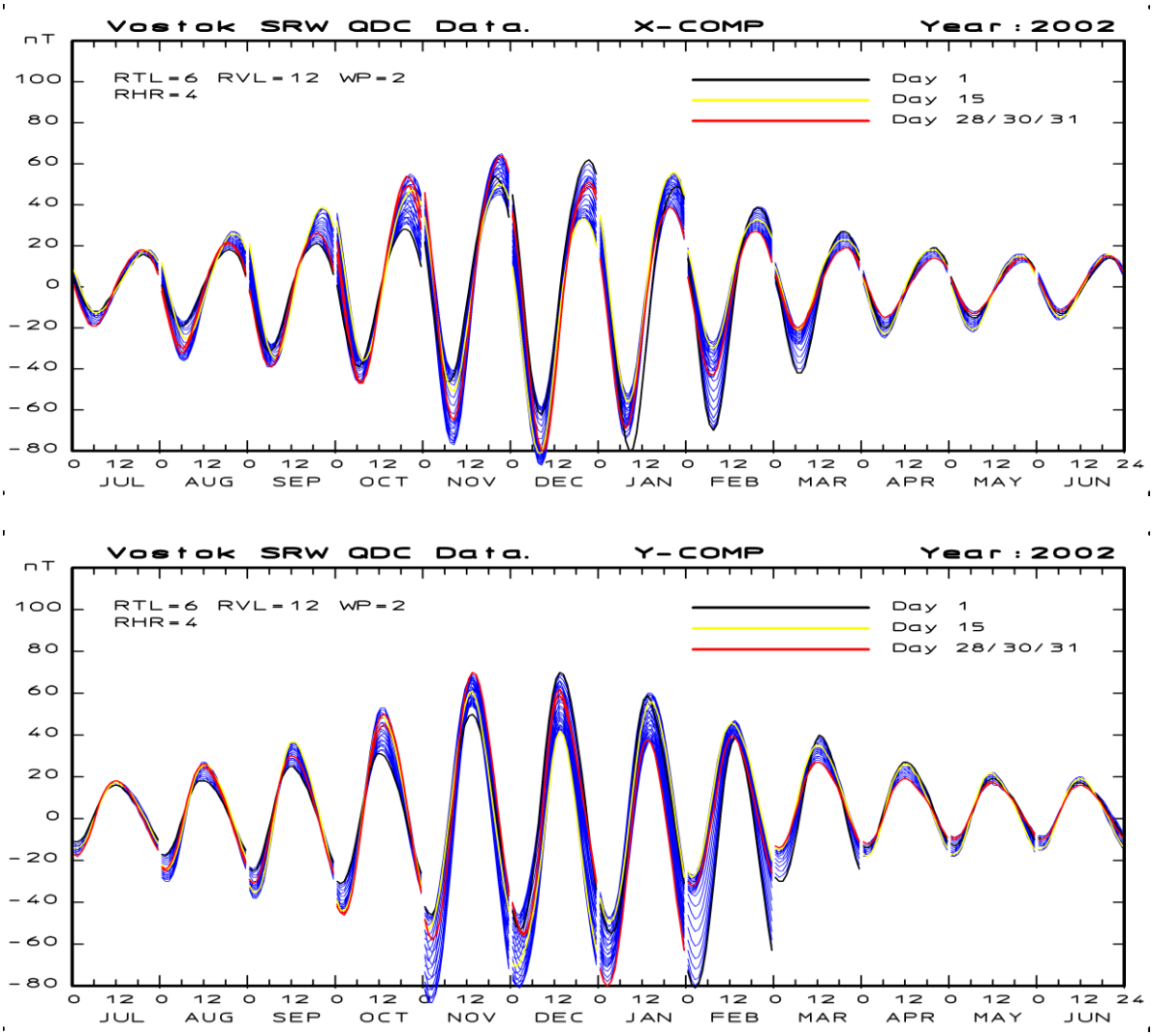

Figure 22. Top field: QDCs for X-component. Full Solar rotation (through - to + 40 days) weighted (SRW) minimum variance hourly QDC values through 2002. There is a scale for the UT hour (00-24) in each monthly section. QDCs for start, middle, and end days of the months are plotted in different colours. The QDCs for other days are plotted in thin blue line. Bottom field: QDCs for Y-component.

12. Calculation of optimum direction angles for Vostok

The calculations of optimum direction angles for Vostok proceed largely with the same procedure as that used for Thule. The antipodal position of Vostok compared to Thule implies a shift in the sign between the two terms of the formula (28) for the projected magnetic variation term, which now reads:

$$\Delta F_{PROJ} = \Delta X \cdot \sin(V_{PROJ}) + \Delta Y \cdot \cos(V_{PROJ}) \qquad (36)$$

In order to obtain the same statistical basis for handling of Vostok data as for Thule, the epoch used for calculations of PCS index angles and coefficients starts at 1997 and ends in 2009. The division in subintervals is: 1997-2000, 2001-2005 (2003 excluded, no data), and 2006-2009. Questionable data were excluded from the processing to derive PCS index angles and coefficients.

The summary diagram (corresponding to Fig. 13) of subinterval values and average optimum direction angles, based on merging electric field values derived from OMNI files and QDC-corrected geomagnetic data from Vostok, is presented in Fig. 23. Note that the sequence of months has been changed in order to make the diagram for the southern polar cap appear comparable to the corresponding diagram for the northern polar cap (local summer at the middle of the diagram).

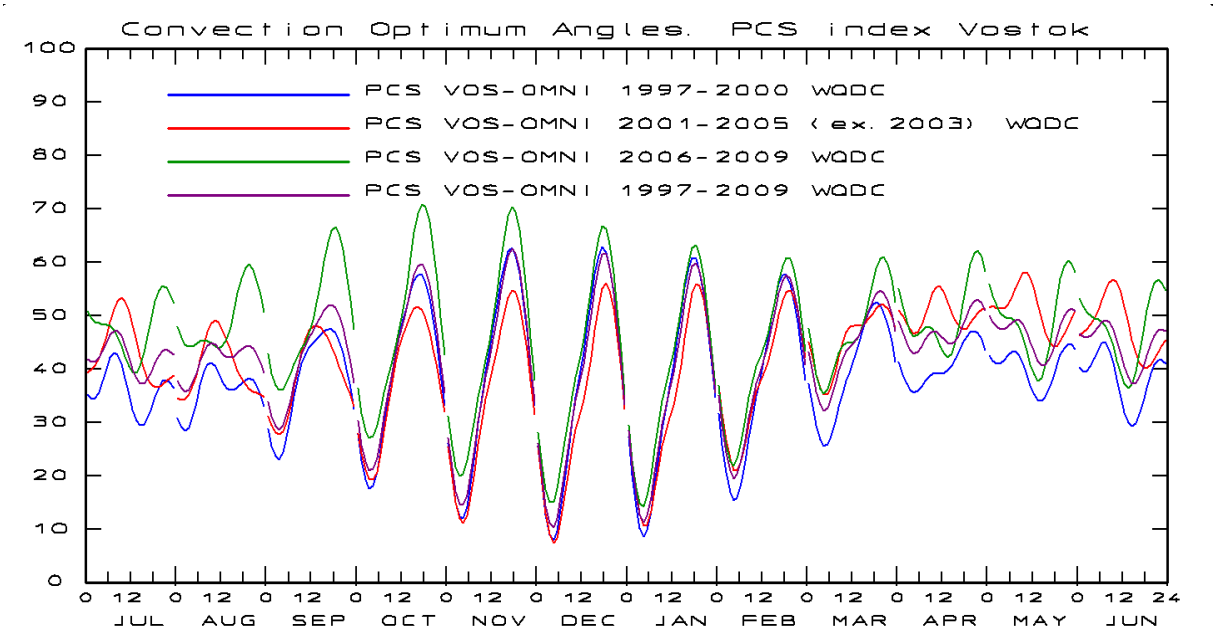

Fig. 23. Derivation of optimum direction angle for Vostok using data from epoch 1999-2002 (blue line), 2003-2006 (red), 2007-2009 (green), and the average through 1999-2009 (magenta line).

In the presently used program to derive the optimum direction angles (the same program as that used for Thule except for the different projection formulas in Eq. 28 vs. Eq. 36), the QDC correction is invoked in a single command line and can easily be switched on or off. For June and November, respectively, Figs. 24a and 24b display the variations of the derived optimum direction angles for Vostok with and without QDC correction as well as with and without smoothing. It is seen, that for the smoothed as well as the raw values, there are negligible differences between the QDC and no-QDC cases.

The values in these diagrams are directly comparable to those of Fig.1a of *Troshichev et al.* (2011) that shows considerable differences between optimum direction angles derived with and without QDC correction. However, as has been pointed out directly to the authors, the two sets of values displayed in Fig. 1a,b,c of *Troshichev et al* .(2011) have apparently been derived from different epochs of data and, therefore, are not directly comparable.

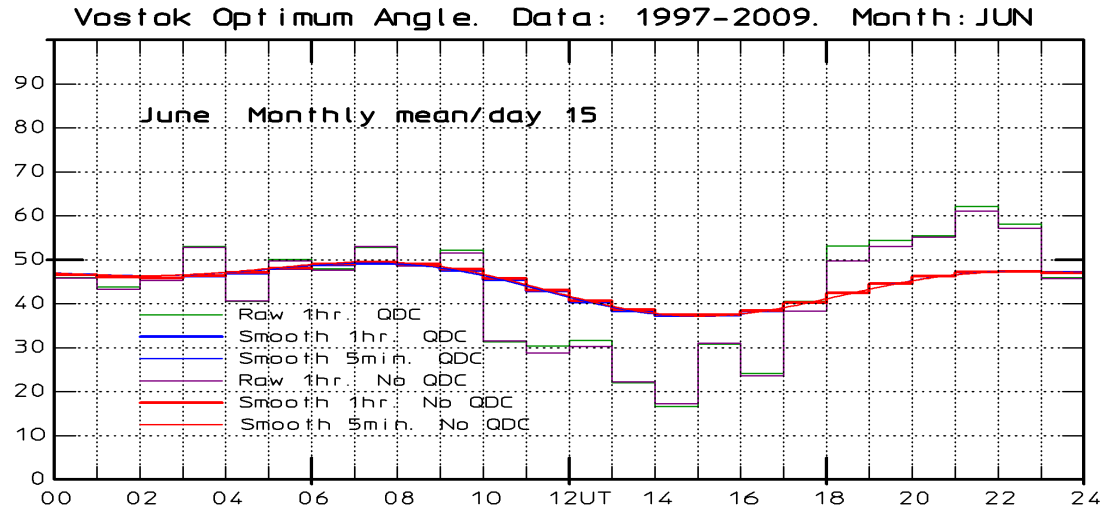

Fig. 24a. Optimum direction angle for Vostok. Raw and smoothed 1-hr monthly averages for June and 5-min values for 15 June. Values derived with and without QDC correction of data.

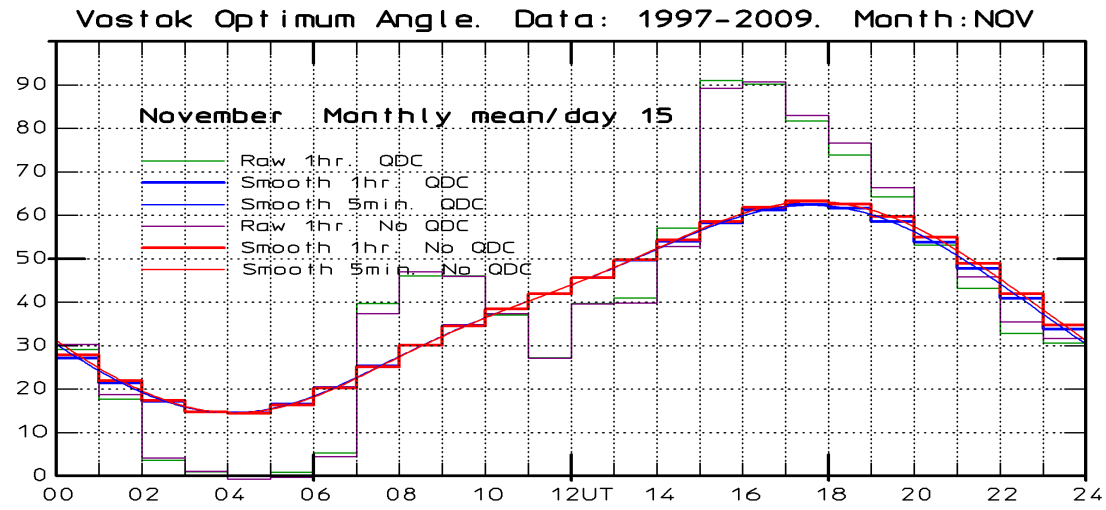

Fig. 24b. Optimum direction angle for Vostok. Raw and smoothed 1-hr monthly averages for November and 5-min values for 15 Nov. Values derived with and without QDC correction of data.

For the assessment of the effects of smoothing it should be noted that the raw values have been exposed to 2-D Gaussian smoothing over time-of-day and month-of-year simultaneously. The normalization parameters for Vostok are the same as those used for Thule, i.e., XHR0=4 hours, XMD0=2 months, and the smoothing ranges are twice the parameter values.

13. Regression slope and intercept for Vostok.

The calculations of slope and intercept parameters for Vostok follows the same course as that outlined for Thule in section 9. The "Solar Rotation Weighted" (SRW) procedure was applied to derive QDC values for Vostok as described in section 11. Optimum direction angles were calculated as shown in section 12 (20 min delay from BSN to Polar Cap, strong NBZ cases excluded). In the first step the values were derived as monthly average 1-hr samples based on data for the epoch 1997-2009 (with intervals of missing or questionable data excluded). Subsequently, 15-min, 5-min and 1-min optimum direction angle values were derived for each day of the year by 2-D Gaussian interpolation.

Now, a data set was built of coincident values of Vostok horizontal geomagnetic variation vectors projected to the optimum direction using Eq. 36, and merging electric field values referred to the Polar Cap by adding a delay of 20 min to the Bow Shock Nose (BSN) values in the OMNI data files. From the 15-min samples of this data set, values of the slope, α, and intersept, β, were found using Eqs. 34 and 35 for subintervals (1997-2000, 2001-2005, 2006-2009) from which the average values are derived for the total interval (1997-2009). The process is illustrated in Fig. 25 for the slope and Fig. 27 for the intercept.

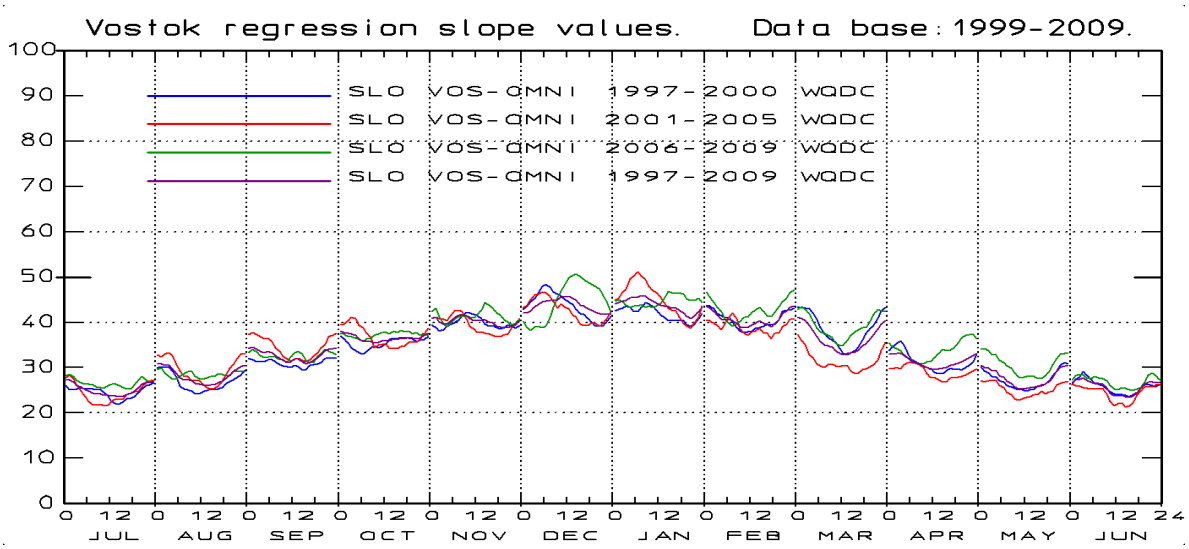

Fig. 25. Derivation of slope values for Vostok using data from epoch 1997-2000 (blue line), 2001-2005 (red line), 2006-2009 (green line), and the average through 1997-2009 (magenta line).

In Fig. 25 the sequence of months has been modified to facilitate the comparison with the corresponding diagram in Fig. 15 for the slope values for Thule. Taking the hemispherical differences into account, the slope levels and the seasonal slope variations are quite similar for Vostok and Thule. However, the daily variations at Vostok are not as simple as the corresponding variations for Thule. For Thule (cf. Fig. 15) there were maxima in slope values at local noon for all months and for all three subintervals of the epoch 1997-2009. At Thule, local solar noon at 16.61 UT is fairly close to local magnetic noon at 15.05 UT. Hence, maxima related to maximum ionization (solar noon) and maximum transpolar convection (magnetic noon) are overlapping. For Vostok, local solar noon at 07.12 UT is quite far from local magnetic noon at 13.02 UT. Hence, the two potential maxima will not overlap and the one or the other may dominate in different seasons.

For Vostok, the raw (non-smoothed) and smoothed hourly slope values are presented in Fig. 26a for June and in Fig. 26b for November (same months as those selected for Fig. 1 in *Troshichev et al.*, 2011). In addition, the figures display interpolated 5-min slope values for day 15 of the months. Note that the data have been 2-D Gaussian smoothed such that the resulting hourly slope values in these monthly plots are not just the mean of the non-smoothed initial values for the month.

Figs. 26a and 26b for Vostok include displays of the raw and smoothed hourly slope values and of the interpolated 5-min slope values for the case where QDC correction is not used. It is evident, that the difference between cases where QDC correction of the geomagnetic data is used or not used is quite marginal for the slope values.

Intercept (β) values were also derived from Eq. 35. Corresponding to the handling of the slope values, the results were exposed to Gaussian 2D-weighted smoothing and amplitude enhancement (*XHR*=4 hours, *XMD*=2 months, and A=0.25). The subinterval results as well as the final result for the total epoch 1997-2009 are presented in the Fig. 27.

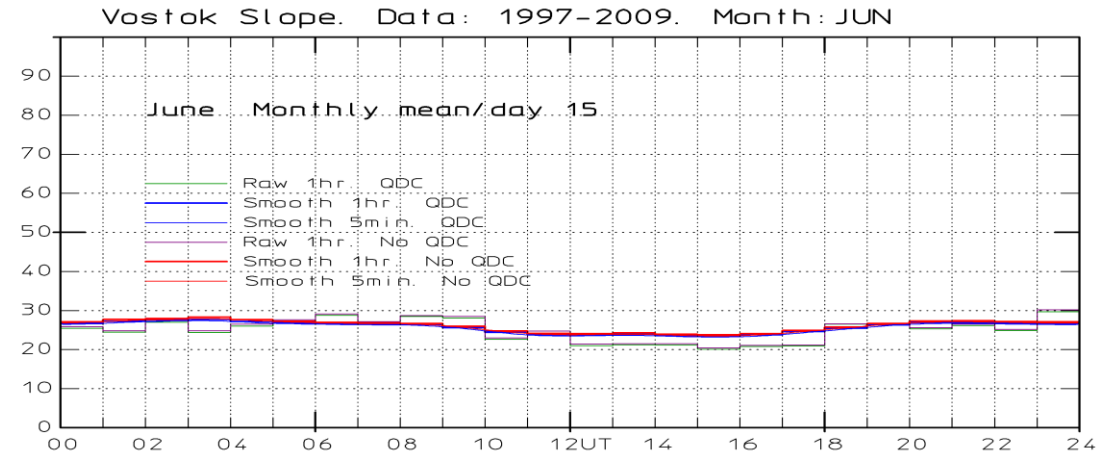

Fig. 26a. June slope values for Vostok. Mean hourly values for June with/without smoothing, with and without QDC correction. Five-min values for day 15 with/without QDC correction

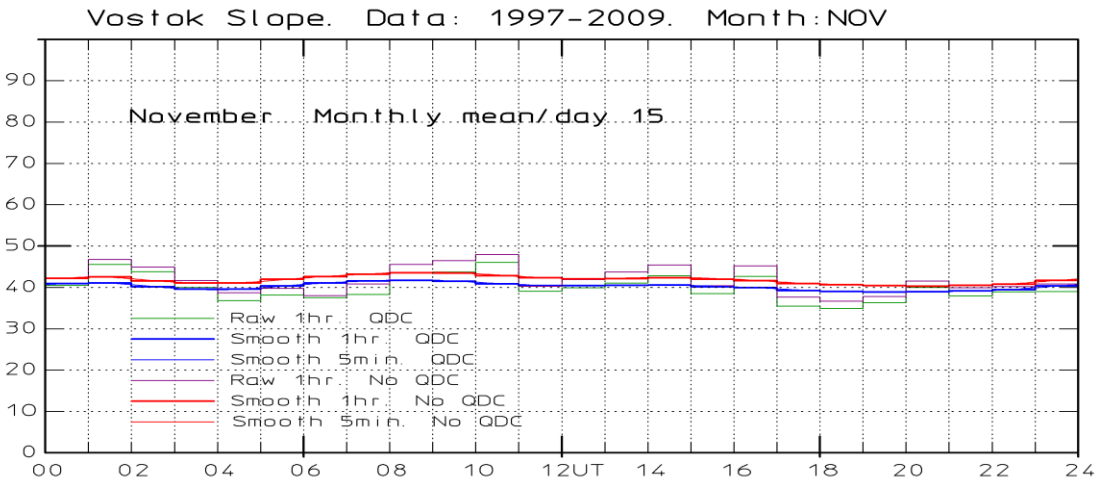

Fig. 26b. November slope values for Vostok. Mean hourly values for November with/without smoothing, with and without QDC correction. Five-min values for day 15 with/without QDC.

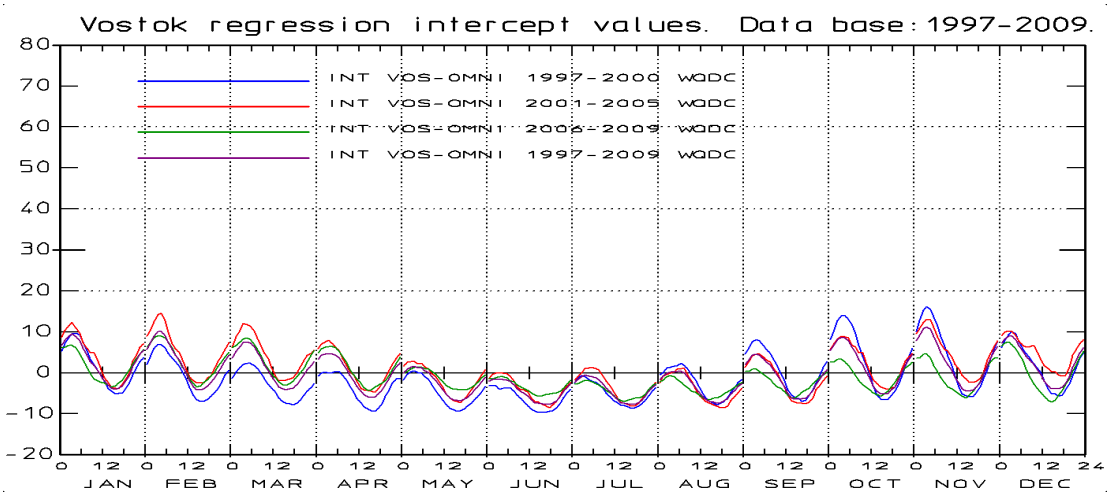

Fig. 27. Derivation of intercept values for Vostok using data from epoch 1997-2000 (blue line), 2001-2005 (red line), 2006-2009 (green line), and the average through 1997-2009 (magenta line).

The monthly mean hourly values are interpolated to give 5-min values. The raw and smoothed hourly intercept values and the 5-min interpolated values for day 15 of June and November are presented in Figs. 28a and 28b for Vostok. Like for the calculations of slope values, the QDC correction of the geomagnetic data can easily be switched on and off without changing neither data base nor data handling. Both cases are presented in Figs. 28a and 28b. For the intercept values there are significant and systematic differences between the QDC and non-QDC cases.

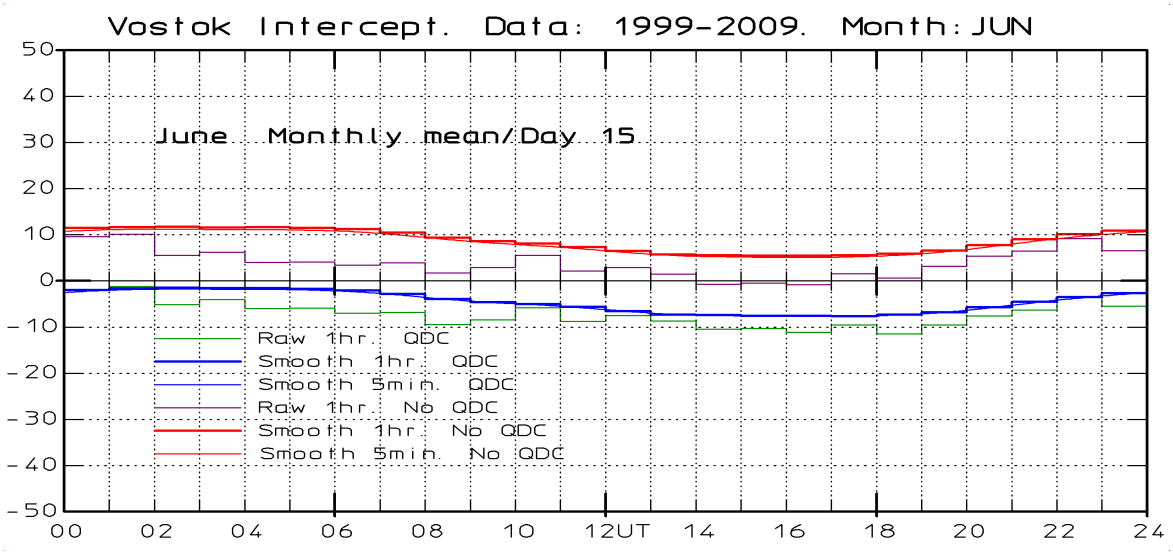

Fig. 28a. June intercept values for Vostok. Mean hourly values for June with/without smoothing, with and without QDC correction. Five-min values for day 15 with/without QDC correction.

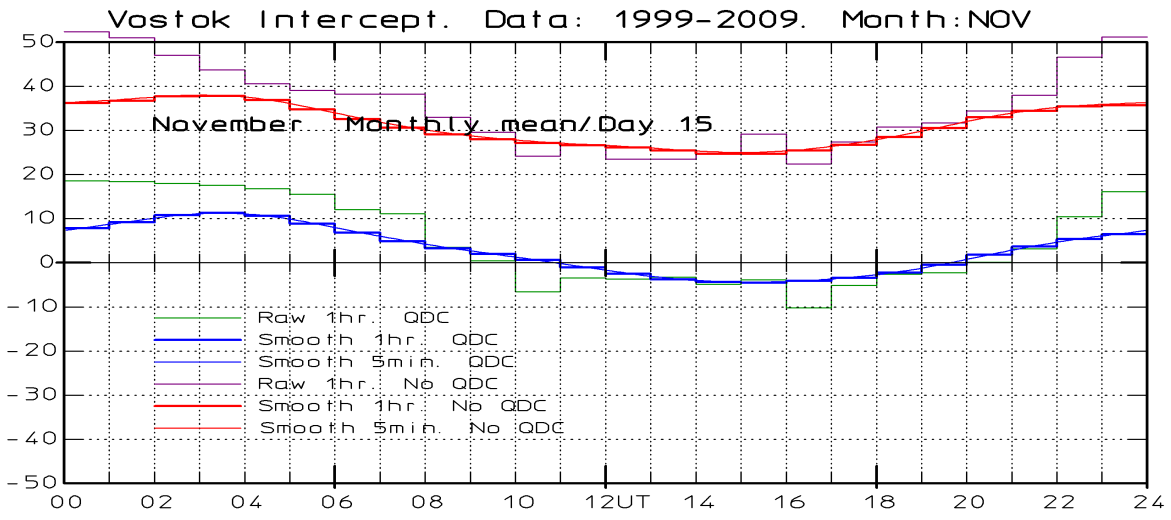

Fig. 28b. November intercept values for Vostok. Mean hourly values for November with/without smoothing, with and without QDC correction. Five-min values for day 15 with/without QDC.

Fig. 29 displays combined plots of optimum direction angle, slope, and intercept coefficients for Vostok. Like the corresponding diagrams for Thule in Fig. 19, the diagrams in Fig. 29 are divided in columnar fields for each month through the year marked along the horizontal axes. Each monthly field is subdivided in hours through a day. Monthly mean hourly values for a day of the index angle and coefficients are plotted within each columnar field. Parameters are derived with and without QDC correction of the geomagnetic data.

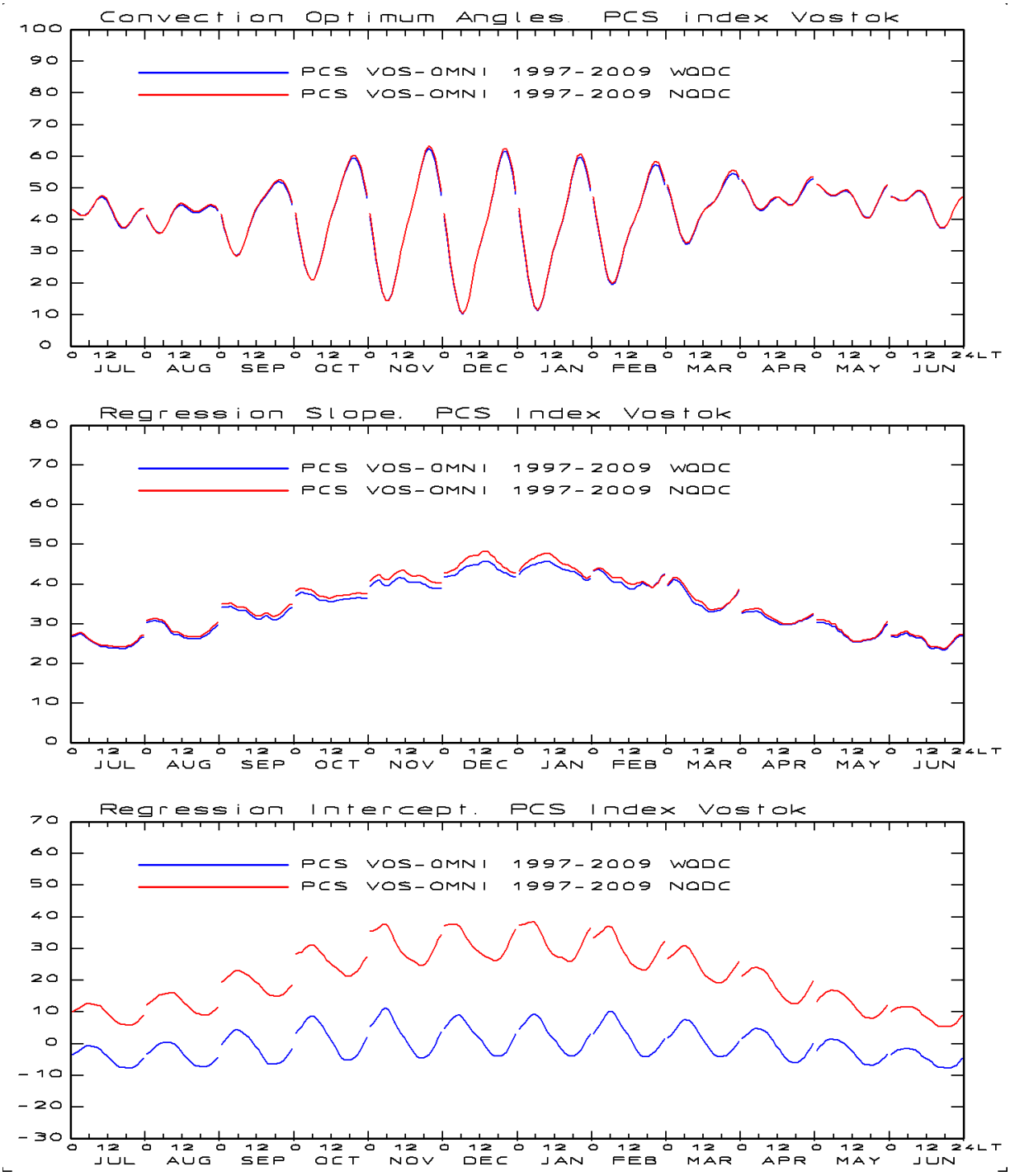

Fig. 29. Summary plot of optimum direction angle (upper field), slope (middle), intercept (bottom).

In Fig. 29, like in Fig. 19 for PCN parameters, the optimum direction angle is hardly affected by the QDC correction. The slope coefficient is little affected, while the intercept parameter, as expected, is substantially different in the QDC and no-QDC cases. The anticipated differences between the QDC and no-QDC cases are further discussed in section 15.4. There are large differences between the QDC/no-QDC variations presented here and the corresponding variations displayed in Fig. 1 of *Troshichev et al.* (2011).

14. PC index calculations for Vostok.

With tables of available PC index parameters, i.e., optimum direction angle, slope and intercept coefficients, interpolated to 1-min resolution it is now straight-forward to derive PCS index values. Recorded 1-min data for the horizontal geomagnetic vector (X_{RAW},Y_{RAW}) are corrected for the baseline and the relevant QDC values are derived using either the Solar Rotation Weighted (SRW) procedure for historical data (data from most of ±40 days must be available) or the HSRW procedure for actual (on-line) data (data from most of preceding 40 days must be available).

The QDC values (X_{QDC},Y_{QDC}) are subtracted from the baseline-corrected values in order to derive the geomagnetic variation vector value ($\Delta \boldsymbol{F}$) according to Eqs 25a,b. Now, the actual UT time and the observatory longitude are used with the tabulated optimum direction angle (φ) for that time to derive the projection angle (V_{PROJ}) according to Eq. 29. The projected scalar disturbance value (ΔF_{PROJ}) is derived according to Eq. 36. Finally, with the tabulated slope, α, and intercept, β, coefficients for the time and date in question, the PC index value is derived according to Eq. 3 (PC = (ΔF_{PROJ} – β)/ α)

To provide an example, PCS index values for 1-16 January 2002 are displayed (red line) in Fig. 30. Values of the related merging electric field (shifted by 20 min) are included (black line) in the diagram for comparison. The plotting is based on 5-min samples. This year is a solar maximum year.

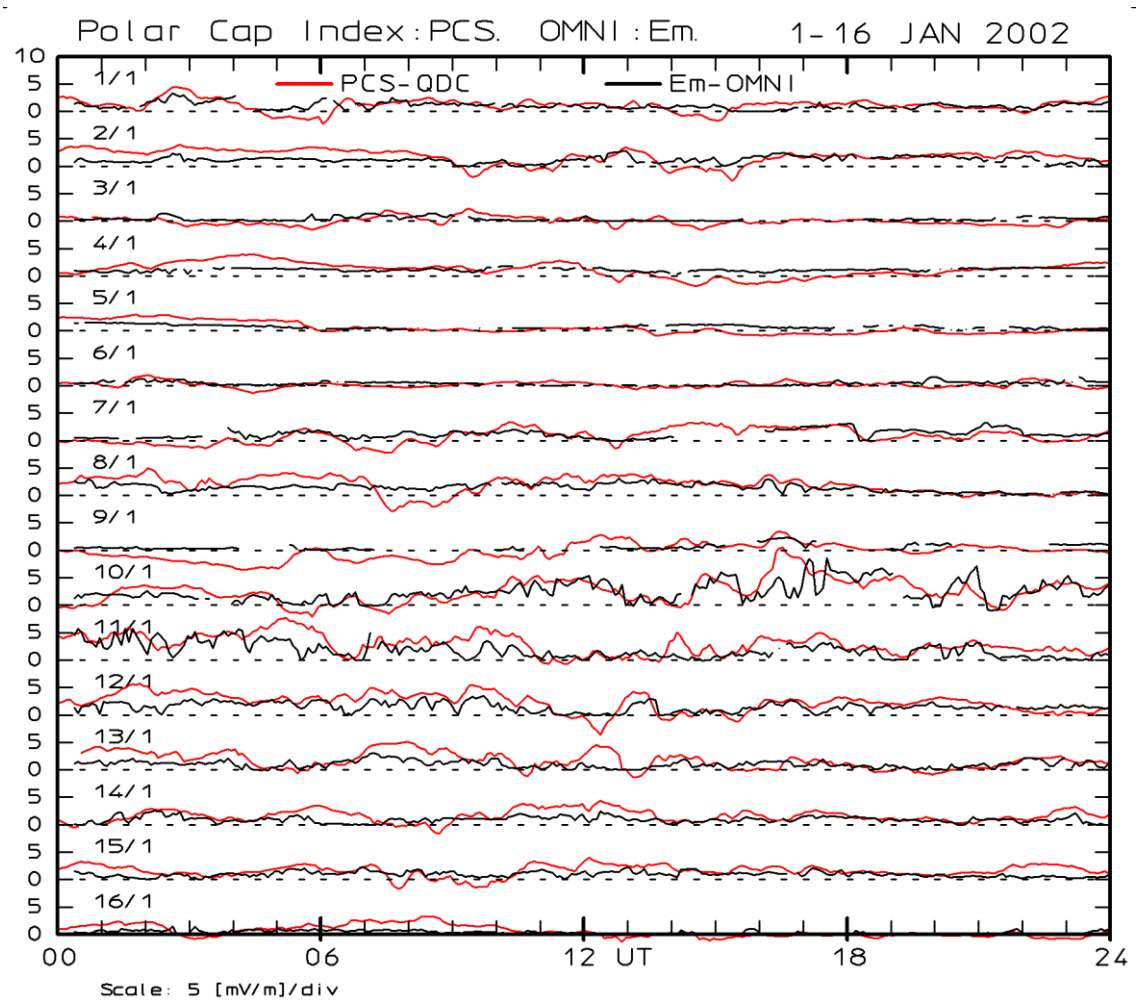

Fig. 30. Southern Polar Cap (PCS) index values (red line) for 1-15 January 2002. Values of the merging electric field ($\mathbf{E_M}$) are plotted in black line for comparison.

15. Discussions on PC index procedures

The discussion here relate to the validity of the above data handling processes and details for deriving QDC values, PC index coefficients, and PC index values with the procedure formulated in sections 2-14.

15.1. Accuracy requirements for PC index values.

The requirements on the accuracy of the derivation procedure in providing a reliable PC index value depend, of course, on the actual application. Cases of systematic uncertainties (or errors) in the index parameters (α, β, φ) are particularly troublesome for scientific studies. Such systematic uncertainties include non-justified variations in the parameters with time of day, season of the year, or IMF conditions. Such systematic uncertainties (errors) in the parameters could lead to incorrect interpretation of the daily or seasonal variations or might give false relations to further solar-terrestrial features.

From extensive investigations of the relations between PC index values and the ring current Dst index, *Troshichev et al*., 2011b, state "*It has been found that all examined storms, lying in the (*Dst*) range from -30 to -373 nT, started when the PC index and, correspondingly, the* E_M *field firmly exceeded the threshold >2 mV* m^{-1}". Correspondingly, *Stauning* (2007) and *Stauning et al*. (2008) found that PC values below 2 mV/m signal quiet conditions, while index amplitudes between 2 and 5 mV/m predict moderately disturbed conditions, and PC values above 5 mV/m indicate strong magnetic disturbances. From an investigation on the use of the PC index to forecast power line disturbances, *Stauning* (2013c) concluded that conditions, where the PC index maintains a level > 10 mV/m through more than one hour, would imply an imminent risk for the development of substorms intense enough to become a threat to power grids. *Troshichev and Janzhura* (2009, 2012) have studied the relations between PC index increases and substorm developments. They have reported that the growth phase, on the average, starts at PC index values of 0.24 mV/m for weak substorms, 0.25 – 0.55 mV/m for isolated substorms, and 1.6 mV/m for repetitive bay-like disturbances. The related sudden substorm onset, correspondingly, would happen, on the average, as the increasing PC index exceeded levels of 1 mV/m, 1.6 – 2.9 mV/m and 3.8 mV/m.

From the above examples, it might be concluded that uncertainties (or errors) below 0.1 mV/m are insignificant, systematic uncertainties between 0.2 and 1 mV/m are troublesome for scientific studies but minor for space weather forecasts, while systematic uncertainties (or errors) above 2 mV/m are prohibitive for science and critical for space weather applications. Through the basic formula in Eq. 3 these numbers can be transformed into corresponding geomagnetic disturbance values. The slope, α, ranges from 20 nT/(mV/m) during winter nights to 50 nT/(mV/m) during summer midday. Thus, the PC levels 0.1 and 2.0 mV/m correspond to levels of 2 and 40 nT, respectively, during winter nights and levels of 5 and 100 nT for either the projected magnetic deflection, the projected QDC level, or the intercept parameter, β. Uncertainties related to the slope parameter, α, give approximately proportional uncertainties in the PC index values. Uncertainties, δφ, in the optimum angle, φ, are transferred to the amplitude of the PC index with approximately a factor sin(φ)δφ.

15.2. Smoothing and interpolation of data.

The PC index parameters, generally, are derived as average values over an ensemble of selected data, for instance, all available samples through a specific hour for all days of a specific month, and through a series of years. The results could be strongly fluctuating and would need smoothing to become generally applicable. The smoothing should remove discontinuities in parameter values and slopes at transitions between intervals but be kept at a minimum. Furthermore, the smoothing should be robust to occasional occurrences of excessive data values. This requirement favours Gaussian-type smoothing (cf. Eq. 32) over, for instance, Cubic Spline or other higher order polynomial-based smoothing schemes.

There is no prescribed method for the level of smoothing. For the quiet day curve (QDC), to be discussed in section 15.5, the amplitude-reducing effects of smoothing is adjusted to balance the amplitude-increasing effects of including samples not completely quiet (cf. Fig. 35). From this process a set of

values of the half width for the Gaussian weight function and the range of summation of samples is defined. The method of smoothing has been applied to further parameters. Here, half widths of 4 hrs in time and 2 months in season are generally used, while the summation ranges are extended to twice the half widths. This choice has been justified through the appearance of the processed data as the level of smoothing was gradually increased until odd jumps have disappeared.

A further issue is the conversion of stepped average values, for instance hourly samples, to a smooth function (finer resolution). The integral of the that function through the step length should equal the step average value. This condition may work properly in-between extreme values. However, at maxima the smoothed function values will be less than and at minima larger than the step values. This deficiency is counteracted by introducing a "peak amplitude enhancement" modification of the data samples (cf. Eq. 33). The enhancement constant, A=0.25, used here was found by comparing the integral of the smoothed function to the original step values for a range of relevant data sets. Typical results of the smoothing and peak amplitude enhancement modifications were shown in Figs. 14a,b, 16a,b, and 18a,b for Thule and in the corresponding diagrams in Figs. 24a,b, 26a,b, and 28a,b for Vostok.

15.3. Handling of solar cycle variations.

The possibility that PC index parameters (α, β, φ) could have variations with the level of solar activity should be considered. In its extreme consequence one could think of deriving different sets of parameters for low, moderate and strong solar activity, respectively. Different opinions have appeared in past investigations. *Papitashvili et al.* (2001) deduced considerable variations in index parameters over the solar cycle. On the other hand, *Troshichev et al.* (2011a) claim "*Invariability of the relationship between the polar cap magnetic activity and geoeffective interplanetary electric field*" (title of their paper). Their work was based on examination of the PCS index. However, Fig. 63 here compares the PCN index coefficients (AARI#3 version) displayed in *Troshichev et al.* (2006) based on the solar max. epoch 1998-2001 with the IAGA-endorsed PCN coefficients (http://pcindex.org) based on a complete solar cycle, 1997-2009 (includes solar min years), and discloses considerable differences in index coefficients. At midday hours in the summer season the AARI#3 coefficient values are α=95 nT/(mV/m), β=-105 nT, while the IAGA values (also derived by AARI) are α=65 nT/(mV/m), β=-40 nT (cf., Figs. 52 and 59).

The problem of possible variations in PC index coefficients is handled here by subdividing the epoch, a full solar cycle, over which the parameters are derived, into subintervals of which the two represent conditions of moderate to strong solar activity, while the third represents conditions of low to very low solar activity. As a by-product, the subdivision also serves to disclose whether erroneous data have entered the statistics in one subinterval to give unreasonable deviations from the results derived for the other two intervals.

For Thule, results of the subdivision are displayed in Figs. 13 (φ), 15 (α), and 17 (β). For the optimum direction angles (φ) there are no systematic differences. For the slopes (α) there is a tendency that the slopes are a little larger, and that the intercept values are a little more negative, at midday during low solar activity than otherwise. For Vostok, the results are displayed in Figs. 23 (φ), 25 (α), and 27 (β). Here, there is the tendency that the optimum direction angles are a little larger during low solar activity, while there are little systematic variations in the slope and intercept coefficients. In summary, the variations with the level of solar activity are considered so small that using separate sets of coefficients would be an unreasonable complication compared to just using the averages over the three subintervals.

There is a simple explanation to the above conflicting results. The large differences in the PCN coefficients over the solar cycle, as will be explained in section 15.6, relate to the inclusion of strong reverse convection cases in the data base used for calculation of index coefficients by *Papitashvili*, 2001, and *Troshichev et al*., 2006. Such events are much more frequent at solar max. than at solar min. epochs and more frequent at Thule than at Vostok. For the index procedure presented here, the strong reverse convection events are excluded (cf. section 15.6) and the variations in PCN as well as the PCS index coefficients are small for different phases of the solar cycle.

15.3. Inclusion of QDC in PC index calculations.

It has been argued in publications (e.g. *Lukianova et al*., 2002, 2007; *Troshichev et al*., 2011) that large differences would arise between PC indices derived by different procedures which did or did not include QDC correction of the geomagnetic data. In Lukianova (2007) it is argued that "*It is important to understand that the factor that crucially affects the final value of PC is the choice of QD curve versus QWL line. If we choose the QD approach, the PC is more sensitive to the variations in the IMF and SW.*" This statement is illustrated in Figure 3 of that paper (QWL is Quiet Winter Level, also termed QWNL for Quiet Winter Night Level).

However, the argument is not correct! Omitting QDC in the processing of data, in reality, corresponds just to use, through the intercept parameter, the same set of daily and seasonally varying QDC values year after year. There is no substantial change in index "sensitivity" to E_M. This is explained in Fig. 31. Observations made at the same UT time on several consecutive days are considered. For these days the projected QDC level is assumed to be Fq ($=F_{QDC,PROJ}$) at the selected UT time. For the 2 days we assume that corresponding values of E_M and ΔF_{PROJ} are known. Hence, from these two days we can calculate the slope and intercept parameters without and with QDC correction.

The figure illustrates that the slope (i.e. α in Eqs. 1 and 3 in section 2.2), which could be termed index "sensitivity" to E_M , is precisely the same in the two cases ($\alpha_2 = \alpha_1$). The intercept β in the figures is changed by the amount Fq in case 2 relative to case 1 ($\beta_2 = \beta_1 - Fq$). No matter how many points we add to calculate regression coefficients for this time, the result is the same. When, subsequently, the PC indices are calculated from new values of ΔF_{PROJ} by using in Eq. 3 the slope and intercept parameters estimated in the two cases without and with QDC correction the results are:

Case 1: $PC_1 = (\Delta F_{PROJ} - \beta_1)/ \alpha_1$ (29)

Case 2: $PC_2 = ((\Delta F_{PROJ} - Fq) - \beta_2)/ \alpha_2 = ((\Delta F_{PROJ} - Fq) - (\beta_1 - Fq))/ \alpha_2$

$= (\Delta F_{PROJ} - \beta_1)/ \alpha_1 = PC_1$ (30)

The incorrect conclusion on the large improvement in sensitivity to E_M variations by the QDC correction as argued in *Lukianova* (2007) is conveyed by the stated assumption: "*For simplicity in the following discussion we will neglect* β." As shown here the "sensitivity" (the $1/\alpha$ value) remains the same whereas the intercept value (β) is changed with the QDC correction compared to the result without this correction. From Fig. 31 it is also easy to see that possible variations in Fq with the activity level in the solar cycle at this time of the day and day of the year will have the same effect as possible modifications in the intercept parameter over the solar cycle (cf. Papitashvili et al., 2001).

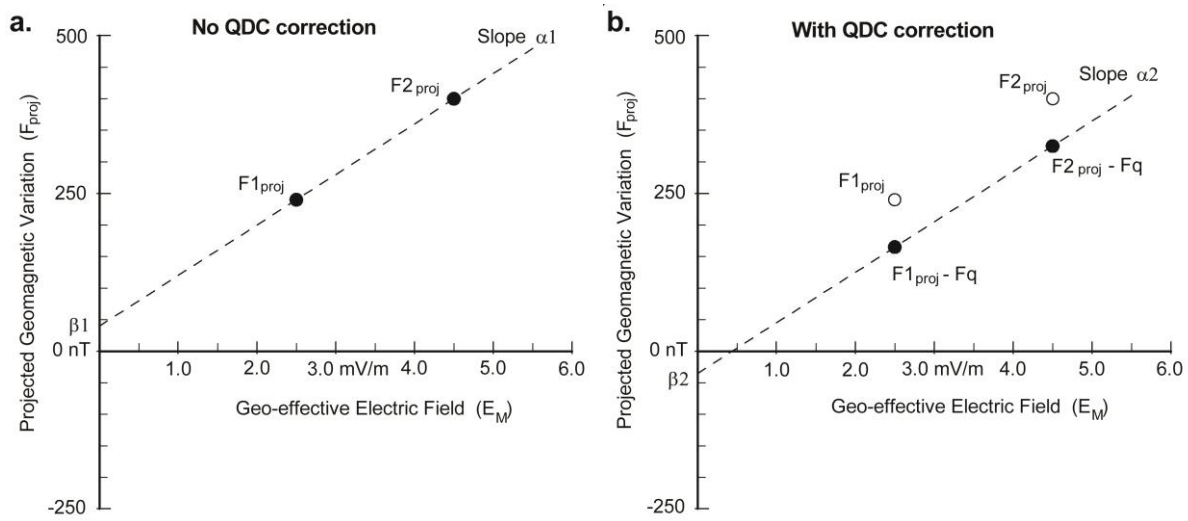

Figure 31. Illustration of calculation of slope and intercept parameters without QDC correction (left field, case 1) and with QDC correction (right, case 2). (from *Stauning*, 2013)

For the calculation of PC index values the QDC handling should, of course, be the same for the calculation of coefficients (angle, slope, and intercept) as for the final calculation of index values. When this is done properly, the actual differences in the PC indices calculated with and without QDC corrections are fairly small in most cases. This is illustrated in Fig. 32 with a display of the differences between PCN index values (5-min samples) calculated with and without QDC correction through 2002, a solar maximum year. Here, the differences are numerically largest in the summer season and mostly negative since the no-QDC intercept increases (cf. Fig. 29) are smaller than the projected QDC.

In solar minimum years the no-QDC intercept increases are generally larger than the projected QDC level and the differences between PCN values calculated with and without QDC are mostly positive. In either case the differences are less than 1 mV/m in magnitude. Hence, for applications of PC index values for space weather forecasts, the use of no-QDC coefficients would make the calculations simpler and reduce the risk that missing or incomplete data for the foregoing days could give erroneous QDC levels and thus cause false real-time PC index values.

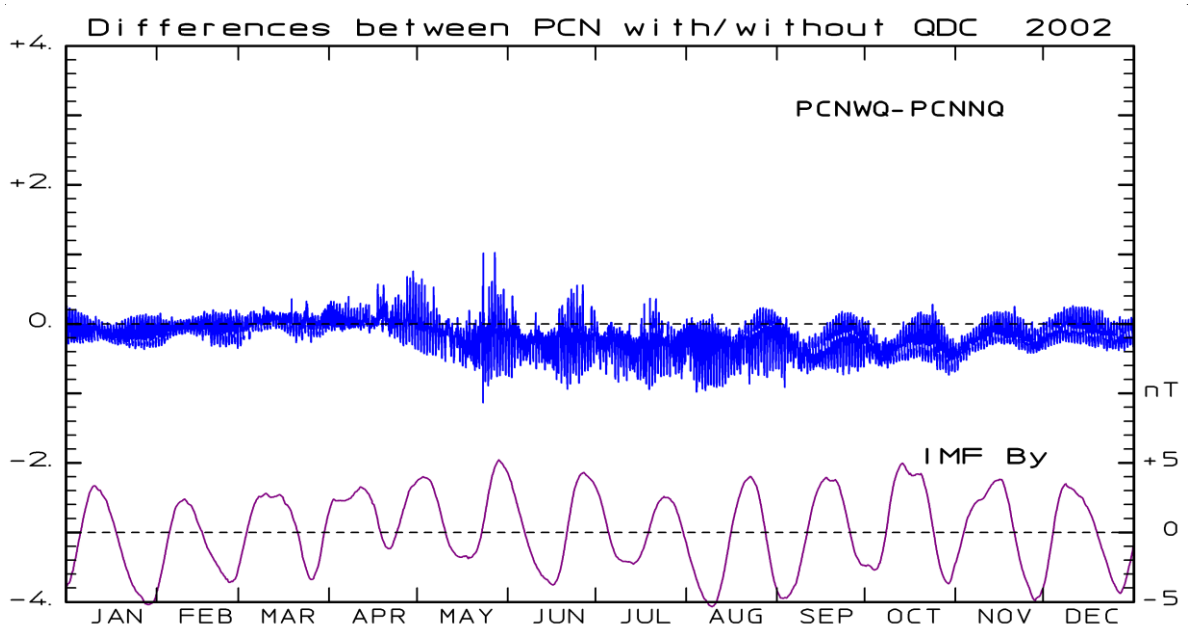

Fig 32. Differences between PCN indices calculated with and without QDC correction. Smoothed IMF By values included for reference to possible solar wind sector effects. Data from 2002.

It should also be noted that the QDC has very little effect on the calculation of the optimal direction since this direction is based on optimum correlation of the projected polar magnetic variations with the merging electric field. The QDC is derived, in principle, for conditions where the merging electric field is vanishingly small. Hence, its inclusion could not affect the correlation of magnetic variations with the merging electric field other than adding to the "noise " level.

15.5. Discussions of the QDC procedure.

This section first discusses the QDC derivation scheme. The selected functions and parameters are explained and the possible consequences associated with the specific choice of parameters are outlined in order of appearance in the steps of the QDC procedure described in section 6.

15.5.1. Baseline values and reduction of raw data. For the calculation of PC index parameters and index values, the reduction of the raw data before calculation of QDC values is not important. For such application the important parameter is the total quiet level, QL=Baseline+QDC, which is subtracted from the raw data to determine the desired magnetic variations. The primary advantage of the baseline subtraction resides in the potential for correction of effects related to discontinuities in the recorded levels caused, for instance, by replacement of instruments. Another issue is the reference of the QDCs to ionospheric properties. If the baseline values represent the levels for "internal" contributions to the field then the derived QDC values reflects the ionospheric (and magnetospheric) current systems and their induced counterparts in the ground. Thus the QDCs derived for different stations or different years and seasons may be compared on a consistent basis for mutual verifications.

15.5.2. Data variability functions and parameters. We use here in the solar rotation-weighted (SRW) QDC procedure (*Stauning*, 2011b) the variability in the horizontal magnetic vector rather than the variability in the individual components in order to make the selection of quiet intervals independent of the representation of the magnetic components (e.g., *X*,*Y* vs. *H*,*E*).

The use of two different variance quantities, the max. time derivative, δHt, and the average variability, δHv, shall prevent mistakes in the selection of quiet intervals. Basically, recordings appear to be "quiet" when they are smooth (low time derivative values), but they should also have small variations with respect to the mean level (i.e., small slopes) within the hour (low average variances) in order to be classified as truly quiet. The functional representation of the weight function should enable a moderate reduction in weight for values close to minimum variance and a strong reduction in weight for large-amplitude magnetic deflections and possible outliers. The actual values of the exponent range parameters, *RTL* and *RVL*, are based on a compromise between wanting them as small as possible to select very quiet samples and the need for a substantial data basis for the QDC comprising many valid samples. In general the QDC amplitudes increase with increasing variance range parameter values but, as to be discussed in section 15.3.4. and illustrated in Fig. 35, this tendency can be counteracted through the smoothing.

For the calculation of initial QDC values the use of hourly samples is a reasonable choice. A time interval of some length is needed to decide whether a sample is quiet or disturbed. Furthermore, in the derivation process, the QDC values are smoothed over several hours. Hence, a more detailed sampling of initial QDC values would have no practical effect. At applications of QDCs (for instance, for calculation of PC indices), the hourly QDC values are interpolated to give the same time resolution (e.g., 5-min or 1-min samples) as that provided in the component data.

15.5.3 Date difference and solar rotation functions and parameters. It is necessary to consider a range of data in order to reliably construct a QDC from quiet segments. These segments should refer as closely as possible to the conditions prevailing at the QDC day in question. Starting from the day in question, many of the solar features of importance for the QDC (e.g., solar magnetic field structure, coronal holes, active sunspots) will gradually change with the progressing solar rotation to be completely different at the face of the Sun seen from the Earth half a solar rotation later. Then, with somewhat reduced probability, they may gradually re-appear during the second half of a full rotation period.

The most important parameter to be considered in this connection is the IMF B_Y variations associated with the sector structure in the IMF. The potential effect of the IMF B_Y parameter is evident in Fig. 33. There are substantial differences between the average daily variation in the geomagnetic H-component for conditions with strongly positive IMF B_Y>3 nT (red, dashed line), numerically small values -2<IMF B_Y<2 nT, and strongly negative values IMF B_Y<-3 nT. Like shown in Fig. 54, these differences appear the same if just quiet values are considered.

It should be noted that the H-component levels are almost equal irrespective of the IMF B_Y level during local night (00 – 10 UT), while the largest differences develop around local noon (~ 16 UT).

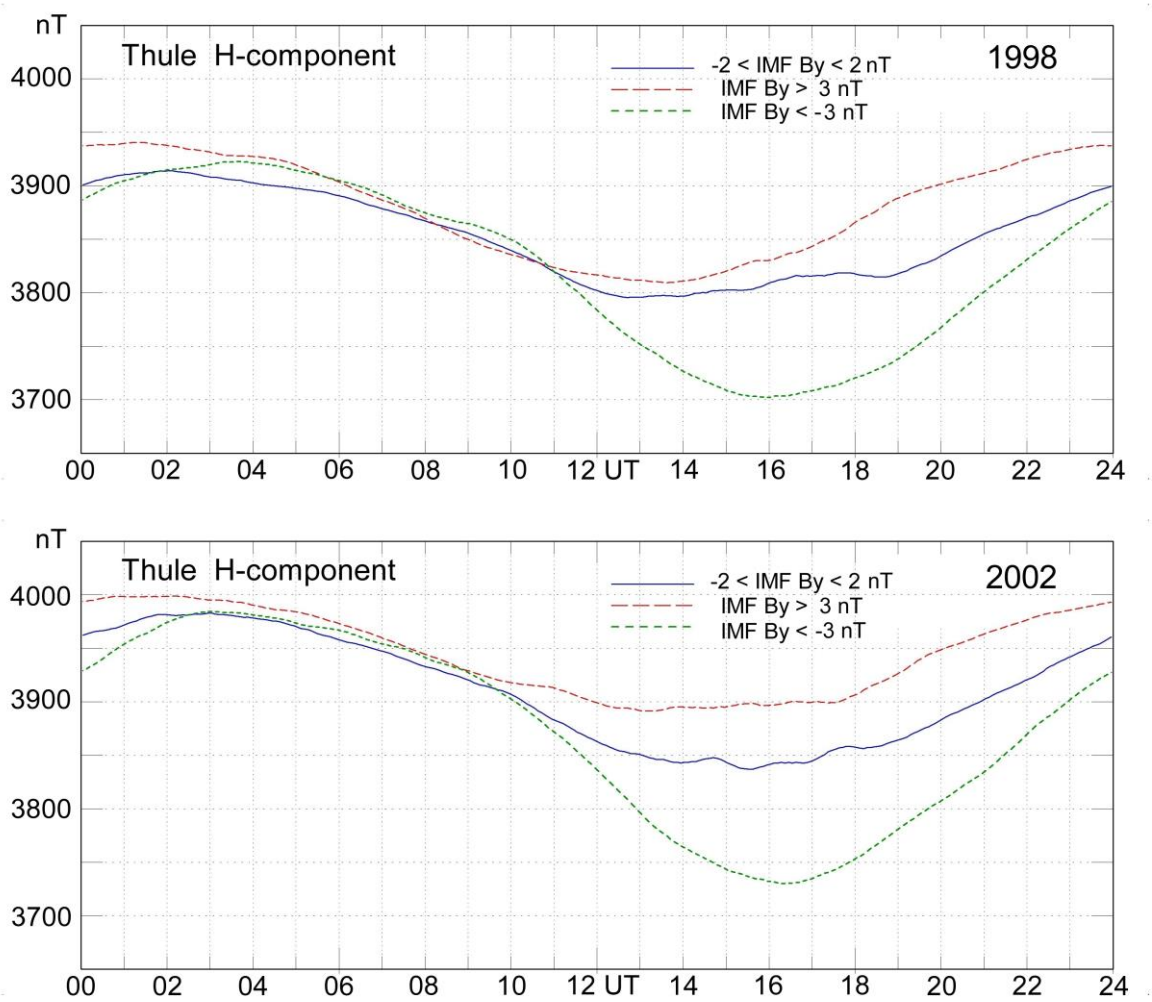

Fig. 33. Average daily variation of the Thule H-component for different levels of the IMF B_Y parameter in a solar quiet year (1998) and a solar active year (2002). Local noon is at ~ 16 UT.

The level of solar ultraviolet radiation, assumed proportional to the *F10.7* microwave level, is important for the QDC variations, and the solar wind velocity could also affect the QDC level. Fig. 34 displays the auto-covariance (recurrence) for IMF B_Y, *VSW*, and *F10.7* for single years and averaged over the entire interval (red line). It is evident from the top field of Fig.34, that the average recurrence tendency with IMF B_Y is as high at a shift of 27 days as found after a shift of less than 2 days. For the solar wind velocity the average recurrence at 27 days equals that found at a shift of around 2 days with respect to the day in question. For the 10.7 cm radio flux (*F.10.7*) the average recurrence at 27 days equals that found at a shift of 7 days.

The selection of days used to build a QDC should primarily comprise the days closest to the day in question supplemented with some days shifted by a solar rotation period (*LSR*) of around 27 days. The solar rotation weight factor should resemble the combined auto covariance (recurrence) function for the parameters of importance for the QDC to give highest weights to days where the conditions with high probability are the same as those on the QDC day in question. The exact shape of the weight function used to implement the selection must build on a compromise between the selection of the few optimal days and the need for a substantial data base for the QDC. The selected function, the cosine squared of half the solar rotation angle, complies with these constraints.

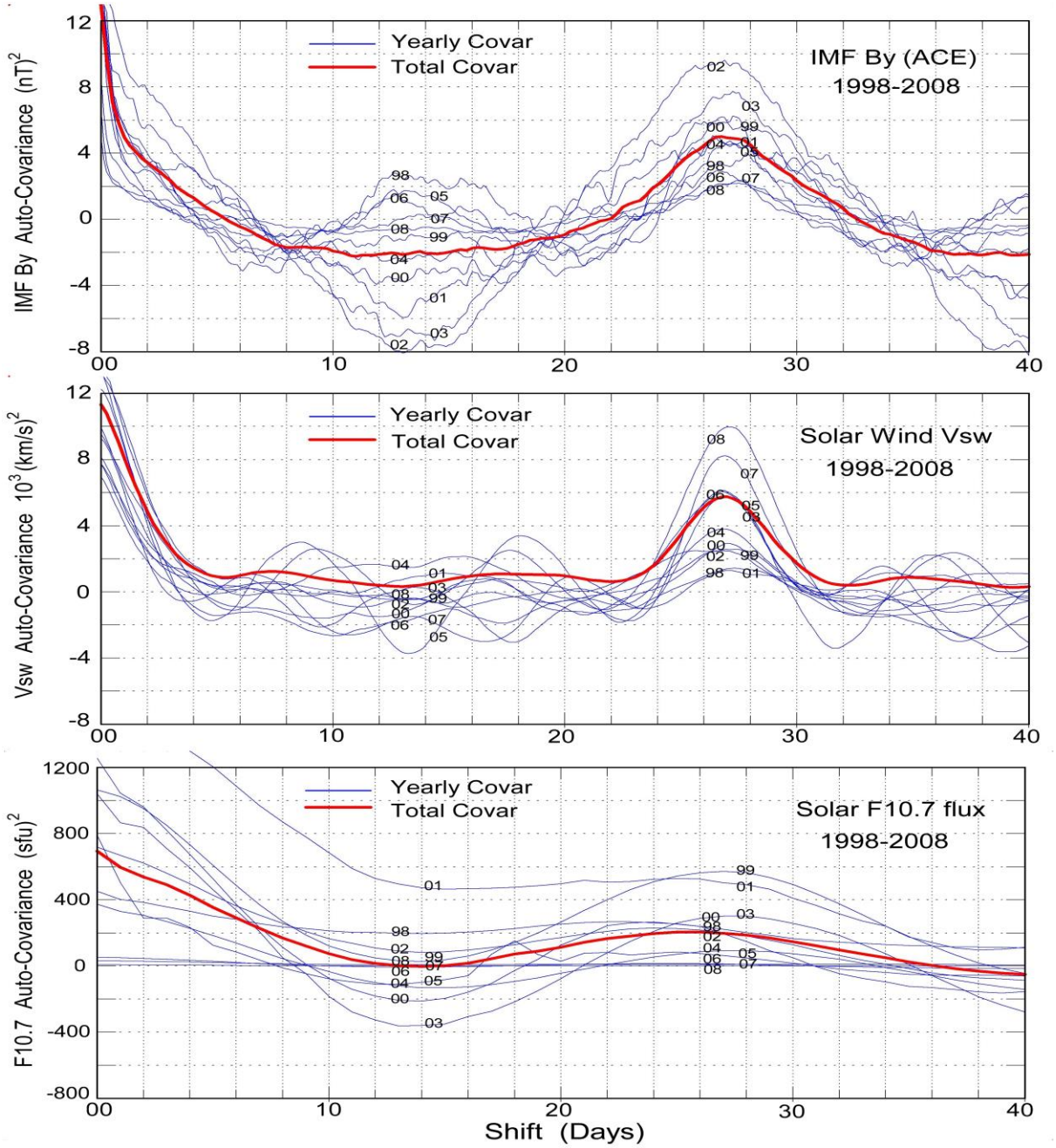

Fig. 34. Plot of covariance (recurrence) features for IMF B_Y (upper field), solar wind velocity, V_{SW} (middle field), and solar *F10.7* flux (UV proxy) (bottom field). Data year (2 digits) noted at the curves (from *Stauning*, 2011b).

In order to take into account the reduced probability that the same seasonal, solar, and solar wind features are present at days separated widely from the day in question, the date difference should be included in the weighting. A Gaussian function is used here and the argument, *RDD*, is selected such that the total weight of the combined date difference and solar rotation weight factors over the solar rotation period around the day in question equals the total weight of the two solar rotation periods displaced by one *LSR* to earlier and later dates, respectively. The use of oppositely displaced data intervals compensate for the gradual changes in QDC values with season, which are strongest at equinoxes.

At solstices the seasonal changes are minimal and the use of displaced intervals may enhance (winter) or reduce (summer) the QDC amplitudes by tiny amounts only. The limits at – and + *LDD* amount of days of the interval of data used to build a QDC are set at ±40 days to include one full solar rotation interval (*LSR*) preceding and one following the rotation period centered at the day in question. At either limits the weight function values are at minimum (near zero), which implies that the shift to the next (or the preceding) QDC day, with a shift of the data interval by one day, will not involve sudden large contributions that could give erratic variations in the derived QDCs.

15.5.4. Smoothing of QDC values.

The smoothing of initial QDC values is also an essential step in the processing. The smoothing should not impose any specific functional shape onto the QDCs, and the inevitable reduction in QDC amplitudes should be minimized. Hence a Gaussian smoothing procedure has been selected over, for instance polynomial smoothing, Fourier smoothing schemes, or smoothing by simple running averages. The degree of smoothing is controlled by the scale parameter, *RHR* (4 hours, cf. Table 3), in combination with the length, *LHR* (8 hours), of the interval used for the smoothing. It is important to control the reduction in QDC amplitude caused by the smoothing. Therefore, the QDCs have been calculated for varying degrees of smoothing, that is, for varying values of the scale parameter, *RHR*. Examples of such calculations for Thule QDC data are displayed in the four panels of Fig. 35 for the months Jan, Apr, Jul, and Oct 2002. The diagram within each panel has a vertical scale for the monthly average total QDC amplitudes (min-to-max). Along the horizontal axis there is a scale for the smoothing parameter, *RHR* (0-10 hours).

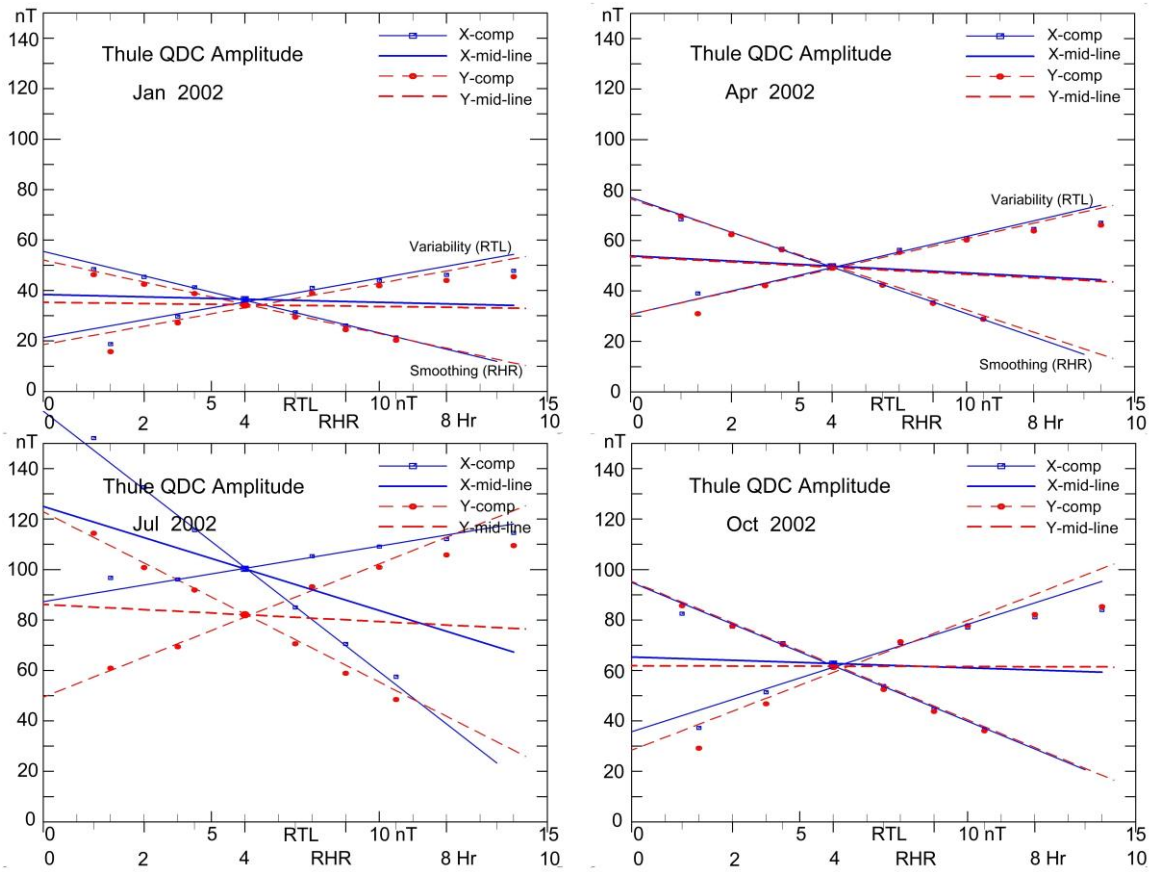

Fig. 35. Effects of the variance and smoothing parameters, RTL and RHR, on the amplitudes of the derived QDCs through selected months (different seasons) (from *Stauning*, 2011b).

The two downward sloping sets of points in Fig. 35, one for the QDC-X amplitudes marked with blue squares, the other for the QDC-Y amplitudes marked with red circles, display the monthly average QDC amplitudes calculated using the related smoothing parameter, *RHR*, while all other parameters have been given their normal values (cf. Table 3). The lines plotted along the sets of points have been derived by regression based on the points closest to the standard value of *RHR* (4 hours). The intersects of the lines with the vertical axis (*RHR*=0) correspond, in principle, to the QDC amplitudes derived without smoothing.

The horizontal axes also have a scale (0-15 nT) for the data variance weight parameter, *RTL*. In calculations of the QDC values the other variance parameter, *RVL*, has been given twice the value of *RTL*. The upward sloping sets of points represent QDC amplitudes calculated for varying values of *RTL* (and *RVL*) while other parameters have been given their standard values (cf. Table 3). For large values of *RTL*, the QDC amplitudes would be more than 100 nT. Corresponding to the smoothing cases, lines derived by regression based on the points closest to the standard values, *RTL*=6 nT and *RVL*=12 nT, have been drawn to intersect the vertical axis (*RTL*=*RVL*=0). The intersect values correspond, in principle, to extremely quiescent conditions. The mean QDC amplitude between the intersects for the "smoothing" and the "variance" lines can be considered the optimum QDC amplitude for very quiet conditions and little smoothing. The points marked by larger squares and circles represent the use of standard parameters (cf. Table 3) for variance weighting and smoothing. If these points display the same amplitudes as the "optimum" mean intersects (giving horizontal connecting lines), then the effects of using the standard variance and smoothing scaling parameters are considered to balance each other properly for the derivation of final QDC values.

This condition works nicely for the winter and equinox months but not quite as well for midsummer. In the diagram for July (lower left panel of Fig. 35) the "middle" line for the *QDC-Y* component has a negative slope, which would indicate too much smoothing. However, referring to the representative example weight function list for 1 July, 2002, displayed in the rightmost section of Table 4, the weight function values are very low for this summer month, particularly around noon (~16 UT) where the *QDC-Y* component maximizes. The small weight function values indicate that the samples used to construct the QDC are far from quiet and may thus take values above the true level. Thus, the apparent strong smoothing is in this case well placed to damp excessive peak values in the QDC amplitudes.

15.6. Reverse convection cases

As explained in section 9.2., with an overhead reverse convection flow, the magnetic deflections at ground are opposite to those of the forward convection mode. Accordingly, the projected disturbance vector may become less than the QDC level or even strongly negative. The defining equation, on which the PC index concept relies, assumes proportionality between the projected polar magnetic variations and the merging electric fields ($\Delta F_{PROJ} = \alpha \cdot E_M + \beta$, cf., Eq. 1). Recalling that $\Delta F_{PROJ} = (\boldsymbol{F} - \boldsymbol{F}_{QDC})_{PROJ}$ where $\boldsymbol{F}$ is the baseline-corrected magnetic deflection vector, while $\boldsymbol{F}_{QDC}$ is the QDC vector, we could rewrite Eq. 1. to the equivalent form:

$$(\boldsymbol{F} - \boldsymbol{F}_{QDC})_{PROJ} = \alpha \cdot E_M + \beta \qquad (31)$$

Now, for extremely quiescent conditions, where the merging electric field, E_M, is zero, we would expect that the magnetic deflection shall resort to just depict the QDC variation (i.e., $\boldsymbol{F} = \boldsymbol{F}_{QDC,}$). Hence the intercept value, β, must be close to zero. When actual calculations of the intercept give another result then the calculations are possibly influenced by cases of reverse convection.

Fig. 36 (from *Stauning*, 2013) illustrates the consequences of reverse convection cases for the calculation of regression coefficients. We consider observations made at the same UT time on several consecutive days (as in Fig. 34). For these days the projected QD level is assumed to be *Fq* at the selected UT time. For the 3 days we assume that corresponding values of E_M and ΔF_{PROJ} are known. Hence, from these three days we can calculate the slope and intercept parameters, for instance, with QD correction as suggested in the figure.

Now, we assume that one day is a reverse convection case ($\Delta F_{PROJ} < 0$), while the two remaining days are normal forward convection cases ($\Delta F_{PROJ} > 0$). E_M is always positive or zero (non-negative).

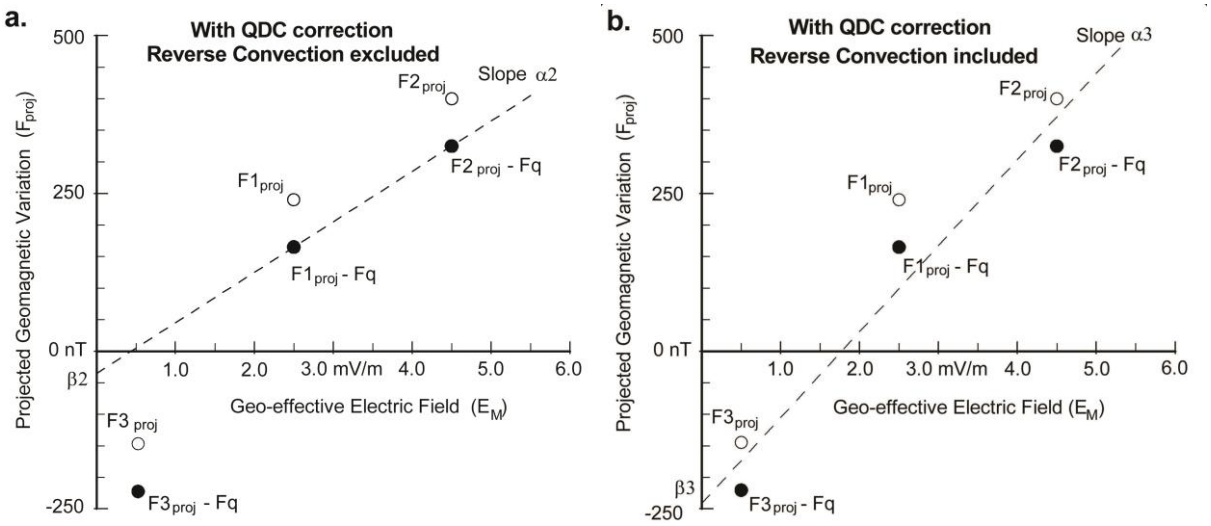

Figure 36. Illustration of effects of reverse convection cases on calculation of regression coefficients.

In the left field of Fig. 36, the slope, α2, and the intercept, β2, have been calculated without the reverse convection case. Usually β2 would be quite small. In the right field, the reverse convection case is included in the best fit (least squares) calculation of the slope, α3, and intercept, β3. It is obvious in Fig. 36 that the slope is larger (α3 > α2) and the intercept more negative (β3 << β2) when reverse convection cases are included. This trend will hold also when more points are added to the statistics.

The calculation of PC index values should, of course, proceed from values of the actual magnetic disturbances using the calculated set of regression coefficients. Some obvious consequences for the PC index values of using either of the different sets of coefficients from the two cases are the following:

(i) For cases of medium disturbances (medium $\Delta F_{PROJ} = F_{PROJ} - Fq$, $Fq=F_{QDC,PROJ}$) the differences between PC indices calculated by using either of the two sets of regression coefficients in Eq. 3. will be fairly small. The smaller value of the slope term ($\Delta F_{PROJ}/\alpha$) will be compensated by the larger intercept term (- β/α).

(ii) For large disturbances (large ΔF_{PROJ}) the slope term ($\Delta F_{PROJ}/\alpha$) will dominate and calculated PC indices will be smaller using the larger slope coefficient (α3), derived with reverse convection cases included, than the index values calculated using the slope (α2) derived without reverse convection cases.

(iii) For weak disturbances (small ΔF_{PROJ}) the intercept term (-β/α) will be important, and the PC index values will be larger when calculated using regression coefficients derived with reverse convection cases included. Although the α value is larger, the much larger negative value of β makes index values larger than values calculated using coefficients derived without reverse convection cases included, where β≈0..

(iv) For intervals of vanishingly small disturbances, i.e., extremely quiet conditions ($\Delta F_{PROJ} = F_{PROJ} - Fq \sim 0$) , there will be an odd "hump" in the PC indices (ΔPC = -β/α). The humps are strongest around local noon and in the summer season where the reverse convection cases are most frequent.

For the PC index to be considered a valid index of geomagnetic disturbance level in response to solar wind and IMF conditions, it must be required that the index values are close to zero for very quiet conditions. From this requirement it follows immediately that the intercept values must be numerically small for the calculations with QDC corrections and close to the values of the projected QDC for calculations without QDC corrections.

This requirement implies that reverse convection cases must be excluded whether or not QDC corrections are implemented. There are various methods to implement this condition. One way is to use previously calculated regression coefficients with the actual projected magnetic variations to calculate a preliminary index value and then omit data where this value turns out strongly negative (for instance less than -1).

The method implemented here uses a combination of actual IMF values and projected magnetic variations. For the IMF it is required that IMF B_Z < | IMF B_Y | + 3.0 nT. This condition excludes cases where the northward IMF B_Z is a strong and dominant component. A further condition imposed on the selection of data requires that the projected magnetic variation, ΔF_{PROJ}, is larger than -50 nT (corresponding to PC index values larger than -1 mV/m). This condition ensures that cases with strong reverse convection, which may continue for a while after the driving northward IMF has been reduced or has changed polarity, are also omitted from the data base used to calculate the coefficients.

Both methods affect the regression results such that the resulting intercept parameter in the QDC-corrected cases could be kept at low values ($|\beta|$ less than ~ 10 nT) or, correspondingly, β values close to projected QDC values when the coefficients are calculated without QDC correction. Actually, it would not change much in the final PC index values calculated with QDC correction if the intercept parameter was completely discarded after adjustments of the reverse convection limits to keep the intercept at low values.

For index procedures where QDC corrections are not applied, the intercept parameter makes sense to provide a solar cycle-average QDC-equivalent quantity. However, when QDC corrections are applied then there is no physics-based, rational argument for the intercept parameter. Furthermore, in this case calculations of the intercept value from different data base intervals indicate values that fluctuate inconsistently around zero (cf. Figs. 17,19,27,29).

16. Discussions on PC index properties.

16.1. Impact of IMF By and sector structure variations.

Like mentioned in section 4, the solar wind magnetic field variations are to some degree ordered by the so-called “sector structure” detected by Svalgaard (1968) and Manzurov (1969) from studies of polar magnetic variations. On either side of the magnetic ecliptic plane, the large-scale magnetic field extending from magnetic regions at the Sun is associated with outgoing or ingoing field lines and thus divides conditions at the Earth in sectors where the preferred interplanetary field direction is either “toward” the Sun (positive IMF B_X component) or “away” (negative IMF B_X).

A further feature is the stretching of the field lines by the outward streaming solar wind plasma. Due to the solar rotation (~27.4 day’s period) the stream of plasma will have a spiral look (garden hose effect). This spiral shape is to some extent transferred to the magnetic field lines. Consequently, the sign of the azimuthal component, IMF B_Y, is coupled to the sign of the IMF B_X component such that positive IMF B_X values in “toward” sectors are generally associated with negative IMF B_Y values while negative IMF B_X values in “away” sectors are associated with positive IMF B_Y values.

The sign of the IMF By component affects the patterns of the transpolar convection within the central polar cap. For the northern polar cap the transpolar convection patterns and the associated geomagnetic variations are generally rotated CW for positive IMF B_Y with the strongest effects appearing at the dayside. The rotation of convection patterns causes phase variations in the components of the magnetic variations. In the projection to the optimum direction, which is an average over IMF B_Y values, the projected geomagnetic variations and thus the PC index values may be affected by the B_Y component beyond its effects on the merging electric field, E_M, where the sign of B_Y has no impact (cf. Eq.2). The IMF B_Y effects are mitigated by using a QDC method like the Solar Rotation Weighted (SRW) method that includes B_Y effects on the convection patterns during the stronger, repetitive cases (cf. Fig. 3).

16.2. Negative PC index values.

The two-cell polar ionospheric "forward" convection is the most common convection mode. It applies to solar wind conditions where the interplanetary magnetic field (IMF) is either southward oriented or only weak in magnitude when northward directed. The transpolar convection flow that generates the QDC variations are generally oriented much the same as the two-cell forward convection patterns. During NBZ conditions the forward convection associated with the QDC would be impeded and reverse convection may result. Now the magnetic deflections are opposite of those of the forward convection mode. Accordingly, the projected disturbance vector, and thus the PC index values, calculated during NBZ conditions may turn out to be negative. Since the interplanetary merging (geo-effective) electric field (E_M) by definition is always non-negative (cf. Eq. 2) then the concept of the PC index as a proxy for the E_M breaks down. For cases of northward oriented IMF the E_M values will be rather small but still positive, while the PC index could take large negative values, which in no way are proportional to the merging electric field.

In consequence of this problem one should disregard the reverse convection cases in the derivation of regression parameters (optimum direction angle, slope and intercept) while the calculated negative PC index values, of course, should be retained in the index series but just taken to indicate northward IMF of some undefined magnitude.

16.3. Epoch of reference data.

For the derivation of PC optimum correlation angle, and the slope and intercept regression parameters an extended selection of data is required in order to avoid meaningless fluctuations. Furthermore, the parameters may change with the phase of the solar cycle. Hence the range of data should span several years, ideally several solar cycles, in order to estimate a parameter set that will give optimum correspondence between the PC index and the E_M throughout solar activity variations.

Some of the published PC data series have been based on only a few years of reference data while other series have been based on reference data spanning several decades. The secular variations could be important, in particular, for the values of the optimum direction angle. For Thule, for instance, the declination has changed as a result of secular variations by over 20 degrees during the epoch 1975 to 2016 for which PC index values have been calculated.

16.4. Smoothing of QDC optimum direction angle, and regression parameters.

Even when an extended reference data interval is used, some degree of smoothing of QDC values, and of the optimum direction angle and regression parameters (ASI) will be necessary. The smoothing should be strong enough to reduce random statistical fluctuations while not so strong that this process in itself influences significantly the physical interpretation of the resulting PC index values. This is a delicate balance. One possible solution, implemented in the present procedure, is to subdivide the reference data epoch in separate intervals. The smoothing should then remove the features which appear differently in the subintervals while retaining features which systematically appear the same way in the different intervals.

16.5. Coordinate system.

Earlier, most magnetic data were expressed through the magnitude H of the total horizontal component and the value of the declination angle D (and inclination angle I). This convention was more or less a result of the function of the available types of mechanical magnetic instruments. With new instruments like the flux gate triaxial magnetometers the magnetic variations were expressed in orthogonal coordinates H, D and Z oriented with the H-axis in the direction of the local horizontal magnetic vector. Now, most magnetic data are expressed as elements X, Y and Z in a local geographic coordinate system.

The choice of coordinate system should, in principle, have no consequence for the calculation of PC index values. Contrary to other QDC methods (e.g., *Janzhura and Troshichev*, 2008), variations in the geomagnetic vectors (and not in the individual components) have been used here to make the selection of quiet samples for the QDC independent of the representation of the components. The derivation of optimum direction angles and regression parameters, slope and intercept, as well as the calculation of PC index values are based on the projection of the magnetic variation vectors to the optimum direction and thus not dependent on the vector representation whether in (H,D) or (X,Y) components.

16.6. Hemispherical differences.

The Northern Polar Cap index, PCN, as well as the Southern Polar Cap index, PCS, are based on calibration of the geomagnetic variations against the merging electric field, E_M, which is common to the two hemispheres. The geomagnetic variations in the two polar caps have both been corrected for the seasonally varying QDC values. Accordingly, the PCN and PCS values should be equal if the northern and southern polar cap convection patterns and intensities have the same response to the merging electric field. However, there are two significant factors dividing between the ionospheric convection patterns in the northern and southern polar caps.

One factor is the asymmetry caused by the azimuthal component, IMF B_Y, which has opposite effects on the convection patterns in the northern and southern polar caps, and thereby also different effects on the PC index values. Thus, PCN and PCS index values have differences that relate to the sign of IMF B_Y and not reflected in the value of the merging electric field, E_M. Forming a mean of the PCN and PCS indices is a possible way to mitigate the IMF B_Y effects that goes beyond the direct influence via the magnitude of merging electric field (cf. Eq. 2).

Another factor of importance for the development of differences in PCN and PCS index values is the occurrence of reverse convection. There are two significant features. Reverse convection events are most frequent during daytime and in the summer season. Thus, the differences in season and in local time between Thule and Vostok may give different convection responses to NBZ conditions in the IMF. For the same IMF conditions one hemisphere may experience reverse convection giving negative values of the PC index, while the other hemisphere just experiences reduced forward convection and reduced, but still positive PC index values.

A significant feature for the derivation of index parameters is the different frequencies and strengths of strong reverse convection events for the two PC index observatories, Thule and Vostok. While the occurrence of strong forward convection is about the same for the two observatories, then the occurrence of strong reverse convection events is much more frequent at Thule compared to Vostok. The reverse convection transpolar channel seen by a polar observatory at local magnetic noon is fairly narrow (cf. Fig. 1). The convection-related current intensities are enhanced by the large conductivities around local solar noon. At Thule local solar and geomagnetic noon are close which enhances the reverse convection, while at Vostok they are widely separated, which weakens the reverse convection intensities. The transpolar channel for forward convection is fairly wide (cf. Fig. 1). Hence the differences between local solar and local geomagnetic noon are not so important.

The occurrence of strong forward convection is illustrated in Fig.37 (from *Stauning*, 2015) that presents the bi-monthly values of intensity times duration [nT*hours] for projected, QDC-corrected magnetic variations above +50 nT through 1997-2009 for Thule (blue line) and for Vostok (red line). For both stations there are seasonal and solar cycle variations with stronger forward convection intensities during local summer in solar maximum years, but the yearly totals are about the same for the two sites. The summations through the epoch (exempting 2003) give about the same intensities of strong forward convection for the two stations with a small surplus at Vostok.

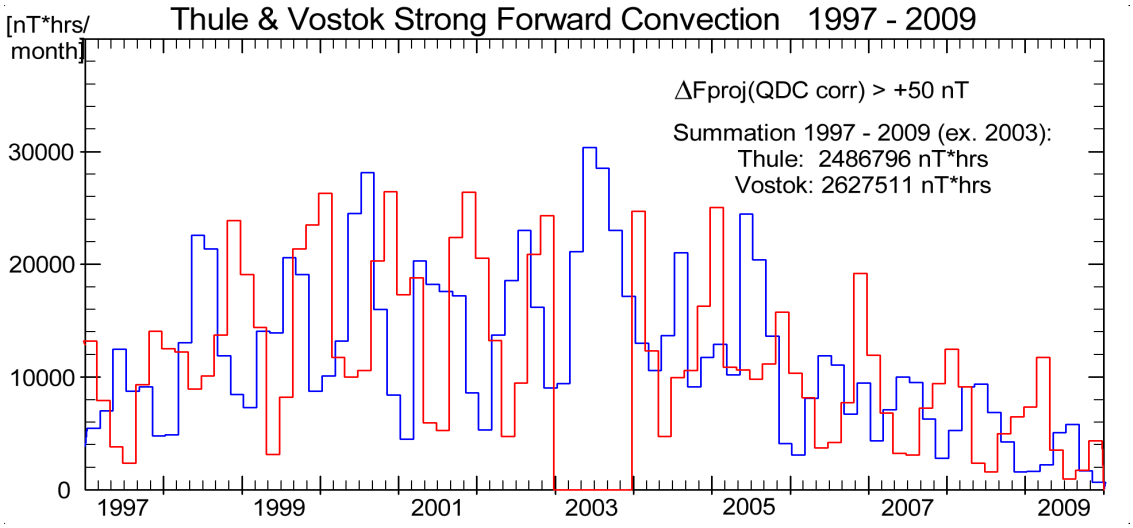

Fig. 37. Forward convection cases illustrated by the bi-monthly sums of intensity times duration [nT·hrs]) for strongly positive values (ΔF_{PROJ}(QDCcorr)>+50 nT) of the projected horizontal variation for Thule (blue line) and Vostok (red). (Note: No Vostok data in 2003)

Fig. 38 illustrates the occurrences of strong reverse convection cases measured again in nT*hours with projected, QDC-corrected magnetic variations more negative than -50 nT. There are, again, strong seasonal and solar cycle variations with maximum intensities of reverse convection during local summer months in solar maximum years, but the yearly totals are very different for the two stations. The summations over the entire epoch from 1997 to 2009, noted in the diagram, indicate more than 3 times more intense reverse convection at Thule than at Vostok.

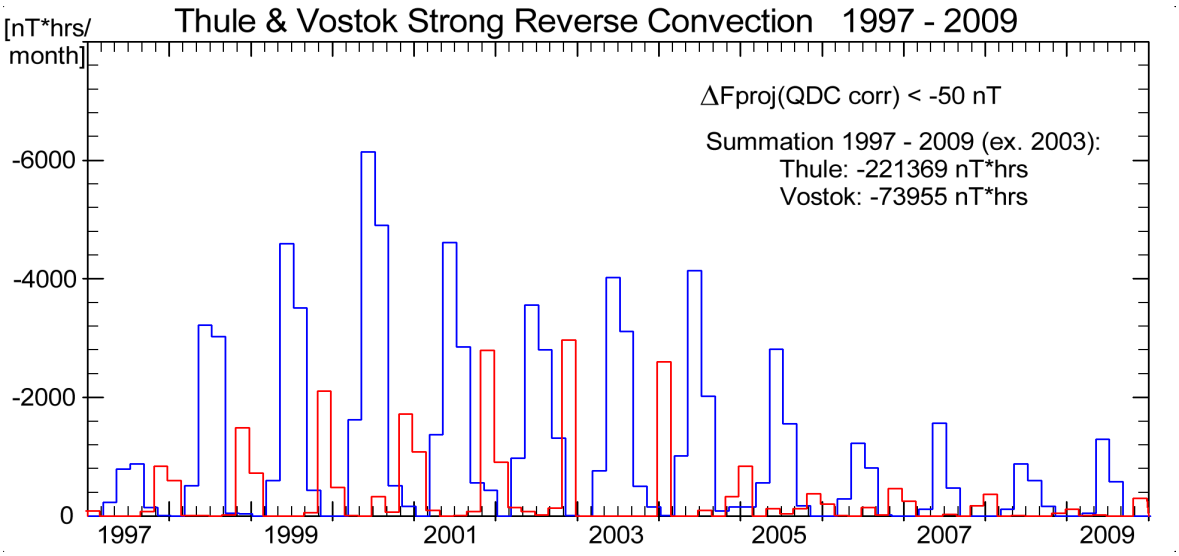

Fig. 38. Strong reverse convection cases illustrated by the bi-monthly sums of intensity times duration [nT·hrs]) for strongly negative values (ΔF_{PROJ} (QDCcorr)<-50 nT) of the projected horizontal deviations for Thule (blue line) and Vostok (red). (Note: No Vostok data in 2003).

The discrimination against reverse convection in the procedure to derive optimum direction angle and regression coefficients for PC index derivation was spurred by the aim to develop an index for the dominant forward convection mode, where energy is transferred most effectively from the solar wind to the Earth, without confusing interference from the reverse convection mode, where the energy transfer is

much smaller and mostly restricted to the near-pole regions. Avoiding the reverse convection effects on the index derivation parameters helps to make them comparable for the PCN and PCS indices taking seasonal and local time differences into account. This feature is illustrated in Fig. 39 presenting optimum direction angle, slope and intercept parameters derived with QDC correction of the geomagnetic data for Thule (blue line) and Vostok (red line). In order to facilitate comparison the sequence of months for Vostok has been modified to have the summer season at the middle of the diagram. Furthermore, the monthly mean daily variations have been plotted vs. local time taken as the average of solar and corrected geomagnetic time (cf. Table 1) such that noon (12 LT) for Thule is at 16 UT, while noon for Vostok is at 10 UT.

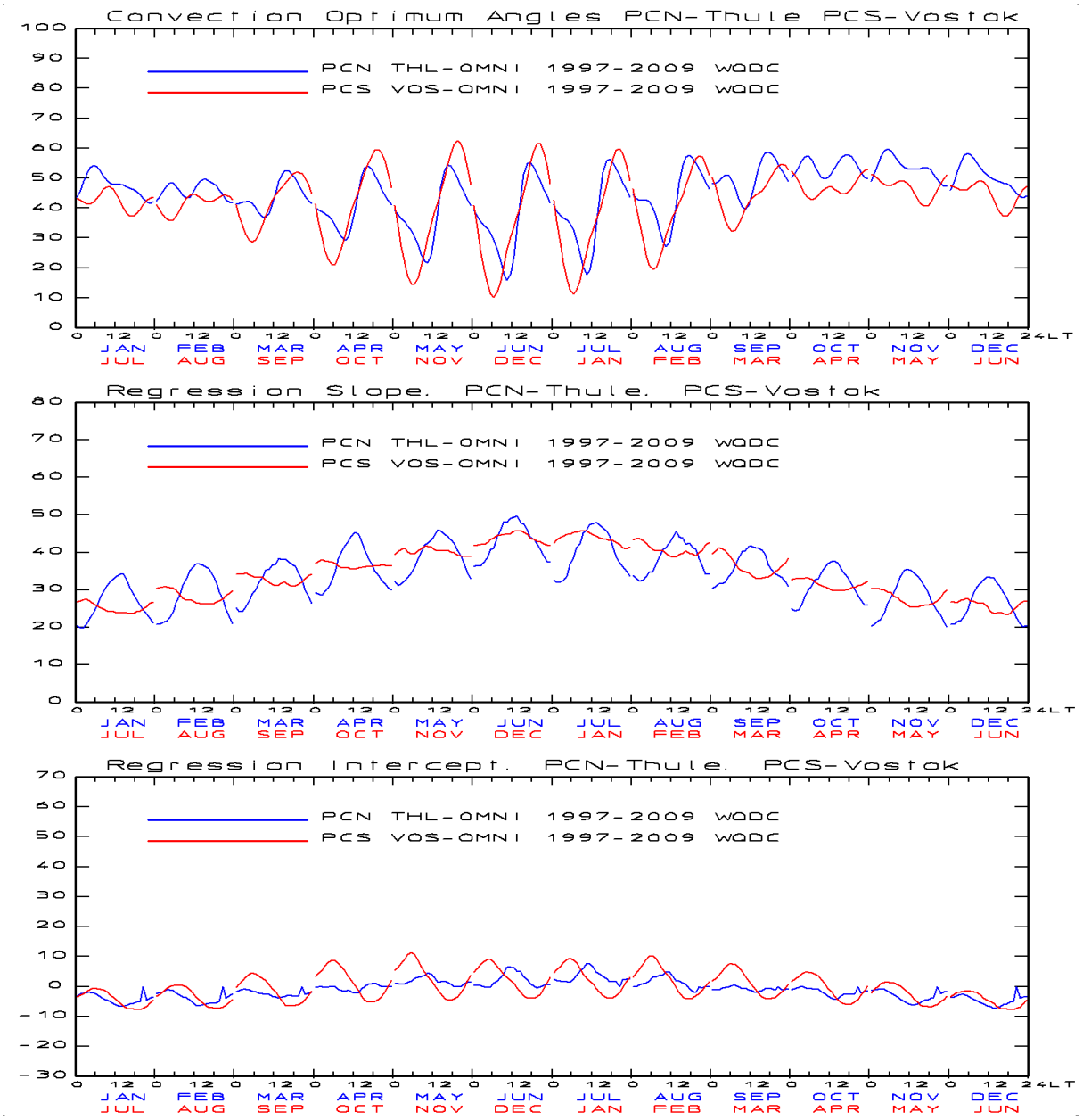

Fig. 39. Summary plots of optimum direction angle (upper field), slope (middle), and intercept (bottom field) for Thule (blue line) and Vostok (red). Parameters derived with QDC correction.

Note in Fig. 39 that the parameters for Thule and Vostok have rather similar levels. Part of the remaining differences arrives from the different relations between local solar time and corrected geomagnetic time for the two stations (cf. Table 1).

16.7. Relations between merging electric fields and PC indices.

With the derived series of PC index values and the available series of merging electric field values derived from the OMNI files, it is now possible to calculate correlation coefficients for various groupings of data. Here, the seasonal and solar cycle effects are examined. Furthermore, the variations in correlation with time shift between Bow Shock Nose (BSN) E_M values and Polar Cap index values are examined. In the derivation of parameters (angle, slope, intersect) a delay of 20 min was estimated in the initial step and then used further on. This delay value can now be tested. For the correlation we use textbook's product-momentum formula provided in Eq. 30 with $X = E_M$ and Y = PCN or PCS , while the summation is extended over all available 5-min samples through the data intervals from 1999 to 2002 solar maximum and 2005-2008 for solar minimum years. The results are presented in Table 7. Reverse convection cases where PC index values are negative are handled in the last rowsof the table.

Table 7. Correlation of PCN index with OMNI-based E_M values at various BSN-Polar Cap delays.

Delay	PCN>-0.5 Epoch 1999-2002			PCN>-0.5. Epoch 2005-2008			Average
Minutes	N. Winter	Equinox	Summer	N. Winter	Equinox	Summer	Correlation
10	0.661	0.724	0.676	0.700	0.716	0.712	0.698
15	0.679	0.735	0.693	**0.711**	0.735	**0.722**	0.713
20	**0.683**	**0.736**	**0.699**	0.708	**0.738**	0.721	**0.714**
25	0.678	0.731	0.697	0.697	0.730	0.712	0.708
30	0.671	0.722	0.689	0.685	0.717	0.700	0.698
Delay	PCN<0	Epoch 1999-2002		PCN<0	Epoch 2005-2008		Average
Minutes	Winter	Equinox	Summer	Winter	Equinox	Summer	Correlation
20	-0.043	-0.102	0.026	-0.162	-0.032	-0.032	-0.062

From Table 7 it is seen that in most specific cases, and on the average, the correlation is maximum at a delay of 20 min. In a parabolic interpolation the maximum correlation is found at a delay of 18 min, which is also the value derived from the correlation between E_M and values of the projected geomagnetic variations shown in Table 5. The agreement confirms that the processing of the index parameters (optimum direction angle, slope, and intercept) has not affected the timing for best correlation. Furthermore, Table 7 indicates that the correlation is highest during equinoxes and during solar minimum years and lowest during the winter season in solar maximum years. Like anticipated, the correlation between negative values of the PCN index and values of the merging electric field is close to zero (i.e., neither correlated nor anticorrelated) throughout.

The correlation coefficients listed in Table 8 for the PCS indices with E_M values have much the same magnitude as the corresponding coefficients for the PCN indices and they also maximize for a delay of 18 min from the Bow Shock Nose to the Southern Polar Cap. Contrary to the PCN indices, in the solar quiet epoch (2005-2008) the correlation of PCS with E_M maximizes at local winter (not equinox).

Table 8. Correlation of PCS index with OMNI-based E_M values at various BSN-Polar Cap delays.

Delay	PCS>-0.5 Epoch 1999-2002			PCS>-0.5. Epoch 2005-2008			Average
Minutes	S.Winter	Equinox	Summer	S. Winter	Equinox	Summer	Correlation
10	0.711	0.726	0.668	0.729	0.684	0.691	0.702
15	0.727	**0.737**	0.685	**0.744**	0.704	**0.703**	**0.717**
20	**0.730**	**0.737**	**0.687**	**0.744**	**0.705**	0.699	**0.717**
25	0.724	0.731	0.679	0.736	0.695	0.685	0.708
30	0.714	0.721	0.665	0.726	0.681	0.668	0.696
Delay	PCN<0	Epoch 1999-2002		PCN<0	Epoch 2005-2008		Average
Minutes	Winter	Equinox	Summer	Winter	Equinox	Summer	Correlation
20	-0.276	-0.052	-0.037	-0.228	-0.045	-0.112	-0.125

In the definition (cf. Eqs. 1-4) of the Polar Cap (PC) index, the polar magnetic variations projected to the optimum direction are scaled to equal, on the average, the interplanetary merging electric field, E_M. However, at large amplitudes, the PC index values no longer follow linearly the E_M values but appear to saturate. The resulting relations between the merging electric fields and the PC indices are displayed in Fig. 40a for PCN, in Fig. 40b for PCS, and in Fig. 40c for PCC.

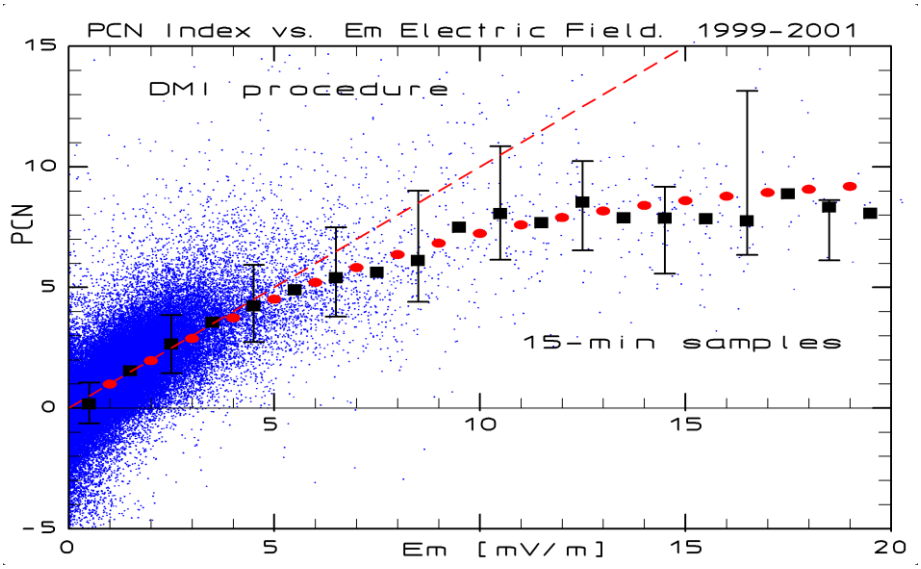

Fig. 40a. Polar Cap PCN index vs. E_M merging electric field. 15 min samples. Delay 20 min.

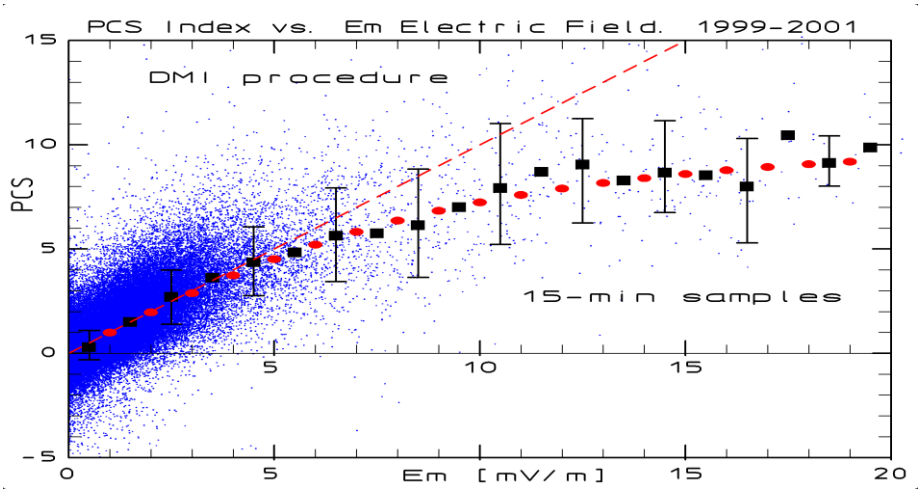

Fig. 40b. Polar Cap PCS index vs. E_M merging electric field. 15 min samples. Delay 20 min.

Mean values of the PCN index are indicated by the black squares for each unit in E_M. Standard deviation is indicated by error bars every other unit in E_M. The dashed oblique line indicates equality between PCN and E_M values, which is quite close for the averages up to around 5 units. The reference relation indicated by the red dots reads:

$$\mathrm{PCN} = E_M / \sqrt{(1 + (E_M / E_0)^2)} \quad \text{with } E_0 = 10.5 \text{ mV/m} \qquad (32)$$

Part of the non-linear development is caused by a changing geometry. The merging electric fields derived from the solar wind and its embedded magnetic field create electric voltages extended over the Magnetosphere from dawn to dusk. These voltages (reduced by boundary processes and field-aligned voltage drops) are carried down to the polar ionospheres along field lines and extended over the "open" polar caps between the "last closed" dawn and dusk field lines.

During strong events the widths of the polar caps expand as the latitudes of the last closed field lines decrease. Hence, for the same total voltage extended across the Magnetosphere, the dawn-dusk

ionospheric electric fields that drive the transpolar convection decrease, and the transpolar current densities, consequently, are reduced compared to the values attained for polar caps of constant width. In addition there are, no doubt, further non-linear features of the transfer of electric fields from the Magnetopause to the polar ionospheres.

Like mentioned earlier, the PCN and the PCS indices could be combined to improve the index performance in relations not specifically relating to the Northern or Southern hemisphere, such as relations to the equatorial ring current or to magnetospheric substorms. Instead of a simple average of the two indices it was suggested by *Stauning* (2006) to combine them into a PCC index by the relation:

PCC = ((PCN if >0 or else 0) + (PCS if >0 or else 0))/2. (33)

The PCC index is non-negative like the merging electric field. Hence, it could be expected to be better correlated with the E_M value than either PCN or PCS. Table 9 presents the coefficients derived for the correlation of PCC with E_M for the same conditions as those used for the results shown in Tables 7 and 8.

Table 9. Correlation of PCC index with OMNI-based E_M values at various BSN-Polar Cap delays.

Delay	Epoch 1999-2002			Epoch 2005-2008			Average
Minutes	N. Winter	Equinox	Summer	N. Winter	Equinox	Summer	Correlation
10	0.711	0.756	0.740	0.728	0.715	0.754	0.734
15	0.731	**0.768**	0.757	**0.739**	0.736	**0.768**	0.750
20	**0.734**	**0.768**	**0.762**	0.735	**0.738**	0.767	**0.751**
25	0.727	0.761	0.757	0.722	0.728	0.758	0.742
30	0.714	0.751	0.746	0.705	0.714	0.746	0.730

The delay for maximum correlation is again 18 min. Table 9 documents that the PCC index correlates much better with the merging electric field than either PCN or PCS with a peak average correlation coefficient of 0.751 compared to 0.714 for the PCN and 0.717 for the PCS index. A further advantage is the rather uniform correlation between PCC and E_M through seasonal and solar cycle variations.

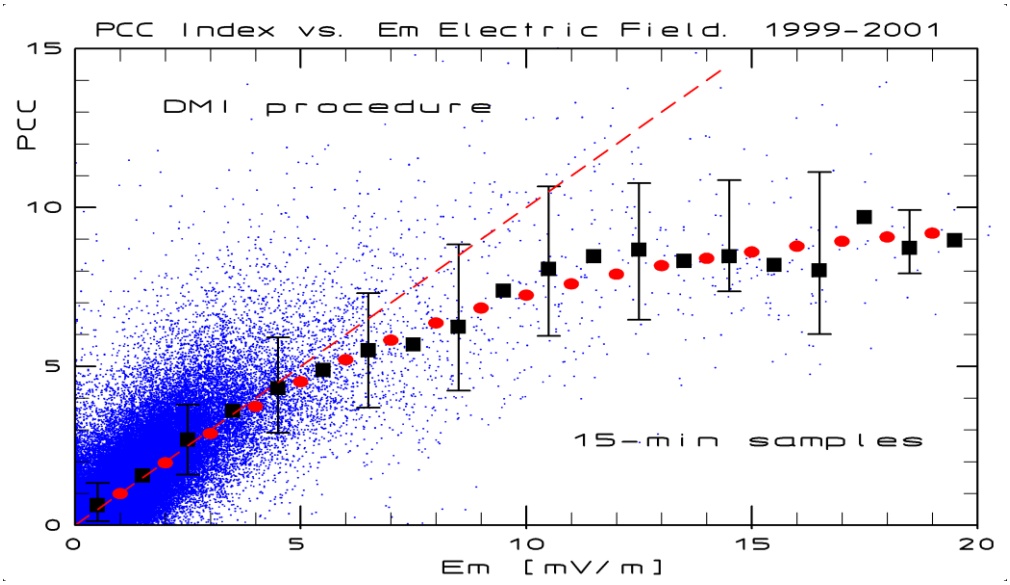

Fig. 40c. Polar Cap PCC index vs. E_M merging electric field. 15 min samples. Delay 20 min.

For all applications not specifically constrained to either Polar Cap it is recommended, whenever possible (i.e., when both PCN and PCS are available), to use the PCC index.

17. Further PC index versions

17.1. Introduction

Since the initial Polar Cap index concept published in *Troshichev and Andrezen* (1985) and further developed by *Troshichev et al.* (1988), 7 different PCN index versions and 5 different PCS versions have been issued (*Stauning*, 2013b). In 2013 a IAGA panel endorsed the PCN and PCS index versions provided jointly by the Arctic and Antarctic Research Institute (AARI) and the Danish DTU Space Institute. These recent versions were mostly built on the latest AARI PC index procedures. However, it was pointed out in *Stauning* (2015) that the IAGA-endorsed PCN and PCS versions have some adverse features, which would reduce their usefulness both for statistical analyses and for Space Weather purposes. The PCN-PCS procedure described in the previous sections of the present report shall be termed "DMI-version". It is built on the "DMI#4-version" but uses data from epoch 1997-2009 for PCN and PCS coefficients (same as the IAGA version) excluding 2003 (no Vostok data).

For a review and naming of the various PC index versions prior to 2013 and a listing of publications using the various versions, see Appendix C or *Stauning* (2013b). In summary, the DMI#1 PCN values have been used in all publications dealing with the PCN index and issued between 1991 and 2001. The DMI#2 (=DTUS#1) PCN values have been used in most publications dealing with the PCN index issued since 2001 except those written (first author) by *Janzhura*, *Lukianova*, *Stauning*, or *Troshichev*. The publications issued by *Janzhura* or *Troshichev* (first author) have used the AARI#3 or AARI#4 PCN index values while publications issued by *Stauning* (as first author) have used the DMI#4 PCN index values. Publications by *Stauning* (first author) have used DMI#4 PCS indices while *Troshichev*, *Lukianova*, *Janzhura*, and other authors have used the AARI#1, AARI#2, AARI#3 or AARI#4 PCS indices. Thus, it is possible in most cases to deduce the PC index versions used in publications from the author names and the publication dates.

In order to demonstrate the differences between the index versions, Fig. 41 (from *Stauning*, 2013b) displays the PCN index values derived by different procedures. There are non-systematic differences by up to a factor two between the peak values of the different PCN versions. Note, in particular, the differences between PCN indices in versions DMI#1 and DMI#2 derived from the same set of index coefficients (COEF24G3.FIL) but differing because of a programming error to be explained below.

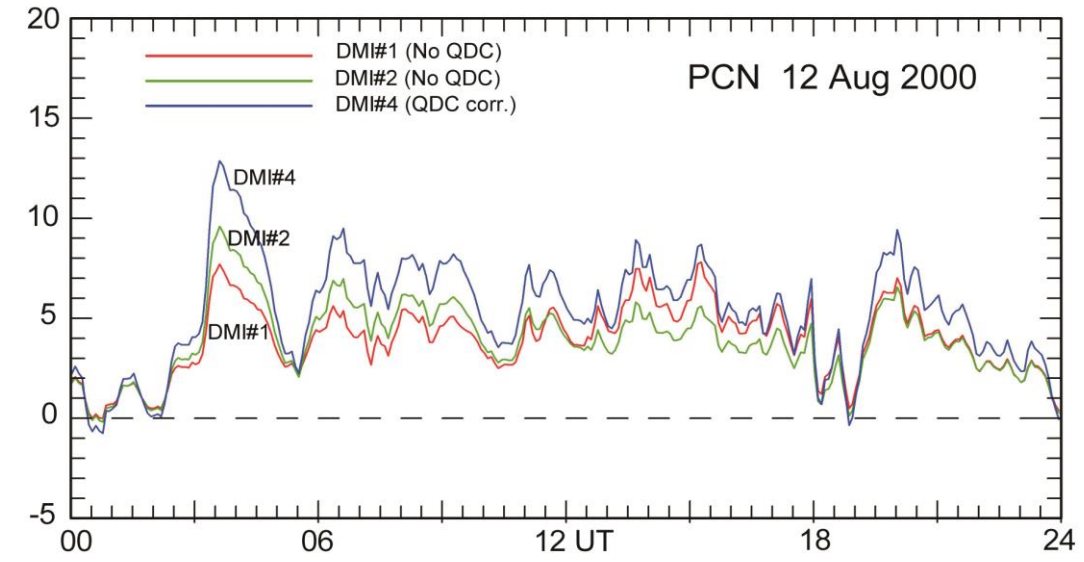

Fig. 41. PCN index values derived by different DMI versions. The version named DMI#2 (=DTUS#1) has been taken over by DTU Space and now named PCN2 (available as PCN in OMNI files).

An example of the large differences between the different PCS index versions is provided in Fig. 42 (from *Stauning* (2013b).

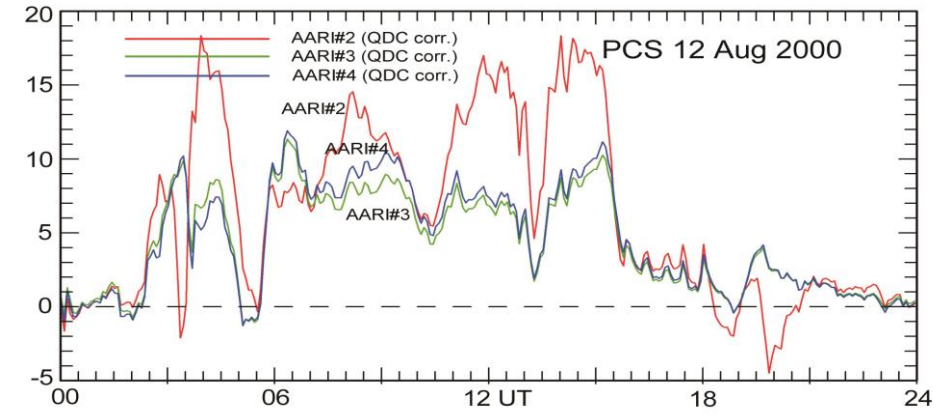

Fig. 42. PCS index values derived by different AARI procedures. (*Stauning*, 2013b)

In the next sections some of these different versions are analysed and contrasted to the version presented here. In addition to providing some comments on the index procedures, the index coefficients shall be displayed graphically in the same format as that used in Figs 19, 29, and 39. The relation of the index values to the merging electric field shall be illustrated in diagrams of the format used for Figs. 40 a,b,c, and the differences between index values shall be illustrated in diagrams of the format used in Fig. 32.

17.2. DMI#1 and DMI#2 (=DTUS#1 PCN2) PCN indices.

The DMI#1,#2 index procedure is described in the dissertation by *S. Vennerstrøm* (1991). It uses IMP-8 (intermittent) solar wind data and Thule geomagnetic data corrected only for the QWNL base level (not QDC) from the epoch 1976-1980. The procedure is much the same as that described here for the no-QDC case except for the regression step that uses a least squares regression method dealing with the deviations perpendicular to the regression line. The "orthogonal" regression formulas in *Vennerstrøm* (1991) (corresponding to Eqs. 1, 34 and 35 above) are here shown in Fig. 43. The equations are reproduced from *McCreadie and Menvielle* (2010). Specifications of units are added in the comment by *Stauning* (2011a).

$$F_{s,\phi} = \alpha_{\perp} E_{m(s)} + \beta_{\perp}$$

$$\alpha_{\perp} = \frac{S_y - S_x \pm \left((S_y - S_x)^2 + 4S_{xy}^2 \right)^{1/2}}{2S_{xy}}$$

$$\beta_{\perp} = \overline{E_m} - \alpha_{\perp} \cdot \overline{F_{s,\phi}}$$

$$S_x = \frac{1}{N-1} \sum_s \left(F_{s,\phi} - \overline{F_{s,\phi}} \right)^2 \qquad [\text{nT}]$$

$$S_y = \frac{1}{N-1} \sum_s \left(E_{m(s)} - \overline{E_m} \right)^2 \qquad [\text{mV/m}]$$

$$S_{xy} = \frac{1}{N-1} \sum_s \left(F_{s,\phi} - \overline{F_{s,\phi}} \right) \left(E_{m(s)} - \overline{E_m} \right) \qquad [\text{nT,mV/m}]$$

Fig. 43. Regression formulas to derive PCN slope and intersect parameters (*McCreadie and Menvielle*, 2010; after *Vennerstrøm*, 1991). Specification of units added in *Stauning*, 2011a.

In regression calculations the choice of dependent and independent parameter is important. In the derivation of PC index coefficients, the merging electric field is usually taken to be the independent parameter like implied in Eq. 1. The use of both parameters in the orthogonal regression attempted like in Fig. 43 makes sense only if the two parameters are supplied in the same unit. However, the equation to derive the slope, $\alpha_{\perp}$, holds the differences between the summation terms S_x and S_y of which one is in nT while the other is in mV/m. The calculations may proceed regardless since the computer is fed with the numerical values and don't care about the units. In addition, the two parameters, E_m and F_φ (and thus their variances) have magnitudes differing by up to 2 orders of magnitude. Thus, the effects of the smaller quantity (S_y) in the difference of variances, S_y and S_x, are highly uncertain.

The problem was brought up to the scientist responsible for the calculation and distribution of this version of the PCN index and later published in a commentary in Ann. Geophys. (*Stauning*, 2011a). Still the distribution of the PCN index (now named PCN2) continued and the index was made available via the DTU Space ftp site: ftp://ftp.space.dtu.dk/WDC/indices/. Furthermore, PCN indices in this version are still made available in the OMNIweb files and have been used in many scientific publications; among other in recent scientific works actually submitted at this time (June 2016) for publication.

The original program and the data base from the processing of data for the epoch 1976-1980 by *Vennerstrøm* (1991) no longer exists. However, the PCN index parameters, optimum direction angle, slope, and intersect, have been kept in an available file of coefficients (COEF24G3.FIL). From this file, the hourly mean optimum direction angles through the day and for all months are shown in green line in Fig. 44 for the DTU#1 (=DMI#1,#2) procedure used to derive DTU Space PCN2 index values. The corresponding angles for the present PCN-DMI procedure are included in magenta line for reference.

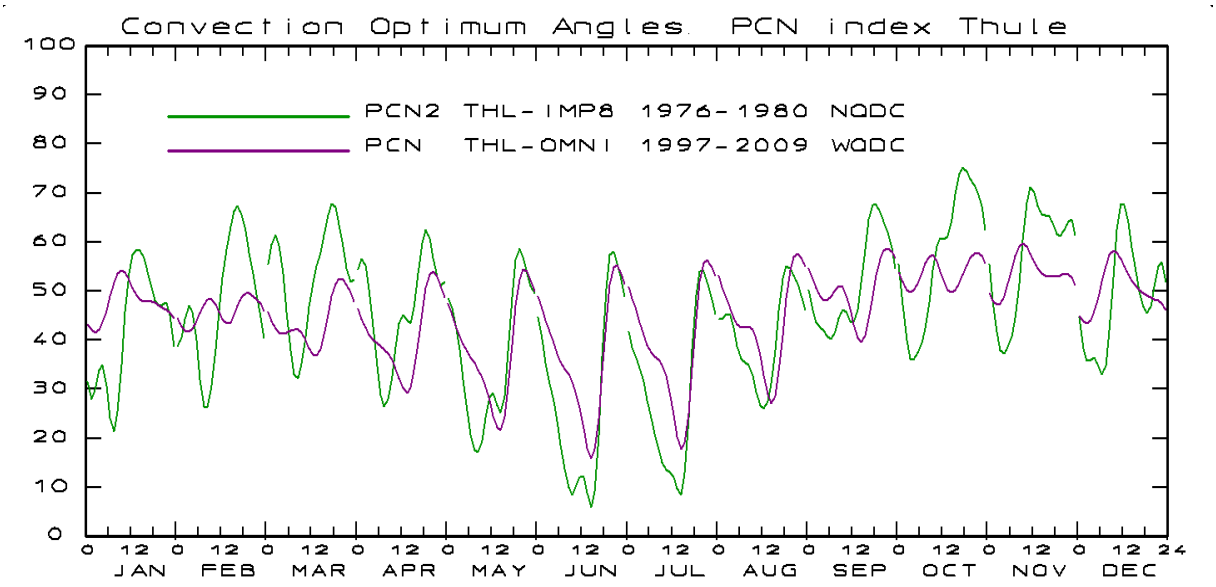

Fig. 44. Optimum direction angles for the PCN2 index (green). Present procedure (magenta).

The match between the two sets of optimum direction angles is fair taking into account the sparser amount of available data due to the shorter epoch and the intermittent IMP8 position in solar wind for calculation of PCN2 parameters compared to the basis for the present PCN index. Possible differences in the smoothing of values can not be assessed since the original program (*Vennerstrøm*, 1991) for deriving scaling parameters for the DMI#1,#2 versions has been lost.

From the file of coefficients (COEF24G3.FIL), the slope and intercept parameters for the DTUS#1 (=DMI#1,#2) PCN2 index version are shown in Fig. 45 in the format corresponding to Fig. 19. Note however, that the scale values have been doubled to include the large amplitudes of the PCN2 scaling coefficients.

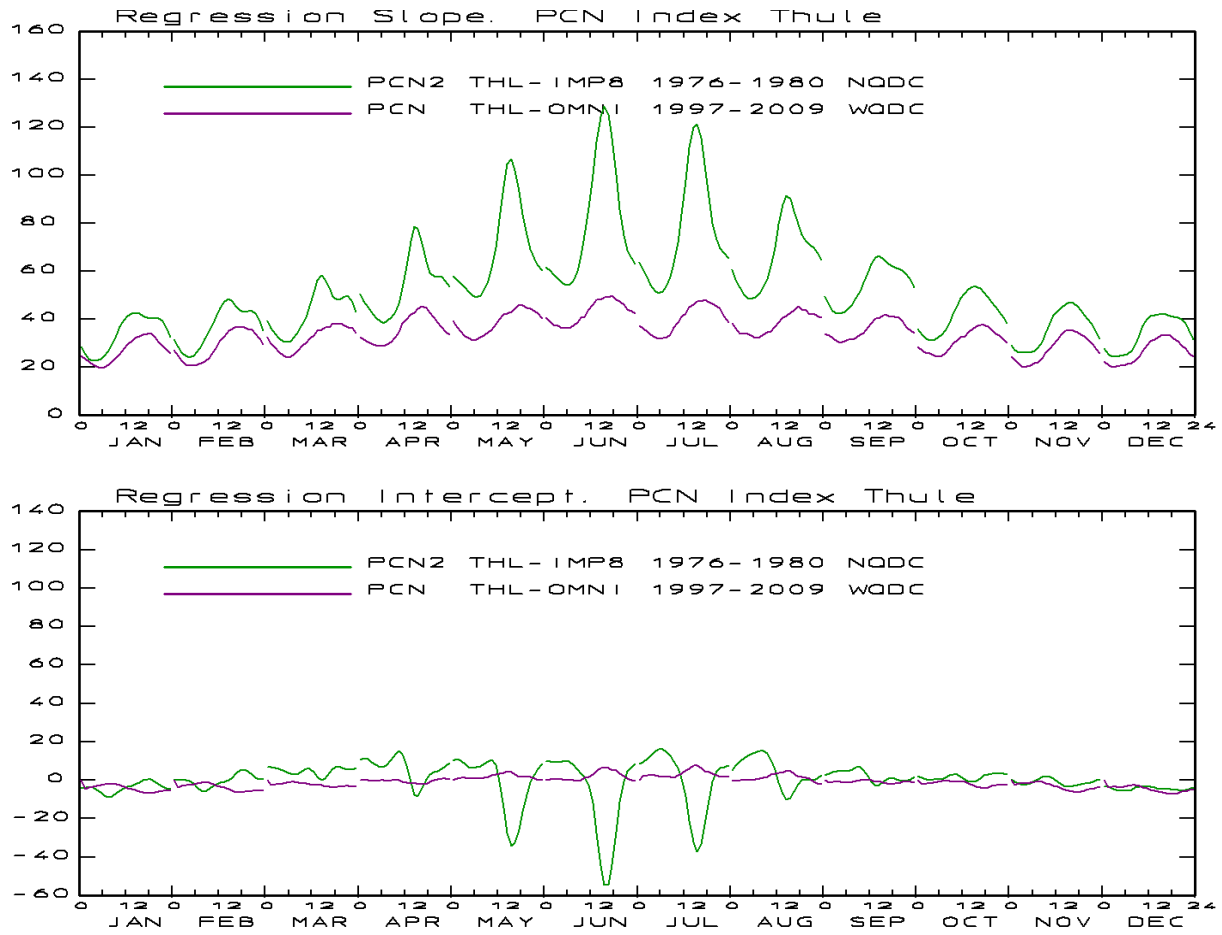

Fig. 45. Slope and intercept parameters for the PCN2-DTUS#1 (DMI#1,#2) index (green line). Parameters for the present PCN-DMI index (magenta line) included for reference.

Control calculations of the PCN coefficients using the same data (epoch 1976-1980, Thule and IMP-8 data) as those used in the original approach (*Vennerstrøm*, 1991) have shown, that the slope and intercept coefficients used for the DTU#1 PCN2 index are closer to those derived using the projected geomagnetic variations as the independent parameter rather than those found by using the merging electric field as the independent parameter. Furthermore, reverse convection cases have not been excluded from the data base for deriving PCN2 coefficients. The lack of discrimination against reverse convection cases contributes to make the slope steeper and the intercept more negative (cf. Fig. 36).

These features are responsible for the very large slope values, and the strongly negative intercept values, particularly those seen during midday hours in summer months, where the slope exceeds 120, i.e., almost three times the maximum slope for the PCN-DMI version presented here. The intercept values seen in Fig. 45 reach -60 nT at midday in the summer (June), while the corresponding values for the present PCN version are held between + and – 10 nT.

In order to assess the relation of the DTU#1 PCN2 index values to the merging electric field, Fig. 46 presents in the format of Figs. 40a,b the 15-min PCN2 values plotted vs. the merging electric field referred to the Polar Cap with a delay of 20 min imposed on the Bow Shock Nose (BSN) parameters derived from the OMNI files. From Fig. 46 it may be noted that at small values (E_M <3 mV/m) the PCN2 equals the merging electric field (on the average), while at larger values the PCN2 indices are systematically much smaller than the corresponding electric fields and even much smaller than the reference shown by the red dots here like in Figs. 40 a,b,c and defined by Eq. 32. At E_M=10 mV/m the PCN2 index is only half the value of the merging electric field.

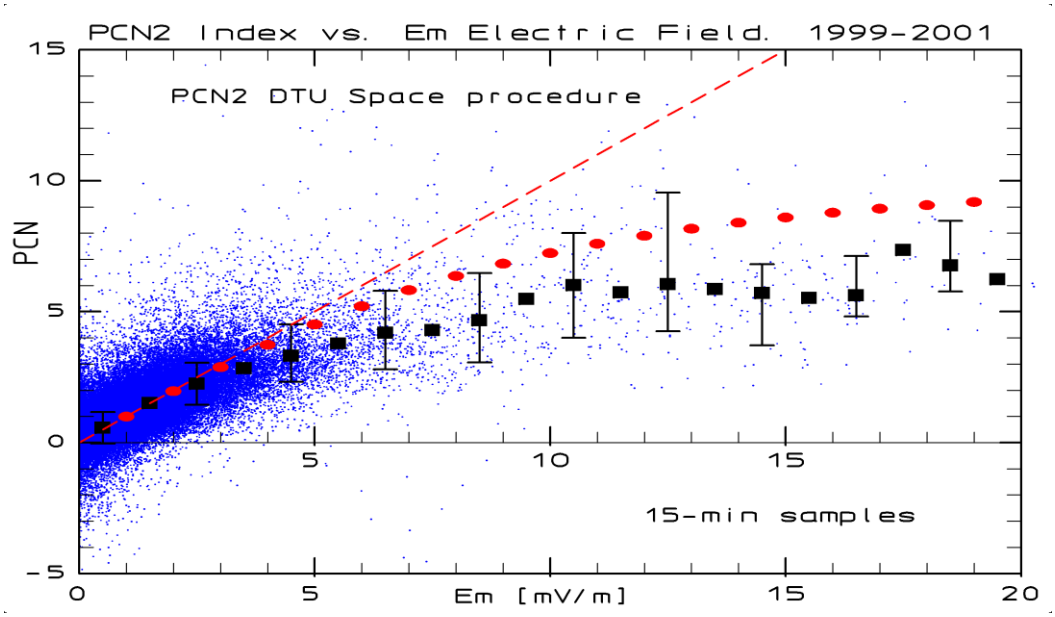

Fig. 46. Polar Cap PCN2 index vs. E_M merging electric field. 15 min samples. Delay 20 min

The effects of the large slope values and the strongly negative intercept values may become even more remarkable if just values from midday hours in summer months are included in the diagram like shown in Fig. 47.

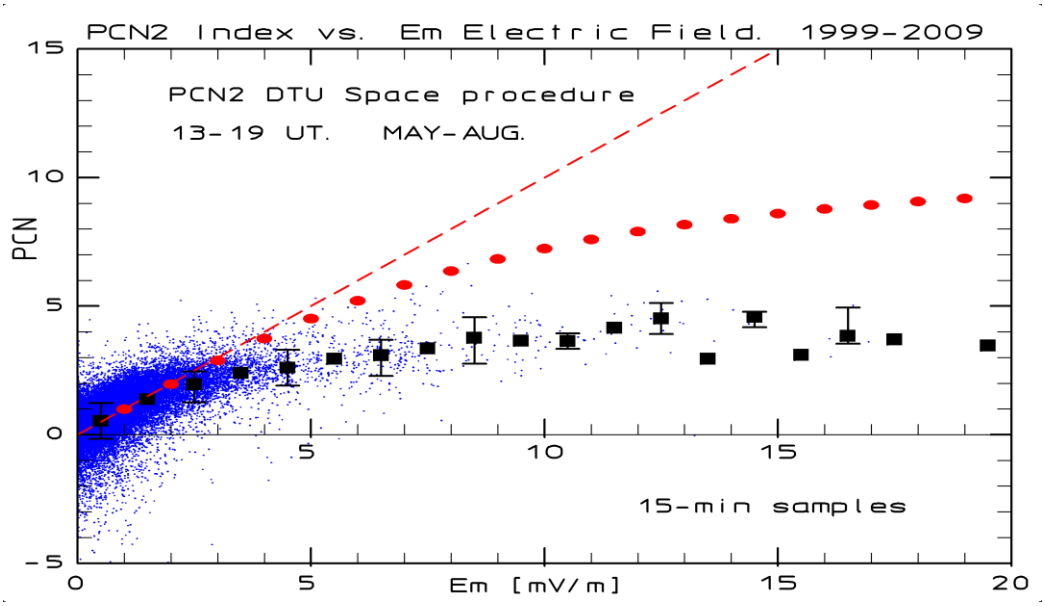

Fig. 47. Polar Cap PCN2 index vs. E_M merging electric field during midday hours 13-19 in summer months May-August through years 1999-2009. 15 min samples. Delay=20 min.

PCN index values in the DMI#1 version (*Vennerstrøm*, 1991) were made available for 1975-2000. In addition to the above-mentioned principal error (cf. Fig. 43) in the coefficient calculations (*Stauning*, 2011a), there was an error detected by *K. Mursula* (*Papitashvili et al.*, 2001) in the index program. Instead of using the daily varying index coefficients to derive PCN index values from the geomagnetic variations, the values provided at 00 UT were used throughout the day. Thus, the resulting PCN index values were then given the systematic daily variation that should have been removed through the scaling to the merging electric field in the solar wind outside the Earth's domain.

The PCN index data in version DMI#1 (cf. *Stauning*, 2013b) have been used in *Chun et al.* (1999), *Nagatsuma et al.* (1999), *Nagatsuma et al.* (2000), *Papitashvili and Rasmussen* (1999), *Takalo and Timonen* (1998a, 1998b,1999), *Troshichev et al.* (1991), *Trochichev et al.* (1996), *Vassiliadis et al.* (1996), *Vennerstrøm* (1991), *Vennerstrøm et al.* (1991, 1994).

With version DMI#2 (=DTUS#1), upon program modifications in 1999 and 2001 by *V. O. Papitashvili* and *O. Rasmussen* (*Papitashvili et al.*, 2001), PCN index values were re-calculated for 1975-2000. The principal error (cf. *Stauning*, 2011a, 2013b) in coefficient calculations (cf. Fig. 43) has not been corrected. Index values for 1975 to 2012 were made available from DTU Space via the DTU Space ftp site: ftp://ftp.space.dtu.dk/WDC/indices/ and are still included in OMNIweb files.

The PCN2 index values have been used in *Chun et al.* (2002), *de Campra and Artigas* (2004), *Fiori et al.* (2009), *Gao* (2012), *Gao et al.* (2012a, 2012b, 2012c), *Henderson et al.* (2006), *Huang* (2005), *Johnsen and Lorentzen* (2012), *Lee et al.* (2004), *Liou et al.* (2003), *Liou et al.* (2004), *Lukianova* (2003, 2007), *Lukianova et al.* (2002), *Nagatsuma* (2002a, 2002b), *Nagatsuma et al.*, (2003), *Ridley and Kihn* (2004).

Instead of having been used in so many published works, this index should (could) have been abandoned long time ago.

17.3 DMI#3 PCN version

The DMI#3 PCN version by *Papitashvili et al.* (2001) (cf. *Stauning*, 2013b) was based on IMP-8 satellite data and Thule geomagnetic data from the epoch 1976-2000. Index values were calculated for 1975-2000 for analyses of solar cycle effects. Data base and software for calculation of PCN index coefficients are not available. The index values are also not available. The results that indicate considerable solar cycle effects are published in DMI report SR 01-01 (*Papitashvili et al*., 2001).

17.4 DMI#4 PCN and PCS version.

The DMI#4 version of the PCN and PCS index procedure (*Stauning et al*, 2006) was developed in 2006 to improve the DMI#1,#2 PCN versions as well as the AARI index versions (*Troshichev et al*., 2006). The index procedure is described in the DMI Scientific Report SR06-04 (*Stauning et al*., 2006). The report was circulated to the co-authors in an initial version, which was subsequently modified and then made available on-line at http://www.dmi.dk/fileadmin/Rapporter/SR/sr06-04.pdf .

Compared to versions DMI#1 and DMI#2 based on data from 1976-80, the DMI#4 version use a much larger data base for index coefficients extending from 1975 to 2003 for the PCN index (1995-2005 for the PCS index), and the regression is based on the concept of the merging electric field being the independent parameter. Furthermore, the DMI#4 version, contrary to the DMI#1,#2 versions, uses QDC correction of the geomagnetic data according to the concept introduced in *Lukianova et al.*, (2002) and *Troshichev et al*. (2006), but with an improved method, the Solar Rotation Weighted (SRW) technique, to derive QDC values (see *Stauning*, 2011b).

Finally, for the DMI#4 version, contrary to the DMI#1,#2 and AARI versions, the strong reverse convection cases were omitted from the data base used to derive index parameters (not index values). The PCN and PCS coefficients are displayed in Fig. 48 for mutual comparison and for comparison with the coefficients displayed in Fig. 39. There is fair match between PCN and PCS coefficients in both versions and a good match between the parameters in the DMI#4 version and the present DMI version.

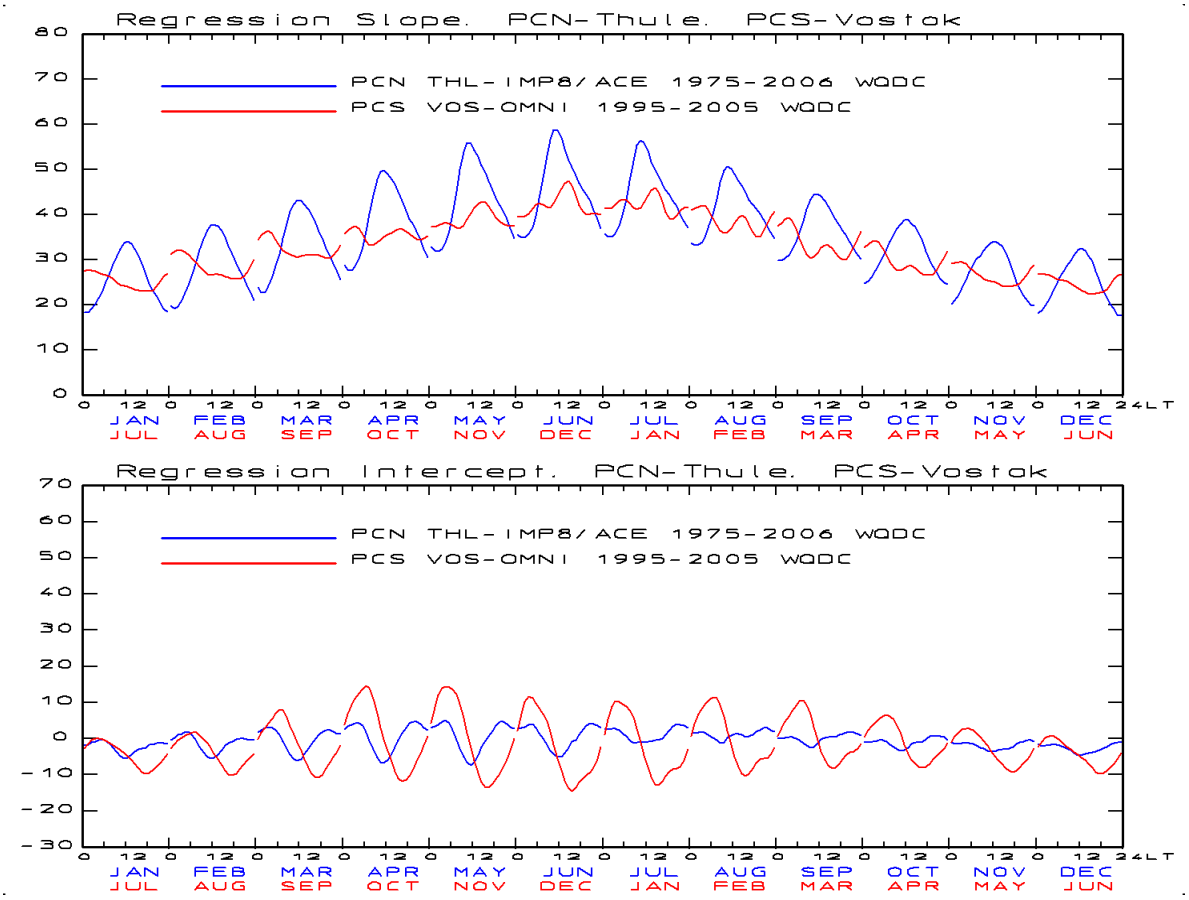

Fig. 48. Slope and intercept coefficients for PCN and PCS in DMI#4 version. (cf. Fig. 39)

The PCN and PCS values derived with the DMI#4 procedure have been used in: *Stauning* (2007, 2011a,b, 2012, 2013a,b,c, 2015), *Stauning and Troshichev* (2008), *Stauning et al.* (2006, 2008).

17.5. AARI#1 PCS index version

The AARI#1 PCS index version was based on Vostok magnetometer data and is described in *Troshichev et al.* (1988). The programming for this index version was developed by *V. G. Andrezen*. Data base, software and coefficients are not available. PC index values are available in a WDC-B2 report. PCS values calculated with this version have been used in: *Troshichev and Andrezen* (1985), *Troshichev* (1988), and *Troshichev et al.* (1988).

17.6. AARI#2 PCS index version.

AARI#2 PCS index values are based on Vostok magnetometer data. PCN index values are based on Thule data. There is no published description. Programmer: *R. Yu. Lukianova*. Data base for PCS coefficients is the Vostok magnetometer recordings and IMP-8 satellite data through the years 1992, 1995, and 1997. Software is not available. PCS index values in this version are available for the years 1992, 1995, and 1997-2000. QDC correction of the recorded magnetometer data was introduced in this version (*Troshichev and Lukianova*, 2002; *Lukianova et al.*, 2002).

Due to the sparse amount of available data and insufficient averaging and smoothing of the derived index parameters they appear quite erratic as seen in Fig. 49.

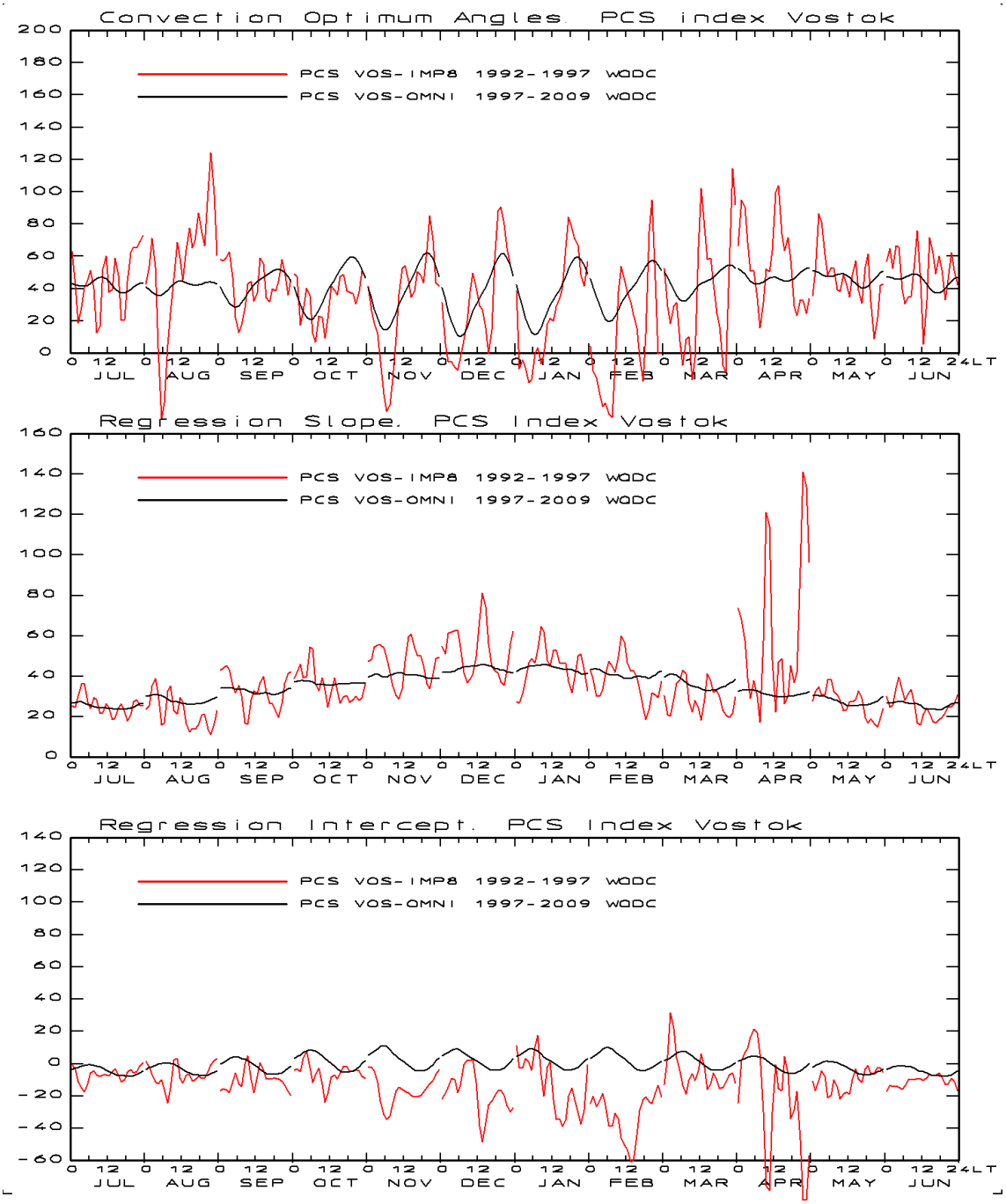

Fig. 49. PCS parameters, angle, slope, and intercept. AARI version #2 (red line). Present PCS-DMI version (black line) included for reference.

The PCS index values derived by using these fluctuating parameters display the corresponding erratic variations like seen in Fig 42. During most months, the average levels of the AARI#2 parameter are not so different from the level of the parameters in the present version.

Fig. 50 displays in a format like that used for Figs. 40a,b, 46, and 47, the distribution of PCS samples vs. corresponding values of the merging electric field delayed 20 min to account for the propagation from the Bow Shock Nose to the Polar Cap.

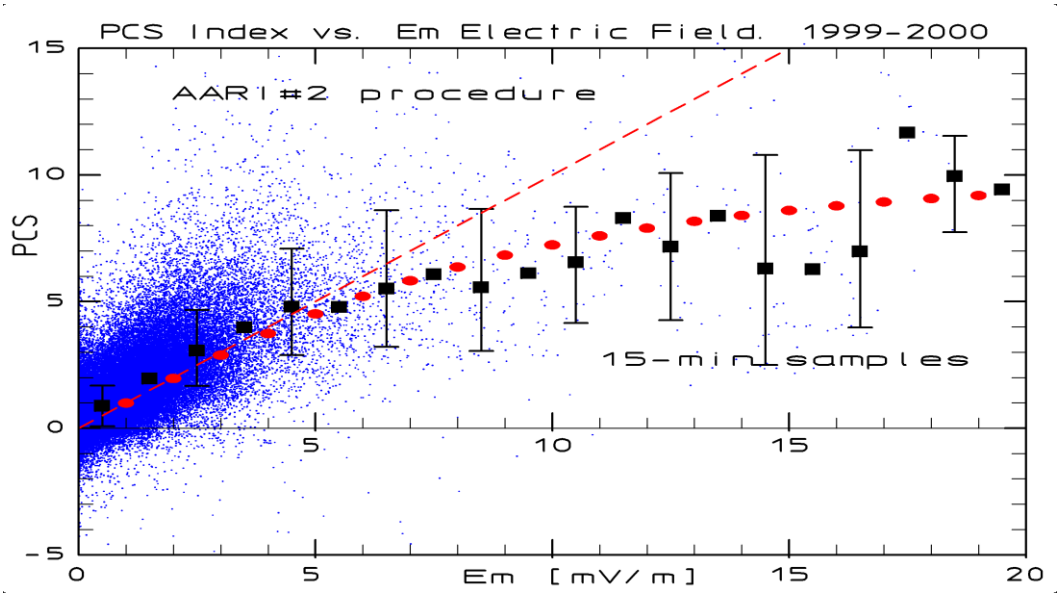

Fig.50. Version AARI#2 15-min PCS samples vs. corresponding merging electric field values based on OMNI BSN data. Delay 20 min.

In Fig. 50 it is seen that the PCS values are a little too high up to around 5 mV/m possibly due in part to the intersect values being more negative than those of the present PCS-DMI version. For the larger values where the slope is the dominant parameter, the PCS values track the approximation given be Eq. 32 (cf. Figs. 40a,b). It was (correctly) noted in *Lukianova et al*. (2002) that these PCS values are much larger than the contemporary PCN index values in the DMI#2 version (cf. Figs. 46 and 47)..

PCS values in this version have been used in *Lee et al*. (2004), *Lukianova* (2003, 2007), *Lukianova et al.* (2002), *Stepanova et al.* (2005a, 2005b, 2005c), *Troshichev and Lukianova* (2002), *Troshichev et al.* (2000). A modified version of the coefficients for the PCS and PCN indices have been presented in Lukianova (2007).

17.7. AARI#3 version of the PCS and PCN indices

A published description of the AARI#3 procedure is provided in *Troshichev et al*. (2006). The computer software was developed by *A. Janzhura*. Data base for the PCS and PCN coefficients was epoch 1998-2001. PCS and PCN coefficients are available in the graphical presentation in Fig. 51. PCN coefficients are available in tables. PCS and PCN index values have been made available for 1995-2006.

Several feature in the AARI#3 version have been improved compared to the previous AARI#2 version. The epoch of the data base for the coefficients have been extended to 4 years (instead of the 3 years 1992, 1995, 1997): Moreover, through this epoch, solar wind data have been continually available from the Wind and ACE spacecrafts, which helps to extend the data base compared to earlier versions using data from the IMP-8 satellite positioned in the undisturbed solar wind and having telemetry coverage in less than half the time (cf. section 4.1.) The quiet daily variation (QDC) used to correct the geomagnetic data from Vostok and Thule is now derived by an automated, objective technique (*Janzhura and Troshichev*, 2008) rather than based on the manual, subjective method used earlier. Furthermore, the averaging and smoothing techniques have been greatly improved in this version compared to the AARI#2 version.

The parameters (angle, slope, intercept) for the AARI#3 PCN and PCS indices are displayed in Fig. 51 in a color-coded version (Troshichev et al., 2006). Note the large differences in slope and intercept values. α(PCN-peak)≈90, α(PCS-peak)≈50. β(PCN-peak)≈-120, β(PCS-peak)≈-15. The large values of the slopes and the large negative values for the intercept for the PCN index vs. the PCS are caused by the high frequency of strong reverse convection events at Thule compared to Vostok (cf. Fig. 38), particularly at local midday hours (~ 16 UT) in the summer months, and during the solar maximum years used here.

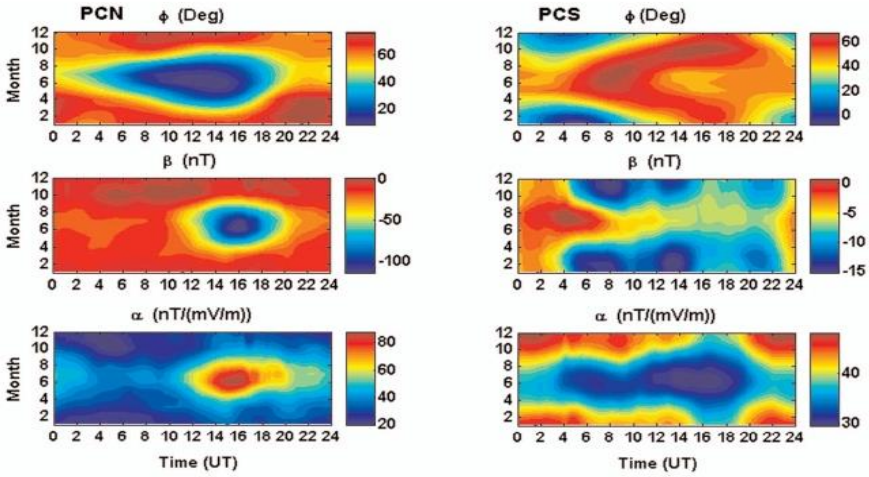

Fig. 51. PCN (left) and PCS (right) index parameters in AARI version #3.

The PCN index parameters for the AARI#3 version are shown in Fig. 52 in the format used for Fig. 39. The corresponding parameters for the present DMI PCN index are included in the diagrams for reference.

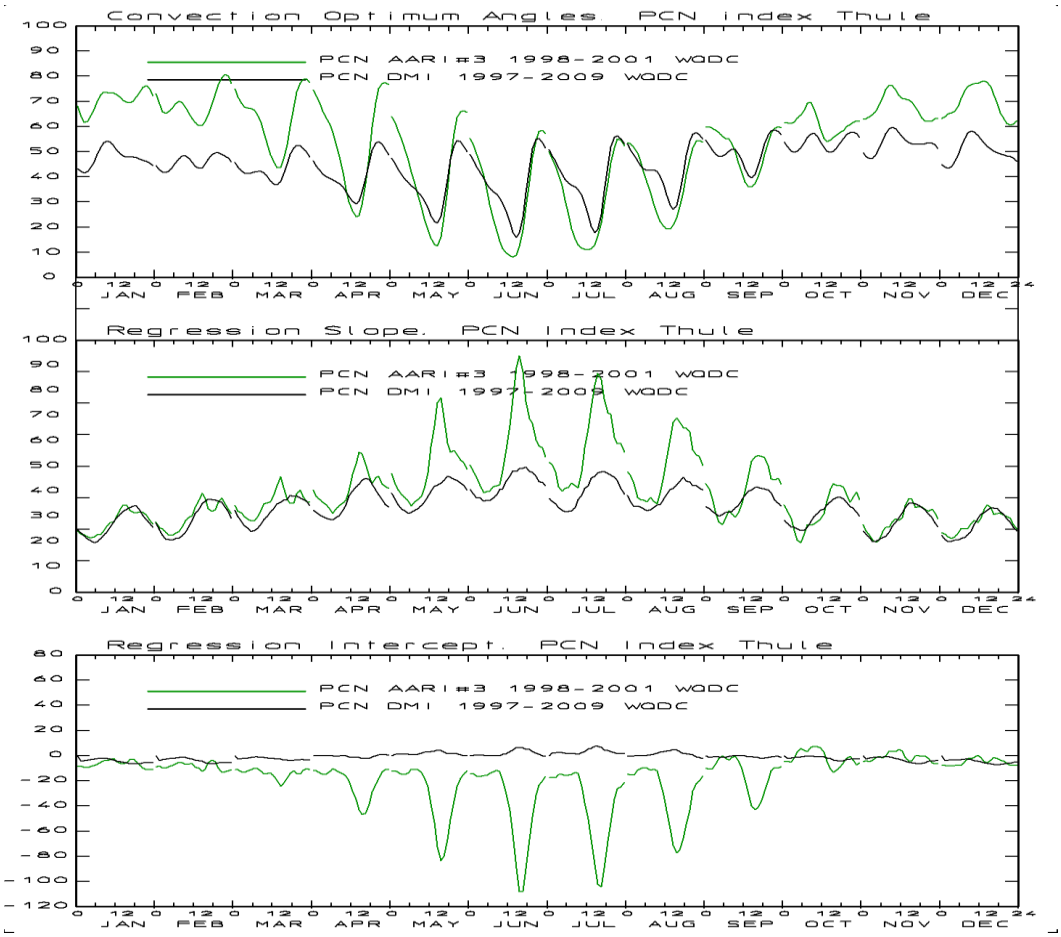

Fig. 52. Version AARI#3 PCN parameters (angle, slope, intersept) in green line. Corresponding PCN-DMI parameters in black line included for reference.

PCN and PCS index values derived with the AARI#3 procedure have been used in: *Janzhura and Troshichev* (2008), *Janzhura et al.* (2007), *Troshichev et al.* (2006, 2007a, 2007b).

17.8. AARI#4 version of the PCS and PCN indices.

A published description can be found at http://geophys.aari.ru/Description.pdf (*Troshichev*, 2011). Software was developed by *A. Janzhura*. Data base for the coefficients: 1995-2005. PCS index parameters (angle, slope, intersept) are available. PCN and PCS index values for 1995-2012 are available.

Compared to AARI#3 index version, the epoch for deriving index coefficients has been extended from 4 years at solar maximum (1998-2001) to 7 years (1998-2005) with less active years included. Like in the earlier AARI PC index versions, the strong reverse convection cases have not been omitted in the calculation of index coefficients. Therefore, the slope values are larger and the intercept more negative than those found in the DMI#4 and the recent DMI index version with the adverse concequences outlined in section 15.6.

For the quiet reference level to be subtracted from the observed data before calculations of index parameters and index values, a solar sector correction of QDC has been introduced (*Janzhura and Troshichev*, 2011). The solar sector modification of the QDC is meant to remove the effects of the changing sign of the IMF B_Y component in the "away" and "toward" sectors of the solar wind. However, the added term has little effect on the PC index values for the daytime hours but large, unfounded effects at the night and morning hours where the real IMF B_Y effects are small (*Stauning*, 2013a, cf. Fig. 33 here).

PCN and PCS index values derived with the AARI#4 version have been used in: *Frank-Kamenetsky and Troshichev* (2012), *Troshichev* (2010), *Troshichev and Janzhura* (2009, 2012a), *Troshichev et al.* (2011a, 2011b, 2011c, and 2012).

18. IAGA-endorsed version of PCN and PCS Indices.

A PC index version issued jointly by Arctic and Antarctic Research Institute (AARI) in St. Petersburg, Russia, and the Danish Space Research Institute, DTU Space, was endorsed by a IAGA committee in 2013. This version is mostly based on the AARI#4 index procedure. Programmer is *A. Janzhura*. PCN index values based on Thule geomagnetic data and PCS index values based on Vostok data were made available in 2014 at the web site http://pcindex.org that holds actual index values as well as archival data. The web site includes the document "Polar Cap (PC) Index" written by *O. A. Troshichev* (2011). However, a full description of the procedure is not found. Some statements on the index procedure and transcripts of some of the software involved may be found at the DTU Space ftp web site for PC indices: ftp://ftp.space.dtu.dk/WDC/indices/pcn/ .

The adverse features of the IAGA-endorsed PC index procedure and the lack of proper documentation were mentioned in *Stauning* (2015). The main issues discussed there were the derivation of the QDC level and the handling of reverse convection events. The IAGA endorsement implies the risk that the PCN and PCS indices derived by this version are being used in scientific analyses by unsuspecting scientists. The method, therefore, shall be analyzed in some dept here using the material provided in the referenced publications by *Troshichev* (2011) and *Janzhura and Troshichev* (2008, 2011). The latter publication was critizised in a commentary by *Stauning*, 2013a. No reply from the authors has been published.

18.1. The QDC method. The QDC method adopted in the IAGA-endorsed version has three steps. From the baseline-corrected geomagnetic data, daily values of solar sector (SS) terms are derived for both components. The method is described in *Janzhura and Troshichev* (2011). Next, initial QDCs are derived for both components using the method described in *Janzhura and Troshichev* (2008). Finally, the SS terms are added to the initial QDCs to create "effective" QDCs (*Janzhura and Troshichev* (2011).

The initial concept of the reference Quiet Day Curve (QDC) for Polar Cap (PC) index calculations was defined in *Troshichev et al.* (2006), by the statement: "*Magnetic deviations δD and δH are calculated from a certain level, "curve of quiet day", which presents the daily magnetic variation, observed at the particular station during extremely quiescent days*".

The QDC procedure developed at AARI (*Troshichev et al*, 2006; *Janzhura and Troshichev*, 2008) as well as the SRW QDC procedure developed at DMI (*Stauning*, 2011b) were built on this concept. However, in the AARI#4 version and in the IAGA-endorsed version, solar wind sector IMF B_Y related (SS) quantities

derived from the daily median geomagnetic component values (whether quiet or disturbed) have been added to the initial QDC values. This term makes the level of the resulting "effective" QDC vary with the varying IMF B_Y component without affecting the amplitude of the daily variation. An example for the H-component from *Janzhura and Troshichev*, 2011 (their Fig. 1) is shown in Fig. 53 here. The wavy envelope with amplitudes up to ~ 100 nT for the QDC corresponds to the IMF B_Y variations. For this interval (summer, 2001) the average effects on the quiet level is shown in Fig. 54 (local noon~16UT).

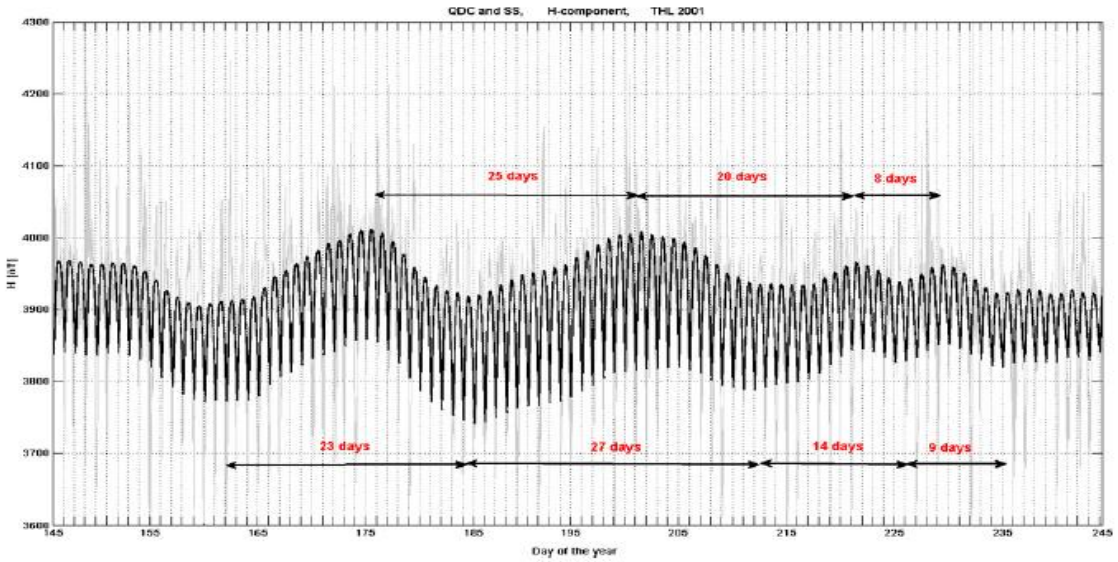

Fig. 1. Superposition of the actual variation of 1-min values of the geomagnetic H-component observed at Thule station in the summer season of 2001 (thin lines) and the quiet daily curve (QDC) characterizing the daily variation of the quiet geomagnetic field (thick solid lines).

Fig. 53. H-component (Thule) in faint grey line and superposed "effective" QDC in black line (from *Janzhura and Troshichev*, 2011).

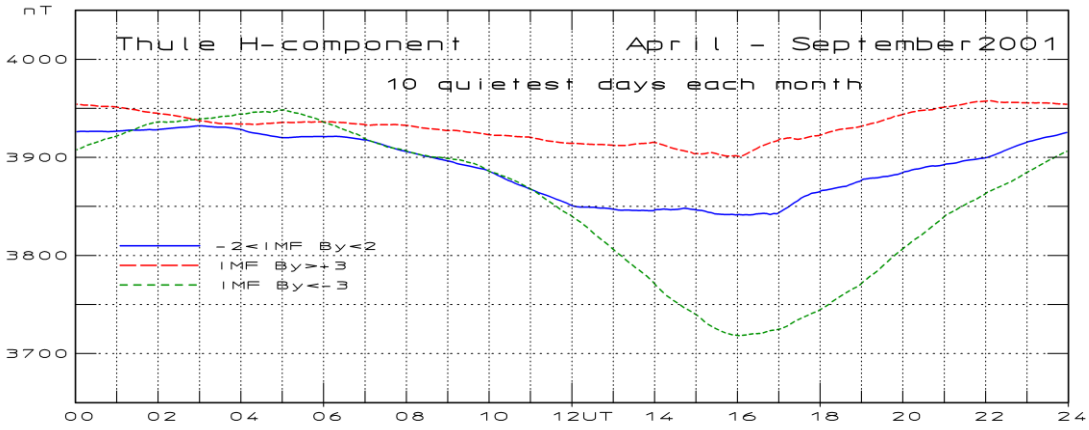

Fig. 54. Average daily variation of the H-component (Thule) for IMF B_Y>3 nT (red line), -2<IMF B_Y <+2 nT (blue), and IMF B_Y <-3 nT (green) during the 10 quietest (QQ) days each month.

The varying top values of the QDC-H in Fig. 53 are local night values. However, it is very clear from the daily H-component variations for different IMF B_Y levels in Fig. 54 that the night values of the H-component are not affected by the varying IMF B_Y while the daytime values and thus the amplitude in the daily variation are strongly affected by the IMF B_Y level and quite different for positive and negative levels. Consequently, the upper envelope (night values) of the varying QDC-H should have been fairly steady with regard to IMF B_Y variations while the lower level (the daytime H-component values) should vary with IMF B_Y to provide the varying QDC amplitudes from night to daytime.

In order to get further insight in the QDC method, the three steps in the derivation method described in *Janzhura and Troshichev* (2011) are repeated here. Fig. 55 displays for the interval presented in Fig. 53, i.e., days 145-245 of 2001, the recorded H-component values in blue line. The initial H_{QDC} values from a file supplied by *A. Janzhura* have been superimposed in red line. On top of these data the smoothed daily median values have been plotted in heavy black line. At the bottom of the diagram, smoothed IMF B_Y values derived from ACE satellite data have been plotted. Note the correspondence between the median values and the IMF B_Y values. Also note the uniform or slowly varying amplitude of the QDC values.

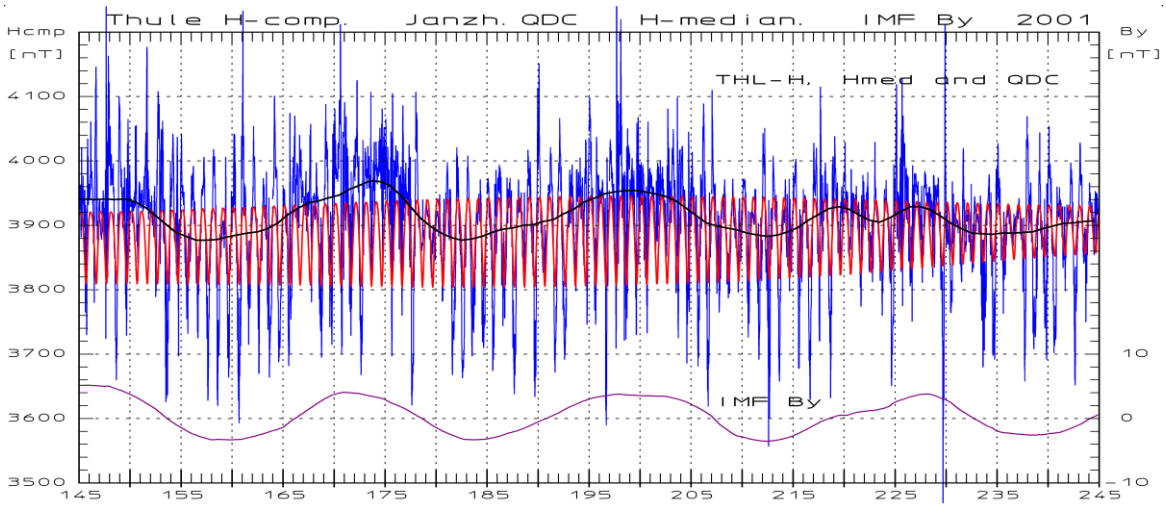

Fig. 55. Thule H-component (blue line), initial QDC (*Janzhura*) in red line, and smoothed daily median H-component values (black) for days 145-245, 2001. Smoothed IMF B_Y in magenta line.

The solar sector term, ΔH_{SS} , is the amplitude of the daily median value counted from the component baseline and processed to derive a smooth sequence. In *Janzhura and Troshichev*, 2011 (*J&T2011*), details of the the real-time processing are provided in p. 1196, while steps in a corresponding smoothing process on past data are illustrated in their Fig. 6. However, the two methods appear to give strongly differing results.

The real-time method aims at producing the solar sector term for an actual day numbered n=0 based on Cubic Spline extrapolation of a set of 3-days average median values from the preceeding days: (i) days n-9 to n-7, (ii) n-7 to n-5, (iii) n-5 to n-3, and (iv) n-3 to n-1. This method has apparently given the sets of values ranging for the ΔH_{SS} term from -50 nT to +150 nT for June and July as illustrated in their Fig. 8. However, in their Fig. 6 for June, the month where the largest excursions occur, the range for ΔH_{SS} is from -35 nT to +65 nT, i.e., only around half the values found from Fig. 8 of *J&T2011*. The cause of the differences in ΔH_{SS} seen from their Fig. 6 to Fig. 8 is not known.

The steps in the smoothing processing of the H-component medians illustrated in Fig. 6 of J&T2011 are repeated in Fig. 56 here using the same basic data from Thule. The 1-day, 3-day, and 5-day median values in Fig. 56 are close to the corresponding values in Fig. 6 of J&T2011. The heavy magenta line in Fig. 56 displays 1-day median values that have been Gaussian-smoothed over current day ±3 days. This curve ressembles the corresponding smoothed values in J&T Fig. 6. The dotted black line in Fig. 56 displays values found by applying Cubic Spline extrapolation according to the procedure defined in p. 1196 of *Janzhura and Troshichev* (2011) to a sequence of 3-day median values scaled from their Fig. 6.

As an example, from *J&T2011* Fig. 6, the sequence of values from the 3-day medians (green line) leading to the ΔH_{SS} on 22 June are (i) 48 nT on 14 June, (ii) 43 nT on 16 June, (iii) 58 nT on 18 June, and (iv) 84 nT on 20 June. With a Cubic Spline polynomium fitted to this steeply rising series and extrapolation from the end point with the slope defined there, gives on 22 June the value 114 nT. The raw 1-day median value (blue line) is 95 nT, the 3-day value (green line) is 80 nT, while the smoothed value (magenta line) gives 65 nT on 22 June. The plot in Fig. 56 and the example here illustrate the confusion of defining proper solar sector terms and the risk of deriving strongly fluctuating, excessive SS terms by using the real-time method from *J&T2011*.

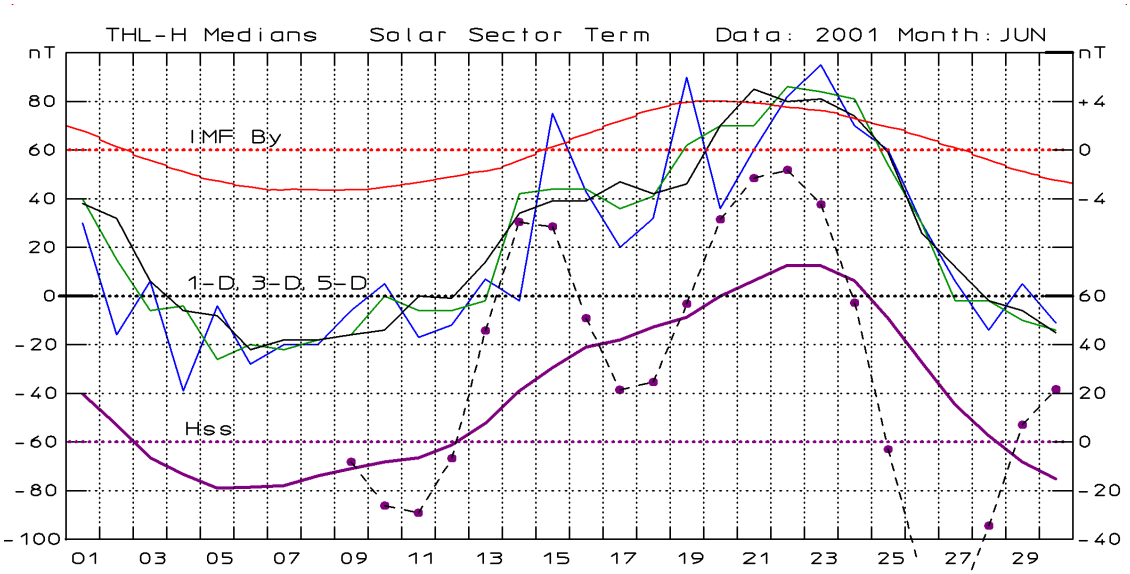

Fig. 56. June 2001. 1-day median ΔH-component values (blue line), 3-day median (green), 5-day median (black). Smoothed median ΔH_{SS} (heavy magenta) and "real-time" Cubic Spline extrapolated ΔH_{SS} (dotted black) values are displaced by -60 nT (scale to the right). IMF B_Y (red) are multiplied by 5 and displaced +60 nT to separate the curves. (cf. Fig. 6 of *Janzhura and Troshichev*, 2011)

With the smoothed ΔH_{SS} values presented in Fig. 56, the "effective" H_{QDC} can now be derived by adding the solar sector terms to the initial (Janzhura) H_{QDC} shown in Fig. 54. The result is shown in Fig. 57.

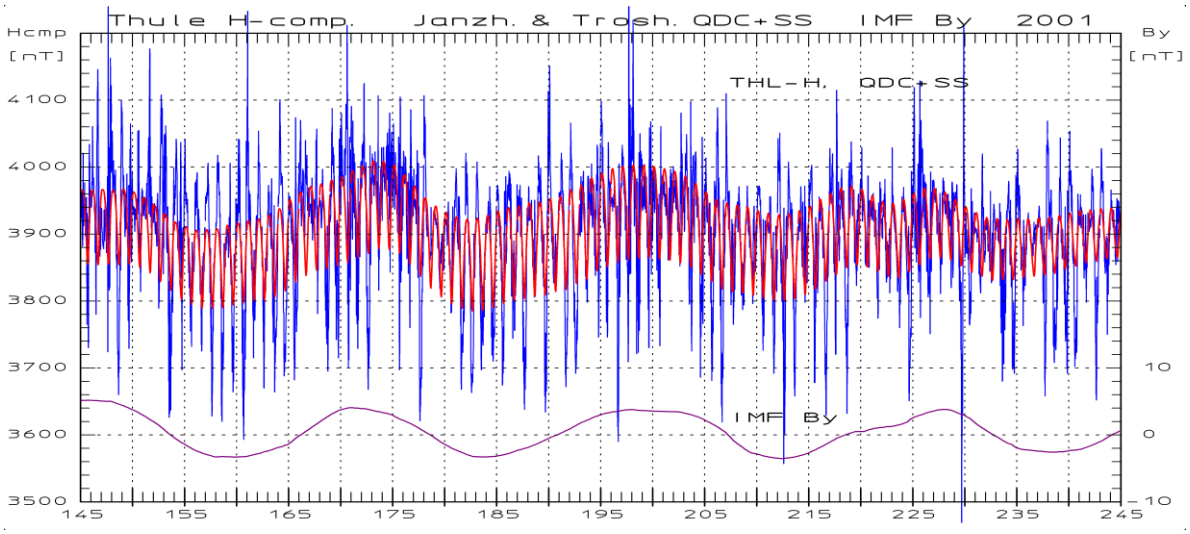

Fig. 57. Thule H-component (blue line), "effective" H_{QDC}=initial H_{QDC} (Janzhura) + ΔH_{SS} (red line). IMF B_Y in magenta line with separate scale (right). ΔH_{SS} from the strongly smoothed curve in Fig. 56.

The display of the H-component and the "effective" H_{QDC} in Fig. 57 is the same as the corresponding display (in grey-tone) in Fig. 1 of *Janzhura and Troshichev* (2011) or (in color) in Fig. 4.10 of Troshichev and Janzhura (2012). The adverse features of this QDC are also the same: the varying H-component night level (upper envelope) and the fairly constant amplitude (separation between upper and lower envelope).

The effects of the solar sector contribution to the QDC is seen by specifying the QDC (vector) terms, $\boldsymbol{F}_{QDC,EFF} = \boldsymbol{F}_{QDC,INIT} + \Delta\boldsymbol{F}_{SS}$, in the PC index formula in Eq. 3:

$$PC = \{(\boldsymbol{F} - \boldsymbol{F}_{BL} - \boldsymbol{F}_{QDC,\,EFF})_{PROJ} - \beta\}/\alpha = \{(\boldsymbol{F} - \boldsymbol{F}_{BL} - \boldsymbol{F}_{QDC,INIT} - \Delta\boldsymbol{F}_{SS})_{PROJ} - \beta\}/\alpha \qquad (34)$$

Thus, an extra contribution from the solar sector term, $\Delta \boldsymbol{F}_{SS} = (\Delta H_{SS}, \Delta D_{SS})$ based on the daily median component values, is added to the PC index values throughout day and night regardless of whether there at the actual time is any geomagnetic variation to justify the contribution:

$$\Delta PC = - \Delta \boldsymbol{F}_{SS,PROJ} / \alpha \qquad (35)$$

The basic error in this procedure is the addition of a constant term ($\Delta \boldsymbol{F}_{SS}$) to the QDC whether justified in the real effects of the IMF B_Y variations (e.g., at the dayside) or not (e.g., at the night side) cf. Fig. 54. Moreover, the contribution depends, as shown in Eq. 35, on the projection to the optimum direction and on the value of the slope. Both parameters change during the day. The projection of the solar sector term ($\Delta \boldsymbol{F}_{SS}$), a constant vector in the rotating local coordinate system, to a rather steady direction in space, changes the sign of the contribution to the PC index forth and back during a day. The slope, α, is smaller (the effect larger) during night time than during midday hours.

The effect by using this QDC term was estimated in *Stauning* (2015) to give unfounded index contributions, $\Delta PCN = \Delta F_{SS,PROJ}/\alpha$, of up to 2.4 mV/m during local night and morning hours. For the example case presented in Fig. 58 from *Stauning* (2012) based on data for the solar sector term, ΔF_{SS}, provided in *Janzhura and Troshichev* (2011), the unfounded contribution to the PC index on 22 June, 2001, was found to peak at 06 UT (~ 02 LMT) on -2.4 mV/m. For quiet geomagnetic fields this contribution would be the final PC index value and would indicate NBZ conditions. At onset of a geomagnetic storm, usually indicated by PC>2 mV/m (cf. section 15.1), the unfounded contribution would add to indicate just quiet conditions, i.e., PC≈0. Still worse, if the forward projection estimate of the solar sector term (*Janzhura and Troshichev*, 2011) is used for real-time derivation of PC index values for Space Weather forecasts, then the unfounded contribution to the index could be twice as large due to the effects of steep gradients in the sequence of median values (cf. the example discussed above).

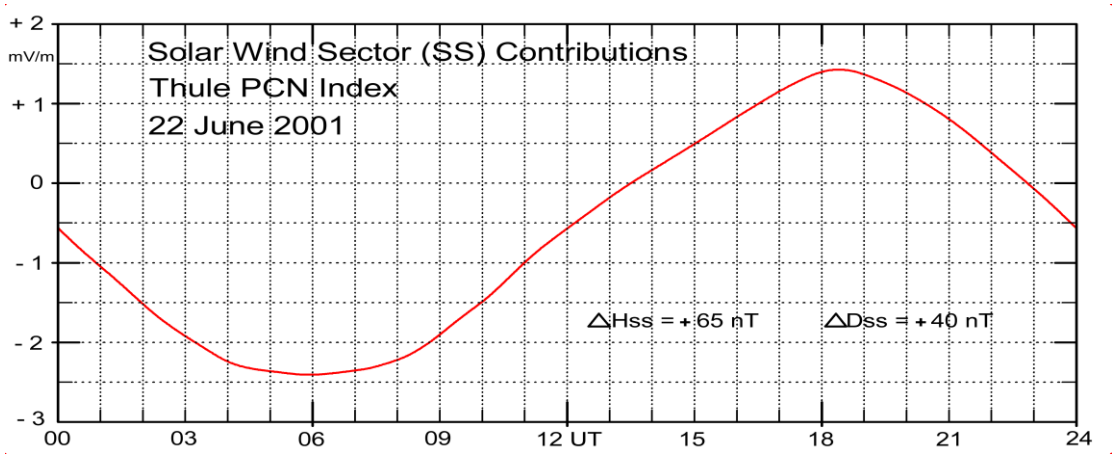

Fig. 58. IMF B_Y-related solar wind sector (SS) contributions to the PCN index values derived according to the "effective QDC" procedure defined in *JT2011* with the excursions ΔH_{SS} = 65 nT defined in their Fig. 6b and ΔD_{SS} = 40 nT. Index coefficients are from http://pcindex.org.

18.2. Effects of reverse convection on the IAGA-endorsed PC index procedure.

In addition to pointing to the problems, particularly the unfounded night and morning contributions to the PC indices, caused by the addition of the solar wind sector (SS) term to the QDC values, the adverse effects of including reverse convection cases in the data base for the index coefficients was documented in *Stauning* (2015). Like for the AARI#1- #4 and the DMI#1- #3 versions, the lack of discrimination against strong reverse convection events during northward IMF B_Z (NBZ) conditions (cf. section 15.6) has adverse consequences for the IAGA-endorsed index procedure. It was demonstrated in section 15.6 here that including the reverse convection events in the data base for regression made the slope larger and the intersept more negative. Since reverse convection events are more frequent and stronger at Thule than at Vostok, as shown in section 16.6 (see Fig. 38), these events, furthermore, cause imbalance between

coefficients for PCN and PCS. The imbalance between slope and intersept values for PCN and PCS is clearly seen in the plot of coefficients in Fig. 59.

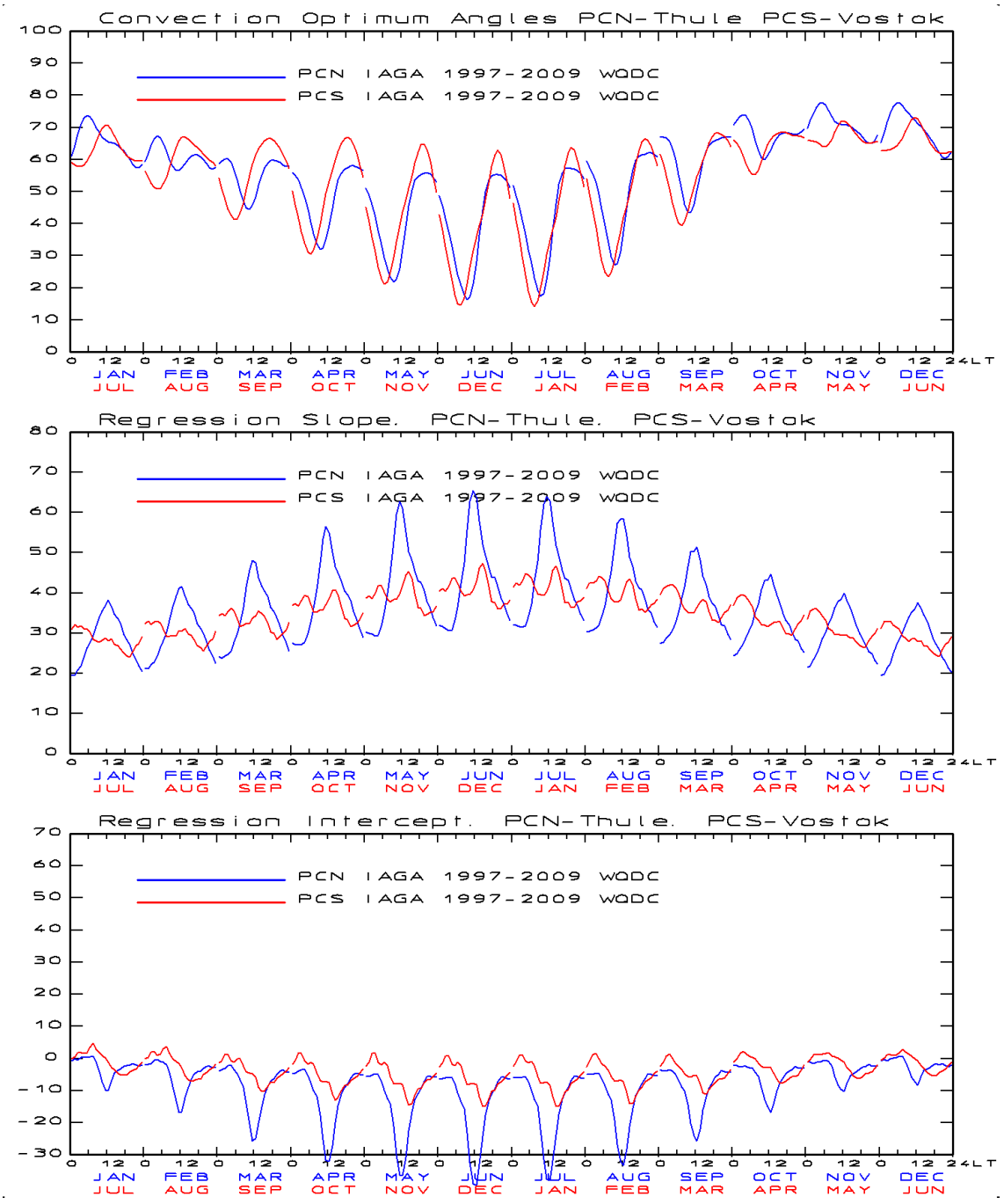

Fig. 59. Monthly mean values vs. local time of parameters for PCN (blue line) and PCS (red line) in the IAGA version. The sequence of months has been modified for PCS values.

18.3. Examples of adverse consequences of the IAGA-endorsed PC index procedure.

Examples of the adverse consequences of the use of a solar sector term added til the QDC level are shown in *Stauning* (2015). Fig. 60 shows the mean values of the PCN index and the merging electric field for an interval of 8 days, 18-25 June 2001, through a period with strong positive IMF B_Y values (see Fig. 3). In its definition the PCN index should be equal to the merging electric field on the average. The systematic smaller values of PCN compared to E_M by ~ 1 mV/m between 00 and 09 UT matches the estimated effect

of the solar wind sector (SS) contribution that maximizes at around -2 mV/m in the local morning hours (at ~ 06 UT) on 22 June (cf. Fig. 58) at the middle of the data interval.

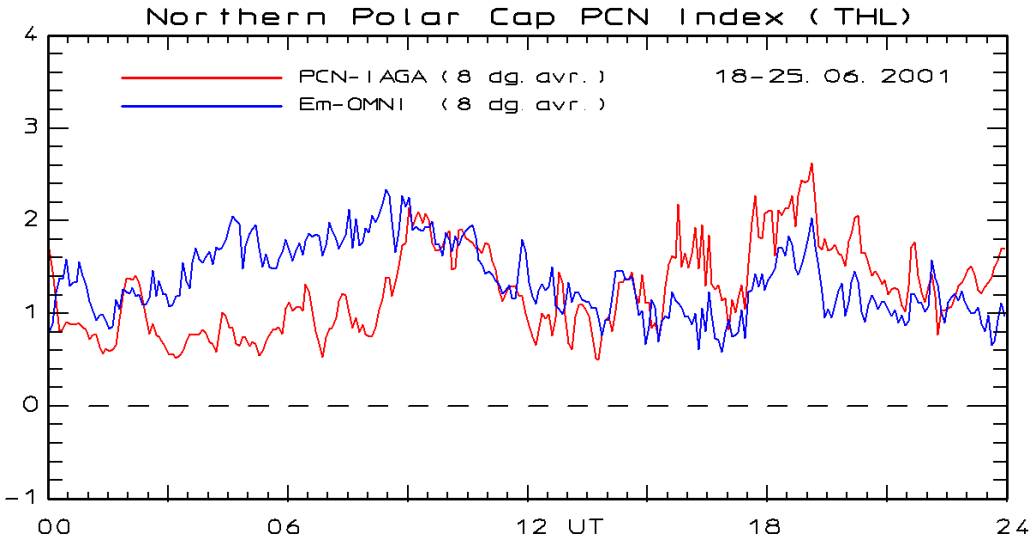

Fig. 60. Mean PCN and E_M values through 18-25 June 2001 with strong positive IMF B_Y. (from *Stauning*, 2015)

The effect of including strong reverse convection events in the data base for calculation of index coefficients are most distinctly seen at midday hours in summer months during intervals of quiet conditions, where $\Delta F_{PROJ} \approx 0$ such that PC $\approx -\beta/\alpha$ (cf. Eq. 3). An example from *Stauning* (2015) is presented in Fig. 61. The enhancement of PCN over E_M by almost 1 mV/m corresponds well to the values of $\beta/\alpha \approx -40/55$ at this time (cf. Fig. 59).

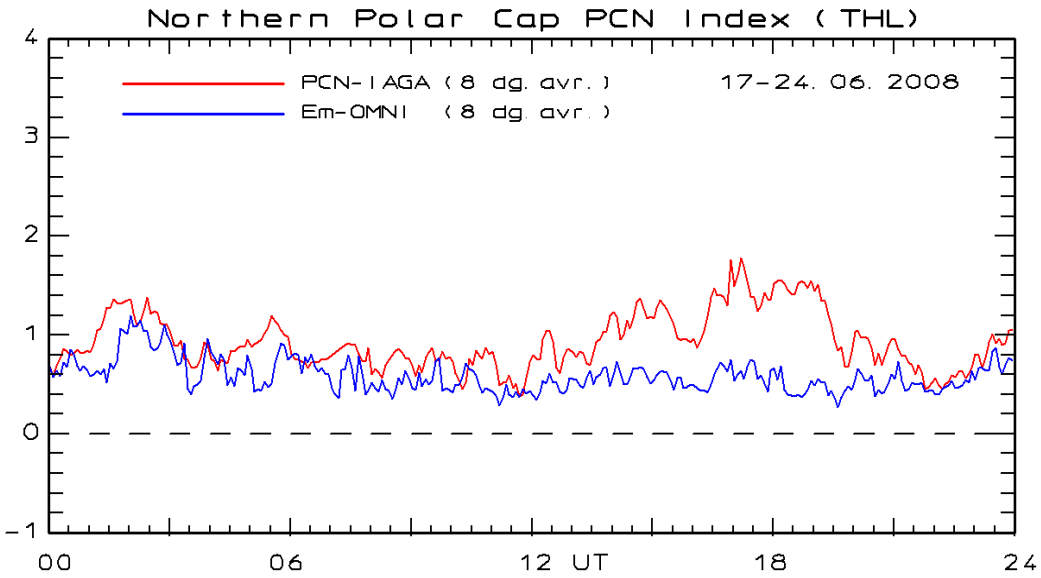

Fig. 61. Mean PCN and E_M values through 17-24 June 2008 with quiet conditions. (from *Stauning*, 2015)

The adverse effects of the solar sector term in the QDC and the inclusion of reverse convection cases in the regression seriously devaluate the value of the IAGA PC index for scientific analyses of solar wind-magnetosphere interactions as well as space weather forecasts.

Indices in this version have been used in: Troshichev, O. A. and D. A. Sormakov (2015); Troshichev,O., N. A. Podorozhkina , D. A. Sormakov, A. Janzhura (2014).

19. Summary

For the derivation of Polar Cap indices, in spite of the simple formulation in Eqs. 1-3, two basic problems still need final solutions. One is the proper definition of the quiet level from which disturbances are counted. Here, the formulation defined in *Troshichev et al.* (2006) by the statement: "*Magnetic deviations δD and δH are calculated from a certain level, "curve of quiet day", which presents the daily magnetic variation, observed at the particular station during extremely quiescent days*" is advocated. The QDC is built from the quietest samples taken at conditions as similar as possible to the day in question. The recurrence statistics presented in Fig. 34 is the basis for the solar rotation weighted (SRW) QDC method. The result is the robust determination of reliable QDC levels that include proper variations with the IMF B_Y solar sector structure. An example is presented in Fig. 62.

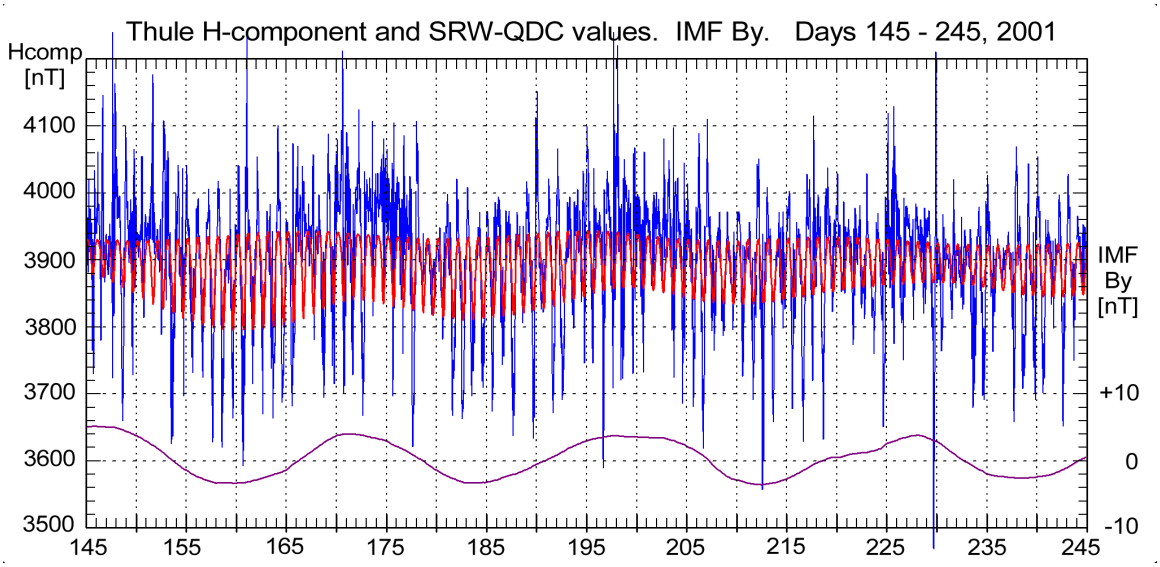

Fig. 62. Thule H-component (blue line) with superposed QDC (red line) for days 145 to 245 of 2001.Smoothed IMF B_Y variations in magenta line. (from *Stauning*, 2015)

Note in Fig. 62 the steady upper envelope for the QDCs (night values) while the lower envelope (day time values) varies considerably to let the QDC amplitude (range between upper and lower envelope) vary with the IMF B_Y conditions (sector structure) in agreement with Figs. 33 and 54. Note the contrast to the QDC variations displayed in Fig. 53 from *Janzhura and Troshichev*, 2011 (their Fig. 1).

The handling of reverse convection cases in the regression to derive index coefficients, slope and intercept, is another issue that should be settled. The basic idea behind the PC index (e.g., *Troshichev et al*, 2006) is the scaling of polar magnetic variations with a parameter in the solar wind to create a disturbance index that is independent of local time, season, and location within the Polar Cap. The solar wind parameter selected for this purpose is the *Kan and Lee* (1979) merging electric field (cf. Eq. 2). This parameter is considered to represent the energy input from the solar wind to the magnetosphere, which is a property that the PC index is supposed to inherit.

Thus, conditions that produce negative values of the PC index violate the proportionality of the projected magnetic variations with the non-negative merging electric field and could not possibly represent the energy input from the solar wind to the magnetosphere. The reverse convection cases, consequently, belong to a different class of Polar Cap conditions that should not be allowed to enter the calculation of parameters for scaling of geomagnetic variations at forward convection cases vs. the merging electric field to produce PC index values. The occurrence of negative PC index values could still be used to indicate the intensity of reverse convection conditions.

In addition to the different handling of the definition of the quiet level from which the geomagnetic disturbance values to be used in the calculation of PC indices are counted, there are large differences between the parameters of the various PC index versions. Fig. 63 displays the slope and intersept regression coefficients, for the DTUS#1 (=DMI#2, cf. section 17.2), the AARI#3 (cf. section 17.7), the IAGA (cf. section 18), and the actual DMI PCN versions. The optimum direction angles are not so different in the different versions. These values are based on largely the same procedure where the differences in handling the QDC and the reverse convection cases are not so important.

On the contrary, the slope and intersept values are strongly different for the different versions. Most notable are the large slope values and strongly negative intersept values at midday hours in the summer months. For the DTUS#1 (PCN2) version the excessive slope and intercept values could be the result of the odd regression procedure outlined in section 17.2 (cf. Fig. 43). For the AARI#3 (and AARI#4 not shown) and the IAGA-endorsed PCN versions, the excessive slope and intersept values were the results of including reverse convection cases in the regression. The AARI#3 version was built on data from the solar maximum years 1999-2002, where the strong reverse convection cases were much more frequent (cf. Fig. 38) than the average occurrence frequency for the interval 1997-2009 on which the IAGA version is built. The slope and intersept values in the IAGA version are reduced compared to those of the AARI#3 version but not brought down to the levels of those of the DMI version where strong reverse convection events were excluded from the data base used for calculations of coefficients.

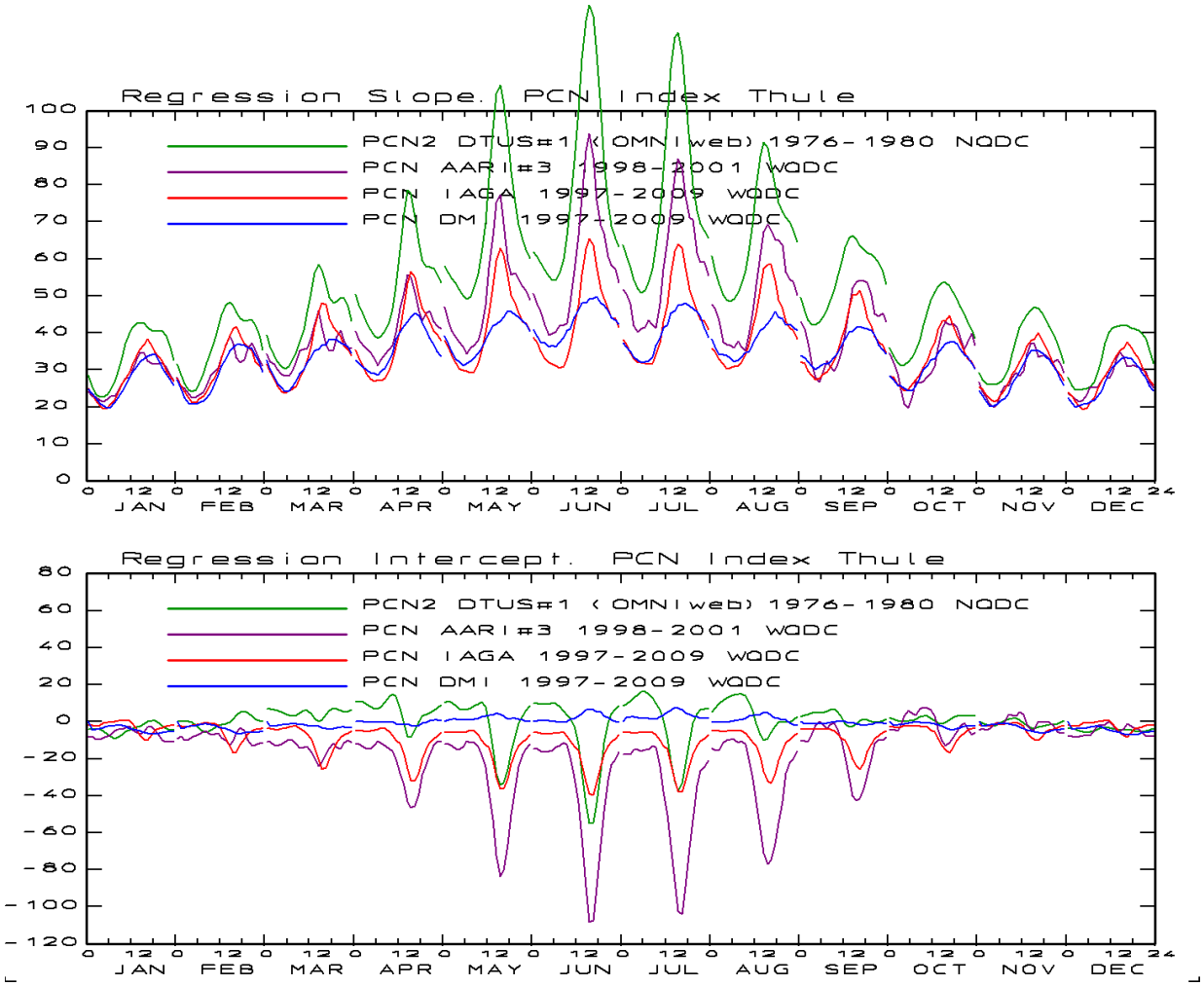

Fig. 63. Slopes (top), and intersepts (bottom) for PCN2 (DTUS#1, green line), PCN (AARI#3, magenta), PCN (IAGA, red), and PCN DMI (blue) versions.

In addition to the adverse consequences of the excessive slope and intersept values for the PCN indices as seen most distinctly in Fig. 47 for the PCN2 index during midday hours in the summer months, these parameters are out of balance with the corresponding parameters for the PCS indices based on geomagnetic observations from Vostok. Such a balance could be expected from the similarity of forward convection intensities displayed in Fig. 37. Thus, possible differences between the levels of slope and intersept coefficients (taking differences in season and local time into account) are caused by the different occurrence of strong reverse convection events at Thule and at Vostok. Fig. 64 displays the PCS parameters for the AARI#4 (green line), IAGA-endorsed (red line), and DMI (magenta) index versions. The optimum direction angles are not so different between Fig. 63 and Fig. 64. However, while the slope and intersept values for the AARI#4, and IAGA PCS versions that agree quite well with the DMI PCS version, they disagree strongly with the corresponding coefficient values in the PCN versions. The coefficients for the DMI PCN and PCS versions agree quite well as shown in Fig. 39.

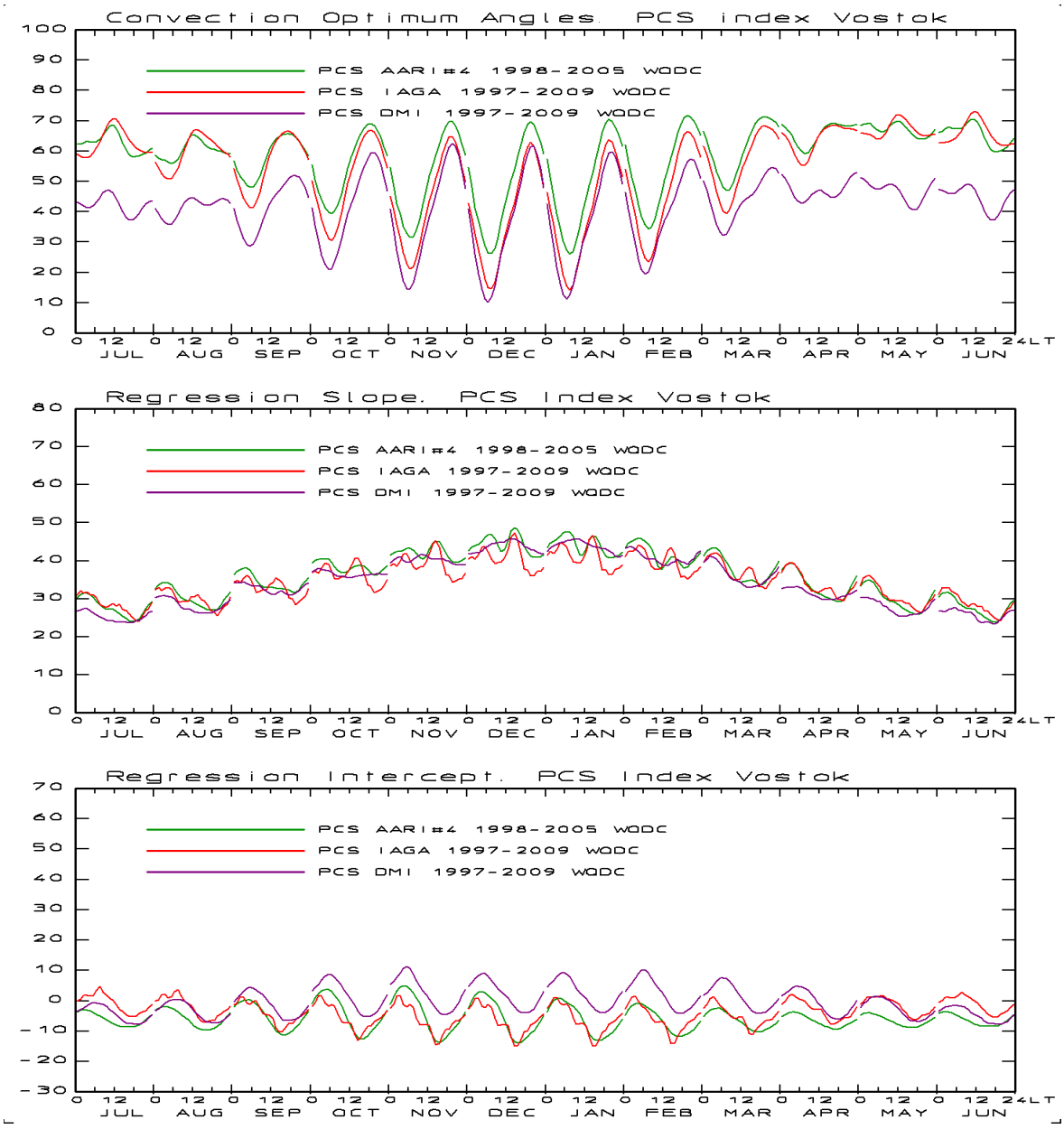

Fig. 64. Optimum direction angle (top field), slope (middle), and intersept (bottom) for PCS (AARI#4, green), PCS (IAGA, red), and PCS (DMI, magenta) versions.

A direct comparison between PCN index values derived by the DMI version and the PCN values in the IAGA-endorsed version available at http://pcindex.org is shown in Fig. 65 for the year 2008 and in Fig. 66 for year 2001.

Solar activity was very low in 2008 and the polar magnetic variations, ΔF, were generally rather small. From Eq. 3 for the PC index it may be seen that the contributions from the ΔF_{PROJ} /α term would then be fairly small, while the contributions from the intercept could dominate in much the same way as shown in Fig. 61, that is, by generating a PCN enhancement of -β/α ≈ 0.5 – 1.0 mV/m during daytime hours (cf. Figs. 59 or 63). For the DMI version, the intercept is fairly small (cf. Figs. 29 or 63) and the corresponding contribution from β/α would be within ± 0.25 mV/m at all times. The resulting differences between PCN(DMI) and PCN(IAGA) take (mostly negative) values between 0.0 and 1.0 mV/m.

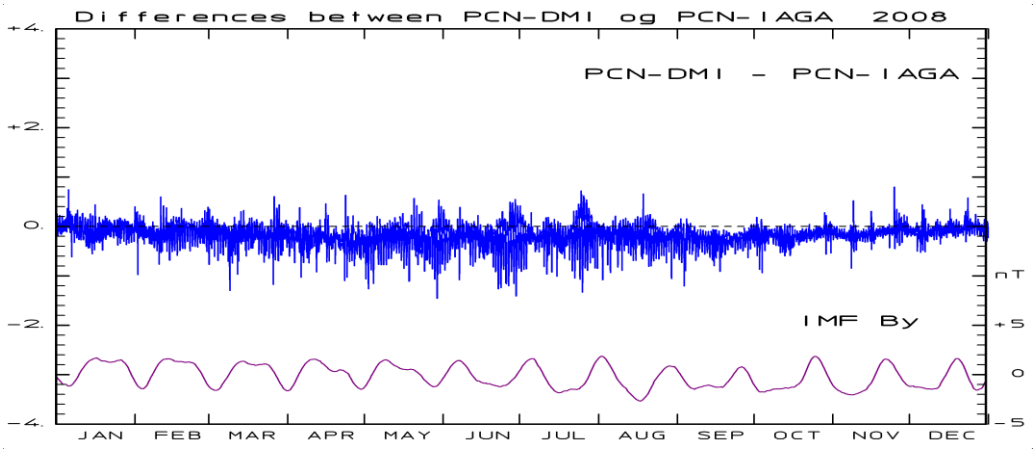

Fig. 65. Differences (in mV/m) between PCN (DMI) and PCN(IAGA) values during 2008. Smoothed IMF B_Y included for reference.

The corresponding diagram for the differences between PCN(DMI) and PCN(IAGA) through a year with high solar activity is shown in Fig. 66 for 2001. Through this year the level of polar magnetic activity is very high. Thus, the first PC index term in Eq. 3, ΔF_{PROJ} /α, will dominate over the intercept term, β/α. The slope values, α, for the IAGA version are much higher than the corresponding values for the DMI version (due to reverse convection cases). Hence, the PCN(IAGA) index would be smaller than PCN(DMI). Furthermore, the different methods to derive QDC levels, particularly the IMF B_Y-related solar sector term in the IAGA-endorsed procedure (cf. Figs. 58 and 60), enhance the differences, positive as well as negative.

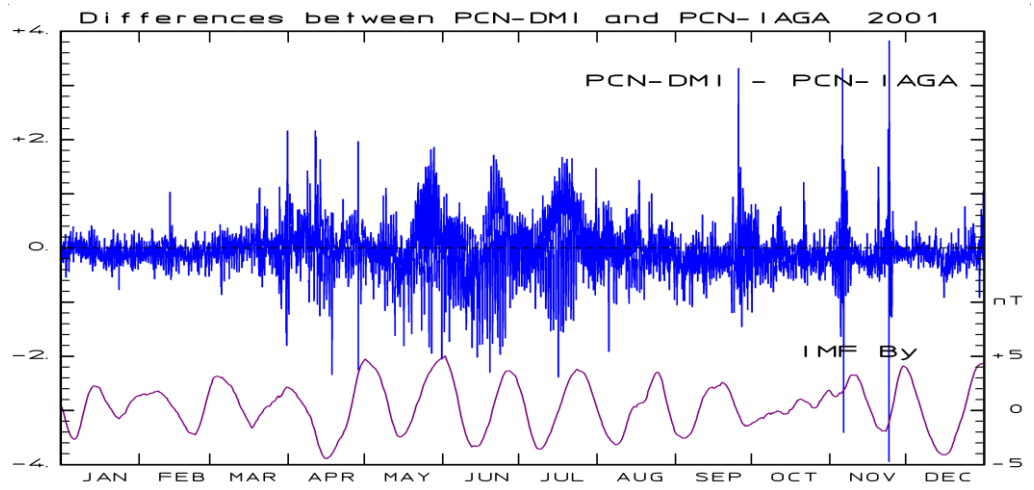

Fig. 66. Differences (in mV/m) between PCN (DMI) and PCN(IAGA) values during 2001. Smoothed IMF B_Y included for reference.

In Fig. 66, the PCN differences often reach levels between 1 and 2 mV/m, at times they reach between 3 and 4 mV/m. Note the strong modulation related to IMF B_Y during the summer months. The large excursions are probably the result of the solar sector term included in the QDC for the IAGA-endorsed version (cf. discussion in section 18.1).

The corresponding diagrams for the differences between PCS indices in the DMI version and the IAGA-endorsed version are presented in Fig. 67 for the solar quiet year, 2008, while Fig. 68 presents the differences between the two versions for the solar maximum year, 2001.

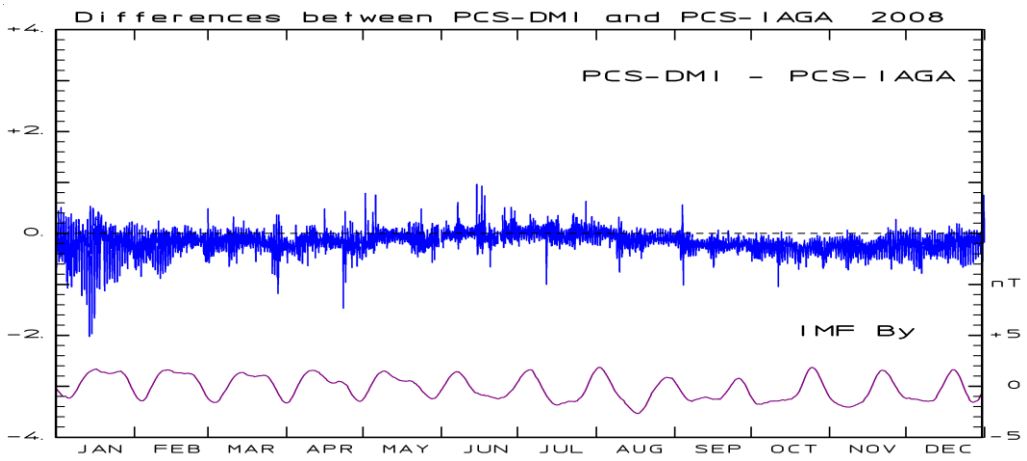

Fig. 67. Differences (in mV/m) between PCS (DMI) and PCS(IAGA) values during 2008. Smoothed IMF B_Y included for reference.

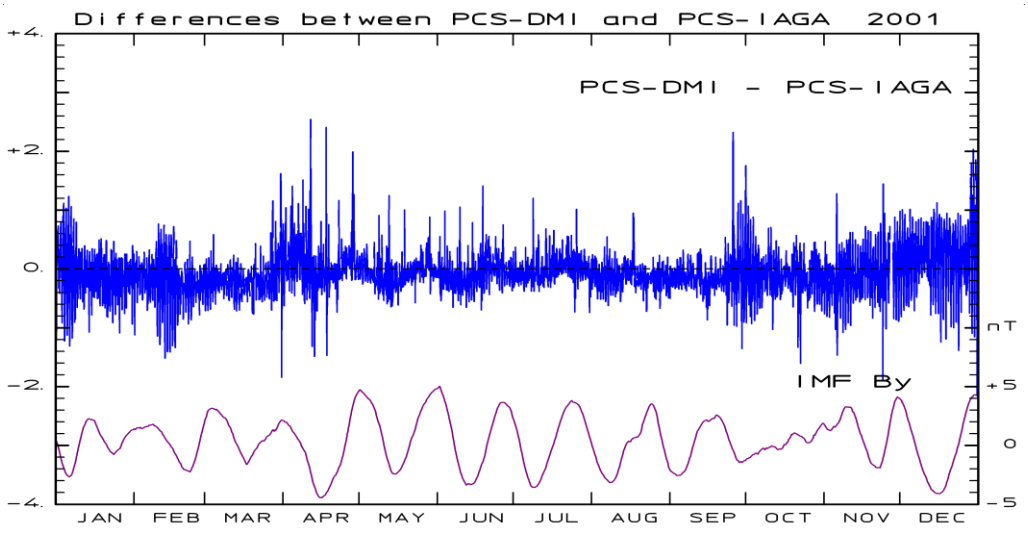

Fig. 68. Differences (in mV/m) between PCS (DMI) and PCS(IAGA) values during 2001. Smoothed IMF B_Y included for reference.

The differences between PCS values during the year of high solar activity appear related to the IMF B_Y variations in much the same way as seen for PCN in Fig. 66. This feature is probably related to the use of a solar sector contribution to the QDC level in the IAGA-endorsed version. Unfortunately, the lack of documentation of the IAGA-endorsed PC index procedures precludes a more thorough investigation.

According to the accuracy criteria defined in section 15.1, one of the two PCN/PCS versions is definitely not suitable for use in scientific analyses, and hardly reliable enough for space weather forecasts.

20. Conclusions.

For the calculation of coefficients, α, β, and φ, for PCN and PCS indices in the different versions, there are essential differences, which relate to:

- The epoch of data used for the calculation of PC index coefficients.
- The choice of reference satellite and the estimate of the timing relations between the satellite data and the polar cap magnetic variations.
- Handling (omission or inclusion) of reverse convection cases occurring during strong northward IMF conditions.
- Inclusion or omission of the quiet daily variation (QDC) in the base level used for the calculation of the magnetic variations.
- The method of QDC calculations, if QDCs are included in the procedure.
- The type (absolute or relative) and the representation (*X,Y*) or (*H,D*) of geomagnetic data.
- The statistical methods used to derive optimum angles and regression coefficients.
- Averaging and smoothing procedures.

These important issues and their effects on the PC index coefficients and actual PC index values have been discussed in the preceding sections.

The present DMI PCN and PCS versions both use geomagnetic data from the epoch 1997-2009. OMNI files are used to provide merging electric field data. The DMI#4 PCN version (*Stauning*, 2006) was based on Thule geomagnetic data from the epoch 1975-2003 while the PCS version used Vostok data from 1995 to 2006. IMP-8 (1975-1998) and ACE (since 1998) satellite data were used for the merging electric field. Both versions use the Solar Rotation Weighted (SRW) method for QDC determination. Strong reverse convection events are omitted by the requirement IMF B_Z<|IMF B_Y|+3 nT on solar wind data, while cases of strongly negative projected variations with $\Delta F_{PROJ} < -2\ F_{\mathrm{QDC,PROJ}}$ (DMI#4) or $\Delta F_{PROJ} < -50$ nT (present DMI version) were excluded. In spite of the differences, the index coefficients are almost equal for the two versions (cf. Fig. 39 and Fig. 48). In both versions the PCN and PCS coefficients are nearly equal taking differences in local time and season into account.

The program error for the DMI#1 version and the odd regression method used for the DMI#1 and DMI#2 (=DTUS#1) versions (cf. section 17.2 and Fig. 43) disqualifies the derived PCN values and seriously devaluate the scientific publications having used these indices (see section 17.2).

The strongly fluctuating index parameters for the AARI#2 version (cf. Fig. 49) make the derived index values less useful for scientific analyses and devaluate the publications using them (see section 17.6).

For the AARI#3, AARI#4, and IAGA-endorsed PCN index versions, the lack of discrimination against reverse convection event in the regression procedure could give unfounded index contributions of up to ~ 1 mV/m (*Stauning*, 2013) and strong asymmetry between PCN and PCS index coefficients. The use of a "solar wind sector" (SS) term added to the QDC level (*Janzhura and Troshichev*, 2011) can introduce unfounded PC index contributions of up to + or – 2.4 mV/m (*Stauning*, 2012, 2015). Use of the real-time forecast method to estimate the solar sector terms might cause unfounded contributions to the PC index of twice the above values. The adverse features should give reservations against scientific publications that use PC indices in these versions and cautions against using the IAGA-endorsed real-time PC indices in Space Weather forecasts (see section 18 and 19). Documentation of the index procedures is incomplete.

Recommendations:

For Space Weather forecasts based on irregular datasources, a no-QDC PC index version is recommended to remove the need of constructing a reliable QDC level.

For all applications not specifically constrained to either Polar Cap it is recommended, whenever possible (i.e., when both PCN and PCS are available), to use the PCC index.

It is recommended that a modified IAGA-endorsed version of the PCN and PCS index procedures includes the principles implied in the present DMI version described in sections 1-16.

Acknowledgments. The observatories in Qaanaaq and Vostok and their supporting institutes are gratefully acknowledged for providing high-quality geomagnetic data for this study. The excellent service at the OMNIweb data center at GSFC, NASA, to provide processed solar wind satellite data, and the efficient provision of geomagnetic data from the InterMagnet data center are greatly appreciated. The author gratefully acknowledges the good collaboration and many rewarding discussions with Drs. O. A. Troshichev and A. S. Janzhura at the Arctic and Antarctic Research Institute in St. Petersburg. The extensive assistance generously provided by Professor Alan Rodger, Cambridge University, to improve clarity and precision in the manuscript is most gratefully appreciated.

References:

Chun, F. K., D. J. Knipp, M. G. McHarg, G. Lu, B. A. Emery, S. Vennerstrøm, S. and O. A. Troshichev (1999): Polar cap index as a proxy for hemispheric Joule heating, *Geophys. Res. Lett.*, *26* , 1101-1104, doi:10.1029/1999GL900196.

Chun, F. K., D. J. Knipp, M. G. McHarg, J. R. Lacey, G. Lu, and B. A. Emery (2002): Joule heating patterns as a function of polar cap index, *J. Geophys. Res.*, *107* (A7), 1119, doi:10.1029/2001JA000246.

de Campra, P. F., M. Z. de Artigas (2004): Comparison between indices during geomagnetic disturbances, *Geofisica Internacional*, *43*(1), 113-117.

Fiori, R. A. D., A. V. Koustov, D. Boteler, R. A. Makarevich (2009): PCN magnetic index and average convection velocity in the polar cap inferred from SuperDARN radar measurements, *J. Geophys. Res*., *114*, A07225, doi:10.1029/2008JA013964.

Frank-Kamenetsky, A. and O. Troshichev (2012): A relationship between auroral absorption and the magnetic activity in the polar cap, *J. Atm. Solar-Terr. Phys*., 77, 40-45. http://dx.doi.org/10.1016/j.jastp.2011.11.007

Förster, M., S. E. Haaland, G. Paschmann, J. M. Quinn, R. B. Torbert, H. Vaith, and C. A. Kletzing (2008): High-latitude plasma convection during Northward IMF from in-situ magnetospheric Cluster EDI measurements, Ann. Geophys., *26(9)*, 2685-2700. http://www.ann-geophys.net/26/2685/2008/

Gao, Y. (2012): On anomalous departures from a linear relation between the polar cap index and its controlling factors in the solar wind and magnetotail, *J. Geophys. Res.*, *117* (A6), A06201, doi:10.1029/2012JA017721.

Gao, Y., M. G. Kivelson, and R. J. Walker (2012a): On the linear dependence of polar cap index on its controlling factors in the solar wind and magnetotail, J. *Geophys. Res*., *117* (A5), doi:10.1029/2011JA017229.

Gao, Y., M. G. Kivelson, Aa. J. Ridley, J. M. Weygand, and R. J. Walker (2012b): Utilizing the polar cap index to explore strong driving of polar cap dynamics, *J. Geophys. Res*., *117* (A7), A07213, 19 pp, doi:10.1029/2011JA017087.

Gao, Y., M. G. Kivelson, R. J. Walker, and J. M. Weygand (2012c): Long-term variation of driven and unloading effects on polar cap dynamics, *J. Geophys. Res*., *117* (A7), A02203, doi:10.1029/2011JA017149.

Haaland, S. E., G. Paschmann, M. Förster, J. M. Quinn, R. B. Torbert, C. E. McIlwain, H. Vaith, P. A. Puhl-Quinn, and C. A. Kletzing (2007): High-latitude plasma convection from Cluster EDI measurements: method and IMF dependence, *Ann. Geophys*., *25*, 239-253; http://www.ann-geophys.net/25/239/2007/

Henderson, M. G., et al. (2006): Substorms during the 10–11 August 2000 sawtooth event, *J. Geophys. Res*., *111(A6)*, A06206, doi:10.1029/2005JA011366.

Huang, C.-S. (2005): Variations of polar cap index in response to solar wind changes and magnetospheric substorms, *J. Geophys. Res.*, 110, A 01203, doi:10.1029/2004JA010616.

Janzhura, A. S. and O. A. Troshichev (2008): Determination of the running quiet daily geomagnetic variation, *J. Atmos. Solar-Terr. Phys.*, 70, 962–972. doi:10.1016/j.jastp.2007.11.004.

Janzhura, A. S. and O. A. Troshichev (2011): Identification of the IMF sector structure in near-real time by ground magnetic data, *Ann. Geophys.*, 29, 1491-1500. doi:10.5194/angeo-29-1491-2011.

Janzhura A., O. A. Troshichev, and P. Stauning (2007): Unified PC indices: Relation to the isolated magnetic substorms, *J. Geophys. Res.*, *112*, A09207, doi: 10.1029/2006JA012132.

Johnsen, M. G., D. A. Lorentzen (2012): A statistical analysis of the optical dayside open/closed field line boundary, *J. Geophys. Res.*, *117(A2)*, A02218, 12 pp, doi:10.1029/2011JA016984.

Kan, J. R. and L. C. Lee (1979): Energy coupling function and solar wind-magnetosphere dynamo, *Geophys. Res. Lett.*, *6*(7), 577– 580. doi:10.1029/GL006i007p00577

Liou, K., J. F. Carbary, P. T. Newell, C.-I. Meng, and O. Rasmussen (2003): Correlation of auroral power with the polar cap index, *J. Geophys. Res*., *108* (A3), 1108, doi:10.1029/2002JA009556.

Liou, K., P. T. Newell, C.-I. Meng, C.-C. Wu, and R. P. Lepping (2004): On the relationship between shock-induced polar magnetic bays and solar wind parameters, *J. Geophys. Res*., *109*, A06306, doi:10.1029/2004JA010400.

Lukianova, R. (2003): Magnetospheric response to sudden changes in solar wind dynamic pressure inferred from polar cap index, *J. Geophys. Res*., *108(A12)*, 1428, doi: 10.1029/2002JA009790.

Lukianova, R. (2007), Comment on "Unified PCN and PCS indices: method of calculation, physical sense, dependence on the IMF azimuthal and northward components" by O. Troshichev, A. Janzhura, and P. Stauning, *J. Geophys. Res*., *112(A7)*, A07204, doi:10.1029/2006JA011950.

Lukianova, R., O. Troshichev, and G. Lu (2002): The polar cap magnetic activity indices in the southern (PCS) and northern (PCN) polar caps: Consistency and discrepancy, *Geophys. Res. Lett.*, *29*(18), 1879, doi:10.10292002GL015179.

Mansurov, S. M. (1969): A new evidence of connection between Space and Earth's magnetic fields, *Geomag. and Aeron*., 9, 768-770.

McCreadie, H. and M. Menvielle (2010): The PC index: review of methods, *Ann. Geophys*., *28*, 1887-1903, doi:10.5194/angeo-28-1887-2010, (http://www.ann-geophys.net/28/1887/2010/)

McCreadie, H. and M. Menvielle (2011): Corrigendum to: "The PC index: review of methods" published in *Ann. Geophys*., 28, 1887-1903, 2010. *Ann. Geophys*., *29*, 813-814, 2011. doi:10.5194/angeo-29-813-2011. (http://www.ann-geophys.net/29/813/2011/)

Nagatsuma T. (2002b): Saturation of polar cap potential by intense solar wind electric fields, *Geophys. Res. Lett.*, *29* (10), doi:10.1029/2001GL014202.

Nagatsuma, T., T. Obara, H. Ishibashi, K. Hayashi, and D. J. McEwen (1999): Real-time monitor of geomagnetic field in the near-pole regions as an index of magnetospheric electric field, *Adv. Polar Upper Atmos. Res*., *13*, 132-138.

Nagatsuma, T., T. Obara, and H. Ishibashi (2000): Relationship between solar wind parameter and magnetic activity in the near-pole region: Application to space weather forecasting, *Adv. Space Res*., *26* (1), 103-106.

Nagatsuma, T., K. Hayashi, D. J. McEwen, and T. Obara (2003): Real time collection of geomagnetic field data from northern near-pole region, *Adv. Space Res*., *31*(4), 1081-1085.

Papitashvili, V. O. and O. Rasmussen (1999): Effective area for the northern polar cap magnetic activity index, *Geophys. Res. Lett*., *26(19)*, 2917-2920.

Papitashvili V. O., L. I. Gromova, V. A. Popov, and O. Rasmussen, (2001): Northern Polar Cap magnetic activity index PCN: Effective area, universal time and solar cycle variations, *Scientific Report 01-01*, Danish Meteorological Institute, Copenhagen, Denmark, 57 pp.

Ridley A. J. and E. A. Kihn (2004): Polar cap index comparisons with AMIE cross polar cap potential, electric field, and polar cap area, *Geophys. Res. Lett*., *31*, L07801, doi:10.1029/2003GL019113.

Stauning, P. (2007): A new index for the interplanetary merging electric field and geomagnetic activity: Application of the unified polar cap indices, *Space Weather*, *5*, S09001, doi:10.1029/2007SW000311.

Stauning, P. (2011a): Comments to "McCreadie, H. and Menvielle, M.: The PC index: review of methods, *Ann. Geophys*., *28*, 1887-1903, doi:10.5194/angeo-28-1887-2010, 2010." and their corrigendum: "McCreadie, H. and Menvielle, M.: Corrigendum to: "The PC index: review of methods" published in *Ann. Geophys*., 28, 1887-1903, 2010. *Ann. Geophys*., *29*, 813-814, 2011.", *Ann. Geophys*., *29*, 1137-1146 (http://www.ann-geophys.net/29/1137/2011)

Stauning, P. (2011b): Determination of the quiet daily geomagnetic variations for polar regions, *J. Atm. Solar-Terr. Phys.*, 73, pp. 2314-2330. doi:10.1016/j.jastp.2011.07.004.

Stauning, P. (2012): The Polar Cap PC Indices: Relations to Solar Wind and Global Disturbances, in: *Exploring the Solar Wind*, Marian Lazar (Ed.), ISBN: 978-953-51-0339-4, InTech, doi: 10.5772/37359.

Stauning, P. (2013a): Comments on quiet daily variation derivation in "Identification of the IMF sector structure in near-real time by ground magnetic data" by Janzhura and Troshichev (2011), *Ann. Geophys.*, 31, 1221-1225. doi:10.5194/angeo-31-1221-2013.

Stauning, P. (2013b): The Polar Cap index: A critical review of methods and a new approach, *J. Geophys. Res.* Space Physics, 118, 5021-5038. doi:101002/jgra.50462.

Stauning, P. (2013c): Power grid disturbances and polar cap index during geomagnetic storms, *J. Space Weather Space Clim. 3*, A22, doi:10.1051/swsc2013044.

Stauning, P. (2015): A critical note on the IAGA-endorsed Polar Cap index procedure: effects of solar wind sector structure and reverse polar convection, Ann. Geophys., 33, 1443-1455, doi:10.5194/angeo-33-1443-2015, www.ann-geophys.net/33/1443/2015

Stauning, P. and O. Troshichev: (2008) Polar Cap convection and PC index during sudden changes in solar wind dynamic pressure, *J. Geophys. Res*., *113*, doi:10.1029//2007JA012783.

Stauning, P., O. Troshichev, and A. Janzhura (2006): Polar Cap (PC) index. Unified PC-N (North) index procedures and quality. *DMI Scientific Report, SR-06-04*. (revised 2007 version available at http://www.dmi.dk/fileadmin/Rapporter/SR/sr06-04.pdf).

Stauning, P., O. A. Troshichev, and A. Janzhura (2008): The Polar Cap (PC) index. Relations to solar wind parameters and global magnetic activity level, *J. Atmos. Solar-Terr. Sci*., *70*, 18, 2246-2261, doi:10.1016/j.jastp.2008.09.028.

Stepanova, M., E. Anatova, O. A. Troshichev (2003): Intermittency of magnetospheric dynamics through non-Gaussian distribution function of PC-index fluctuations, *Geophys. Res. Lett*., 30, 1127, doi:10.1029/2002GL016070.

Stepanova, M., E. Anatova, O. A. Troshichev (2005a): Forecasting of Dst variations from Polar Cap indices using neural networks, *Adv. in Space Res*. *36*(12), 2451-2454.

Stepanova, M., E. Anatova, O. A. Troshichev (2005b): PC-index fluctuations and intermittency of the magnetospheric dynamics, *Adv. Space Res*., 36(12), 2423-2427.

Stepanova, M., E. Anatova, O. A. Troshichev (2005c): Prediction of Dst variations from Polar Cap indices using time-delay neural network, *J. Atmos. Solar-Terr. Phys*., 67, 1658-1664.

Svalgaard, L. (1968): Sector structure of the interplanetary magnetic field and daily variation of the geomagnetic field at high-latitudes, *Scientific Report, R-8*, Danish Meteorological Institute.

Takalo, J. and J. Timonen (1998a): Comparison of the dynamics of the AU and PC indices. *Geophys. Res. Lett*., *25* (12), 2101-2104, doi:10.1029/98GL01614.

Takalo, J. and J. Timonen (1998b), On the relation of the AE and PC indices, *J. Geophys. Res*., *103(A12)*, 29393-29398, doi:10.1029/98JA02390.

Takalo J. and J. Timonen (1999): Neural network prediction of the AE index from the PC index, *Physics and Chemistry of the Earth*, Part C: *Solar, Terrestrial and Planetary Science*, *24* (1-3), 89-92. doi: 10.1016/S1464-1917(98)

Troshichev, O. A. (1988): The physics and meaning of the existing and proposed high-latitude geomagnetic indices, Ann. Geophys., *6* (6), 601-610.

Troshichev, O. (2010): Relationship between magnetic activity in the polar cap and atmospheric processes in the winter Antarctica, *J. Atmos. Solar-Terr. Phys*., *72*, 943-950.

Troshichev, O. A. (2011): Polar Cap (PC) Index, http://geophys.aari.ru/Description.pdf .

Troshichev, O. A. and V. G. Andrezen (1985): The relationship between interplanetary quantities and magnetic activity in the southern polar cap, *Planet. Space Sci*., *33*, 415-419.

Troshichev, O. A. and A. Janzhura (2009): Relationship between the PC and AL indices during repetitive bay-like magnetic disturbances in the auroral zone. *J. Atmos. Solar-Terr. Phys*., *71(12)*, 1340-1352. doi: 10.1016/j.jastp.2009.05.017

Troshichev, O. and A. Janzhura (2012a): Physical implications of discrepancy between summer and winter PC indices observed in the course of magnetospheric substorms, *Adv. Space Res.*. *50* (1), 77-84.

Troshichev, O. A., and A. Janzhura (2012b): Space Weather monitoring by ground-based means, *Springer Praxis Books*. doi:10.1007/978-3-642-16803-1.

Troshichev, O. A., and R. Lukianova (2002): Relation of the PC index to the solar wind parameters and substorm activity in time of magnetic storm, *J. Atmos. Solar.Terr. Phys*., *64(5-6)*, 585-591.

Troshichev, O. A. and D. A. Sormakov (2015): PC index as a proxy of the solar wind energy that entered into the magnetosphere: 2. Relation to the interplanetary electric field E_{KL} before substorm onset, Earth, Planets and Space 67:170, doi:10.1186/s40623-015-0338-4.

Troshichev, O. A., V. G. Andrezen, S. Vennerstrøm, and E. Friis-Christensen (1988): Magnetic activity in the polar cap – A new index, *Planet. Space Sci*., *36(11)*, 1095-1102.

Troshichev, O. A., V. G. Andrezen, S. Vennerstrøm, and E. Friis-Christensen (1991): Polar Cap index (PC) geomagnetic activity index for 1975-1982, *WDC-B2*, Soviet Geophysical Committee, Academy of Sciences of the USSR, Moscow, 1-142.

Troshichev, O. A., H. Hayakawa, A. Matsuoka, T. Mukai, and K. Tsuruda (1996): Cross polar cap diameter and voltage as a function of PC index and interplanetary quantities, *J. Geophys. Res*., *101(A6)*, 13,429-13,435. doi:10.1029/95JA03672

Troshichev, O. A., R. Yu. Lukianova, V. O. Papitashvili, F. J. Rich, and O. Rasmussen (2000): Polar Cap index (PC) as a proxy for ionospheric electric field in the near-pole region, *Geophys. Res. Lett.*, *27*, 3809-3812. doi:10.1029/2000GL003756.

Troshichev, O. A., Janzhura, A., and P. Stauning, P. (2006): Unified PCN and PCS indices: method of calculation, physical sense and dependence on the IMF azimuthal and northward components, *J. Geophys. Res.*, 111, A05208. doi:10.1029/2005JA011402.

Troshichev, O. A., A. Janzhura, and P. Stauning (2007a): Reply to Comment of R. Lukianova, R. on paper "The unified PCN and PCS indices: method of calculation, physical sense, dependence on the IMF azimuthal and northward components" by O. Troshichev, A. Janzhura, and P. Stauning, *J. Geophys. Res*., *112(A7)*, A07205, doi:10.1029/2006JA012029.

Troshichev, O. A., A. S. Janzhura, and P. Stauning (2007b): Magnetic activity in the polar caps: Relation to sudden changes in the solar wind dynamic pressure, *J. Geophys. Res.*, *112*, A11202, doi:10.1029/2007JA012369.

Troshichev, O., A. Janzhura, and P. Stauning (2009): Correction to "Unified PCN and PCS indices: Method of calculation, physical sense, and dependence on the IMF azimuthal and northward components", J. Geophys. Res., *114*, A11202, doi:10.1029/2009JA014937.

Troshichev, O. A., N. A. Podorozhkina, and A. S. Janzhura (2011a): Invariability of relationship between the polar cap magnetic activity and geoeffective interplanetary electric field, *Ann. Geophys*., 29, 1479-1489. doi:10.5194/angeo-29-1479-2011.

Troshichev, O. A., D. A. Somarkov, A. Janzhura, (2011b): Relation of PC index to the geomagnetic storm Dst variation, *J. Atmos. Solar-Terr. Phys*., *73(5-6)*, 611-622. doi:10.1016/j.jastp.2010.12.015

Troshichev, O. A., N. A. Podorozhkina, and A. S. Janzhura (2011c): Invariability of relationship between the polar cap magnetic activity and geoeffective interplanetary electric field, *Ann. Geophys*., *29(8)*, 1479-1489, 2011. doi:10.5194/angeo-29-1479-2011.

Troshichev, O. A., N. A. Podorozhkina, and A. S. Janzhura (2011d): Relationship between PC index and magnetospheric substorms observed under conditions of northward IMF, *J. Atmos. Solar-Terr. Phys*., *73* (16), 2373-2378.

Troshichev, O., A ., D. A. Sormakov, A. Janzhura (2012): Relations between PC index and substorm (AL) and storm (SYM, ASYM) indices under conditions of the steadily high solar wind energy input into the magnetosphere, *Adv. Space Res*. , *49* (5), 872-882. doi:10.1016/j.asr.2011.12.011.

Troshichev, O., N. A. Podorozhkina , D. A. Sormakov, A. Janzhura (2014): PC index as a proxy of the solar wind energy that entered into the magnetosphere: 1. Development of magnetic substorms, J. Geophys. Res. Space Physics 119, doi:10.1002/2014JA019834.

Vassiliadis, D., V. Angelopoulos, D. N. Baker, and A. J. Klimas (1996): The relation between the northern polar cap and auroral electrojet geomagnetic indices in the wintertime, *Geophys. Res. Lett*., *23*, 2781. doi:10.1029/96GL02575

Vennerstrøm, S. (1991): The geomagnetic activity index PC, PhD Thesis, *Scientific Report 91-3*, Danish Meteorological Institute, 105 pp.

Vennerstrøm, S., E. Friis-Christensen, O. A. Troshichev, V. G. Andrezen (1991): Comparison between the polar cap index PC and the auroral electrojet indices AE, AL and AU, *J. Geophys. Res*., *96(A1)*, 101-113. doi:10.1029/90JA01975.

Data availability:

Live PC index values and PCN and PCS index series are now made available through the web site: http://pcindex.org. The web site, furthermore, holds PCN and PCS index coefficients derived by the IAGA-endorsed procedure. QDC values are not included. The web site includes the document "Polar Cap (PC) Index" written by O. A. Troshichev.

The Space-DTU (2014) ftp web site for PC indices: ftp://ftp.space.dtu.dk/WDC/indices/pcn/ includes documents: *PC_index_description_main_document.pdf* and PC_index_description_*Appendix_A.pdf*, and a directory, *PC_index_description_Appendix_A___file_archive*, with program transcripts and data files (neither including QDC values nor solar wind sector terms).

Geomagnetic data from Thule were supplied in part from the InterMagnet service center at http://intermagnet.org and in part directly from the former DTU Space ftp data server at ftp://ftp.space.dtu.dk/WDC/. This service is now transferred to WDC for Geomagnetism, Edinburgh, available at http://www.wdc.bgs.ac.uk

Geomagnetic data from Vostok was supplied in part from the web site http://pcindex.org, and in part directly from the Arctic and Antarctic Research Institute in St. Petersburg, Russia, available at http://geophys.aari.ru .

Solar wind data and PCN (DTUS) values were provided from the OMNIweb data service at Goddard Space Flight Center, GSFC, NASA at http://omniweb.gsfc.nasa.gov .

Appendix A.

Table A1. Quiet winter night baseline values for Thule magnetometer (QWNL file).

YEAR	D	I	H	X	Y	Z	F	ELE
	Deg	Deg	nT	nT	nT	nT	nT	
1973.0	282.250	86.018	3936	835	-3846	56543	56680	DHZ
1974.0	282.550	86.024	3934	855	-3840	56596	56733	DHZ
1975.0	282.917	86.030	3931	879	-3832	56638	56774	DHZ
1976.0	283.333	86.034	3929	906	-3823	56664	56800	DHZ
1977.0	283.800	86.036	3928	937	-3815	56681	56817	DHZ
1978.0	284.333	86.038	3926	972	-3804	56690	56826	DHZ
1979.0	284.833	86.037	3927	1005	-3796	56691	56827	DHZ
1980.0	285.267	86.033	3930	1035	-3791	56676	56812	DHZ
1981.0	285.667	86.032	3930	1061	-3784	56655	56791	DHZ
1982.0	286.033	86.034	3927	1085	-3774	56640	56776	DHZ
1983.0	286.350	86.035	3925	1105	-3766	56622	56758	DHZ
1984.0	286.667	86.038	3919	1124	-3754	56582	56718	DHZ
1985.0	286.983	86.046	3909	1142	-3739	56555	56690	DHZ
1986.0	287.300	86.054	3899	1159	-3723	56520	56654	DHZ
1987.0	287.700	86.062	3888	1182	-3704	56486	56620	DHZ
1988.0	288.067	86.071	3878	1203	-3687	56465	56598	DHZ
1989.0	288.450	86.073	3875	1226	-3676	56447	56580	DHZ
1990.0	289.050	86.084	3863	1261	-3651	56430	56562	DHZ
1991.0	289.417	86.089	3856	1282	-3637	56400	56532	DHZ
1992.0	289.917	86.090	3855	1313	-3624	56395	56527	DHZ
1993.0	290.467	86.089	3853	1347	-3610	56362	56494	DHZ
1994.0	291.083	86.093	3848	1384	-3590	56350	56481	DHZ
1995.0	291.850	86.090	3850	1433	-3573	56335	56466	DHZ
1996.0	292.567	86.097	3842	1474	-3548	56315	56446	DHZ
1997.0	293.433	86.090	3848	1530	-3531	56304	56435	DHZ
1998.0	294.333	86.088	3850	1586	-3508	56300	56431	DHZ
1999.0	295.333	86.077	3862	1652	-3491	56310	56442	DHZ
2000.0	296.333	86.060	3878	1720	-3476	56310	56443	DHZ
2001.0	297.333	86.048	3890	1786	-3456	56310	56444	DHZ
2002.0	298.417	86.035	3903	1857	-3433	56315	56450	DHZ
2003.0	299.483	86.016	3922	1930	-3414	56320	56456	DHZ
2004.0	300.483	86.001	3938	1998	-3394	56336	56473	DHZ
2005.0	301.467	85.986	3953	2063	-3372	56333	56472	DHZ
2006.0	302.433	85.970	3967	2128	-3348	56312	56452	DHZ
2007.0	303.417	85.953	3984	2194	-3325	56315	56456	DHZ
2008.0	304.400	85.937	3999	2259	-3300	56299	56441	DHZ
2009.0	305.400	85.916	4019	2328	-3276	56286	56429	DHZ
2010.0	306.417	85.894	4039	2398	-3250	56269	56414	DHZ
2011.0	307.400	85.871	4061	2467	-3226	56258	56404	DHZ
2012.0	308.400	85.850	4081	2535	-3198	56247	56395	DHZ

Table A2a. OMNI Em – Thule correlations (no QDC corr.)

Correlation of ΔFproj (No QDC) vs. Em (OMNI). Years: 1997-2009

UT	JAN	FEB	MAR	APR	MAY	JUN	JUL	AUG	SEP	OCT	NOV	DEC
0	0.694	0.728	0.803	0.771	0.756	0.776	0.809	0.780	0.694	0.753	0.694	0.741
1	0.667	0.699	0.772	0.774	0.754	0.729	0.807	0.763	0.791	0.791	0.751	0.700
2	0.738	0.677	0.781	0.823	0.714	0.790	0.735	0.763	0.799	0.769	0.744	0.733
3	0.708	0.626	0.759	0.806	0.729	0.758	0.770	0.747	0.789	0.787	0.746	0.764
4	0.681	0.663	0.779	0.821	0.757	0.782	0.796	0.805	0.769	0.754	0.695	0.743
5	0.593	0.689	0.764	0.729	0.726	0.771	0.799	0.766	0.707	0.721	0.741	0.745
6	0.652	0.680	0.791	0.794	0.742	0.763	0.755	0.756	0.754	0.757	0.775	0.719
7	0.664	0.690	0.809	0.764	0.736	0.755	0.732	0.747	0.748	0.770	0.807	0.714
8	0.698	0.700	0.773	0.763	0.719	0.776	0.654	0.775	0.736	0.777	0.793	0.749
9	0.698	0.743	0.766	0.769	0.724	0.739	0.722	0.707	0.719	0.770	0.795	0.744
10	0.658	0.762	0.770	0.810	0.726	0.732	0.761	0.765	0.766	0.782	0.809	0.753
11	0.685	0.747	0.733	0.797	0.760	0.766	0.782	0.786	0.764	0.816	0.862	0.752
12	0.760	0.719	0.767	0.830	0.767	0.783	0.792	0.744	0.774	0.792	0.821	0.729
13	0.747	0.787	0.752	0.765	0.728	0.734	0.777	0.773	0.760	0.813	0.826	0.749
14	0.757	0.767	0.746	0.766	0.687	0.750	0.785	0.757	0.735	0.830	0.795	0.667
15	0.805	0.773	0.715	0.716	0.651	0.742	0.752	0.724	0.721	0.800	0.767	0.756
16	0.748	0.771	0.752	0.653	0.620	0.700	0.691	0.685	0.721	0.837	0.837	0.770
17	0.683	0.772	0.769	0.700	0.614	0.607	0.588	0.696	0.698	0.839	0.769	0.775
18	0.723	0.748	0.798	0.723	0.707	0.630	0.660	0.741	0.748	0.812	0.762	0.729
19	0.730	0.759	0.786	0.792	0.746	0.733	0.737	0.814	0.794	0.773	0.777	0.735
20	0.702	0.758	0.773	0.775	0.742	0.773	0.777	0.825	0.749	0.761	0.793	0.754
21	0.709	0.759	0.786	0.755	0.789	0.776	0.794	0.841	0.774	0.781	0.762	0.708
22	0.696	0.765	0.798	0.797	0.810	0.782	0.789	0.842	0.777	0.710	0.763	0.665
23	0.676	0.757	0.773	0.738	0.770	0.776	0.766	0.841	0.707	0.743	0.711	0.661

Average correlation: 0.7504

Table A2b. OMNI Em – Thule correlations (QDC corr.)

Correlation of ΔFproj (QDC-corr) vs. Em (OMNI). Years: 1997-2009

UT	JAN	FEB	MAR	APR	MAY	JUN	JUL	AUG	SEP	OCT	NOV	DEC
0	0.690	0.715	0.801	0.755	0.698	0.726	0.800	0.765	0.678	0.742	0.693	0.733
1	0.661	0.687	0.769	0.769	0.693	0.677	0.803	0.741	0.768	0.782	0.742	0.697
2	0.743	0.656	0.776	0.815	0.654	0.741	0.745	0.735	0.779	0.757	0.732	0.728
3	0.714	0.603	0.759	0.804	0.654	0.697	0.769	0.724	0.767	0.772	0.739	0.755
4	0.665	0.646	0.787	0.819	0.676	0.701	0.799	0.783	0.746	0.748	0.672	0.736
5	0.574	0.660	0.761	0.723	0.627	0.676	0.805	0.749	0.675	0.715	0.708	0.734
6	0.640	0.656	0.764	0.791	0.698	0.678	0.767	0.736	0.731	0.740	0.762	0.718
7	0.651	0.690	0.790	0.757	0.697	0.666	0.719	0.724	0.722	0.761	0.802	0.712
8	0.682	0.692	0.766	0.756	0.685	0.694	0.664	0.763	0.721	0.772	0.790	0.738
9	0.685	0.743	0.755	0.765	0.681	0.713	0.739	0.698	0.705	0.761	0.789	0.735
10	0.648	0.753	0.758	0.807	0.691	0.723	0.761	0.752	0.747	0.778	0.798	0.750
11	0.674	0.745	0.731	0.794	0.741	0.755	0.786	0.780	0.749	0.805	0.851	0.743
12	0.752	0.715	0.765	0.826	0.739	0.778	0.783	0.737	0.760	0.778	0.810	0.730
13	0.738	0.775	0.742	0.759	0.701	0.732	0.757	0.765	0.749	0.803	0.824	0.752
14	0.750	0.758	0.733	0.766	0.656	0.754	0.768	0.751	0.725	0.822	0.793	0.666
15	0.799	0.768	0.704	0.719	0.632	0.743	0.727	0.722	0.720	0.794	0.759	0.756
16	0.748	0.764	0.747	0.661	0.614	0.704	0.663	0.666	0.717	0.837	0.826	0.770
17	0.670	0.767	0.760	0.703	0.617	0.608	0.574	0.703	0.698	0.835	0.765	0.769
18	0.715	0.739	0.783	0.714	0.707	0.619	0.624	0.750	0.743	0.805	0.758	0.724
19	0.722	0.757	0.767	0.780	0.740	0.699	0.707	0.813	0.782	0.770	0.768	0.726
20	0.695	0.753	0.762	0.771	0.720	0.744	0.768	0.820	0.727	0.752	0.776	0.745
21	0.699	0.747	0.772	0.737	0.766	0.737	0.787	0.832	0.747	0.771	0.750	0.704
22	0.684	0.751	0.791	0.783	0.779	0.739	0.779	0.830	0.762	0.698	0.762	0.656
23	0.664	0.751	0.765	0.732	0.726	0.744	0.759	0.837	0.678	0.739	0.700	0.655

Average correlation: 0.7367

Table A3a. PCN parameters (no QDC corr.).

Smoothed optimum projection angle. No QDC corr. Excl. rev. conv. Years: 1997-2009.
Smoothing: XH0= 3 XM0= 2

UT	JAN	FEB	MAR	APR	MAY	JUN	JUL	AUG	SEP	OCT	NOV	DEC
0	42.84	43.27	44.36	45.19	46.12	47.80	50.04	52.06	52.90	51.47	47.94	44.41
1	41.45	41.31	41.86	42.33	43.05	44.71	47.17	49.50	50.60	49.47	46.42	43.21
2	40.79	40.02	39.94	39.90	40.24	41.73	44.28	46.92	48.48	48.03	45.69	42.81
3	41.14	39.69	38.81	38.05	37.80	38.89	41.45	44.52	46.87	47.45	45.98	43.44
4	42.59	40.34	38.46	36.82	35.80	36.34	38.85	42.55	46.05	47.89	47.39	45.19
5	45.08	41.85	38.78	36.15	34.32	34.23	36.75	41.28	46.11	49.30	49.79	47.99
6	48.26	43.96	39.60	35.96	33.37	32.79	35.44	40.89	46.99	51.36	52.78	51.46
7	51.46	46.17	40.62	36.06	32.90	32.09	35.05	41.31	48.33	53.53	55.72	54.89
8	53.88	47.84	41.39	36.13	32.64	31.91	35.24	42.03	49.51	55.14	57.88	57.47
9	54.99	48.47	41.46	35.78	32.14	31.55	35.14	42.11	49.73	55.60	58.74	58.66
10	54.72	47.94	40.66	34.70	30.84	30.15	33.68	40.66	48.47	54.72	58.28	58.48
11	53.51	46.61	39.20	32.88	28.43	27.14	30.32	37.40	45.81	52.84	56.99	57.37
12	51.97	45.19	37.77	30.82	25.19	22.77	25.45	32.98	42.54	50.75	55.53	55.94
13	50.69	44.43	37.28	29.53	22.22	18.26	20.47	28.79	39.83	49.25	54.41	54.64
14	50.01	44.85	38.52	30.25	21.23	15.66	17.48	26.60	38.81	48.86	53.81	53.64
15	49.97	46.45	41.64	33.75	23.84	17.13	18.55	27.87	40.14	49.61	53.61	52.93
16	50.29	48.64	45.92	39.60	30.40	23.66	24.64	33.02	43.68	51.19	53.58	52.38
17	50.49	50.55	50.03	46.18	39.31	33.91	34.54	40.84	48.45	53.08	53.59	51.82
18	50.22	51.47	52.81	51.55	47.74	44.55	45.05	48.88	53.08	54.82	53.56	51.17
19	49.44	51.28	53.79	54.48	53.34	52.30	52.92	54.82	56.41	56.07	53.50	50.43
20	48.40	50.30	53.22	54.91	55.41	55.87	56.76	57.69	57.99	56.63	53.29	49.64
21	47.28	48.96	51.68	53.53	54.68	55.91	57.14	57.93	57.98	56.39	52.72	48.74
22	46.03	47.36	49.56	51.11	52.33	53.86	55.44	56.57	56.87	55.32	51.55	47.55
23	44.50	45.43	47.05	48.21	49.30	50.93	52.86	54.47	55.08	53.57	49.83	46.02

Slope. No QDC. Excl. rev. conv. Years: 1997-2009.
Smoothing: XH0= 3 XM0= 2

UT	JAN	FEB	MAR	APR	MAY	JUN	JUL	AUG	SEP	OCT	NOV	DEC
0	25.07	27.75	32.99	33.16	40.15	41.75	37.88	39.03	34.41	28.99	24.66	22.93
1	23.77	25.10	30.32	32.09	37.50	39.70	36.65	36.76	33.68	27.79	23.34	21.37
2	22.62	22.85	28.39	31.03	35.20	38.12	35.23	34.62	32.50	26.36	21.67	20.34
3	21.29	21.21	26.55	30.33	33.18	37.97	33.66	34.62	31.42	26.15	20.36	20.63
4	20.61	21.03	25.43	29.59	32.50	36.75	32.67	34.24	30.68	25.46	20.59	21.00
5	19.87	20.88	24.33	29.25	31.37	37.24	32.11	33.63	31.51	24.79	21.15	21.04
6	20.15	21.44	24.65	29.08	31.91	37.10	32.45	32.83	32.23	25.07	21.97	21.63
7	21.47	21.81	25.68	30.16	32.82	38.45	32.89	33.36	32.33	26.28	22.49	22.08
8	22.88	22.59	27.46	31.07	33.80	39.91	34.30	34.43	32.94	28.59	24.19	23.19
9	24.42	24.27	29.41	33.37	35.42	42.35	37.84	35.80	34.61	30.60	26.61	24.71
10	26.06	27.01	30.70	35.51	36.90	43.16	40.09	36.18	35.65	31.88	28.39	27.28
11	28.50	29.19	32.70	39.44	39.55	46.95	43.39	38.78	38.16	33.46	29.93	29.77
12	30.03	31.89	34.30	41.98	41.70	49.95	45.02	41.00	39.97	34.08	32.13	31.42
13	31.62	33.43	36.15	43.97	44.29	52.29	48.43	43.22	41.74	35.59	34.25	32.51
14	32.69	35.94	36.56	45.04	45.07	52.74	49.22	43.97	42.01	36.99	36.06	33.41
15	33.58	36.81	37.42	46.26	46.46	54.10	50.64	45.21	43.27	38.09	36.28	34.31
16	34.18	37.70	37.78	47.24	47.35	54.67	50.90	45.93	43.52	38.50	36.08	34.08
17	34.76	37.61	39.41	46.64	49.24	54.69	51.35	47.48	43.00	38.73	35.47	33.87
18	34.87	37.35	39.21	44.57	48.85	52.45	50.39	45.67	42.61	38.02	34.50	32.60
19	33.07	36.81	39.24	42.13	47.96	51.32	49.43	45.35	41.97	36.70	33.60	31.45
20	31.07	36.43	38.26	39.82	46.81	49.04	47.86	43.38	40.59	35.02	31.78	29.80
21	29.27	34.65	37.70	37.86	45.19	46.33	46.06	43.36	37.43	34.20	30.16	28.33
22	28.00	32.56	36.90	35.75	43.88	45.21	42.44	42.31	36.03	32.39	27.91	26.31
23	26.22	29.89	34.99	34.43	41.60	43.53	39.70	41.39	34.87	30.89	26.31	24.82

Intercept. No QDC. Excl. rev. conv. Years: 1997-2009.
Smoothing: XH0= 3 XM0= 2

UT	JAN	FEB	MAR	APR	MAY	JUN	JUL	AUG	SEP	OCT	NOV	DEC
0	6.83	8.48	12.22	18.66	21.59	23.17	25.11	19.02	16.02	12.30	9.53	7.03
1	6.27	8.43	12.25	18.52	23.15	24.73	25.99	19.89	15.69	11.61	9.08	6.43
2	6.08	8.52	12.31	18.60	24.49	26.26	27.24	21.04	15.90	11.74	9.13	6.24
3	6.07	8.78	12.55	18.95	25.72	27.49	28.62	21.69	16.12	11.73	9.19	5.81
4	6.30	8.89	12.89	19.66	26.80	29.26	30.03	22.84	16.69	12.25	9.27	5.59
5	7.10	9.52	13.83	20.70	28.33	30.84	31.43	24.36	17.30	13.21	9.73	6.04

6	7.90	10.34	14.82	21.92	29.87	32.85	32.94	26.36	18.42	14.43	10.50	6.87
7	8.67	11.46	15.69	22.73	31.56	34.24	34.46	28.09	19.98	15.59	11.53	7.94
8	9.47	12.44	16.29	23.91	33.22	35.58	35.57	29.59	21.30	16.04	12.07	8.68
9	10.25	12.92	16.66	24.58	34.50	36.48	36.17	31.04	22.27	16.56	12.36	9.16
10	10.64	12.88	17.11	25.10	35.48	37.77	37.42	32.52	23.26	17.17	12.55	9.35
11	10.55	12.93	16.97	23.93	35.13	37.17	37.65	32.57	23.12	17.43	12.70	9.60
12	10.83	12.92	17.00	22.97	34.16	36.82	37.86	32.04	22.77	17.67	12.57	9.94
13	11.07	13.17	16.82	22.08	32.74	36.38	37.22	31.40	22.13	17.39	12.41	10.13
14	11.37	12.82	16.98	21.72	31.71	36.33	37.24	31.25	21.99	16.99	12.19	10.18
15	11.13	12.38	16.26	20.15	29.38	33.85	35.33	29.86	20.76	16.16	12.01	10.01
16	10.97	11.83	15.70	18.81	26.55	31.30	32.59	27.86	19.71	15.44	11.68	10.00
17	10.55	11.54	14.75	17.98	23.53	28.42	29.29	25.24	18.64	14.85	11.24	9.57
18	10.41	11.76	15.00	18.68	22.49	27.15	27.51	24.29	18.47	14.92	11.37	9.67
19	10.37	11.66	14.97	18.99	21.90	25.02	25.96	22.86	18.32	15.12	11.48	9.56
20	10.31	11.25	14.98	19.78	21.67	24.01	25.34	22.12	18.75	15.36	11.78	9.56
21	9.66	10.49	14.36	19.90	21.20	23.12	24.38	20.29	18.52	14.52	11.04	8.88
22	8.81	9.75	13.51	19.88	20.74	22.35	24.37	19.20	17.70	13.95	10.57	8.46
23	7.74	9.08	12.83	19.17	20.98	22.33	24.38	18.44	16.57	12.79	9.79	7.59

Table A3b. PCN parameters (QDC corr.)

Optimum projection angle. QDC corr. Excl. rev. conv. Years: 1997-2009.
Smoothing: XH0= 3 XM0= 2

UT	JAN	FEB	MAR	APR	MAY	JUN	JUL	AUG	SEP	OCT	NOV	DEC
0	43.30	44.47	45.81	46.55	47.49	48.98	50.91	53.13	54.80	53.88	49.62	44.94
1	42.15	42.90	43.87	44.39	45.16	46.57	48.61	50.97	52.66	51.89	48.10	43.84
2	41.63	41.89	42.37	42.54	42.98	44.14	46.18	48.68	50.61	50.37	47.30	43.46
3	42.08	41.72	41.51	41.09	40.99	41.71	43.65	46.45	49.01	49.73	47.57	44.12
4	43.60	42.43	41.26	40.06	39.26	39.38	41.20	44.55	48.18	50.16	49.00	45.92
5	46.03	43.84	41.47	39.34	37.79	37.29	39.09	43.26	48.23	51.59	51.43	48.71
6	48.96	45.62	41.91	38.78	36.52	35.57	37.54	42.69	49.02	53.64	54.39	52.04
7	51.72	47.27	42.26	38.15	35.33	34.22	36.60	42.71	50.16	55.70	57.17	55.17
8	53.64	48.26	42.19	37.26	34.06	33.06	35.97	42.83	50.98	57.11	59.10	57.40
9	54.30	48.27	41.47	35.97	32.51	31.68	34.99	42.25	50.80	57.33	59.74	58.30
10	53.73	47.30	40.12	34.22	30.45	29.54	32.91	40.33	49.21	56.22	59.11	57.90
11	52.33	45.76	38.46	32.18	27.76	26.30	29.40	36.95	46.39	54.16	57.64	56.63
12	50.65	44.28	37.12	30.29	24.71	22.17	24.82	32.74	43.14	51.93	55.97	55.02
13	49.19	43.50	36.83	29.37	22.19	18.17	20.39	28.96	40.55	50.29	54.60	53.47
14	48.26	43.80	38.16	30.40	21.62	16.06	17.91	27.16	39.65	49.72	53.69	52.17
15	47.89	45.13	41.17	33.92	24.36	17.73	19.22	28.62	40.98	50.28	53.19	51.14
16	47.88	47.00	45.14	39.47	30.66	24.03	25.12	33.63	44.37	51.66	52.95	50.32
17	47.89	48.66	48.93	45.61	39.06	33.73	34.47	41.02	48.89	53.44	52.88	49.65
18	47.65	49.55	51.54	50.62	47.01	43.80	44.37	48.56	53.30	55.21	52.98	49.08
19	47.16	49.59	52.58	53.45	52.39	51.26	51.87	54.20	56.60	56.68	53.23	48.65
20	46.62	49.07	52.32	54.03	54.56	54.88	55.69	57.09	58.37	57.62	53.48	48.34
21	46.14	48.34	51.25	53.00	54.16	55.25	56.35	57.61	58.74	57.86	53.43	48.02
22	45.54	47.40	49.72	51.10	52.32	53.71	55.13	56.68	58.07	57.24	52.75	47.39
23	44.57	46.10	47.86	48.85	49.93	51.42	53.13	55.07	56.68	55.82	51.36	46.29

Slope. QDC. Excl. rev. conv. Years: 1997-2009.
Smoothing: XH0= 3 XM0= 2

UT	JAN	FEB	MAR	APR	MAY	JUN	JUL	AUG	SEP	OCT	NOV	DEC
0	24.77	27.39	32.61	32.65	39.28	40.84	37.27	38.41	33.93	28.44	24.36	22.56
1	23.51	24.79	30.05	31.69	36.88	39.07	36.29	36.26	33.29	27.29	23.11	21.06
2	22.42	22.61	28.16	30.67	34.77	37.57	35.00	34.17	32.14	25.92	21.47	20.07
3	21.12	21.02	26.39	30.05	32.96	37.42	33.60	34.20	31.00	25.79	20.12	20.40
4	20.44	20.90	25.27	29.33	32.35	36.21	32.58	33.83	30.20	25.11	20.36	20.76
5	19.72	20.75	24.15	28.97	31.23	36.60	31.95	33.20	30.96	24.45	20.90	20.81
6	19.98	21.30	24.45	28.69	31.72	36.37	32.14	32.35	31.64	24.69	21.73	21.39
7	21.25	21.64	25.43	29.68	32.55	37.48	32.43	32.70	31.67	25.81	22.21	21.82
8	22.59	22.39	27.11	30.56	33.27	38.74	33.61	33.57	32.14	28.05	23.86	22.86
9	24.09	23.95	28.94	32.64	34.57	40.75	36.74	34.69	33.62	30.03	26.21	24.33
10	25.71	26.56	30.17	34.60	35.84	41.11	38.62	34.81	34.51	31.21	27.92	26.80
11	28.09	28.62	32.05	38.23	38.15	44.18	41.32	37.03	36.77	32.61	29.42	29.21

12	29.56	31.25	33.42	40.21	40.01	46.19	42.29	38.82	38.46	33.05	31.55	30.79
13	31.07	32.77	35.17	41.93	42.00	48.17	45.23	40.81	40.29	34.58	33.61	31.80
14	32.13	35.25	35.64	42.93	42.46	47.99	46.00	41.35	40.51	35.95	35.30	32.67
15	33.03	36.09	36.61	44.39	43.32	49.17	47.44	42.63	41.61	37.11	35.47	33.50
16	33.64	36.95	36.92	45.36	44.36	49.36	47.71	43.92	41.70	37.59	35.19	33.36
17	34.19	36.87	38.42	44.80	46.04	49.73	48.04	45.71	41.30	37.80	34.52	33.14
18	34.28	36.61	38.14	42.91	45.74	47.98	47.22	44.21	41.06	37.05	33.60	31.96
19	32.52	36.12	38.22	40.70	44.88	47.55	46.58	43.74	40.64	35.66	32.77	30.81
20	30.57	35.78	37.34	38.64	44.38	46.02	45.69	42.18	39.55	34.14	31.13	29.23
21	28.83	34.03	36.92	36.92	43.35	44.10	44.50	42.41	36.64	33.45	29.61	27.75
22	27.61	32.00	36.24	34.97	42.47	43.48	41.30	41.50	35.34	31.74	27.46	25.80
23	25.89	29.43	34.51	33.80	40.51	42.33	38.86	40.72	34.30	30.32	25.93	24.38

Intercept. QDC. Excl. rev. conv. Years: 1997-2009.
Smoothing: XH0= 3 XM0= 2

0	-4.93	-4.63	-3.16	0.23	0.19	-0.19	2.11	-1.22	-1.08	-2.14	-2.94	-4.38
1	-4.49	-3.82	-2.58	0.09	1.06	0.45	2.30	-0.52	-1.09	-2.13	-2.52	-4.02
2	-3.94	-3.08	-2.16	-0.03	1.44	0.80	2.55	0.13	-0.85	-1.59	-1.84	-3.49
3	-3.50	-2.49	-1.86	-0.17	1.43	0.56	2.59	-0.05	-0.89	-1.51	-1.46	-3.49
4	-3.14	-2.35	-1.73	-0.21	1.07	0.59	2.42	-0.06	-0.89	-1.22	-1.38	-3.59
5	-2.52	-1.98	-1.28	-0.14	0.98	0.25	2.07	0.07	-1.14	-0.77	-1.22	-3.33
6	-2.16	-1.67	-0.98	0.01	0.83	0.28	1.80	0.57	-1.07	-0.26	-1.00	-2.95
7	-2.03	-1.25	-0.93	-0.27	0.92	-0.11	1.70	0.89	-0.56	0.09	-0.68	-2.54
8	-2.01	-1.03	-1.16	-0.09	1.34	-0.20	1.52	1.21	-0.23	-0.32	-0.93	-2.58
9	-2.10	-1.32	-1.50	-0.11	1.91	-0.01	1.35	1.87	-0.07	-0.65	-1.48	-2.98
10	-2.61	-2.11	-1.65	0.04	2.75	1.32	2.54	3.03	0.41	-0.71	-2.12	-3.68
11	-3.55	-2.72	-2.14	-0.97	3.05	1.84	3.63	3.42	0.25	-0.84	-2.73	-4.29
12	-4.08	-3.35	-2.28	-1.33	3.37	3.20	5.28	3.67	0.00	-0.91	-3.53	-4.76
13	-4.58	-3.69	-2.62	-1.54	3.72	4.46	6.05	4.01	-0.67	-1.67	-4.33	-5.29
14	-4.93	-4.53	-2.55	-1.12	4.66	6.60	7.68	5.04	-0.44	-2.35	-5.00	-5.84
15	-5.68	-5.38	-3.25	-1.86	4.20	6.43	7.48	4.73	-1.06	-3.28	-5.47	-6.43
16	-6.17	-6.09	-3.47	-2.15	2.98	6.28	6.58	3.54	-1.40	-3.93	-5.90	-6.75
17	-6.64	-6.36	-4.01	-2.06	1.47	5.10	4.85	1.83	-1.97	-4.28	-6.23	-7.21
18	-6.60	-5.92	-3.40	-0.72	1.67	4.96	4.23	1.79	-1.66	-3.83	-5.87	-6.97
19	-6.25	-5.71	-3.19	-0.13	1.76	3.29	3.35	1.21	-1.36	-3.11	-5.33	-6.64
20	-5.70	-5.57	-2.86	0.71	1.47	2.24	2.72	0.76	-0.67	-2.43	-4.50	-6.03
21	-5.47	-5.57	-2.98	0.93	0.76	1.10	1.72	-0.78	-0.47	-2.63	-4.47	-5.82
22	-5.26	-5.34	-3.18	1.13	0.07	0.12	1.74	-1.50	-0.64	-2.35	-3.97	-5.19
23	-5.18	-5.03	-3.21	0.61	0.03	-0.40	1.71	-1.95	-1.10	-2.57	-3.70	-4.94

Appendix B.

Table B1a. Vostok magnetometer. Yearly average component values during quiet days.

Year	X nT	Y nT	Z nT	Year	X nT	Y nT	Z nT
1991	-6629	-11530	-58540	2002	-6978	-11568	-58119
1992	-6641	-11552	-58527	2003	-7019	-11549	-58095
1993	-6653	-11574	-58514	2004	-7030	-11530	-58070
1994	-6658	-11576	-58508	2005	-7077	-11525	-58027
1995	-6767	-11554	-58403	2006	-7098	-11515	-57993
1996	-6873	-11531	-58368	2007	-7143	-11495	-57962
1997	-6792	-11612	-58313	2008	-7181	-11475	-57918
1998	-6823	-11615	-58280	2009	-7243	-11455	-57894
1999	-6848	-11598	-58242	2010	-7307	-11423	-57885
2000	-6889	-11606	-58190	2011	-7356	-11408	-57855
2001	-6933	-11586	-58151	2012	-7415	-11384	-57839

Table B1b. Vostok magnetometer. Monthly average components during quiet days (1997-2009).

Year	Md	X nT	Y nT	Z nT	Year	Md	X nT	Y nT	Z nT	Year	Md	X nT	Y nT	Z nT
1997	1	-6755	-11602	-58326	2001	1	-6919	-11602	-58136	2006	1	-7084	-11519	-57996
1997	2	-6760	-11605	-58327	2001	2	-6920	-11593	-58146	2006	2	-7083	-11516	-58000
1997	3	-6766	-11607	-58327	2001	3	-6922	-11587	-58157	2006	3	-7083	-11514	-58004
1997	4	-6770	-11608	-58326	2001	4	-6925	-11584	-58164	2006	4	-7087	-11513	-58004
1997	5	-6775	-11609	-58324	2001	5	-6928	-11583	-58164	2006	5	-7092	-11513	-58001
1997	6	-6779	-11610	-58321	2001	6	-6931	-11582	-58161	2006	6	-7096	-11514	-57998
1997	7	-6783	-11610	-58316	2001	7	-6934	-11583	-58156	2006	7	-7100	-11513	-57994
1997	8	-6787	-11612	-58310	2001	8	-6937	-11585	-58150	2006	8	-7104	-11513	-57989
1997	9	-6793	-11615	-58301	2001	9	-6942	-11588	-58142	2006	9	-7108	-11515	-57983
1997	10	-6798	-11619	-58289	2001	10	-6947	-11592	-58129	2006	10	-7113	-11518	-57973
1997	11	-6803	-11621	-58276	2001	11	-6952	-11596	-58112	2006	11	-7118	-11520	-57963
1997	12	-6806	-11621	-58268	2001	12	-6956	-11596	-58101	2006	12	-7122	-11519	-57958
1998	1	-6808	-11618	-58267	2002	1	-6959	-11591	-58100	2007	1	-7124	-11515	-57958
1998	2	-6808	-11614	-58272	2002	2	-6962	-11582	-58110	2007	2	-7126	-11508	-57964
1998	3	-6810	-11611	-58280	2002	3	-6965	-11573	-58123	2007	3	-7128	-11502	-57971
1998	4	-6814	-11611	-58286	2002	4	-6969	-11566	-58130	2007	4	-7130	-11498	-57976
1998	5	-6818	-11612	-58288	2002	5	-6973	-11562	-58131	2007	5	-7135	-11497	-57975
1998	6	-6822	-11613	-58288	2002	6	-6978	-11562	-58126	2007	6	-7140	-11495	-57970
1998	7	-6824	-11614	-58286	2002	7	-6983	-11562	-58121	2007	7	-7144	-11494	-57963
1998	8	-6827	-11616	-58283	2002	8	-6987	-11563	-58119	2007	8	-7149	-11492	-57955
1998	9	-6831	-11618	-58276	2002	9	-6989	-11564	-58117	2007	9	-7153	-11490	-57950
1998	10	-6835	-11620	-58266	2002	10	-6992	-11566	-58108	2007	10	-7156	-11489	-57945
1998	11	-6840	-11618	-58256	2002	11	-6995	-11567	-58097	2007	11	-7158	-11487	-57940
1998	12	-6843	-11611	-58252	2002	12	-6997	-11568	-58087	2007	12	-7160	-11486	-57936
1999	1	-6844	-11602	-58253	2004	1	-7036	-11561	-58075	2008	1	-7162	-11485	-57933
1999	2	-6844	-11596	-58257	2004	2	-7036	-11556	-58072	2008	2	-7165	-11484	-57932
1999	3	-6843	-11594	-58259	2004	3	-7037	-11550	-58068	2008	3	-7168	-11481	-57931
1999	4	-6842	-11595	-58256	2004	4	-7038	-11544	-58064	2008	4	-7171	-11479	-57930
1999	5	-6841	-11597	-58251	2004	5	-7042	-11539	-58062	2008	5	-7175	-11476	-57927
1999	6	-6843	-11597	-58246	2004	6	-7049	-11535	-58064	2008	6	-7178	-11475	-57924
1999	7	-6846	-11598	-58244	2004	7	-7059	-11530	-58068	2008	7	-7181	-11473	-57921
1999	8	-6852	-11601	-58240	2004	8	-7071	-11522	-58075	2008	8	-7185	-11473	-57917
1999	9	-6859	-11604	-58229	2004	9	-7082	-11513	-58080	2008	9	-7188	-11473	-57910
1999	10	-6866	-11607	-58212	2004	10	-7089	-11509	-58077	2008	10	-7192	-11473	-57899
1999	11	-6872	-11609	-58193	2004	11	-7089	-11512	-58062	2008	11	-7194	-11475	-57887
1999	12	-6875	-11608	-58182	2004	12	-7085	-11520	-58043	2008	12	-7188	-11483	-57877
2000	1	-6877	-11606	-58181	2005	1	-7081	-11528	-58028	2009	1	-7177	-11493	-57873
2000	2	-6878	-11604	-58190	2005	2	-7076	-11531	-58024	2009	2	-7170	-11499	-57876
2000	3	-6878	-11602	-58200	2005	3	-7074	-11528	-58028	2009	3	-7171	-11499	-57883
2000	4	-6879	-11602	-58206	2005	4	-7074	-11524	-58035	2009	4	-7185	-11489	-57889
2000	5	-6881	-11603	-58207	2005	5	-7073	-11522	-58036	2009	5	-7207	-11478	-57892
2000	6	-6883	-11604	-58204	2005	6	-7074	-11522	-58034	2009	6	-7227	-11470	-57891
2000	7	-6886	-11605	-58200	2005	7	-7075	-11522	-58032	2009	7	-7242	-11467	-57886
2000	8	-6891	-11606	-58192	2005	8	-7076	-11523	-58031	2009	8	-7253	-11469	-57872
2000	9	-6897	-11608	-58179	2005	9	-7079	-11524	-58027	2009	9	-7263	-11472	-57844
2000	10	-6904	-11610	-58161	2005	10	-7082	-11525	-58017	2009	10	-7271	-11473	-57811
2000	11	-6911	-11611	-58145	2005	11	-7085	-11524	-58006	2009	11	-7277	-11467	-57793
2000	12	-6916	-11608	-58135	2005	12	-7086	-11523	-57998	2009	12	-7283	-11448	-57806

Table B2a. OMNI Em – Vostok correlations (no QDC corr.)

Correlation of ΔFproj (No QDC) vs. Em (OMNI). Years: 1997-2009

UT	JAN	FEB	MAR	APR	MAY	JUN	JUL	AUG	SEP	OCT	NOV	DEC
0	0.705	0.759	0.791	0.764	0.732	0.722	0.793	0.771	0.688	0.739	0.733	0.743
1	0.709	0.712	0.772	0.772	0.735	0.723	0.766	0.767	0.695	0.773	0.758	0.748
2	0.730	0.765	0.760	0.808	0.724	0.764	0.717	0.763	0.800	0.769	0.771	0.763
3	0.740	0.647	0.722	0.777	0.718	0.746	0.721	0.738	0.790	0.781	0.766	0.817
4	0.725	0.673	0.740	0.776	0.744	0.765	0.609	0.775	0.731	0.711	0.716	0.774
5	0.665	0.645	0.709	0.696	0.689	0.748	0.600	0.700	0.669	0.662	0.763	0.752
6	0.525	0.659	0.631	0.762	0.751	0.775	0.780	0.728	0.714	0.689	0.762	0.596
7	0.490	0.622	0.678	0.709	0.783	0.768	0.686	0.743	0.671	0.733	0.722	0.629
8	0.639	0.647	0.691	0.751	0.778	0.829	0.745	0.764	0.742	0.754	0.761	0.711
9	0.731	0.728	0.733	0.788	0.731	0.799	0.772	0.783	0.754	0.778	0.816	0.790
10	0.771	0.777	0.790	0.816	0.727	0.785	0.804	0.812	0.786	0.796	0.858	0.789
11	0.758	0.764	0.755	0.790	0.750	0.797	0.807	0.817	0.775	0.826	0.835	0.785
12	0.757	0.753	0.776	0.794	0.830	0.767	0.824	0.723	0.803	0.797	0.760	0.741
13	0.696	0.719	0.742	0.760	0.816	0.716	0.835	0.772	0.739	0.824	0.748	0.721
14	0.672	0.699	0.720	0.796	0.792	0.816	0.817	0.813	0.730	0.814	0.765	0.584
15	0.668	0.738	0.742	0.770	0.729	0.799	0.821	0.793	0.717	0.786	0.692	0.620
16	0.693	0.729	0.806	0.747	0.811	0.828	0.783	0.769	0.765	0.805	0.791	0.709
17	0.746	0.710	0.784	0.777	0.725	0.762	0.717	0.789	0.699	0.788	0.792	0.737
18	0.741	0.687	0.784	0.810	0.748	0.801	0.754	0.737	0.757	0.775	0.744	0.731
19	0.724	0.738	0.737	0.808	0.723	0.724	0.745	0.766	0.729	0.760	0.750	0.747
20	0.720	0.716	0.719	0.782	0.714	0.734	0.743	0.782	0.693	0.769	0.749	0.760
21	0.705	0.738	0.748	0.752	0.769	0.753	0.734	0.730	0.789	0.769	0.740	0.770
22	0.724	0.739	0.775	0.776	0.779	0.724	0.707	0.811	0.793	0.719	0.764	0.716
23	0.714	0.745	0.764	0.770	0.719	0.718	0.767	0.829	0.687	0.738	0.746	0.736

Avr. correlation= 0.7466

Table B2b. OMNI Em – Vostok correlations (QDC corr.)

Correlation of ΔFproj (QDC-corr) vs. Em (OMNI). Years: 1997-2009

UT	JAN	FEB	MAR	APR	MAY	JUN	JUL	AUG	SEP	OCT	NOV	DEC
0	0.688	0.703	0.792	0.754	0.721	0.722	0.785	0.747	0.688	0.739	0.726	0.702
1	0.702	0.687	0.774	0.762	0.713	0.727	0.760	0.755	0.697	0.766	0.751	0.705
2	0.735	0.733	0.767	0.793	0.708	0.767	0.711	0.752	0.804	0.765	0.765	0.729
3	0.736	0.635	0.725	0.774	0.711	0.750	0.715	0.735	0.793	0.775	0.752	0.785
4	0.726	0.657	0.749	0.766	0.748	0.760	0.607	0.775	0.730	0.712	0.700	0.759
5	0.659	0.632	0.722	0.693	0.606	0.749	0.596	0.699	0.669	0.666	0.757	0.734
6	0.533	0.662	0.620	0.760	0.753	0.779	0.783	0.728	0.718	0.688	0.767	0.555
7	0.489	0.615	0.680	0.710	0.783	0.770	0.696	0.744	0.671	0.735	0.720	0.605
8	0.642	0.604	0.689	0.747	0.774	0.830	0.745	0.757	0.748	0.751	0.765	0.690
9	0.735	0.701	0.729	0.794	0.730	0.800	0.766	0.780	0.759	0.782	0.813	0.760
10	0.760	0.772	0.792	0.815	0.715	0.784	0.804	0.808	0.785	0.796	0.855	0.747
11	0.752	0.760	0.756	0.790	0.739	0.791	0.813	0.817	0.781	0.829	0.837	0.743
12	0.759	0.746	0.777	0.786	0.832	0.763	0.826	0.723	0.807	0.799	0.763	0.716
13	0.699	0.705	0.746	0.760	0.820	0.715	0.835	0.770	0.737	0.817	0.737	0.695
14	0.679	0.686	0.726	0.798	0.777	0.811	0.817	0.814	0.729	0.812	0.765	0.555
15	0.679	0.725	0.752	0.775	0.728	0.796	0.819	0.793	0.706	0.778	0.693	0.592
16	0.697	0.730	0.809	0.752	0.806	0.826	0.779	0.767	0.754	0.788	0.784	0.704
17	0.745	0.710	0.791	0.780	0.721	0.761	0.714	0.793	0.696	0.773	0.787	0.719
18	0.746	0.685	0.790	0.812	0.751	0.804	0.755	0.736	0.754	0.763	0.741	0.720
19	0.719	0.735	0.739	0.811	0.721	0.724	0.744	0.762	0.724	0.743	0.753	0.707
20	0.716	0.715	0.720	0.767	0.712	0.736	0.748	0.778	0.694	0.757	0.750	0.723
21	0.693	0.739	0.747	0.742	0.769	0.755	0.734	0.730	0.791	0.749	0.731	0.739
22	0.715	0.738	0.771	0.769	0.782	0.729	0.699	0.803	0.791	0.701	0.767	0.697
23	0.701	0.747	0.764	0.758	0.722	0.718	0.760	0.821	0.689	0.730	0.739	0.711

Avr. correlation= 0.7412

Table B3a. PCS parameters (no QDC corr.).

VOSTOK. Smoothed optimum projection angle. No QDC corr. Excl. rev. conv. Years: 1997-2009.
Smoothing: XH0= 4 XM0= 2

UT	JAN	FEB	MAR	APR	MAY	JUN	JUL	AUG	SEP	OCT	NOV	DEC
0	29.21	35.55	43.58	49.19	49.90	46.53	41.86	37.78	34.21	30.75	27.89	26.87
1	22.50	29.80	39.61	47.01	48.88	46.04	41.30	36.33	31.19	26.08	21.95	20.18
2	16.89	24.86	36.12	45.06	48.06	45.90	41.29	35.65	29.20	22.70	17.42	14.83
3	13.10	21.41	33.70	43.77	47.73	46.35	42.07	35.99	28.54	20.98	14.77	11.42
4	11.59	19.89	32.61	43.23	47.78	47.08	43.33	37.23	29.32	21.19	14.41	10.41
5	12.72	20.64	33.15	43.67	48.34	48.12	44.94	39.17	31.33	23.23	16.35	12.02
6	16.12	23.35	34.99	44.70	49.01	49.05	46.52	41.45	34.27	26.75	20.20	15.83
7	20.83	27.18	37.49	45.91	49.46	49.45	47.49	43.43	37.49	31.05	25.13	20.87
8	25.66	31.18	40.01	46.86	49.34	49.04	47.60	44.79	40.48	35.37	30.06	25.93
9	29.89	34.67	42.06	47.30	48.62	47.84	46.78	45.33	42.93	39.29	34.53	30.38
10	33.30	37.35	43.33	46.96	47.06	45.71	45.01	45.07	44.81	42.75	38.44	34.10
11	36.22	39.52	44.09	46.14	45.07	43.15	42.76	44.30	46.22	45.81	41.95	37.38
12	39.36	41.74	44.80	45.26	43.07	40.63	40.50	43.42	47.51	48.87	45.66	40.95
13	43.25	44.44	45.74	44.58	41.41	38.59	38.69	42.77	48.83	52.03	49.82	45.30
14	47.88	47.72	47.20	44.53	40.54	37.43	37.66	42.57	50.25	55.24	54.31	50.32
15	52.82	51.40	49.25	45.35	40.78	37.45	37.60	42.83	51.52	58.02	58.57	55.46
16	57.16	54.81	51.45	46.76	41.92	38.46	38.36	43.41	52.42	59.88	61.79	59.75
17	60.09	57.40	53.54	48.67	43.87	40.30	39.71	44.09	52.69	60.41	63.29	62.28
18	60.84	58.54	55.06	50.63	46.16	42.51	41.28	44.65	52.18	59.39	62.60	62.39
19	59.28	58.02	55.72	52.35	48.45	44.67	42.68	44.78	50.75	56.76	59.70	60.00
20	55.62	55.81	55.25	53.34	50.13	46.25	43.53	44.29	48.41	52.76	54.97	55.47
21	50.25	52.10	53.65	53.51	51.15	47.21	43.79	43.20	45.34	47.77	48.89	49.29
22	43.64	47.18	51.00	52.76	51.30	47.36	43.37	41.53	41.70	42.12	41.95	42.02
23	36.43	41.50	47.52	51.23	50.81	47.07	42.63	39.58	37.80	36.23	34.72	34.32

VOSTOK. Slope. No QDC. Excl. rev. conv. Years: 1997-2009.
Smoothing: XH0= 4 XM0= 2

UT	JAN	FEB	MAR	APR	MAY	JUN	JUL	AUG	SEP	OCT	NOV	DEC
0	45.20	44.13	41.75	33.61	31.17	27.08	27.78	31.38	35.04	39.17	42.22	43.34
1	45.78	43.85	41.55	33.64	30.84	27.69	27.72	31.40	35.33	38.97	42.50	43.59
2	46.36	43.24	41.15	33.93	30.62	27.94	27.23	31.15	34.80	38.73	41.57	44.22
3	46.63	42.56	40.10	33.95	30.01	28.28	26.45	31.06	34.45	38.54	41.12	45.22
4	47.30	41.80	39.12	33.60	29.89	27.65	25.98	30.40	34.11	38.10	41.10	45.73
5	47.42	41.60	37.77	32.87	28.79	27.25	25.41	29.28	34.29	37.40	41.94	46.66
6	47.71	41.77	36.82	32.26	28.36	26.97	25.05	28.28	34.03	36.91	42.60	46.98
7	47.86	41.59	36.07	31.84	27.47	26.83	24.73	27.86	33.35	36.83	43.21	47.22
8	47.73	40.93	35.93	31.38	26.96	26.68	24.57	27.97	32.73	36.76	43.53	47.18
9	47.27	40.18	35.58	31.03	26.11	25.93	24.63	27.58	32.25	36.47	43.47	47.40
10	46.54	40.12	34.80	30.51	25.53	24.77	24.32	27.06	31.91	36.72	42.86	48.21
11	45.89	39.98	33.91	30.12	25.49	24.13	24.35	26.87	32.15	37.03	42.28	48.29
12	45.24	40.30	33.52	29.98	25.62	24.10	24.21	26.76	32.72	37.21	42.03	48.33
13	44.96	40.35	33.61	29.96	25.84	24.26	24.27	26.74	32.77	37.04	42.13	47.43
14	44.89	40.82	33.75	30.10	26.05	23.94	24.10	26.82	32.24	37.43	42.37	46.86
15	44.41	40.10	33.86	30.16	26.10	23.76	24.12	26.77	31.88	37.25	41.98	45.61
16	44.03	39.80	34.23	30.71	26.47	24.07	24.52	27.28	32.20	37.61	41.62	45.14
17	43.46	39.10	34.98	30.83	26.66	24.91	24.74	27.68	32.53	37.59	40.90	44.39
18	42.85	39.81	35.44	31.30	27.39	25.77	25.23	28.31	33.27	37.97	40.63	43.95
19	41.92	40.43	36.50	31.60	28.35	26.71	25.97	29.07	33.96	37.75	40.41	43.34
20	41.53	41.78	37.47	32.12	29.80	27.28	26.79	29.72	34.81	37.60	40.32	42.91
21	42.25	42.52	38.78	32.61	30.67	27.34	27.17	30.43	35.06	37.75	40.48	42.75
22	43.28	43.39	40.02	33.06	31.10	27.18	27.14	30.80	35.06	38.29	40.78	42.89
23	44.33	43.92	40.90	33.57	31.01	27.12	27.42	31.17	35.08	38.74	41.68	43.08

VOSTOK. Intercept. No QDC. Excl. rev. conv. Years: 1997-2009.
Smoothing: XH0= 3 XM0= 2

UT	JAN	FEB	MAR	APR	MAY	JUN	JUL	AUG	SEP	OCT	NOV	DEC
0	37.80	34.73	28.18	22.96	15.39	11.43	11.18	13.70	21.00	29.04	36.20	37.67
1	38.16	35.73	29.35	23.74	16.30	11.66	11.83	14.56	21.82	29.88	36.72	37.76
2	38.42	36.68	30.31	24.06	16.72	11.74	12.45	15.34	22.85	30.77	37.72	37.63
3	38.38	37.17	31.07	24.10	17.01	11.54	12.84	15.65	23.28	31.27	37.82	37.01

4	37.24	36.69	30.78	23.70	16.68	11.60	12.70	15.86	23.12	31.07	36.89	35.67
5	35.56	34.94	30.01	23.18	16.63	11.50	12.53	16.12	22.51	30.28	34.76	33.67
6	33.08	32.56	28.51	22.21	15.97	11.18	12.29	16.25	21.97	29.01	32.56	32.06
7	30.93	30.28	26.82	20.75	15.47	10.43	11.89	16.04	21.49	27.74	30.62	30.81
8	29.30	28.65	24.87	19.17	14.41	9.35	10.92	15.00	20.55	26.45	29.08	30.04
9	28.38	27.15	23.05	17.50	13.38	8.57	9.86	14.15	19.71	25.77	27.99	29.21
10	27.67	25.65	21.75	16.15	12.23	8.07	9.01	13.17	18.90	24.82	27.16	28.26
11	27.24	24.66	20.83	14.92	10.95	7.33	8.06	12.16	17.89	24.04	26.59	27.70
12	27.13	24.06	20.26	13.94	9.83	6.47	7.17	11.13	16.66	23.25	26.16	27.17
13	26.55	23.66	19.58	13.19	8.90	5.72	6.38	10.31	15.68	22.50	25.44	26.79
14	25.90	23.14	19.16	12.69	8.32	5.54	6.12	9.73	15.25	21.56	24.72	26.17
15	25.96	23.50	19.14	12.62	8.10	5.47	6.01	9.49	15.12	21.39	24.69	26.45
16	26.97	24.33	19.64	12.80	8.03	5.45	5.80	9.11	15.02	21.50	25.41	27.03
17	28.59	25.99	20.45	13.71	8.47	5.48	5.89	9.11	15.15	22.27	26.75	28.39
18	30.54	27.54	21.82	14.93	9.12	5.87	6.25	9.31	15.54	23.08	28.44	30.09
19	32.81	29.41	23.25	16.47	10.10	6.57	6.95	9.84	16.42	24.47	30.56	32.33
20	35.11	30.94	24.81	18.23	11.09	7.74	8.01	10.77	17.63	26.23	32.94	34.68
21	36.44	32.30	26.03	19.86	12.27	9.04	9.11	11.52	18.52	27.45	34.42	36.22
22	37.34	33.27	26.89	21.26	13.35	10.08	10.14	12.29	19.33	28.27	35.47	37.24
23	37.56	34.00	27.62	22.13	14.51	10.87	10.74	12.93	20.01	28.67	35.72	37.59

Table B3b. PCS parameters (QDC corr.)

VOSTOK. Optimum projection angle. QDC corr. Excl. rev. conv. Years: 1997-2009.
Smoothing: XH0= 4 XM0= 2

UT	JAN	FEB	MAR	APR	MAY	JUN	JUL	AUG	SEP	OCT	NOV	DEC
0	28.51	35.01	43.21	49.02	49.89	46.58	41.88	37.70	33.96	30.26	27.17	26.07
1	21.94	29.35	39.28	46.83	48.83	46.08	41.38	36.38	31.11	25.81	21.46	19.58
2	16.47	24.47	35.79	44.82	47.93	45.90	41.40	35.77	29.26	22.63	17.15	14.42
3	12.77	21.06	33.32	43.44	47.52	46.31	42.17	36.14	28.68	21.06	14.70	11.18
4	11.35	19.56	32.20	42.81	47.48	46.97	43.36	37.34	29.48	21.37	14.48	10.30
5	12.52	20.31	32.70	43.20	47.98	47.93	44.86	39.15	31.43	23.43	16.51	12.00
6	15.93	23.02	34.55	44.24	48.65	48.81	46.33	41.30	34.27	26.92	20.38	15.83
7	20.64	26.87	37.10	45.50	49.11	49.15	47.17	43.13	37.37	31.15	25.28	20.88
8	25.47	30.91	39.71	46.56	49.05	48.71	47.17	44.36	40.26	35.39	30.17	25.91
9	29.71	34.46	41.88	47.15	48.42	47.50	46.28	44.82	42.62	39.23	34.58	30.34
10	33.15	37.22	43.30	46.97	46.97	45.38	44.46	44.51	44.44	42.62	38.44	34.04
11	36.09	39.46	44.18	46.30	45.09	42.87	42.22	43.74	45.84	45.64	41.93	37.33
12	39.23	41.70	44.95	45.51	43.17	40.41	40.01	42.89	47.11	48.65	45.60	40.89
13	43.07	44.35	45.85	44.81	41.53	38.42	38.26	42.27	48.41	51.75	49.69	45.17
14	47.58	47.49	47.16	44.65	40.63	37.30	37.30	42.12	49.80	54.87	54.07	50.09
15	52.35	50.96	48.96	45.27	40.80	37.37	37.32	42.40	51.02	57.53	58.18	55.07
16	56.49	54.13	50.87	46.43	41.84	38.42	38.14	43.01	51.87	59.26	61.20	59.15
17	59.23	56.50	52.70	48.09	43.68	40.28	39.53	43.68	52.07	59.66	62.50	61.49
18	59.84	57.51	54.05	49.90	45.90	42.48	41.12	44.22	51.50	58.52	61.63	61.41
19	58.21	56.93	54.65	51.58	48.16	44.64	42.52	44.33	50.03	55.81	58.61	58.89
20	54.54	54.77	54.27	52.65	49.90	46.24	43.37	43.84	47.68	51.78	53.81	54.30
21	49.22	51.17	52.84	52.99	51.01	47.22	43.65	42.79	44.66	46.82	47.73	48.12
22	42.68	46.38	50.36	52.40	51.23	47.39	43.27	41.21	41.14	41.28	40.89	40.92
23	35.60	40.84	47.03	50.99	50.79	47.12	42.59	39.37	37.38	35.55	33.81	33.36

VOSTOK. Slope. QDC. Excl. rev. conv. Years: 1997-2009.
Smoothing: XH0= 4 XM0= 2

UT	JAN	FEB	MAR	APR	MAY	JUN	JUL	AUG	SEP	OCT	NOV	DEC
0	44.07	43.72	41.23	33.06	30.48	26.66	27.40	30.83	34.25	38.05	40.88	42.11
1	44.42	43.22	40.90	33.03	30.16	27.27	27.35	30.88	34.54	37.82	41.10	42.13
2	44.80	42.42	40.42	33.24	29.96	27.48	26.89	30.61	34.03	37.58	40.14	42.61
3	44.91	41.57	39.33	33.18	29.38	27.74	26.17	30.48	33.66	37.45	39.56	43.50
4	45.44	40.77	38.27	32.79	29.29	27.14	25.73	29.86	33.36	37.08	39.54	43.92
5	45.43	40.50	36.79	32.06	28.27	26.82	25.16	28.76	33.57	36.32	40.37	44.55
6	45.71	40.69	35.75	31.46	27.90	26.59	24.78	27.77	33.35	35.89	41.05	44.73
7	45.89	40.45	35.04	31.13	27.07	26.50	24.45	27.32	32.68	35.82	41.54	44.86
8	45.74	39.84	34.89	30.79	26.62	26.38	24.26	27.45	32.05	35.87	41.71	44.91
9	45.25	38.99	34.53	30.45	25.87	25.60	24.25	27.10	31.53	35.49	41.51	45.00

10	44.64	38.82	33.81	30.01	25.34	24.42	23.90	26.56	31.13	35.62	40.84	45.59
11	44.32	38.79	33.13	29.72	25.35	23.75	23.91	26.33	31.34	35.90	40.47	45.59
12	43.87	39.43	32.91	29.72	25.46	23.80	23.80	26.19	31.92	36.12	40.40	45.82
13	43.58	39.81	33.13	29.75	25.68	23.95	23.87	26.17	31.95	36.02	40.48	45.31
14	43.48	40.34	33.31	29.90	25.83	23.62	23.71	26.24	31.36	36.35	40.55	44.94
15	43.20	39.76	33.52	30.01	25.85	23.45	23.75	26.21	30.93	36.18	40.15	43.86
16	43.11	39.60	33.97	30.57	26.19	23.77	24.15	26.69	31.23	36.51	39.90	43.55
17	42.71	39.06	34.86	30.66	26.33	24.61	24.35	27.05	31.53	36.45	39.22	43.06
18	42.15	39.86	35.39	31.07	26.99	25.45	24.84	27.66	32.26	36.76	39.03	42.82
19	41.29	40.57	36.42	31.35	27.86	26.35	25.57	28.41	32.95	36.52	38.91	42.32
20	40.91	41.96	37.28	31.83	29.23	26.89	26.37	29.08	33.85	36.40	38.96	41.96
21	41.52	42.62	38.48	32.29	30.05	26.93	26.73	29.79	34.14	36.52	39.13	41.77
22	42.42	43.35	39.64	32.66	30.45	26.76	26.72	30.20	34.21	37.10	39.44	41.87
23	43.34	43.70	40.47	33.09	30.35	26.69	27.02	30.59	34.25	37.59	40.33	41.98

VOSTOK. Intercept. QDC. Excl. rev. conv. Years: 1997-2009.
Smoothing: XH0= 4 XM0= 2

UT	JAN	FEB	MAR	APR	MAY	JUN	JUL	AUG	SEP	OCT	NOV	DEC
0	6.71	5.81	3.72	3.36	-0.04	-2.00	-2.28	-1.67	2.10	5.50	7.82	7.25
1	8.00	7.50	5.24	4.25	0.90	-1.65	-1.55	-0.77	3.16	6.90	9.15	8.37
2	9.01	9.05	6.48	4.68	1.35	-1.46	-0.89	0.01	4.26	8.15	10.76	9.07
3	9.52	10.11	7.47	4.81	1.62	-1.60	-0.52	0.25	4.62	8.77	11.31	9.04
4	8.91	10.21	7.57	4.57	1.27	-1.55	-0.72	0.31	4.28	8.57	10.66	8.18
5	7.89	9.20	7.35	4.28	1.19	-1.72	-0.95	0.39	3.43	7.84	8.85	6.67
6	6.05	7.43	6.41	3.58	0.56	-2.05	-1.26	0.36	2.65	6.50	6.80	5.26
7	4.28	5.68	5.06	2.31	0.10	-2.81	-1.71	0.00	1.93	5.06	4.92	4.02
8	2.81	4.41	3.44	0.91	-0.87	-3.88	-2.71	-1.22	0.65	3.26	3.24	3.04
9	1.86	3.20	1.87	-0.58	-1.83	-4.58	-3.75	-2.27	-0.58	2.07	1.93	2.10
10	0.75	1.63	0.54	-1.87	-2.88	-4.99	-4.59	-3.41	-1.83	0.40	0.61	0.88
11	-0.69	-0.23	-0.92	-3.24	-4.11	-5.67	-5.53	-4.56	-3.31	-1.37	-1.03	-0.47
12	-1.88	-1.97	-2.21	-4.44	-5.20	-6.56	-6.44	-5.67	-4.97	-3.13	-2.49	-2.00
13	-3.05	-3.33	-3.37	-5.30	-6.09	-7.29	-7.20	-6.46	-6.10	-4.38	-3.78	-3.12
14	-3.77	-4.14	-3.91	-5.79	-6.57	-7.45	-7.42	-6.94	-6.40	-5.15	-4.40	-3.86
15	-4.00	-4.16	-4.08	-5.91	-6.74	-7.54	-7.51	-7.08	-6.33	-5.11	-4.49	-3.83
16	-3.74	-3.91	-3.90	-5.86	-6.81	-7.60	-7.70	-7.35	-6.30	-4.93	-4.15	-3.86
17	-3.12	-3.11	-3.65	-5.15	-6.44	-7.65	-7.59	-7.21	-6.04	-4.22	-3.40	-3.46
18	-2.06	-2.35	-2.81	-4.18	-5.88	-7.36	-7.25	-6.86	-5.42	-3.37	-2.26	-2.59
19	-0.45	-1.09	-1.79	-2.89	-5.04	-6.78	-6.58	-6.19	-4.26	-1.85	-0.50	-0.91
20	1.58	0.17	-0.41	-1.35	-4.20	-5.73	-5.58	-5.13	-2.75	0.18	1.82	1.30
21	3.14	1.66	0.82	0.16	-3.15	-4.51	-4.50	-4.23	-1.48	1.94	3.70	3.18
22	4.58	3.05	1.84	1.53	-2.13	-3.50	-3.46	-3.31	-0.28	3.40	5.39	4.87
23	5.58	4.37	2.82	2.44	-0.98	-2.66	-2.81	-2.53	0.79	4.47	6.47	6.13

Appendix C.

Summary of PC index procedures, their data bases and software, their availability and the index uses. The naming of procedures is like the table provided in *McCready and Menvielle* (2010, 2011).

1. **AARI#1:** PCS index based on Vostok magnetometer data.
   Published description: *Troshichev et al*., (1988). Programmer: *V. G. Andrezen*.
   Data base for coefficients: 1976-1980. Software not available.
   PC index values: Available in WDC-B2 report. Possibly available at AARI.
   Used in: *Troshichev* (1988), *Troshichev et al.* (1988)

2. **AARI#2:** PCS index based on Vostok data. PCN index based on Thule data.
   Published description: Not available. Programmer: *R. Yu. Lukianova*.
   Data base for PCS coefficients: 1977-1979. Software not available.
   PCS index values: 1992, 1995, 1997-2000. Available. PCN index not available.
   Data handling: QDC included. Reverse convection events included. Poor smoothing.
   Comments: Coefficients are strongly fluctuating. PCS values are very different from concurrent DMI PCN values.
   Used in: *Lee et al*. (2004), *Lukianova* (2003, 2007), *Lukianova et al.* (2002), *Stepanova et al.* (2003, 2005a, 2005b, 2005c), *Troshichev and Lukianova* (2002), *Troshichev et al*. (2000).

3. **AARI#3:** PCS and PCN indices based on Vostok and Thule data, respectively.
   Published description: *Troshichev et al*. (2006). Programmer: *A. Janzhura*.
   Data base for coefficients: 1998-2001.
   PCS and PCN index values: calculated for 1995-2006. Available.
   Data handling: QDC included. Reverse convection events included.
   Comments: Large PCN slope values and strongly negative intercept values at midday during summer season. PCN and PCS coefficients are quite different.
   Used in: *Janzhura and Troshichev* (2008), *Janzhura et al.* (2007), *Troshichev et al*. (2006, 2007a, 2007b)

4. **AARI#4:** PCS and PCN indices based on Vostok and Thule data.
   Published description: http://geophys.aari.ru/clgmi/geophys/Description.pdf. Programmer: *A. Janzhura*.
   Data base for coefficients: 1995-2005. PCS coefficients available at AARI web site.
   PCS (and PCN) index values: calculated for 1995-2013.
   Data handling: QDC included. Solar sector term. Reverse convection events included.
   Comments: AARI#3 index coefficients modified. Solar sector correction of QDC level.
   Used in: *Frank-Kamenetsky and Troshichev* (2012), *Troshichev* (2010), *Troshichev and Janzhura* (2009, 2012a), *Troshichev et al*. (2011a, 2011b, 2011c, 2011d, and 2012).

5. **IAGA-endorsed version:** PCS and PCN indices based on Vostok and Thule data.
   Published description: Notes at endorsement. Full description not available. Programmer: *A. Janzhura*.
   Data base for coefficients: 1997-2009. PCN and PCS coefficients available at http://pcindex.org.
   PCN values calculated from 1975 to present. PCS index values: calculated from 1995 to present.
   Data handling: QDC included. Solar sector term derived. Reverse convection events included.
   Comments: Solar sector correction of QDC level give examples of unfounded PC index changes of up to 2.4 mV/m. Inclusion of reverse convection events give examples of unfounded index changes of up to ~ 1 mV/m.
   Used in: Troshichev, O. A. and D. A. Sormakov (2015), Troshichev, O., N. A. Podorozhkina , D. A. Sormakov, A. Janzhura (2014).

6. **DMI#1:** PCN indices based on Thule data
Published description: *Vennerstrøm* (1991); *Vennerstrøm et al.* (1994). Programmer: *S. Vennerstrøm*.
Data base for coefficients: 1976-1980. Data base and software not available.
PCN index values: calculated for 1975-2000. Available in WDC-A- report (UAG-103).
Data handling: QDC not included. Reverse convection events included.
Comments: Principal error in coefficient calculations. Software error in index program. PCN data are incorrect.
Used in: *Chun et al.* (1999), *Nagatsuma et al.* (1999), *Nagatsuma et al.* (2000), *Papitashvili and Rasmussen* (1999), *Takalo and Timonen* (1998a, 1998b,1999), *Troshichev et al.* (1991), *Trochichev et al.* (1996), *Vassiliadis et al.* (1996), *Vennerstrøm* (1991), *Vennerstrøm et al.* (1991, 1994).

7. **DMI#2** = **DTUS#1:** PCN indices (PCN2) based on Thule data.
Published description: *Vennerstrøm* (1991), *Vennerstrøm et al.* (1994). Programmer: *S. Vennerstrøm*.
Program modifications: *V. O. Papitashvili* and *O. Rasmussen*.
Data base for coefficients: 1976-1980 (same as above). Data base and software not available.
PC index values: re-calculated for 1975-2013. Available from DTU-Space. Included in OMNIweb.
Data handling: QDC not included. Reverse convection events included.
Comments: Software error in index program corrected in 2001. Principal error in coefficient calculations not corrected. Present DTUS#1 (DMI#2) PCN2 data are questionable.
Used in: *Chun et al.* (2002), *de Campra and Artigas* (2004), *Fiori et al.* (2009), *Gao* (2012), *Gao et al.* (2012a, 2012b, 2012c), *Henderson et al.* (2006), *Huang* (2005), *Johnsen and Lorentzen* (2012), *Lee et al.* (2004), *Liou et al.* (2003), *Liou et al.* (2004), *Lukianova* (2003, 2007), *Lukianova et al.* (2002), *Nagatsuma* (2002a, 2002b), *Nagatsuma et al.*, (2003), *Ridley and Kihn* (2004).

8. **DMI#3:** PCN indices based on Thule data.
Published description: *Papitashvili et al.* (2001) (DMI report SR01-01). Programmer: *V. O. Papitashvili*.
Data base for coefficients: 1976-2000. Data base and software not available.
Data handling: QDC not included. Reverse convection events included.
PCN index values: calculated for 1975-2000 for analyses of solar cycle effects. Not available.
Used in: *Papitashvili et al.* (2001).

9. **DMI# 4:** PCN and PCS indices based on Thule and Vostok data.
Published description: *Stauning et al.* (2006) (DMI report SR06-04). Programmer: *P. Stauning.*
Data base for PCN coefficients: 1975-2006. Data base and software available on request.
PCN index values: 1975-2012. Used in DMI publications. Available on request.
Data handling: QDC included. Reverse convection events excluded.
Comments: PCN and PCS coefficients are similar. The extended data base for calculation of coefficients, differences in QDC calculations, and differences in handling of reverse convection give deviations from concurrent PCN and PCS values calculated by AARI (cf. above AARI#3 and AARI#4).
Used in: *Stauning* (2007, 2011a, 2011b, 2012, 2013a), *Stauning and Troshichev* (2008), *Stauning et al.* (2006, 2008).

10. **DMI (version presented here):** PCN and PCS indices based on Thule and Vostok data.
Published description: DMI report SR16-xx. Programmer: *P. Stauning*.
Data base for PCN and PCS coefficients: 1997-2009. Data base and software available on request.
PCN index values: 1975-2016. PCS index values: 1995-2015. Available on request.
Data handling: QDC included. Reverse convection events excluded.
Comments: PCN and PCS coefficients are similar. Differences in QDC calculations, and handling of reverse convection give deviations from concurrent PCN and PCS values calculated by AARI (cf. above AARI#3 and AARI#4 and IAGA versions).